

## **General Disclaimer**

### **One or more of the Following Statements may affect this Document**

- This document has been reproduced from the best copy furnished by the organizational source. It is being released in the interest of making available as much information as possible.
- This document may contain data, which exceeds the sheet parameters. It was furnished in this condition by the organizational source and is the best copy available.
- This document may contain tone-on-tone or color graphs, charts and/or pictures, which have been reproduced in black and white.
- This document is paginated as submitted by the original source.
- Portions of this document are not fully legible due to the historical nature of some of the material. However, it is the best reproduction available from the original submission.

DOE/NASA/0077-82/1  
NASA CR 167974  
AIRESEARCH 82-19211



# ADVANCED SINGLE PERMANENT MAGNET AXIPOLAR IRONLESS STATOR AC MOTOR FOR ELECTRIC PASSENGER VEHICLES

FINAL REPORT

E.D. Beauchamp, J.R. Hadfield, K.L. Wuertz  
AiResearch Manufacturing Company  
The Garrett Corporation

August 8, 1983

Prepared for  
NATIONAL AERONAUTICS AND SPACE ADMINISTRATION  
Lewis Research Center

Under Contract DEN 3-77

for  
U.S. DEPARTMENT OF ENERGY  
Conservation and Renewable Energy  
Office of Vehicle and Engine R&D  
Washington, D.C. 20585

(NASA-CR-167974) ADVANCED SINGLE PERMANENT  
MAGNET AXIPOLAR IRONLESS STATOR AC MOTOR FOR  
ELECTRIC PASSENGER VEHICLES Final Report  
(AiResearch Mfg. Co., Torrance, Calif.)  
226 p HC A11/MF A01

N83-32687

Unclass

CSC 13F G3/85 28489

DOE/NASA/0077-82/1  
NASA CR 167974  
AIRESEARCH 82-19211

# ADVANCED SINGLE PERMANENT MAGNET AXIPOLAR IRONLESS STATOR AC MOTOR FOR ELECTRIC PASSENGER VEHICLES

FINAL REPORT

E.D. Beauchamp, J.R. Hadfield, K.L. Wuertz  
AiResearch Manufacturing Company  
The Garrett Corporation

August 8, 1983

Prepared for  
NATIONAL AERONAUTICS AND SPACE ADMINISTRATION  
Lewis Research Center

Under Contract DEN 3-77

for  
U.S. DEPARTMENT OF ENERGY  
Conservation and Renewable Energy  
Office of Vehicle and Engine R&D  
Washington, D.C. 20585  
Under Interagency Agreement DE-A-101-77CS51044

# CONTENTS

	<u>Page</u>
ABSTRACT . . . . .	1-1
SUMMARY . . . . .	2-1
Program Accomplishments and Limitations . . . . .	2-1
Program highlights . . . . .	2-1
System limitations . . . . .	2-2
INTRODUCTION . . . . .	3-1
CONCEPT AND DESIGN ANALYSIS . . . . .	4-1
Rotating Machine . . . . .	4-1
Approach . . . . .	4-1
Status and history of concept . . . . .	4-1
Design concept . . . . .	4-2
Optimizing the design . . . . .	4-7
Baseline design . . . . .	4-9
Alternate magnet design . . . . .	4-13
Power Converter . . . . .	4-16
Basic considerations . . . . .	4-16
Voltage-source inverter . . . . .	4-19
Current-source inverter . . . . .	4-19
Converter/PM motor interface . . . . .	4-25
Inverter design considerations . . . . .	4-25
Power transistors . . . . .	4-29
Bipolar single . . . . .	4-31
Bipolar Darlington . . . . .	4-35
Advanced motor converter . . . . .	4-36
Advanced motor control logic . . . . .	4-39
Start mode . . . . .	4-39
Drive mode . . . . .	4-40
Transition mode . . . . .	4-40
Brake mode . . . . .	4-41
Logic circuits . . . . .	4-41
System interface . . . . .	4-42

## CONTENTS (Continued)

	<u>Page</u>
PROOF-OF-PRINCIPLE MODEL MOTOR DEVELOPMENT . . . . .	5-1
Stator assembly . . . . .	5-1
Rotor assembly . . . . .	5-10
Final assembly . . . . .	5-12
Preliminary magnetic circuit tests . . . . .	5-12
Low speed tests in generator mode . . . . .	5-17
Full speed and load tests in generator mode . . . . .	5-19
FUNCTIONAL MODEL MOTOR DEVELOPMENT . . . . .	6-1
Windage tests . . . . .	6-1
Magnetic circuit measurements . . . . .	6-8
Stator assembly . . . . .	6-15
Rotor assembly . . . . .	6-20
End bells . . . . .	6-20
Final assembly . . . . .	6-24
Rotating machine tests in generator mode . . . . .	6-28
FUNCTIONAL MODEL MOTOR TEST CONSIDERATIONS IN MOTOR MODE . . . . .	7-1
Functional model system analysis . . . . .	7-1
CONCLUSIONS . . . . .	8-1
REFERENCES . . . . .	9-1
APPENDIX A - LEAKAGE INDUCTANCE OF IRONLESS STATOR . . . . .	A-1
APPENDIX B - THERMAL ANALYSIS OF THE ADVANCED ELECTRIC VEHICLE . . . . .	B-1
APPENDIX C - ADVANCED ELECTRIC MOTOR STRESS ANALYSIS SUMMARY . . . . .	C-1
APPENDIX D - DESIGN COMPARISON: RARE-EARTH COBALT MAGNETS VERSUS STRONTIUM FERRITE . . . . .	D-1
APPENDIX E - KEY COMPONENT DRAWING LIST . . . . .	E-1
APPENDIX F - SHAFT POSITION SENSOR . . . . .	F-1

# ADVANCED SINGLE PERMANENT AXIPOLAR IRONLESS STATOR AC MOTOR FOR ELECTRIC PASSENGER VEHICLES

E.D. Beauchamp, J. R. Harfield, K. L. Wuertz  
AiResearch Manufacturing Company

## SUMMARY

The purposes of the program were to further develop electric motor technology as it applies to electric passenger vehicles for urban driving service, and to apply this technology toward a potentially attractive "advanced" motor design concept. Furthermore, the goal was to fabricate and test hardware to determine its feasibility for ultimate use in a 1350-kg production electric vehicle. An "advanced" motor in this context implied a motor that did not exist in a form suitable for electric vehicle applications. A prime consideration in determining concept feasibility was a reduction in life-cycle costs, i.e., low manufacturing costs and low maintenance costs, while achieving low weight and high efficiency.

### Program Accomplishments and Limitations

Program highlights.--During the program, an extensive preliminary design phase resulted in the motor concept and predicted performance. The motor is a brushless, rare-earth cobalt permanent magnet, axial air gap, ironless stator, air-cooled design. A proof-of-principle model was fabricated and tested to evaluate the feasibility of the concept. A functional model was fabricated and tested, incorporating improvements based on proof-of-principle model test results. Program goals were not met in that an electronic controller was not built, therefore, no testing was conducted with the rotating machine operating as a motor. However, extensive and significant testing was done with the machine operating in the generator mode. Also, Phase II was not exercised. The Phase II goal was to have fabricated and tested an engineering model, and conducted a preliminary design and performance prediction for the production model.

Significant program results are listed below:

- (1) Validity of basic magnetic flux linkage predication of design program was established.
- (2) Inherent voltage regulation of machine was confirmed.
- (3) An ironless stator was successfully constructed, demonstrating capability of continuous operation at peak current, and establishing the thermal time constant.
- (4) Windage losses were reduced from 5000 W in the proof-of-principle model to 2000 W in the functional model. This reduction resulted in a 10 percent increase in efficiency at full speed/full load.

- (5) Full generator level testing was conducted on the functional model; recording electromagnetic, thermal, aerodynamic, and acoustic noise data.
- (6) A complete engineering drawing package was made, reflecting the new design features in stator construction and support.
- (7) 20.3 kW output with the functional model operating as a generator at 1466 rad/s (14000 rpm), 150 A dc was demonstrated.
- (8) Projected system performance based on functional model machine parameters and a transistor inverter of 23.6 kW output power at 1466 rad/s and 83.3 percent efficiency.
- (9) Rotating machine weight is 23.52 kg with a rotor weight of 13.0 kg and a rotor moment of inertia of  $0.0615 \text{ N}\cdot\text{m}\cdot\text{s}^2$ .

System limitations.--The following factors should be considered when evaluating this concept:

- (1) A windage loss of 2000 W reduces maximum system efficiency to 85 percent.
- (2) Rotor inertia results in an unloaded motor rotor acceleration time from 0 to 100 percent speed at full rated torque of 5.6 s.
- (3) Mechanical considerations resulted in an air gap increase of 0.40 mm and approximately an 11 percent reduction of flux, voltage, and power capability.
- (4) Effective commutating reactance was 50 percent higher than calculated, further reducing the output power if operated with a thyristor bridge inverter.
- (5) The stator winding needs cooling at high torque, low speed conditions. The volume of air supplied should be controlled as a function of stator temperature.
- (6) The rotor magnetic flux leakage (fringing) outside the housing may cause a problem in the external environment. Shielding may be required.

## INTRODUCTION

This program covers the design, development, and evaluation of the performance of an advanced electric motor for passenger vehicle propulsion. It was undertaken to support the Electric and Hybrid Vehicles Division of the Department of Energy and NASA Lewis Research Center in their efforts to reduce the dependency of the United States on petroleum in the transportation system.

The definition of the term "advanced motor" required development of a motor concept not in existence for vehicle propulsion and, utilizing materials, components, and design concepts based on a predictable growth in technology. The motor developed under this contract recognized the goals of low weight, low cost, and high efficiency with speed/torque control capability over the full performance range required by an electric passenger vehicle.

In order to accomplish the stated goals, the program was structured to be performed in two phases.

Phase I was funded while Phase II was held as a follow-on option. This report covers all the activities undertaken in Phase I. The structure of Phase I consisted of seven tasks. The specific technical activities performed in each of the tasks are summarized below.

Task 1.--A design study was conducted that defined the motor and controller parameters for the proposed system. An analytical assessment of the motor/controller performance operating at the required vehicle duty cycles was performed and the basic machine was defined.

Task 2.--A proof-of-principle rotating machine was designed, built, and tested in the generator mode. An electronic controller design was made.

Task 3.--A formal program review documenting the work accomplished and progress made in Tasks 1 and 2 was accomplished.

Task 4.--A functional model rotating machine was designed. This machine incorporated features to improve the motor performance established with the proof-of-principle hardware.

Task 5.--The functional model rotating machine was fabricated and tested as a generator. Data were taken to establish the characteristics of the functional model machine and to establish whether the concept showed sufficient promise to justify further development. The proof-of-principle stator was scheduled to be used on the functional model but the stator suffered irreparable electrical damage. Further work on the electronic controller was de-emphasized until generator tests could confirm the overall rotating machine viability. An analytical evaluation of motor performance was completed with a modified existing controller.



Task 6.--This task provided for the assessment of an alternate magnet material applied to the motor design concept. Because of stator fabrication requirements, most of the funding intended for this task was transferred to Task 5. However, a preliminary computer design using the alternate low-cost ferrite magnet was performed by AiResearch and is included in this report.

Task 7.--A full review of all activities and a summary of the program results through Task 6 was given in an oral presentation with view-graphs to officials of NASA Lewis Research Center. This presentation is summarized in AiResearch Document No. 82-19202, TASK 7, PHASE I PROGRESS REVIEW DOCUMENT, dated July 30, 1982. This report covers the same areas in greater depth and represents the completion of Phase I activities, which fell short of motor mode testing.

The effort undertaken by AiResearch in this program was to develop a motor exhibiting potential advantages in the area of low initial and low life-cycle costs. The motor used advanced technology permanent magnet materials and power electronic devices and attempted to achieve this low cost with little if any penalty in system weight, efficiency, or performance capability. To achieve these goals the motor used only four basic parts in its rotating structure and only strip copper wire in its stator assembly. The unit was configured to pump its own cooling air and to utilize a housing/end bell structure of three parts. All parts of the motor showed excellent promise of being well-suited to economical mass production. The electronic controller to be used with the motor was designed to operate at the highest input voltage option (240 Vdc) to reduce the size of the power semiconductors as well as cables and terminals. The controller concept is a three-phase inverter using power transistors in each leg of the bridge. This provided for operation of the motor at nearly unity power factor to minimize motor size for the required output power.

The potential of this advanced motor concept was such that it merited a full analytical and test evaluation. This program accomplished that assessment.

#### ACKNOWLEDGEMENTS

AiResearch Manufacturing Company wishes to thank the following employees who were instrumental in the development of this unique concept in motor design:

Fred McCarty was responsible for the electromagnetic design of the machine. He developed the leakage inductance calculation procedure presented in Appendix A and the alternate magnet design comparison in Appendix D.

Jack Jones conducted the preliminary thermal analysis in Appendix B, and Yong Kim contributed to the thermal design of the functional model.

Roger Boisjoly conducted the stress analysis presented in Appendix C.

Rudy Schneegas created the mechanical design of the rotating machine, with some of the key drawings contained in Appendix E.

Bill Beck, Everett Geis, and Sid Gorla were significant contributors to the preliminary electronic concept and design, with some of the key schematics presented in Appendix F.

Ed Beauchamp and Pete Walia conducted the electronic analyses for the functional model.

John Dancy and Jeff Hadfield were the development engineers for the proof-of-principle and functional models, respectively.

Frank Echolds and Ken Wuertz were the program managers for the proof-of-principle and functional models, respectively.

The project manager from NASA Lewis was B. R. Hatvani.

## CONCEPT AND DESIGN ANALYSIS

### Rotating Machine

Approach.--The motor is a brushless, dc, rare-earth cobalt, permanent magnet, axial air gap inductor machine, using an ironless stator. Air cooling is inherently provided by the centrifugal-fan action of the rotor poles. This unique new motor concept is based on the Lorentz-Induction concept, but overcomes the disadvantages resulting from high interpolar leakage flux and nonreversing flux linkage that cause a high stator leakage reactance in typical inductor machines.

Status and history of concept.--The ironless stator concept is well-known but has generally been unacceptable for small electromagnetically excited machines since the required exciting magnetomotive force (mmf) results in an intolerable field loss. However, due to scaling laws, a practical design can sometimes be achieved in large machines for certain applications. In 1965, The Garrett Corporation developed a 500-kVA, 2-pole, 60-Hz axial gap machine with an ironless stator and electromagnetic excitation.

In permanent magnet machines, ironless stators have been more widely applied, particularly in the case of the printed-circuit dc motor where the commutator and stator windings are combined to achieve significant cost savings. Such motors have been confined to small ratings, because the scaling laws for permanent magnet machines are different than for field-excited machines. This gives magnets an inherent advantage at small scale. For example, the mmf of a magnet scales linearly with scale factor, but its flux scales as the square. However, both the mmf and flux of an electromagnetic coil increase with the square of the scale factor.

When actual designs are considered, it is found that field-excited machines are at a great disadvantage at small scale so far as complexity, size, and efficiency are concerned. But as size increases, there is a crossover point where the machines are roughly equivalent in size, and beyond that the field-excited machine has an advantage. The advent of very high energy magnets has dramatically raised the point of equivalence and has made it possible to consider entirely new design concepts.

As far as the inductor alternator principle is concerned, it is a classic concept generally limited to applications where a low-cost, high-frequency, high-impedance machine is desired as in induction heating systems. Because of its elegant simplicity, it has great appeal and is frequently misapplied when its deficiencies are not well understood. Fundamentally, the inductor machine is at a disadvantage because utilization of the stator iron and copper is less than 50 percent when compared to flux-reversing machines. Furthermore, the fact that half the coils of the machine are inactive at any given instant means that such machines will have about twice the stator impedance that could be obtained in a flux-reversing machine operating at the same electric loading and air gap flux density.

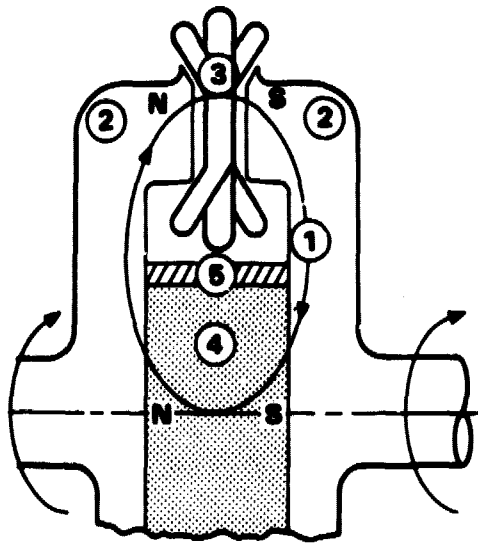
Fortunately, the use of an ironless stator in conjunction with a high energy magnet makes it possible to realize the simplicity of the inductor concept and to obtain acceptable size and performance. This is possible because the ironless stator has a low leakage reactance and the amount of copper required is reasonable (and hence the losses incurred) because relatively small coils are required to embrace the high density pole flux. The axipolar concept is very flexible in allowing magnet weight to be traded for stator loss because air gap flux density is not limited by stator-tooth saturation. It is limited only by pole iron saturation.

Design concept.--Fig. 1 shows a conceptual cross section of the axipolar machine. Magnetic flux from the cylinder magnet is collected and focused by the iron rotor poles. The flux always travels in the same direction across the air gap (left to right in this case). The ironless stator coils all lie in the same plane in the air gap. A high-strength hoop mechanically contains the magnet under all speed and temperature conditions.

A magnetic flux comparison of the axipolar machine with a conventional machine is appropriate at this time. In a conventional machine, a given stator coil sees a flux distribution that completely reverses in direction from some positive, maximum value to the same negative value. Peak flux in the gap corresponds to about 0.70 T. This is shown in fig. 2(a). In the axipolar machine, fig. 2(b), the flux in a given coil is always in the same direction. It varies from some peak value when the coil is in line with the rotor poles to some minimum value when the coil is between the poles. This minimum value of flux is due to flux lines crossing the air path between consecutive rotor poles, and linking the coils in this area.

The difference in magnetic flux distribution of the two machines results in a different way of achieving net torque. Fig. 3 defines the direction of force on a current-carrying conductor in a magnetic field. In a conventional machine, stator coils are arranged such that when the flux field reverses, the direction of current also reverses. Therefore, the force and torque are in the same direction. In the axipolar machine, fig. 4, the flux does not reverse, but the current does. A relatively large positive force results when the conductors are under the poles and a relatively small force in a negative direction results when the conductors are between the poles. This negative component of force and torque is a characteristic of all inductor-type machines.

However, the use of an ironless stator minimizes the negative effect and results in a machine with many desirable characteristics. The permanent magnet can be precisely matched magnetically to the stator so that an economical balance of magnet material versus losses and other materials can be achieved regardless of the type of magnet material or number of poles. Thus, even a low-cost, low-energy product magnet material may be operated at its optimum flux density so that its maximum field energy is obtained. The flux-focusing iron poles result in a much higher magnetic field flux density (approximately 1.09 T) so that relatively small stator coils are required to link the required pole flux. This results in much lower copper loss and stator impedance than if the coils were operating at the magnet flux density.



- ① UNIDIRECTIONAL MAGNETIC FLUX
- ② ROTOR POLES
- ③ IRONLESS STATOR COILS
- ④ MAGNET
- ⑤ NON-MAGNETIC HOOP

A31841

Figure 1.--Axipolar Machine Principles.

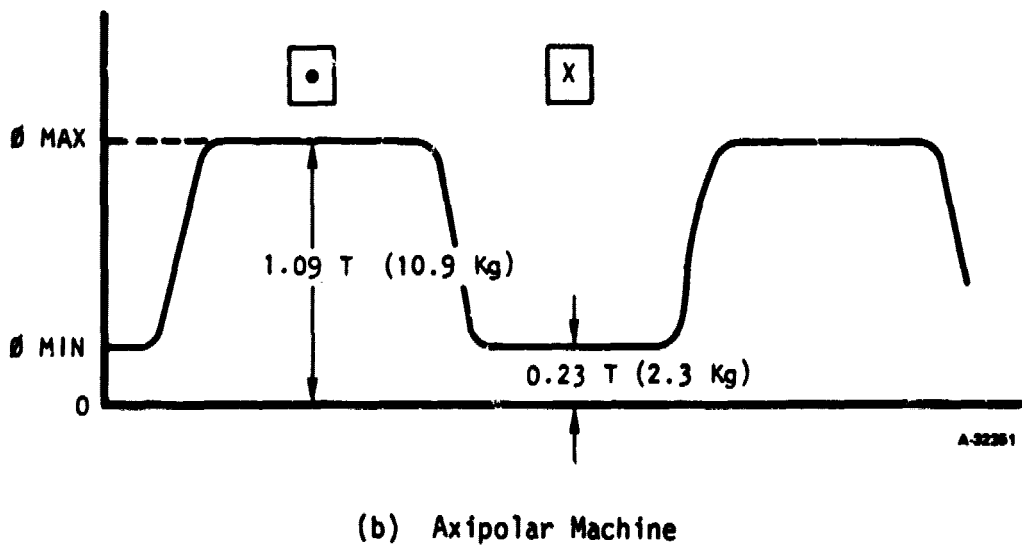
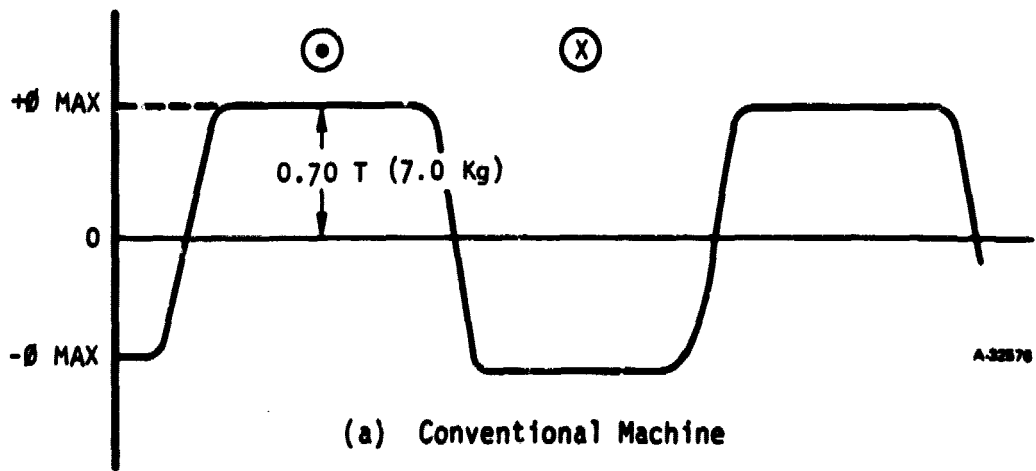


Figure 2.--Magnetic Flux Comparison.

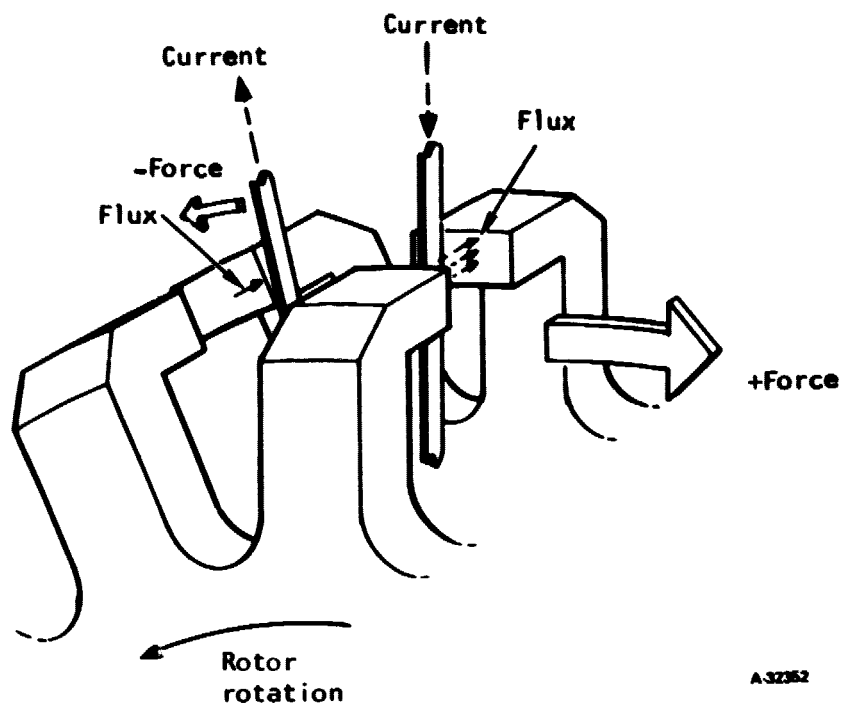


Figure 3.--Direction of Magnetic Force.

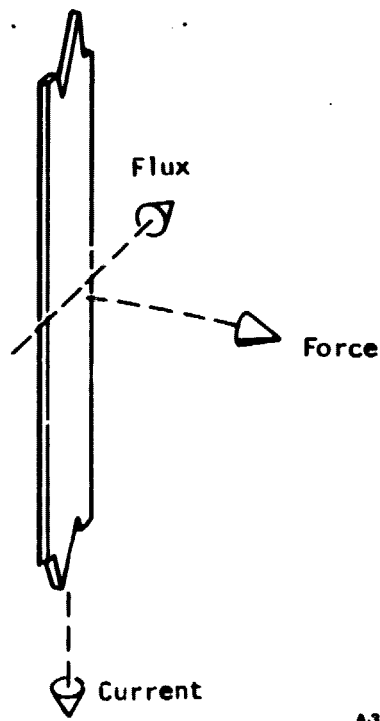


Figure 4.--Axipolar Machine Principles.

Structurally, this rotor design provides a simple, high-strength construction that can operate at high speeds to reduce overall machine size and weight. The magnet rotates at a relatively low tip speed when compared to the rotor poles. This is important, because magnet stress is proportional to the tip speed squared. The magnet is totally supported in compression by a shrink ring so that the rotor's structural integrity is unaffected by poor mechanical properties that are characteristic of rare-earth cobalt, as well as most other magnet materials.

An aluminum shroud covers each of the rotor sections to direct the rotor-induced airflow over the stationary stator coils. The shroud also reduces the overall rotor windage loss.

The ironless stator assembly is a three-phase winding using machine-wound coils with strip copper conductors that are ML-coated for insulation. The strip copper coils result in a "laminated" effect that minimizes eddy current losses in the conductors. All coils are identical except that two-thirds of the coils are formed to permit all "active" surfaces of the coils to lie in the same plane. This is necessary in order to achieve a minimum stator axial thickness. Magnet weight is directly proportional to stator thickness, so a thin stator is required to minimize magnet cost and weight. There are many advantages to this type of stator assembly.

The stator does not contain iron so the iron losses are eliminated. This is particularly important in a high-speed permanent magnet machine because the iron losses increase exponentially with speed, causing efficiency to be low at low-load conditions. Although iron loss can be reduced at low load by schemes that shunt the magnet flux away from the stator, such schemes add to cost and also reduce reliability.

There is one potentially negative aspect of using an ironless stator: it is possible to have substantial eddy current losses in the conductors in addition to the  $I^2R$  loss. The conductors are operating directly in the main field, whereas in conventional machines the conductors perceive only their own leakage field, the main field being diverted by the stator teeth. It is believed that the proposed ribbon construction of the stator coils will make it possible to achieve a conductor configuration in which the eddy loss is minimal. For that reason and because experimental data were not available for coils of this precise configuration, eddy loss has not been included in the estimated performance data.

Due to the absence of stator iron, the disadvantages that are typical of inductor machines are dramatically reduced. The interpolar leakage flux that generates a negative torque component opposing the torque of the main flux is minimized. The low leakage flux, in conjunction with the high flux density in the gap, results in a flux swing with undulation comparable to that obtained in conventional flux-reversing synchronous machines. Further, the elimination of stator teeth substantially reduces the stator leakage reactance. The demagnetizing effect of the stator load current is reduced due to the large reluctances of the stator gap and the magnet.

Ribbon conductors provide superior heat transfer as compared to round wire, mush-wound coils or substrate-mounted printed-circuit conductors. Virtually all



coil surfaces are directly exposed to cooling air (or cooling fluid, if desired), permitting operation at high current densities to reduce the amount of copper required. This reduces the air gap dimension and amount of magnet material required. Ribbon conductors also provide the most efficient utilization of the space between the poles. In the baseline design, the fill factor is 0.61. This compares with 0.15 typically attained in mush-wound coils supported in iron teeth (the teeth occupy about half the available space).

In addition, the possibility of ground faults is virtually nil since the coils are not imbedded in slots in iron. Phase-to-phase faults are very unlikely since conductors of various phases are preformed and not intertwined.

Optimizing the design.--A computer math model of the axipolar machine was created in order to study the effects of certain important design parameters. Losses, magnet weight, total weight, magnet tip speed, and rotor tip speed are tabulated for 26 kW, 0.9 power factor machines in table 1. In this study, speed, poles, current density, and electric loading (ampere-conductors per unit of stator inner periphery) were varied. The study was used to determine a rough size for the machine and indicate significant trends.

Optimization of the design required additional activities:

- (1) Achievable bend radii for the stator coils were determined.
- (2) A method of calculating the winding leakage inductance in ironless stator machines was derived. This method is given in appendix A.
- (3) Electronic converter performance characteristics, limitations, and power dissipation were defined.
- (4) An existing driving cycle performance program was incorporated into the machine design program.
- (5) An estimated cost of materials was included to evaluate the machine on a dollar basis.

Incorporation of all of these system characteristics into a single program allowed the evaluation of many design parameters to determine the most economical system design. For instance, the design study in table 1 assumed a pole face flux density of 1.09 T. This is not necessarily the best design because magnet weight is directly proportional to pole face density, while copper and pole weight, tip speed, and losses are inverse functions of pole face flux density. Also, although the magnet material has the highest cost per pound of the materials used in the machine, the economically optimum design is probably not the one with the lowest magnet weight, since low magnet weight is attained at the expense of greater copper loss, greater windage loss, or both.

Baseline design.--Exercise and evaluation of the system computer program resulted in the selection of a 16-pole motor with a rated speed of 1466 rad/s and a rated power of 26.73 kW. Table 2 summarizes all machine parameters except for the magnetic circuit data, which are presented in fig. 5, and the converter model,

TABLE 1.--AXIPOLAR MOTOR STUDY.

(Magnet = 15 MGO Mischmetal) Assumed pole face flux density = 1.09 Tesla

Speed, rad/s	Poles pairs	Current density, A/m <sup>2</sup> x 10 <sup>-6</sup>	Electric load, A-cond/m x 10 <sup>-3</sup>	I <sup>2</sup> R loss, kW	Windage loss, kW	Total loss, kW	Rotor tip speed, m/s	Magnet tip speed, m/s	Magnet weight, kg	Total weight, kg	
1466 (14k rpm)	10	18.6	39.4	1.17	0.404	1.570	160	105	1.93	17.91	
			31.5	1.019	0.611	1.630	170	113	1.85	20.45	
			47.2	-	-	-	-	-	-	-	-
		23.3	39.4	-	-	-	-	-	-	-	
	8	18.6	31.5	1.23	0.593	1.823	170	113	1.65	19.77	
			47.2	1.58	0.271	1.851	151	100	1.76	15.36	
			39.4	1.38	0.44	1.820	163	105	1.94	18.41	
			31.5	1.21	0.665	1.875	172	112	1.89	20.93	
		23.3	47.2	1.55	0.326	1.876	155	100	2.02	16.99	
			39.4	1.66	0.409	2.069	161	105	1.73	17.41	
			31.5	1.47	0.633	2.103	171	112	1.68	20.05	
			47.2	-	-	-	-	-	-	-	-
12	18.6	39.4	-	-	-	-	-	-	-	-	
		31.5	0.904	0.581	1.485	169	113	1.85	20.18		
	23.3	47.2	-	-	-	-	-	-	-	-	
		39.4	1.25	0.361	1.610	156	105	1.70	16.77		
1676 (16k rpm)	10	18.6	31.5	1.09	0.558	1.648	168	111	1.65	19.45	
			47.2	1.43	0.263	1.693	151	100	1.79	15.23	
			39.4	1.25	0.361	1.610	156	105	1.70	16.77	
		23.3	39.4	1.25	0.361	1.610	156	105	1.70	16.77	
	8	18.6	31.5	1.09	0.558	1.648	168	111	1.65	19.45	
			47.2	1.43	0.263	1.693	151	100	1.79	15.23	
			39.4	1.25	0.361	1.610	156	105	1.70	16.77	
			31.5	1.09	0.558	1.648	168	111	1.65	19.45	
		23.3	47.2	1.43	0.263	1.693	151	100	1.79	15.23	
			39.4	1.25	0.361	1.610	156	105	1.70	16.77	
			31.5	1.09	0.558	1.648	168	111	1.65	19.45	
			47.2	1.43	0.263	1.693	151	100	1.79	15.23	
1676 (16k rpm)	10	18.6	39.4	1.08	0.674	1.754	176	115	1.75	15.91	
			31.5	0.94	1.000	1.948	186	123	1.68	18.09	
			47.2	1.24	0.501	1.740	169	109	1.84	14.68	
		23.3	39.4	1.31	0.612	1.922	173	115	1.54	14.94	
	8	18.6	31.5	-	-	-	-	-	-	-	-
			47.2	1.47	0.453	1.920	166	109	1.60	13.64	
			39.4	-	-	-	-	-	-	-	-
			31.5	1.11	1.103	2.200	189	123	1.71	18.55	
		23.3	47.2	-	-	-	-	-	-	-	-
			39.4	1.54	0.672	2.210	176	115	1.56	15.41	
			31.5	1.35	1.042	2.392	187	123	1.53	17.73	
			47.2	1.72	0.487	2.207	168	109	1.61	14.00	
12	18.6	39.4	0.975	0.635	1.610	174	115	1.77	15.64		
		31.5	-	-	-	-	-	-	-	-	
	23.3	47.2	1.14	0.476	1.616	167	109	1.87	14.86		
		39.4	1.16	0.598	1.758	173	115	1.55	14.86		
12	18.6	31.5	1.01	0.909	1.919	183	123	1.50	17.14		
		47.2	1.32	0.440	1.760	166	109	1.62	18.05		
		39.4	1.16	0.598	1.758	173	115	1.55	14.86		
	23.3	39.4	1.16	0.598	1.758	173	115	1.55	14.86		

shown in fig. 6. In addition, full thermal and stress analyses were conducted on the baseline machine. These results are given in appendix B and appendix C, respectively.

TABLE 2.--AXIPOLAR MACHINE DESIGN DATA.

Nominal motor rating:	81.0 V <sub>l-n</sub> (air gap voltage), -0.993 power factor, 110 A fundamental ac rms current, three-phase, 26.73 kVA, 1466 rad/s, 1774 rad/s overspeed, 16 poles, 1867 Hz
Magnet:	151.3-mm o.d., 11.4-mm thick, rare-earth cobalt, 15.0 MGO at 210C, 13.9 MGO at 930C
Stator:	3.5-mm thick, 255.4-mm o.d., 170.1-mm i.d., 48 coils total, three-phase, 8 circuits, 16 poles, 20 turns/coil of 0.22-mm thick, 3.37-mm wide annealed, bare copper ribbon with 0.05-mm silicone/kapton/silicone interleaf, fill factor = 0.608, electric loading = 36,400 A-cond/m, current density = $4.724 \times 10^7$ A/m <sup>2</sup>
Rotor:	230.6-mm o.d. (excluding flared face), 456 mm <sup>2</sup> of iron section per pole, 8 poles per rotor section, 25.7-mm axial thickness at pole root, material = 4340 steel, R <sub>c</sub> = 36-40
Electromagnetic weights:	Rotor iron = 8.632 kg Magnet = 1.672 kg Copper = <u>.889 kg</u> 11.193 kg
Dimensional data:	Total air gap between mating poles = 5.15 mm Mechanical clearance, pole surface to stator surface = 0.828 mm Mean pole pitch = 41.78 mm Tie bolt clearance hole in magnet = 9.65-mm diam Magnet hoop = 8.37-mm thick 8.274 Pa shrink fit, Inconel 718
Parameters:	Pitch and distribution factor = 0.9225 Pole embrace = 0.6 per unit Copper temperature factor = 1.5 (1490C) Form factor, main poles = 1.027 interpoles = 1.270 Pole factor C <sub>p</sub> = 0.647

Table 2.--Axipolar Machine Design Data--Continued.

Parameters (cont.):	Stator phase resistance, hot	= 0.02464 ohms
		= 0.0335 per unit
	XAD	= 1.44 per unit
	XAQ	= 0.149 per unit
	XL	= 0.150 per unit
	Leakage inductance	= 9.43 mH
	Base $\Omega$	= 0.73636 ohms
Loss summary:	Stator copper loss	= 0.8946 kW
	Stator eddy loss	= 0.1621 kW
	Stator stray loss	= 0.0709 kW
	Pole face loss	= 0.0375 kW
	Windage loss	= 0.717 kW
	Bearing loss	= <u>0.0302 kW</u>
	Total motor loss	= 1.912 kW
	Inverter loss	= <u>1.366 kW</u>
	Total Loss	3.278 kW
Efficiency:	Motor	= 0.9309
	Motor and inverter	= 0.887

$$R_{BASE} = V_{RATED}/I_{RATED} = 81/110 = 0.73636 \Omega$$

$$R_{PU} = R/R_{BASE} = 0.02464/0.73636 = 0.0335 \text{ per unit}$$

ORIGINAL PAGE IS  
OF POOR QUALITY

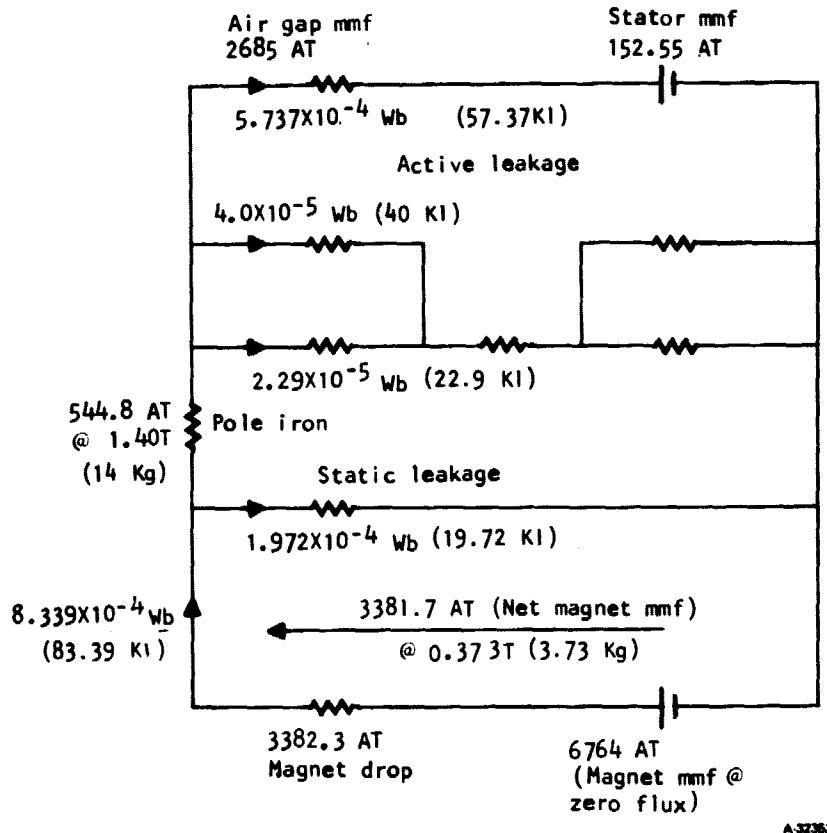


Figure 5.--Magnetic Circuit Data per Pole Pair.

NOTE: Static leakage is the flux that leaks across the gap but does not link any coils.

Active leakage is the flux that links stator coils between poles and creates a negative torque component.

Stator mmf is the demagnetizing component of armature reaction due to current flowing in the stator coils.

ORIGINAL PAGE IS  
OF POOR QUALITY

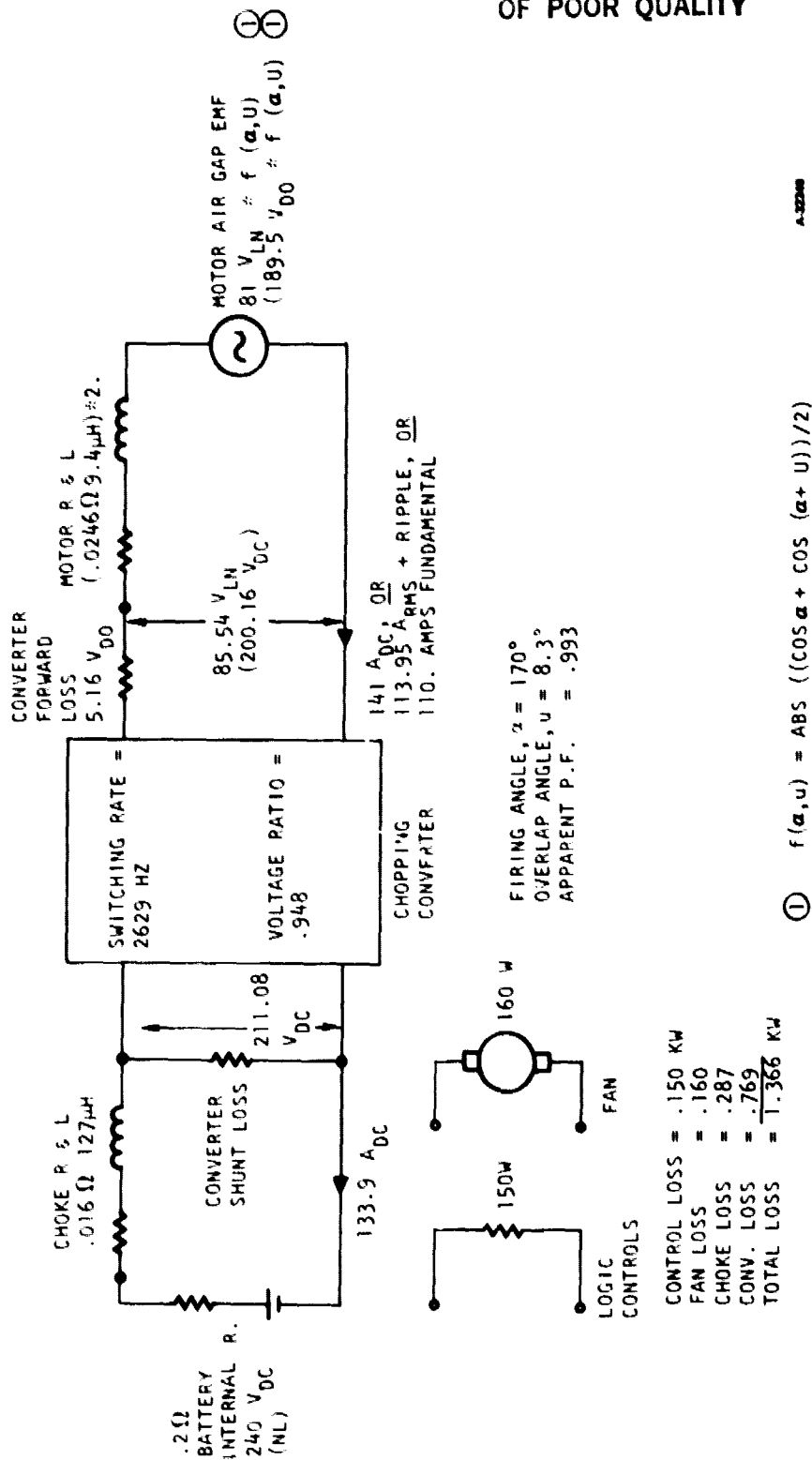


Figure 6.--Predicted Converter Performance at Rated Load.

Performance of the system was analyzed over the SAE J227(a) Schedule D driving cycle with an AiResearch-developed computer program. This program predicts performance, losses, and energy consumption over any given driving cycle in 0.1 s increments. It includes the effects of the rolling resistance, gear losses, aerodynamic drag, cooling system losses, vehicle mass, and event times. It can be used with either mechanical or dynamic braking of the vehicle. Transmission gear ratios and shift point are also considered. The program then plots a curve of vehicle speed, motor speed, motor torque, and various other power and energy curves. The vehicle characteristics assumed for this analysis are given below:

Vehicle curb weight, including passengers	= 1350 kg (3000 lb)
Vehicle frontal area	= 1.86 m <sup>2</sup> (20 ft <sup>2</sup> )
Aerodynamic drag coefficient, C <sub>D</sub>	= 0.3
Tire rolling resistance coefficient, R <sub>R</sub>	= 0.008 N/N (lb/lb)
Rolling radius of tires	= 0.29 m (11.5 in.)

In addition, a two-speed transmission is assumed with automatic gear shifting occurring at 56.6 km/hr (35 mph). Gear ratios are 27.37:1 and 15.996:1, resulting in the motor operating at 100 percent speed (1466 rad/s) at vehicle speeds of 56.6 km/hr (35 mph) and 97.1 km/hr (60 mph). Mechanical braking of 135.5 N·m (100 ft-lb) of wheel torque is applied during regenerative braking to stop within the required time.

The resulting baseline motor and vehicle performance over the J227(a) D driving cycle is shown in fig. 7. Fig. 8 is an example of the various motor curves used by the program in determining vehicle performance. Each variable is plotted as a function of motor speed, with motor current as a third parameter, and for both brake and drive modes.

Alternate magnet design.--A design option that was not chosen for this program was the use of an alternate, lower-cost magnet material than the rare-earth cobalt. However, a preliminary design for the rotating machine was conducted using a strontium-ferrite magnet approach. A discussion and summary of this approach is presented in appendix D.

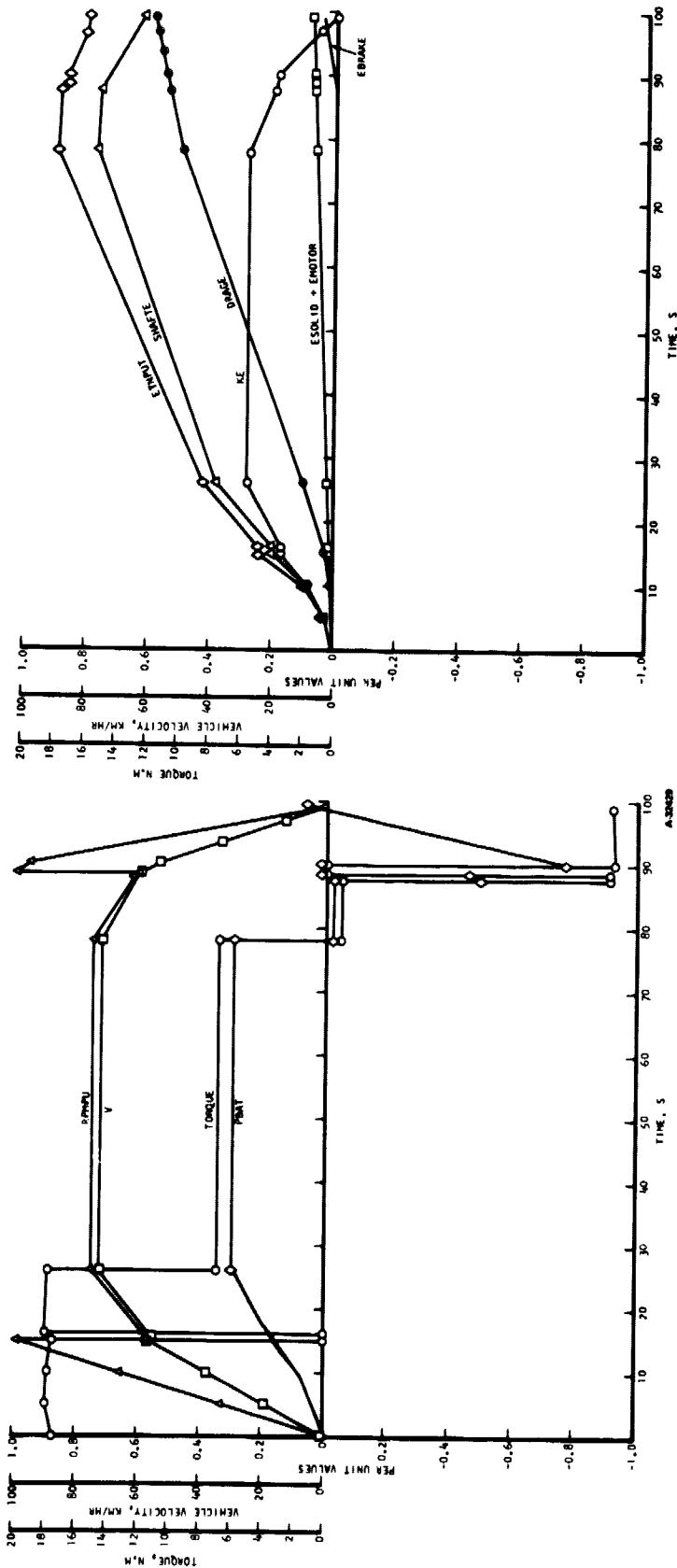


Figure 7.--Vehicle and Motor Performance versus Time.

NOTE:

- V = Vehicle speed, km/hr
- RPMPU = Motor speed per unit, 1 pu = 1466 rad/s.
- EINPUT = Energy delivered at the battery terminals per unit, 1 pu = 1000 kW.s.
- SHAFT = Energy at the motor shaft per unit
- DRAGE = Total vehicle drag energy (aerodynamic, rolling resistance, gear loss) per unit

- KE = Vehicle kinetic energy (1/2 Mv<sup>2</sup>) per unit. Kinetic energy due to wheels, drive train, and motor is ignored.
- ESOLID = Total energy loss due to solid state converter and its auxiliary devices (cooling fan, controls, and choke) per unit
- EBRANE = Energy loss due to mechanical braking per unit
- EMOTOR = Total energy loss due to motor (copper loss, eddy loss, stray loss, pole head loss, bearing loss and windage) per unit
- PBAT = Power at battery terminals per unit, 1 pu = 30 kW.
- TORQUE = Motor torque, N.m



ORIGINAL PAGE IS  
OF POOR QUALITY

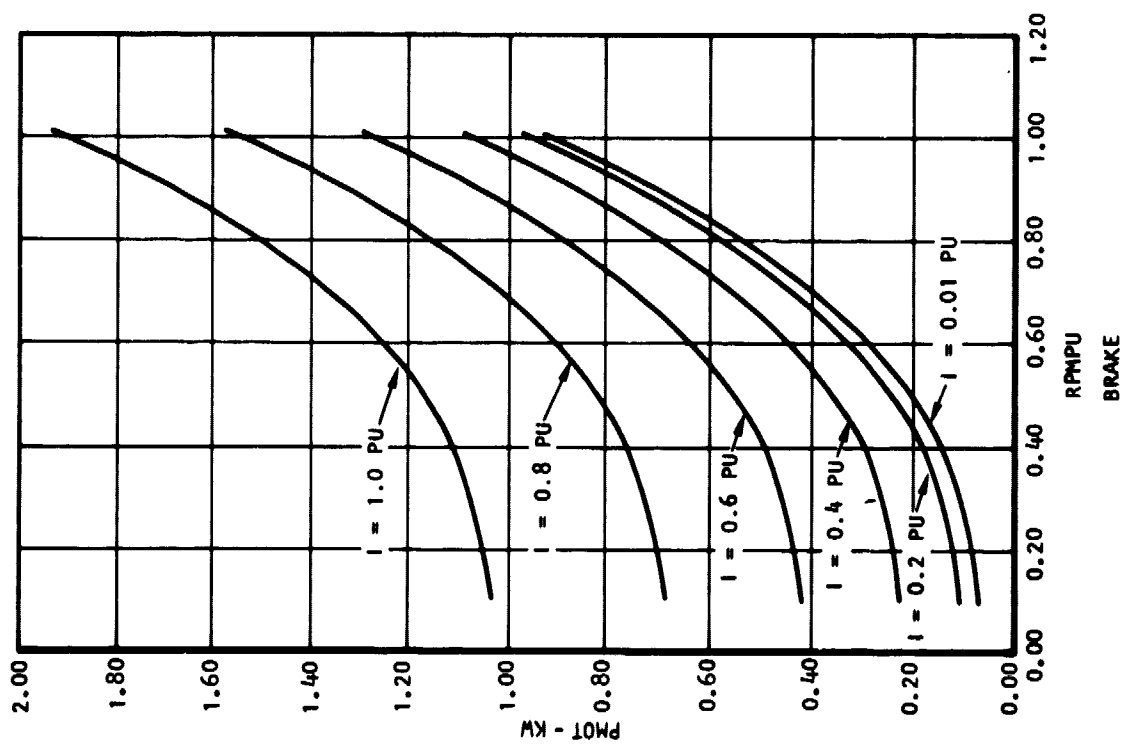
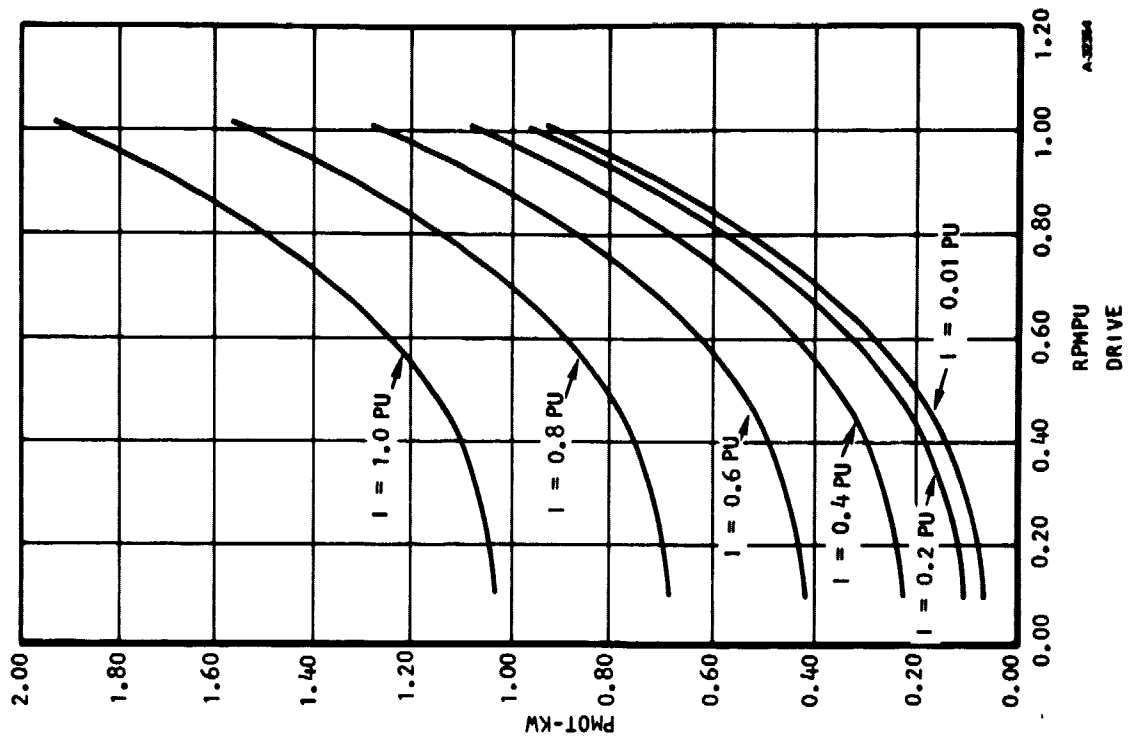


Figure 8.---Total Motor Loss versus Motor Speed.

## Power Converter

Basic considerations--The converter's function is to transform the vehicle primary electric dc power to the variable voltage and frequency power required by the permanent magnet (PM) motor drive assembly. Fig. 9 shows two methods for accomplishing this requirement: conventional and advanced.

The converter selected for the advanced motor program employs a method in which regulation is accomplished by pulse width modulation (PWM) within the inversion process. Thus, as shown in fig. 10, the inverter transistors, indicated as switches, are sequentially closed, then opened, to provide current in a precise and synchronized manner in relationship to the electromotive force (EMF) generated by the PM motor. Each transistor switch can conduct for up to 120 electrical deg; however, during the 120-deg interval, PWM (the turning on and off of the transistor switches) controls or regulates the current flow through the PM motor windings. Thus, in the advanced converter method, power is handled only once. This provides for fewer power and logic-level circuit components. The benefits of this approach are lower converter cost, smaller converter size and weight, and increased overall converter electrical efficiency in comparison with existing two-stage converter technology.

Interface with the PM motor can be achieved by either of two types of inverters: voltage or current source.

Voltage-source inverters have capacitor banks across their dc terminals that maintain a nearly constant dc voltage. Ripple current circulates through these capacitors and is generally the determining factor in bank size and rating. Typically, once capacitors have been selected to withstand the ripple current, the capacitance value is such that the voltage ripple is negligible. Very little of the dc current ripple flows through the source; most of it flows through the dc capacitors. The output waveform from a voltage-source inverter consists of a fundamental voltage and a spectrum of harmonic voltages. Interface of the voltage-source inverter with the PM motor requires some form of rotor position sensor to determine the relationship between the applied-inverter output voltage and the motor rotor position.

Current-source inverters use an inductor in series with one or both of their dc inputs. The inductor is usually sized so that the dc current ripple is small. The input voltage, therefore, has a ripple content reflected from the load current. All of the dc current ripple flows through the source; this ripple may be reduced by using a larger inductor or higher switching frequency. State-of-the-art power transistors can operate at frequencies high enough to allow the internal inductance of the PM motor to serve as the required inductance. Thus, no external or added inductors are required. The output waveform from the current-driven inverter consists of a fundamental current and a spectrum of harmonic currents. Interface of the current-source inverter with the PM motor requires some form of rotor position sensor to determine the relationship between the current delivered to the motor windings from the inverter and motor rotor position.



(a) Conventional method

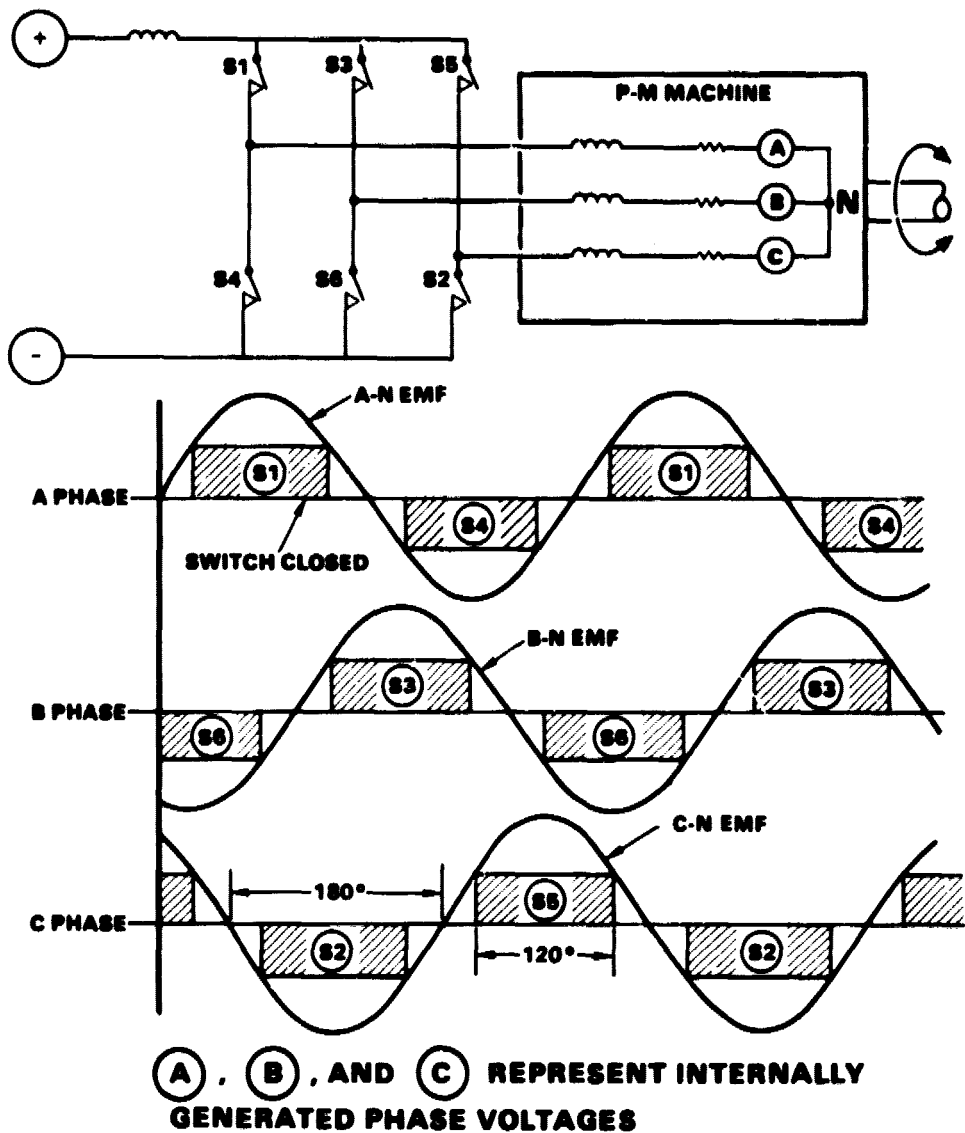


(b) Advanced method

A-32740

Figure 9.--Converter Configurations.

ORIGINAL PAGE IS  
OF POOR QUALITY



A-31621

Figure 10.--Basic Converter and Waveforms, Drive Mode.

For both the voltage- or current-source inverters, the power components are nearly identical. The primary differences are within the logic or control methodology. A brief description and discussion of the functional aspects of each type of converter-PM motor configuration follows.

**Voltage source inverter:** The voltage source inverter provides, at its terminals, a low-impedance voltage that can be supplied to a passive or active load. When the load is passive, as in the case of a resistor, the output current is a function of voltage, and control is relatively simple.

When the load is active, as in the case of a permanent magnet (PM) motor, the situation is different. The single-phase equivalent circuit for a voltage-source inverter is given in fig. 11. For such a system, the real power transfer is accomplished only by varying the phase angle of the voltage source with respect to the motor back-EMF. Current, however, can be increased between the source and motor by adjusting voltage. This circulates power between the load and source, and essentially only heats up the components, contributing nothing to the useful torque of the system.

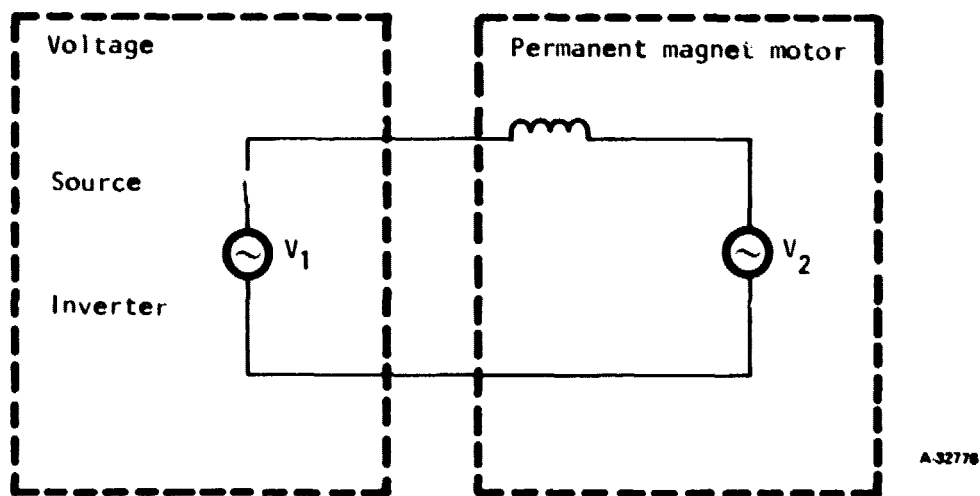


Fig. 11.--Equivalent Circuit, Voltage-source Inverter.

As a consequence, two sense mechanisms and two independent control systems are required to control motor current and torque.

Typically, the control electronics required for such a system are much slower to respond than those used for the corresponding current-source inverter, and are considerably more complex. For these reasons, the voltage-source inverter was not selected for the advanced motor converter.

**Current-source inverter:** The basic inverter schematic is given in fig. 10. In this diagram, the transistors are turned on by the gating logic as a function of rotor position in relation to the stator. Torque is controlled by means of the amplitude of the dc-link current, and regulated by the current source.

The simplest way to consider the operation of the inverter PM-motor is at zero speed in the drive mode. Assuming use of a three-phase, two-pole motor, by exciting two of the windings and taking into account the polarity of excitation, there are six possible vectors associated with the resultant fundamental magnetomotive force (MMF) of the stator (fig. 12). Maximum torque is achieved when the rotor flux and stator MMF are at right angles. With only six possible vectors for positioning the stator MMF, maximum torque cannot be maintained for all relative rotor/stator positions. However, by maintaining the stator MMF at an angle of  $90 \pm 30$  deg to that of the rotor flux, the torque pulsations due to rotor position can be minimized to approximately  $\pm 7$  percent.

To maintain torque as the rotor rotates past 60 electrical deg, a new set of windings is selected based on the rotor position and direction, and the MMF wave is clocked around, thereby maintaining the relative angles at between  $90 \pm 30$  deg.

The MMF can be rotated through the use of transistors or thyristors. The simplest system uses transistors as shown in fig. 13. The switching mechanism turns on the A+ C- transistors for 60 electrical deg, then B+ C-, B+ A-, C+ A-, C+ B-, A+ B-, and finally returns to A+ C- devices.

Complete operation of the inverter requires that it provide for the reactive or lagging current flow due to the inductance of the PM motor windings. For this reason, each transistor has an associated diode to allow for continued current flow. Fig. 14 shows a diode (C+) associated with a transistor (C+) and the resultant current paths through the motor windings during the A+ to C- conduction period.

As noted earlier, to minimize the number of devices used to control the clocking and, at the same time, control the amplitude of the dc link current, the current source and transistor gating scheme can be combined into a single unit.

The current through the motor is determined by the voltage applied across the reactance of the two windings (see fig. 12). Application of a fixed voltage across an inductor causes the current to increase at a rate determined by the ratio of the voltage to the inductance. To limit and regulate the amplitude of the current, one of the two transistors can be turned off when the current reaches its desired value. When this happens, the current in the inductor flows through its corresponding freewheeling diode and the other transistor. This is illustrated in fig. 15(a) in which transistors A+ and C- are both conducting. Fig. 15(b) shows the reactive current flowing through transistor A+ and freewheeling diode C+, when transistor C- is turned off. Fig 15(c) shows the load current timing relationship to the conduction and freewheeling currents.

By modulating the "on time" of one of the power devices with a simple hysteretic comparator/regulator, the current and torque can be controlled in the motor. Further, if only two devices are gated on at any one time, each device being turned on for 120 deg, modulation of current can be achieved by the transistor during its second 60 deg on-time. In this way, the additional heating due to the switching losses associated with the modulating transistor are equally distributed throughout the entire inverter bridge.

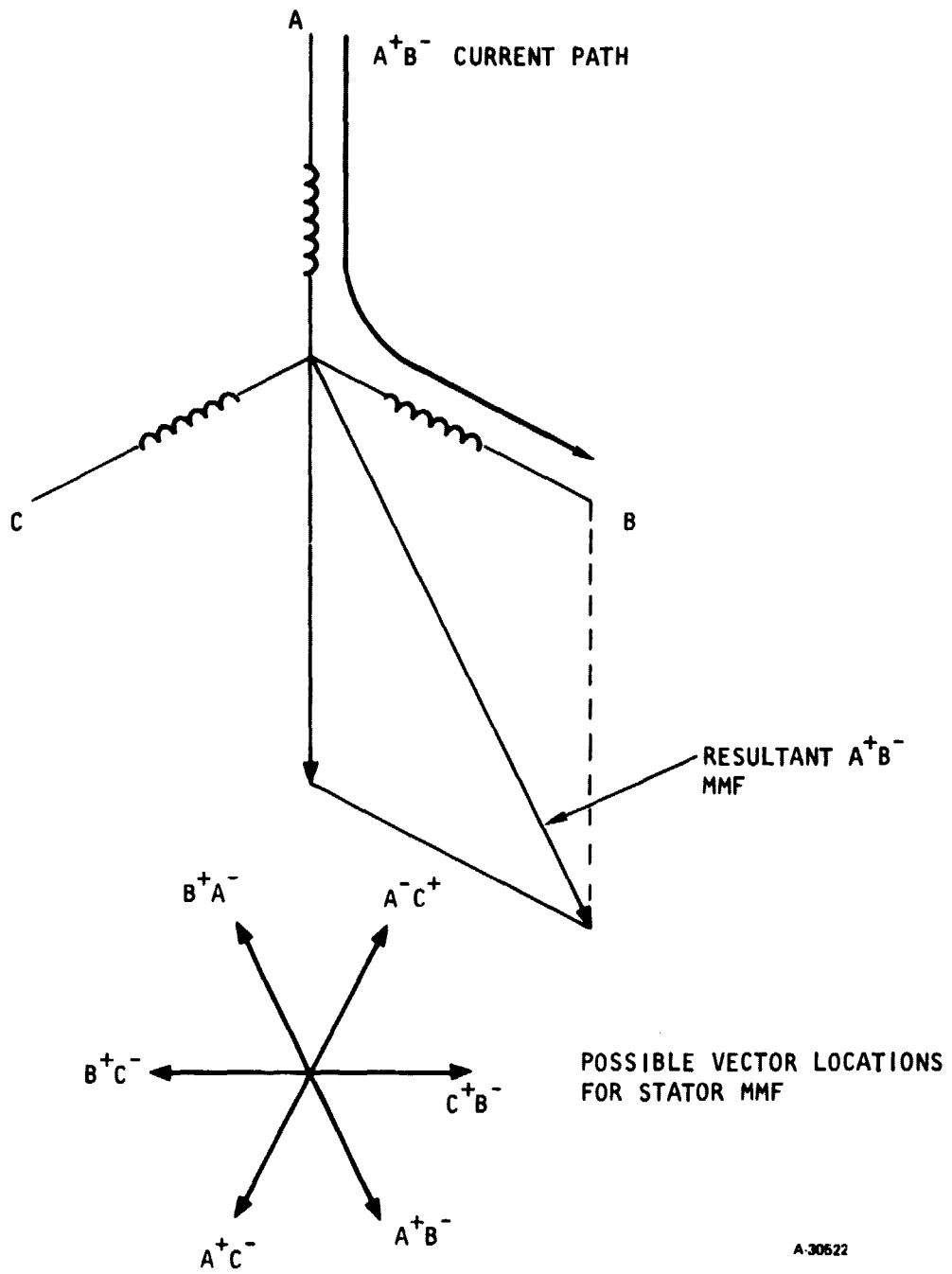
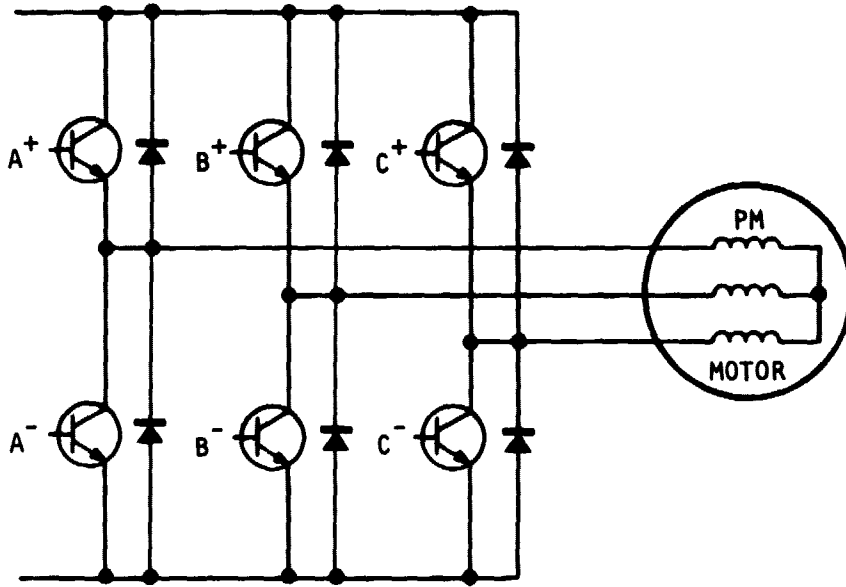


Figure 12.--Possible MMF Vectors for Stator Winding.

ORIGINAL PAGE IS  
OF POOR QUALITY

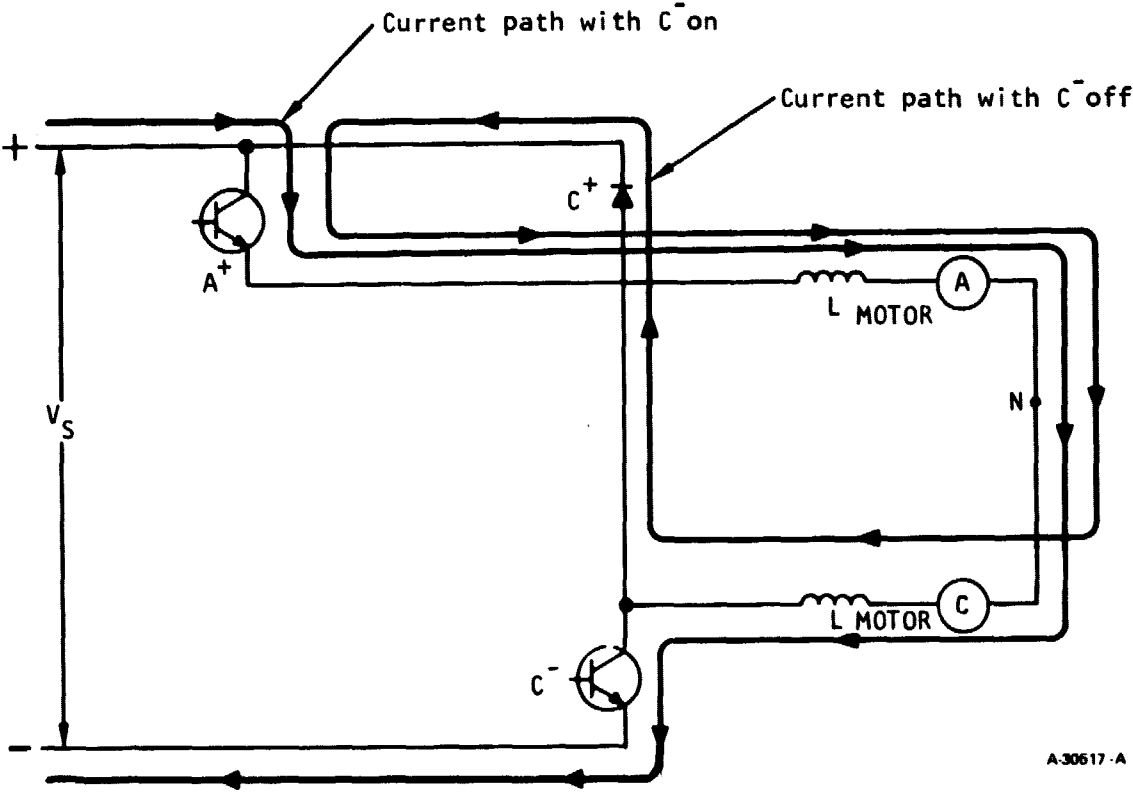


A-48996

Figure 13.--Simplified Inverter Schematic.

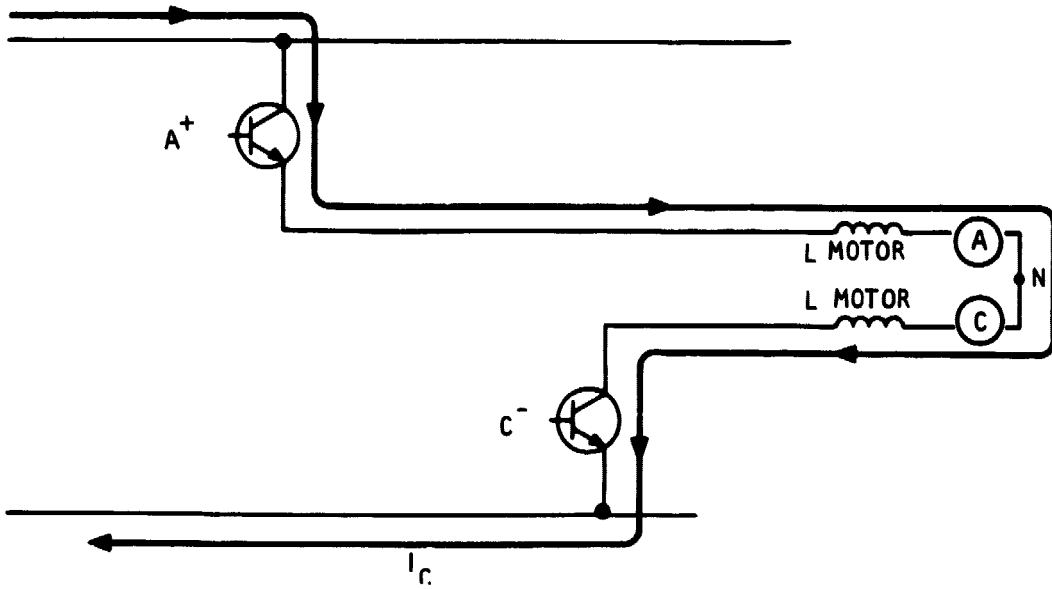


ORIGINAL PAGE IS  
OF POOR QUALITY

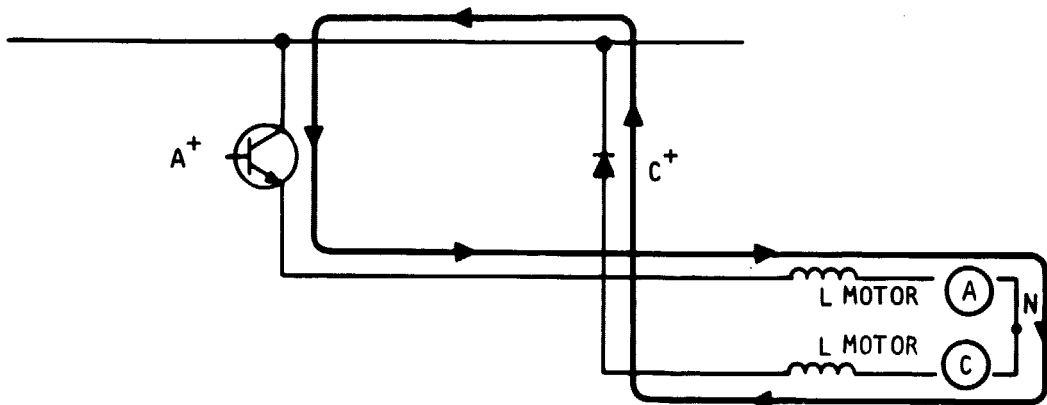


A-30617-A

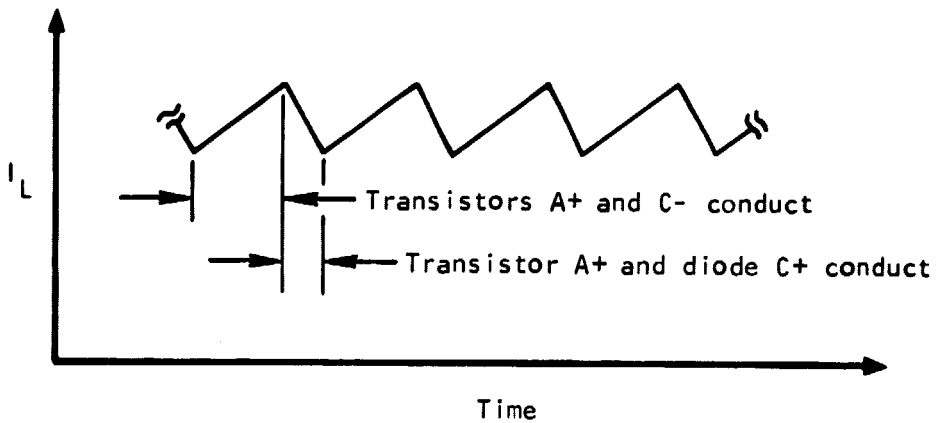
Figure 14.--Current Flow During 60 deg Rotor Rotation.



(a) Transistors A<sup>+</sup> and C<sup>-</sup> Conduct Current



(b) Transistor A<sup>+</sup> and Diode C<sup>+</sup> Conduct Current



(c) Current Waveform in PM Motor

Figure 15.--Current Control.

In the brake mode, it is necessary that the inverter is able to return power to the source, thereby providing an active brake.

One method of achieving this for the current-source inverter is shown in fig. 16. In the brake mode, only one of these lower transistors, A-, B-, or C-, is used to produce braking torque. In fig. 16 this is accomplished by turning on transistor B-, which essentially short-circuits all three of the motor windings through the freewheeling diodes, producing current and torque. When the current reaches its maximum or desired value, the transistor is turned off, and the current freewheels through diodes B+, A-, and C-. This energy is regenerated to the source. If the source is incapable of accepting the energy, a resistor (R) can be placed in parallel to dissipate the energy. The value of this resistor can be modulated by a series transistor (Q) to vary between infinite (transistor off) to the value of the resistor (transistor full on). In this way, a simple control loop can select the duty cycle on the transistor to dissipate exactly that amount of energy that is being regenerated.

Converter/PM motor interface.--Optimization of the converter/PM motor performance requires that the electrical characteristics of each are fully compatible. In establishing the converter design, PM-motor frequency and voltage range as well as specific machine resistances, were critical design factors. For the PM motor design, converter cyclic and subcyclic waveforms, as well as the maximum allowable machine reactances, are critical. The effect and interaction of these parameters have been well established through previously proven AiResearch designs and applications.

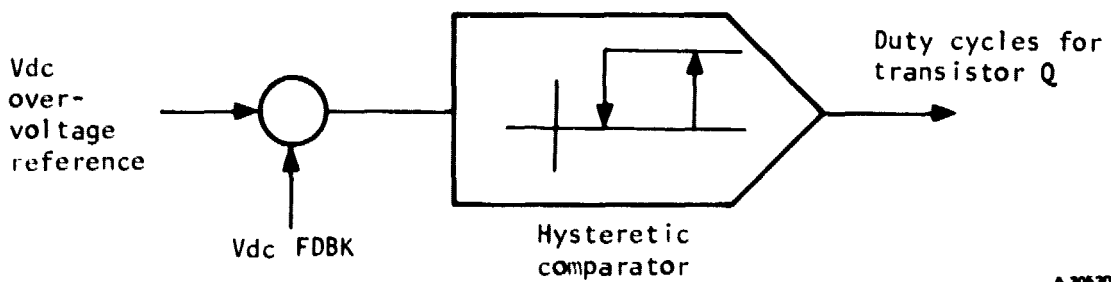
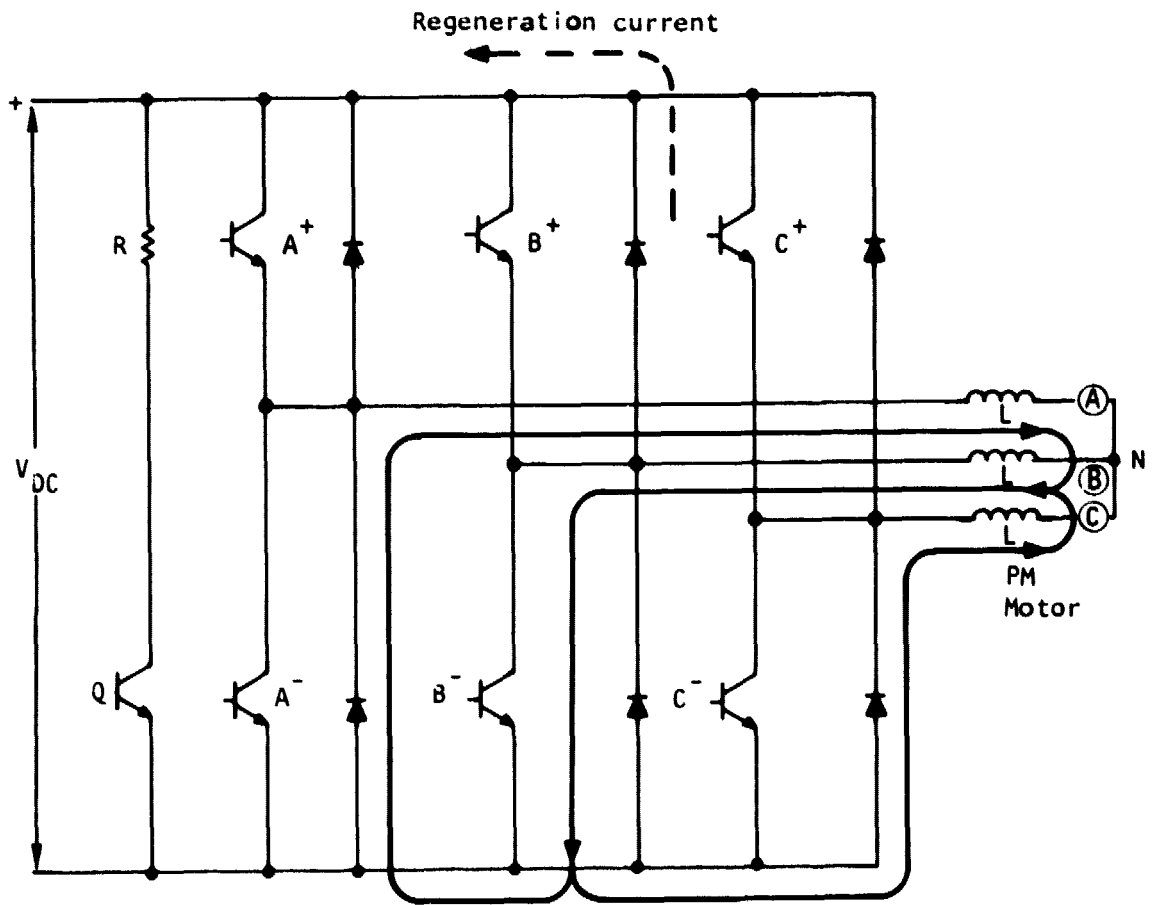
A key element in the analysis and optimization of these interfaces is the use of an AiResearch-developed computer model for predicting the converter/PM-motor interface waveforms and overall performance (figs. 17 and 18). Fig. 17 shows the typical PM-motor EMF voltage and inverter-produced line current at rated speed and load conditions. The shape of the current waveform reflects a full 120 deg transistor conduction. Fig. 18 shows the same parameters except at reduced speed and increased current; typical of the PM-motor acceleration at 50 percent of rated speed. Note that the inverter-current waveform shows more than two peaks, indicating that PWM action is being used to control the inverter-produced line currents.

Inverter design considerations: The baseline PM motor electrical ratings were 26.73 kVA, 0.993 PF, 81.0 V (L-N), 110.46 A, three-phase, 1867 Hz, with an efficiency of approximately 93 percent. The power requirement for the converter is derived through the following equation:

$$P_C = \frac{\text{kVA}_{\text{pm}} (\text{PF})}{E_{\text{pm}}} = \frac{(26.73)(0.993)}{0.93} \text{ kW}$$

$$P_C = 28,540 \text{ W}$$

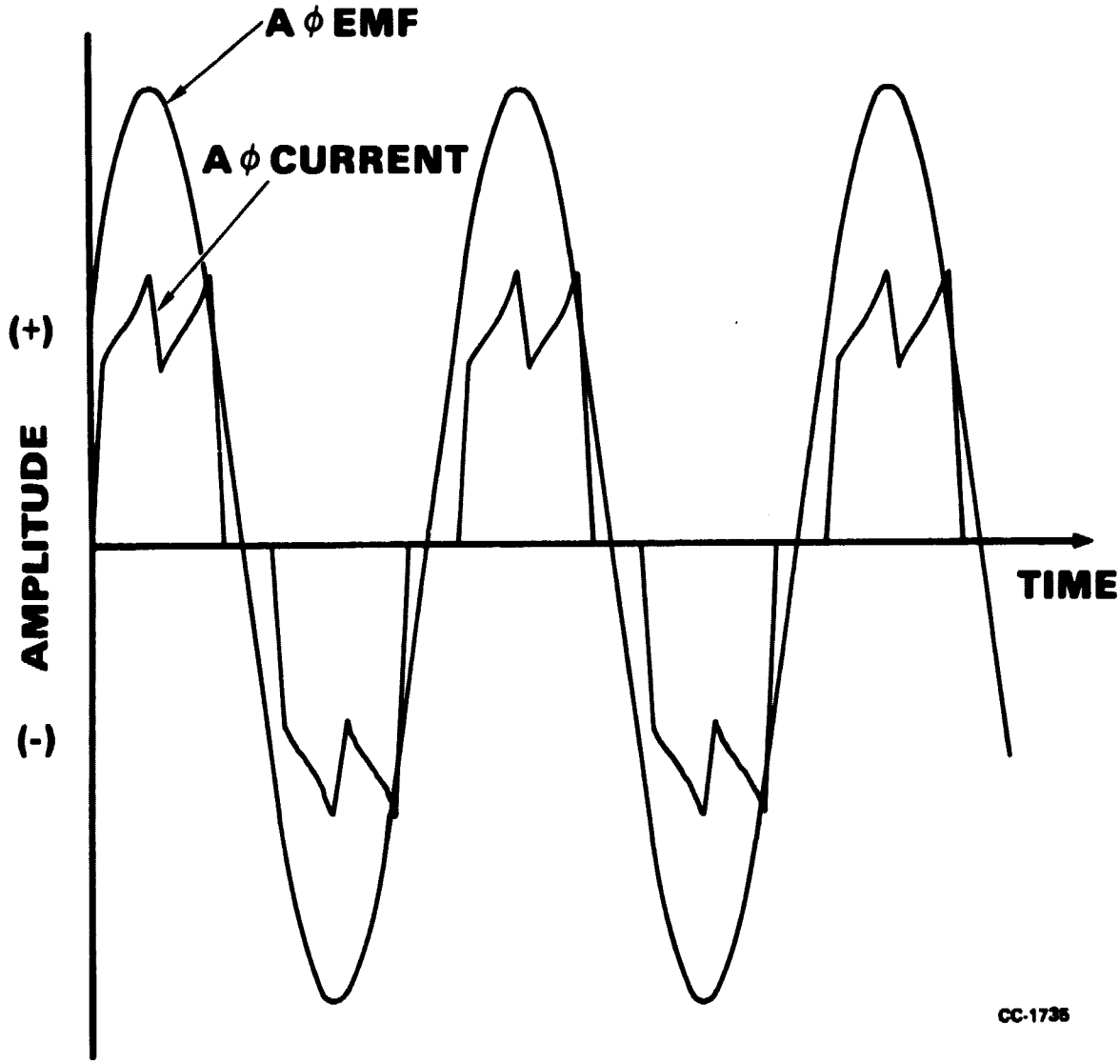
Based on the selected dc battery-source voltage of 240 Vdc, the load current into the converter is calculated to be nominally 118.9 A dc. This value must be



A.30620 A

Figure 16.--Inverter Operation During Regeneration.

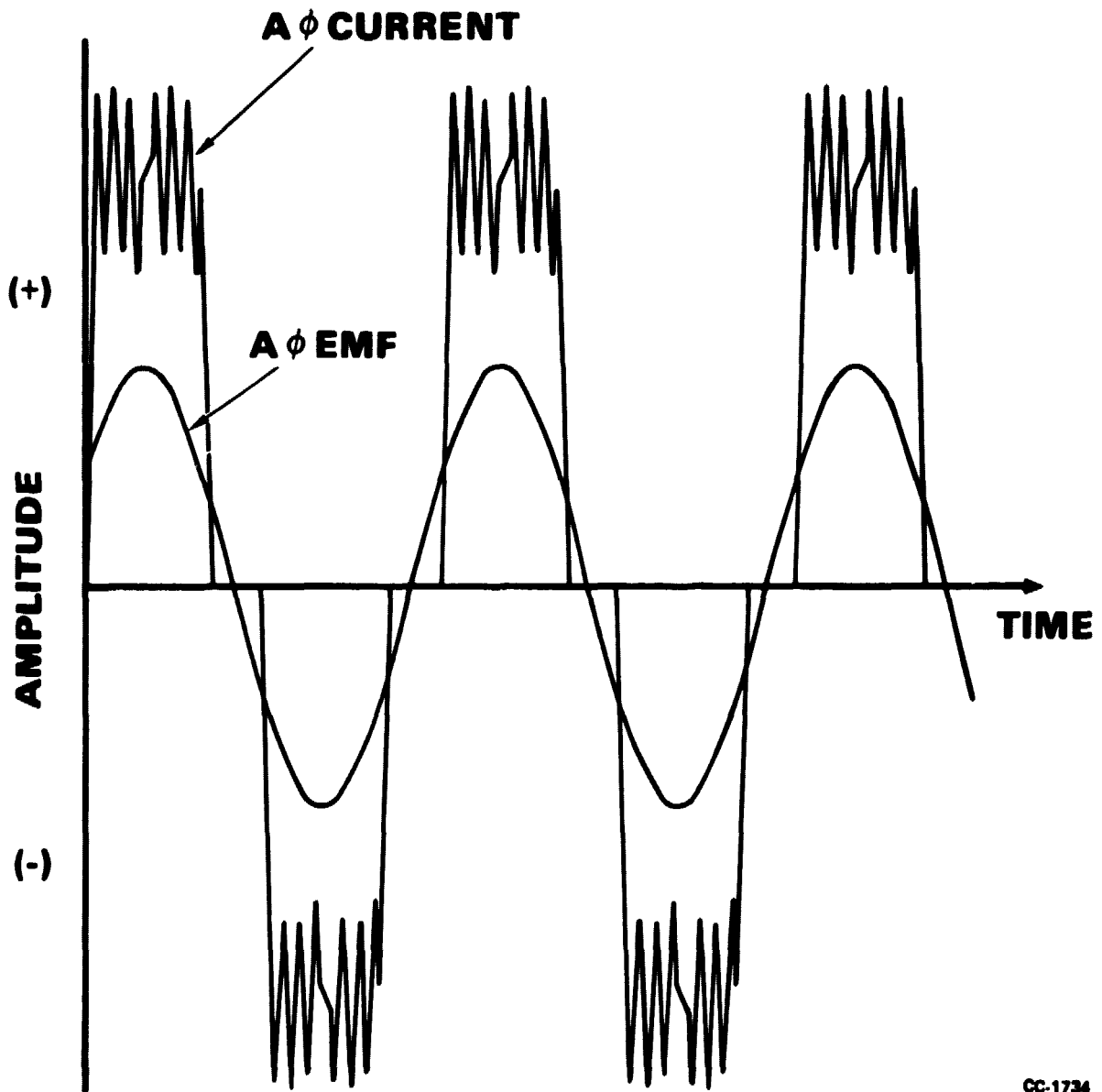
ORIGINAL PAGE IS  
OF POOR QUALITY



CC-1735

Figure 17.--Typical Phase Waveforms at Rated Speed and Load Conditions.

ORIGINAL PAGE IS  
OF POOR QUALITY



CC-1734

Figure 18.--Typical Phase Waveforms During Acceleration.

increased by at least the peak ripple requirements for the aforementioned current control concept. This requires an approximate 15 percent increase, which establishes the maximum nominal load current that each transistor must control, at turn-off, of 136.8 A.

During transistor turn-on, the transistor current consists of the load as well as the recovery current of its associated freewheeling diode. Fig. 19(a) illustrates the inverter circuitry and fig. 19(b) shows the resultant idealized transistor current. At time,  $t_1$ , transistor A- is turned off. The load current then freewheels through diode A+ until it reaches the minimum predetermined load-level at time  $t_2$ . Transistor A- is turned on at a current level consisting of the minimum load plus the recovery current from diode A+. For high-switching applications that are required in a PWM-inverter, unless a high-speed or fast-recovery diode is used, the recovery current can exceed the maximum load current. Therefore, in an PWM-inverter application, the transistor peak-current rating must account for its associated diode characteristics.

In terms of transistor-switching parameters or limitations, the peak turn-on current is associated with its forward bias safe operating area (FBSOA) and the peak turn-off current is associated with its reverse bias safe operating area (RBSOA).

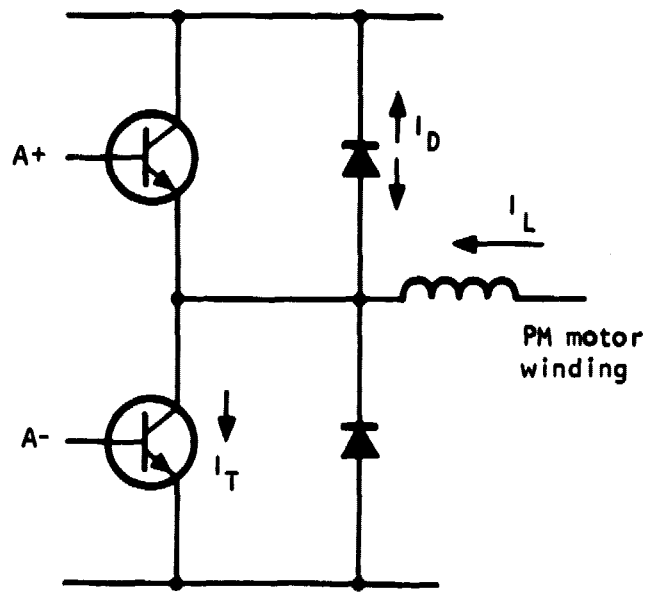
As a result of initial laboratory testing of the selected baseline switching transistor, Power Tech Model PTM 30080A, was judged to have an unsatisfactory switching capability. Also, at that time, there were no other single transistors available with the required capability. As a result, the design of the transistor switch was changed to six Motorola MJ10016 devices in parallel for each of the six switch positions. This action, although it did not affect the inverter concept, produced a significant impact on power unit complexity, size, and parts count. The selection of the Motorola transistors was based on their successful application in similar PM-motor converter drive programs.

During the past four years, significant progress in the development and availability of high-power switching transistors has occurred. Thus, 1982 state-of-the-art transistor technology does allow for a single transistor switch for an inverter rating up to 100 kVA. This fact is, in part, based on AiResearch laboratory testing as outlined in the power transistor section that follows.

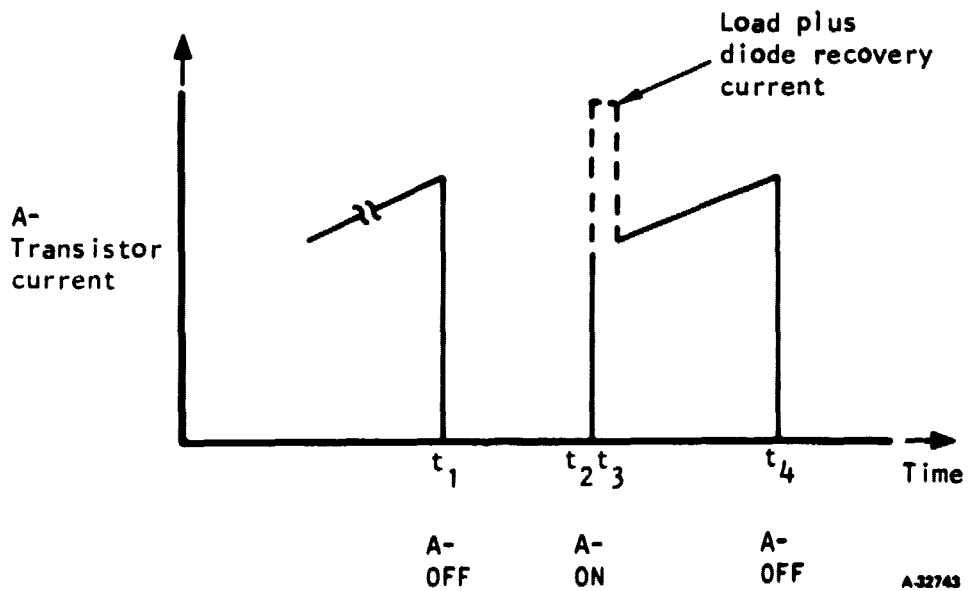
Power transistors: AiResearch continuously monitors the state of the art in power transistors suitable for power-conversion equipment, and maintains an internally funded test program to evaluate the devices. The dedicated test console was designed and fabricated to test and evaluate these power transistors. Testing is conducted to verify manufacturers' ratings according to the following parameters:

(a) Switching characteristics

- Rise time ( $t_r$ )
- Fall time ( $t_f$ )
- Storage time ( $t_s$ )



(a) Inverter Circuitry



(b) Transistor Current

Figure 19.--Transistor Operation.



(b) Conduction characteristics

- Saturation voltage (V<sub>CE SAT</sub>)

(c) Gain characteristics

- Forced beta (h<sub>FE</sub>)

(d) Thermal

- Junction - case thermal resistance (R<sub>θJ-C</sub>)

In addition, the devices are tested to reveal characteristics that are critical but for which ratings may not have been established by the manufacturers. Such characteristics may be:

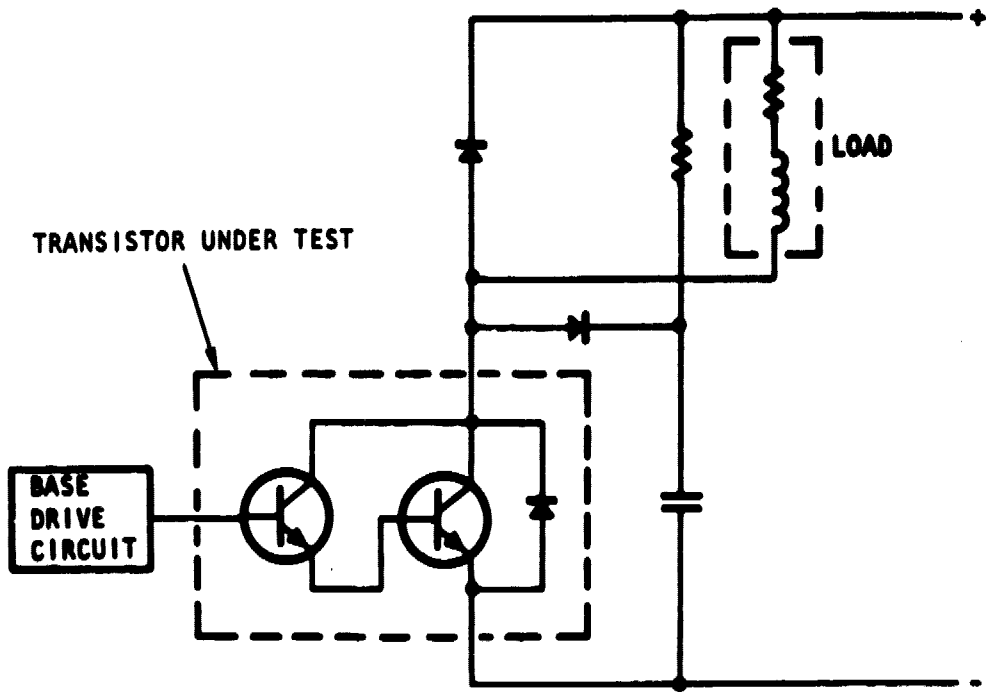
- Forward and reverse bias safe operating area (FBSOA and RBSOA)
- Stored charge time at other than specified conditions
- Static and dynamic parameters that affect the ability of devices to operate in parallel (to achieve greater power capability) or in series (to achieve higher voltage capability)

The test circuits are application-oriented to ensure that observations are as realistic as possible. Primarily, the transistors are tested in the chopper and inverter modes of operation with inductive load switching at frequencies from hundreds of Hz to thousands of Hz. Standard test circuits are used to establish a common basis for the evaluation of each state-of-the-art transistor. Figs. 20 and 21 depict the standard test circuits used.

Basically, two types of bipolar transistors have been evaluated: the bipolar single configuration and the bipolar Darlington configuration. Typical configurations are shown in fig. 22 and a brief comparison follows.

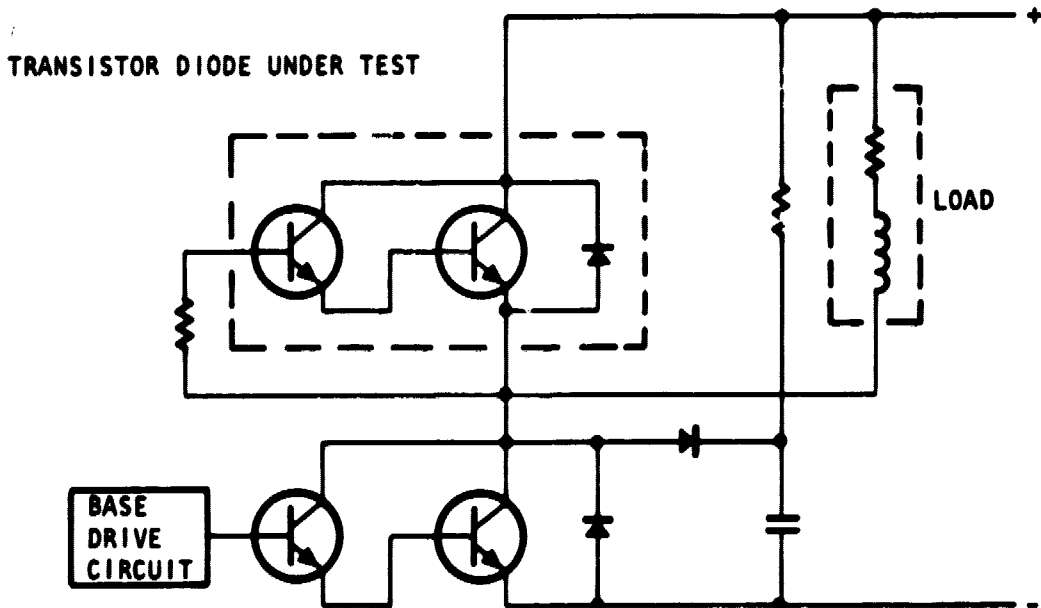
Examples of state-of-the art power transistors that have already been evaluated are shown in Table 3 and fig. 23. In addition, there is a continuous AiResearch R&D program to evaluate the new power transistors as they become available from the manufacturers. Examples of some of the new devices that will be evaluated in the near future are listed in Table 4.

**Bipolar single:** Generally the high-voltage bipolar, single transistors have relatively low gain (h<sub>FE</sub>) at high collector currents, which results in a large base drive requirement. The state-of-the-art power single transistors have a gain of only 5 to 10 at 100 A of collector current. Thus, for a 400-A collector current, the base drive requirements are 40 to 80 A. Such a large base drive usually results in larger size, higher cost, and an overall less efficient system, even though single transistors tend to have lower saturation voltage (V<sub>CE SAT</sub>).



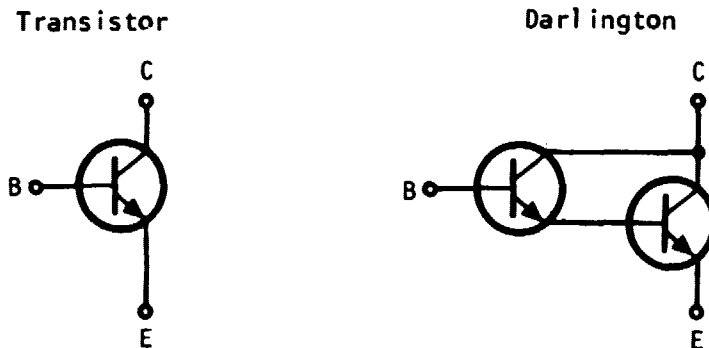
S-40101

Figure 20.--Simplified Test Circuit for Chopper Configurations.



S-40102

Figure 21.--Simplified Test Circuit for Inverter Leg Configuration.



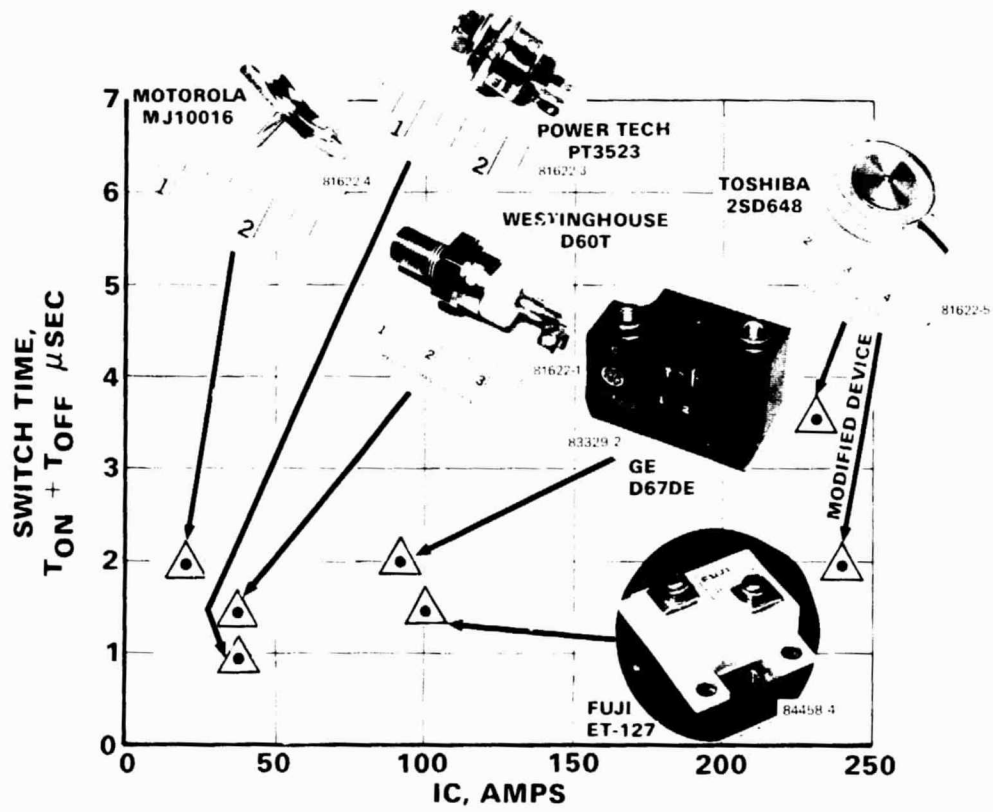
A-32744

Figure 22.--Typical Transistor Configurations.

TABLE 3.--STATE-OF-THE-ART POWER TRANSISTORS.

Manufacturer	Part Number	Manufacturers' Ratings		Transistor Type
		VCE, V	IC, A	
Power Tech	PT3523	400	90	Bipolar
Westinghouse	D60T	500	200	Bipolar
Westcode	WT5705	450	200	Bipolar
Motorola	MJ10016	500	50	Bipolar Darlington
Toshiba	2SD648	300	400	Bipolar Darlington
General Electric	D67DE5	500	150	Bipolar Darlington
Fuji	ET-127	520	250	Bipolar Darlington

ORIGINAL PAGE IS  
OF POOR QUALITY



• SWITCHING LOSSES PROPORTIONAL TO  $T_{ON} + T_{OFF}$

F. 31253 A  
545623

Figure 23.--Comparative Transistor Test Evaluation.

TABLE 4.--NEWEST POWER TRANSISTORS IN PRODUCTION

Manufacturer	Part Number	Manufacturers' Ratings		Transistor Type
		VCE, V	IC, A	
Fuji	ET-109	900	50	Darlington
Toshiba	2SD1034A	450	300	Darlington
Toshiba	2SD1166	900	200	Darlington
Westinghouse	D7ST	500	100	Bipolar
General Electric	D67NGE	500	100	Darlington
Westcode	WT5700	500	350	Bipolar

**Bipolar Darlington:** The bipolar Darlington transistors generally have higher gain, which results in a relatively small base drive requirement. The state-of-the-art high-voltage, high-current Darlington transistors have forced gains ( $h_{FE}$ ) of approximately 50 to 100 at 100 A of collector current. For a 400-A collector current, the base drive requirements are only 4 to 8 A, thus, there is at least an order of magnitude difference for the base drive requirement between the single and the Darlington transistor configurations. There are several different configurations of the state-of-the-art Darlington transistors available on the market. The Darlington transistors that have a second base available outside the package or a built-in speed-up diode have the advantage of faster switching times, which result in lower switching losses and a capability of higher frequency switching operation. Some of the currently marketed Darlington transistors have an inherent substrate (effective) inverse-parallel diode that is not characterized and, in many cases, is incompatible with the Darlington switching speeds and currents. This can cause problems in some inverter applications. AiResearch has studied this phenomenon carefully through internally funded research and development testing. The solution usually results in adding components to block this undesirable inverse-parallel diode.

There are other state-of-the-art power Darlington transistors available that eliminate this inherent substrate (effective) inverse-parallel diode and, at the same time, provide a fully specified and compatible inverse-parallel diode that may be successfully used to replace the external freewheeling diode in inverter applications. Such a Darlington reduces the component count and assembly complexity, providing the benefit of size and cost reductions.

Advanced motor converter.--The functional elements of the power circuits of the advanced motor converter are shown in fig. 24 with the detailed circuit schematic SK820910 included in appendix E.

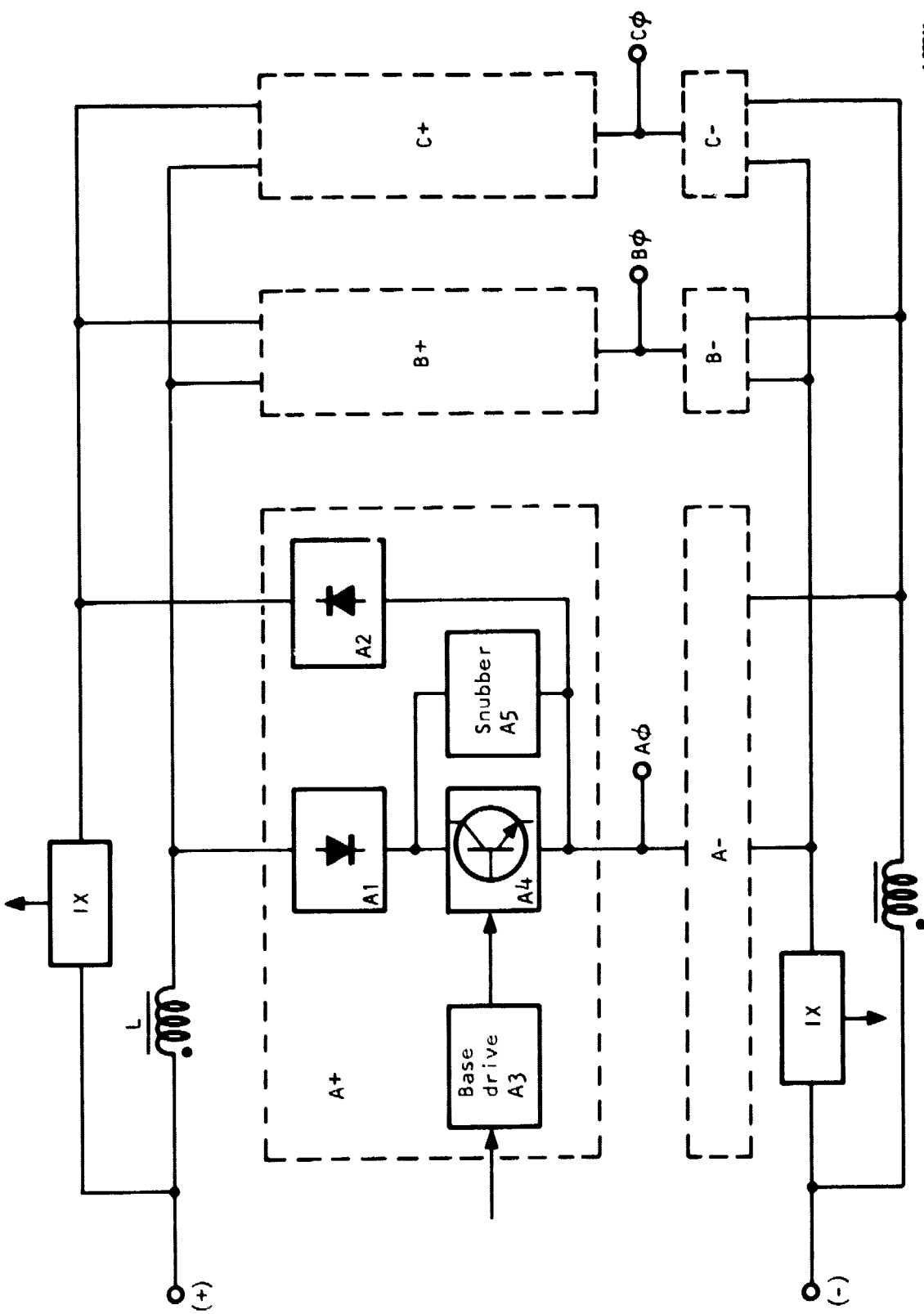
The proposed inverter concept utilizes the inherent motor inductance to limit the rate of rise of current in the power circuit. When the rate of change of current is controlled within reasonable boundaries, the waveform generation and transistor modulation frequency can be held within satisfactory limits. The resultant design of the advanced motor produced an internal inductance far lower than conventional designs. Considerable innovation and redesign of the inverter was necessary to limit the transistor-switching frequency and maintain waveform integrity, while maintaining low weight and high efficiency. The impact of the redesigned inverter concept involved increased control complexity, additional power components, and significant modification to the computer simulation used to investigate the effects of the new design.

A description of the operation and salient features of the converter functional elements follows.

The three diodes in element A1 block the reverse current flow through the slow-recovery inverse-parallel diodes associated with the six power transistors in element A4 (fig. 24). The reverse or freewheeling current is forced through the three diodes in element A2. Both sets of diodes are fast-recovery types (Motorola MR876) that minimize the turn-on stress of the power transistors in the A-inverter leg.

At the outset of the program, it was the opinion of several transistor suppliers that a power-switching transistor could be designed to operate without transient protection, i.e., without snubber networks to limit rate of rise of current ( $di/dt$ ) or rate of rise of voltage ( $dv/dt$ ). Transistor and circuit modeling showed that although  $di/dt$  stress can be controlled by inherent lead length within the inverter layout or through the use of fast-recovery diodes, the  $dv/dt$  stress still requires added components for proper transistor protection. These added components can be minimized, however, by optimum selection of the power transistors and diodes, as well as specific attention to the inverter wiring associated with generation of such voltage stress. For the Motorola MJ10016 transistors and the anticipated breadboard layout of the inverter, the components within element A5 were provided.

The base drive circuitry, element A3, is common to all upper or positive inverter legs. The base drive circuitry for the negative inverter legs are somewhat different: The selection of high-gain Darlington's over the single transistors for the switches in the PWM inverter reduces the base drive requirements considerably. The typical gain of the Darlington's used is in excess of 21 at 25-A collector current; meaning that less than 8 A of base current will be required to drive six paralleled Darlington's per switch location.



A-32741

Figure 24.--Advanced Motor Converter Block Diagram.

Since the drive-current requirement is relatively low, metal oxide semiconductor field effect transistor devices (MOSFETs) can be very effectively used as drivers. MOSFETs have the significant advantage of faster switching speeds, and lower switching losses, if used properly. AiResearch is constantly evaluating the state-of-the-art MOSFET devices under an internally funded R&D program and has proven experience in the successful application of such devices to drive power stages. For this program, state-of-the-art MOSFET devices were selected for the drivers in proven circuit configurations.

Since consideration is given to the selection of circuit techniques that enhance the rapid turnoff of the power Darlington. Faster turnoff results in lower switching losses and safe operation. The upper base drivers utilize a resistor-inductor network in parallel with the power transistor base to emitter terminals. Therefore, when the base drive is turned off, the stored energy in the inductor causes it to reverse its voltage polarity, which forces negative or "sweep-out" current through the base to the emitter junction of the power transistor. The lower drivers utilize a negative 5 Vdc source and a second MOSFET to accomplish a similar function. In either case, the circuit action improves the switching characteristics to maintain the power transistor performance within its RBSOA rating.

The upper and lower transistor turn-off circuitry is different since it was anticipated that the high-frequency switching, or PWM, would be performed by the lower transistors and they required an active turn off method. Subsequent analysis showed that it is better to have all six inverter legs operate in the PWM mode. This is accomplished by logic control wherein each power transistor is used in the PWM mode for 60 deg of its normal 120 deg conduction period.

To monitor the total PM motor load current, two current sensors (IX) are utilized. Their outputs are summed within the logic circuitry, as required for control and protection purposes. The sensor configuration allows for both real (elements A1 and A4) and reactive (element A2) current monitoring.

The series inductors are required to limit the PWM frequency to approximately 15 KHz. The baseline design was based on the use of the PM motor-winding inductance to limit the rate of rise of load current during the PWM intervals. However, the initial PM motor design resulted in only a 0.15 per unit commutation reactance ( $X_{C, pu}$ ), approximately 50 percent of the required value needed to eliminate the need for such external inductances. As seen in fig. 15a, the increase of current through the PM motor-winding inductance is approximately:

$$\Delta I = \frac{V\Delta t}{2LC}$$

where:

$\Delta I$  = Current increase during time  $\Delta t$

$V$  = Circuit-forcing voltage



$\Delta t$  = On-time of the power transistor

$L_C$  = PM motor commutation inductance

and:

$$L_C = \frac{X_{C, pu}}{2\pi f} \frac{V(L-N)}{I}$$

where:

$X_{C, pu}$  = PM motor commutation per unit reactance

$f$  = PM motor rated frequency

$I$  = PM motor rated line current

$V(L-N)$  = PM motor rated line-neutral voltage

Substituting the original design parameters:

$$L_C = \frac{0.15}{2\pi(1867)} \frac{81}{110} = 9.4 \mu\text{H}$$

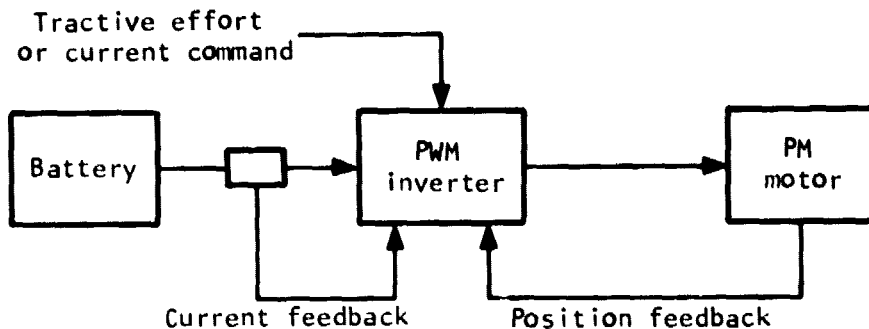
Since the value of  $L_C$  is small, additional external inductance is required to increase  $T$  or decrease  $f_{PWM}$  to the desired 15 kHz limit. The total external inductance required is 66  $\mu\text{H}$  for both the drive and regeneration current loops. Thus, an inductor with a minimum inductance of 66  $\mu\text{H}$  is required in each of the positive and negative input dc lines as shown in fig. 24.

The final functional element associated with the converter power circuit is the power supply for the transistor base drives and the logic control circuitry. The circuit is shown in schematic SK820910 included in appendix E.

The power supply consists of a single-phase, 75 kHz, high-frequency inverter operating from a 12 Vdc battery source. The supply provides two +20 Vdc supplies, four +6.5 Vdc supplies, and one -5 Vdc isolated supply with a combined rating of 253 W.

Advanced motor control logic: The functional basic block diagram for the advanced motor control system is shown in fig. 25. Within the system there are four basic modes of operation: start, drive, transistion, and brake.

Start mode: As previously indicated, proper controller to PM-motor interface requires that the current delivered to the motor windings be synchronized to the motor-generated EMF. However, at stall or low-speed motor conditions, the generated EMF is insufficient to be electrically sensed. Thus, an electro-mechanical position sensor, an integral part of the PM motor, is used to determine sequential operation of the inverter so that the inverter current is applied



A32742

Fig. 25.--Basic System Block Diagram.

to the correct windings and in the required relationship to the machine rotor. At approximately 10 percent of rated motor speed, the inverter logic automatically changes from position to EMF synchronization. Thus, during all PM motor speeds, the inverter current is in phase with the EMF voltage, which results in the PM motor operating at a desirable high input-power factor, or near unity. The position sensor is discussed further in appendix F.

**Drive mode:** Acceleration or deceleration are programmed or commanded by positive or negative tractive effort or torque. Since PM motor torque is proportional to the dc current into the inverter and this current is easily monitored, the actual system will respond to current command signals. Using PWM within the inverter will allow the PM motor to accelerate under constant torque conditions. As the motor nears its rated speed, the commanded torque or current will be automatically reduced by the motor-speed feedback signal.

**Transition mode:** Transitions from the drive-to-brake mode and vice-versa or the forward-to-reverse mode and vice-versa are controlled within the logic circuitry. Adequate safeguards are provided to ensure proper system conditions are met prior to and during these transitions. These transitions are rate-limited so that abrupt changes can not occur in excess of normal vehicle operation except when brake is commanded. In addition, forward-to-reverse transitions require the vehicle to be controlled to a stop mode, followed by system sequence changes that provide for the selected mode.

Brake mode: During brake or deceleration conditions, the PM motor generates an output voltage that is proportional to its speed. Therefore, for a fixed value of brake resistance, the energy available for deceleration would normally decrease as the square of the motor speed or voltage. However, using the PWM capability of the inverter, the energy can be held constant, at its maximum value, from 100 percent to approximately 20 percent of the rated motor speed. This results in the ability of the converter to more rapidly decelerate the PM motor in the event of abnormal operation.

Logic circuits: The baseline control concept uses conventional technology to implement the inverter switching sequences, provide the drive-brake transitions, forward-reverse maneuvers, and protective features. Early in the design phase, the conventional approaches were replaced in favor of field-programmable logic arrays (FPLA) and read only memories (ROM) so that the advanced motor system with increased inverter complexity could have advanced technology control logic. This approach, instituted to provide lower cost for future applications, required considerable evaluation of candidate devices and subsequent design effort to properly interface these relatively new logic elements into a suitable configuration for this application. This effort included design of control functions compatible not only with the basic requirements of the more complex inverter and motor, but also with features that are involved with the application of the advanced motor to a vehicle drive system.

To implement the required control, monitor, and protective functions, six specific circuit designs were completed. The final circuit design, interface logic, was not completed because problems with the PM motor development put all converter activities on hold. The circuit designs are listed in table 5. Completed schematics are included in appendix F.

TABLE 5.--LOGIC CIRCUIT SCHEMATIC DIAGRAMS.

Title	Schematic Drawing Number
Inverter	2001564
Sync and speed decoder	2001592
Current sense and comparator	2001566
Drive-brake direction and tractive effort pause	2001556
Fault protection and tractive effort pause	2001558
Base drive power supply logic	2001570
Power supply	2001560
Interface	Incomplete

Within the schematics various terms are used to define the input/output functions. Of those, the following definitions apply:

**Tractive effort pause:** A protective function wherein the tractive effort (TE) or current command is reset to zero for such time as required to correct the initiating fault condition.

**QSAT:** A protective monitoring function that indicates that a power transistor within the main inverter has not switched to a predetermined low-forward conduction state subsequent to the application of a positive base drive.

System interface: Due to the PM motor problem, the full integration between the converter power, converter logic, and PM motor was not completed. However, fig. 26 indicates the general interface requirements with the exception of the interface logic. Such logic would typically be required for signal conditioning or system status readout functions.

Except for the analysis and preliminary schematic, work on the converter was postponed in April of 1979, until the successful development of the functional model rotating machine. Section 7 covers the follow-on activities.

A-32748

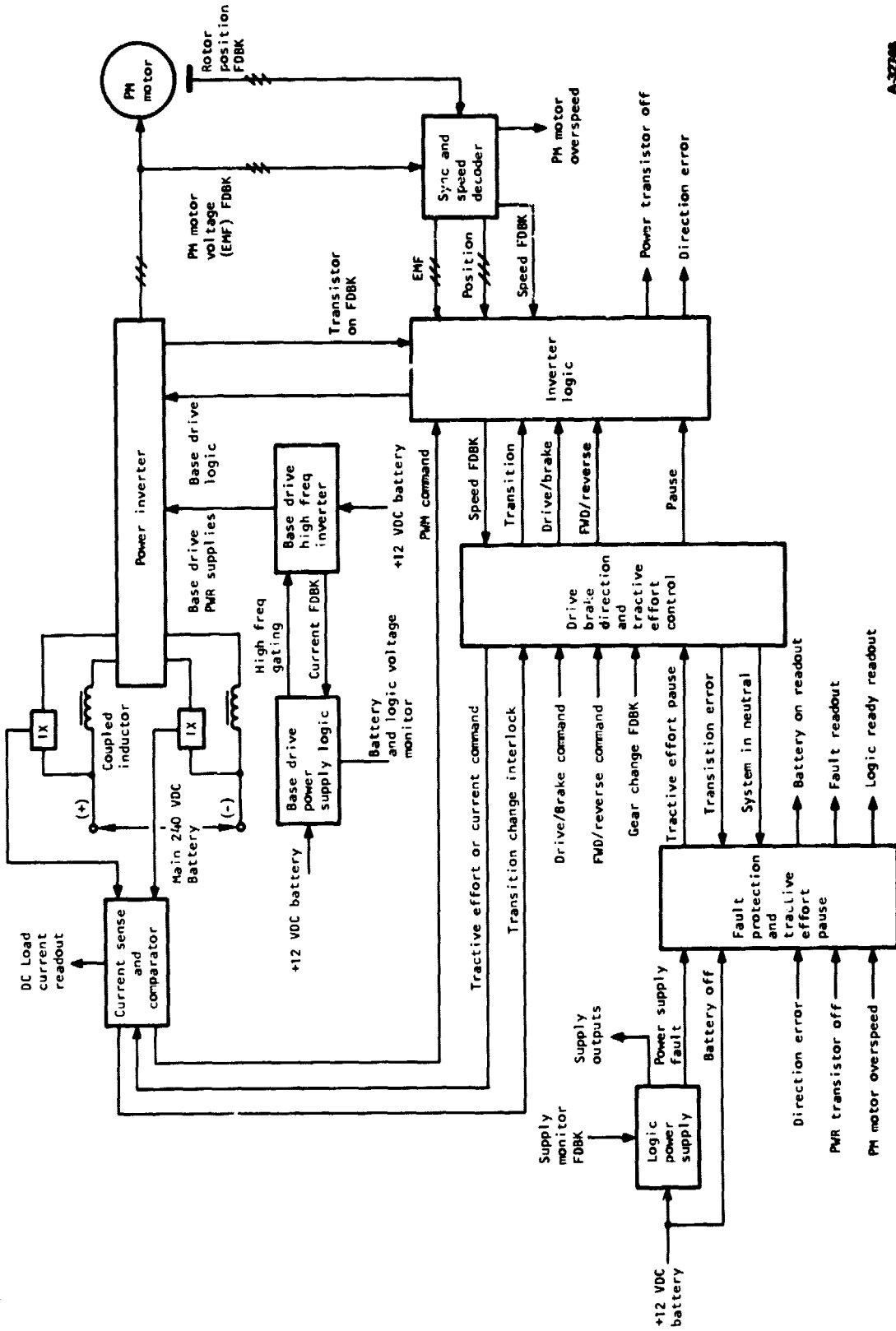


Figure 26.--System Interface Block Diagram.

## PROOF-OF-PRINCIPLE MODEL MOTOR DEVELOPMENT

The unique construction of the axipolar machine with an ironless stator required an extensive amount of development and tooling for fabrication and assembly of both the rotor and stator assemblies. Each of these areas is discussed separately below.

**Stator assembly.**--The first task associated with the stator assembly was determination of achievable bend radii of the individual stator coils. Bending of the coils is necessary in order for coils of all three phases to lie in the same plane. Fig. 27 shows how the coils interleave to achieve a minimum air gap and maximum packing factor in the tangential direction. The information on bend radii was necessary as an input to the computer program so that the proof-of-principle design could be completed. Fig. 28 is a partial schematic of the stator winding, showing how coils are connected and the current path for a given condition.

Initial evaluation of the stator coils was accomplished by procuring a readily available strip copper with approximately the right dimensions. Fig. 29 shows a picture of one of the first coils wound before bending. It was found that the coils could be formed with a 3.4-mm bend radius. This information was used to help select the final design configuration of the coils and stator assembly.

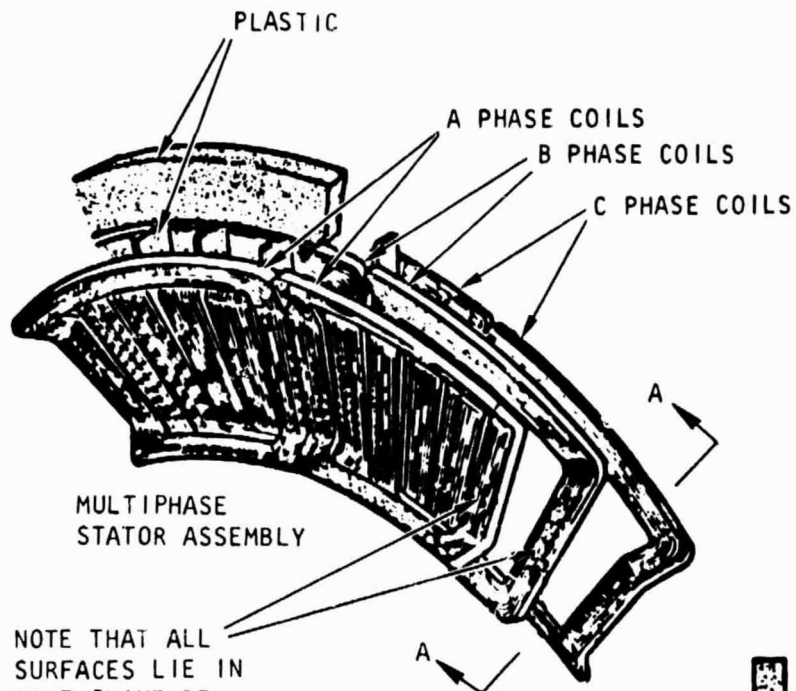
A trapezoidal-shaped winding bobbin was used to machine-wind the coils. The properly sized bare strip copper wire was fed into the winder with a 0.05-mm kapton layer in between each of the 20 turns. Each coil was then impregnated with a silicon varnish (see table 7) to help it retain its shape during bending. Coil bending tooling was designed, and after a few modifications, coils were made that demonstrated the proposed bending technique was suitable. Fig. 30 shows the forming tooling.

Electrical data were taken on the individual coils to check the insulation system and to obtain the actual resistance and inductance values. Typical data, along with calculated values, are presented in table 6 below.

TABLE 6.--ELECTRICAL TEST DATA ON INDIVIDUAL COILS.

<u>Sample Description</u>	<u>Resistance at 21°C, Ω</u>	<u>Inductance, mH</u>
1. Unwound strip (2.845-m long)	0.075	-
2. Wound, unvarnished	.075	0.026
3. Wound, varnished, not formed	.075	.026
4. Wound, varnished, formed	.076	.027
5. Calculated (nominal) value	.066	.031

ORIGINAL PAGE 13  
OF POOR QUALITY



NOTE THAT ALL SURFACES LIE IN SAME PLANE BETWEEN POLES TO MINIMIZE GAP BETWEEN POLES AND ACHIEVE HIGH PACKING FACTOR



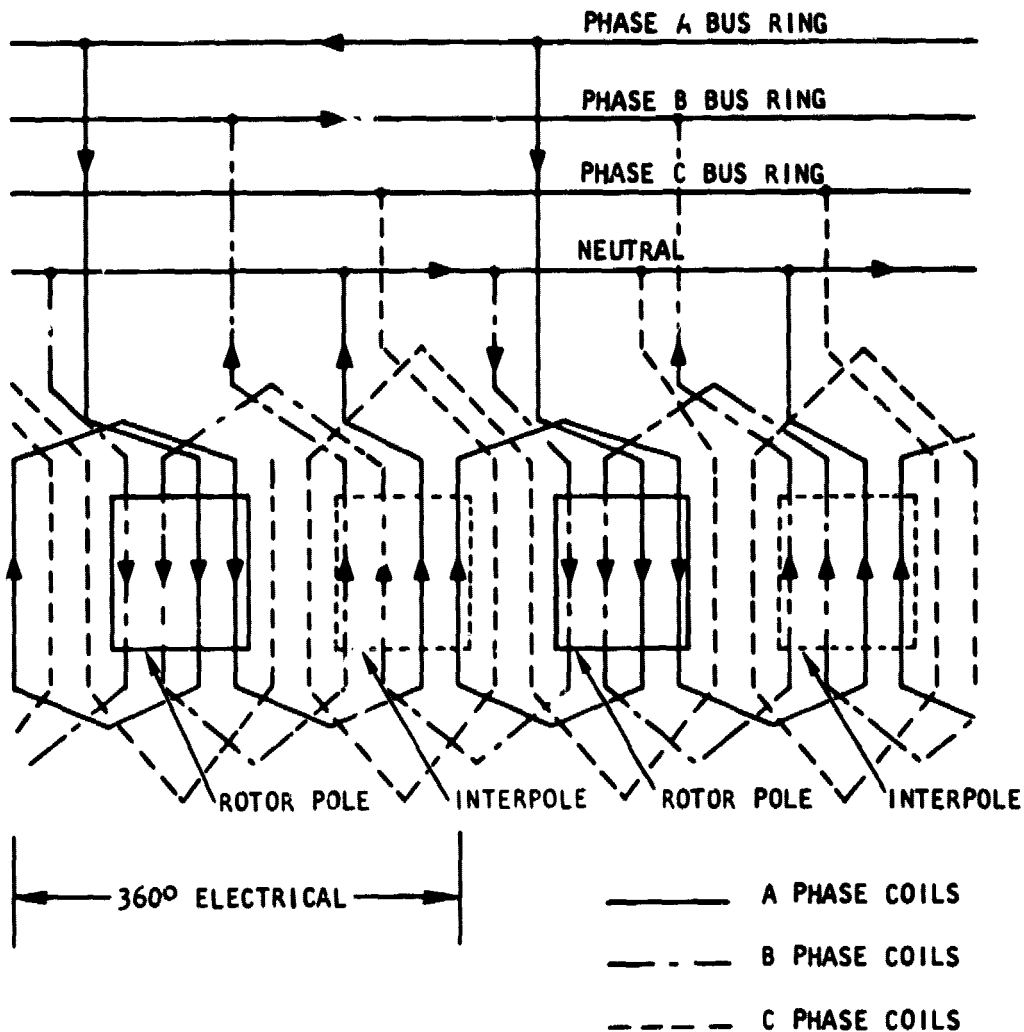
A - A

A-32421

REF: STATOR DRAWING 2043900, APPENDIX E

Figure 27.--Stator Assembly Construction Concept.

ORIGINAL PAGE IS  
OF POOR QUALITY



NOTE: CONDITION SHOWN IN FOR A +, B- CURRENT CONDUCTION

A 38000

REF: STATOR DRAWING 2043900, APPENDIX E

Figure 28.--Stator Winding Schematic with Connection and Pole/Interpole Representation.

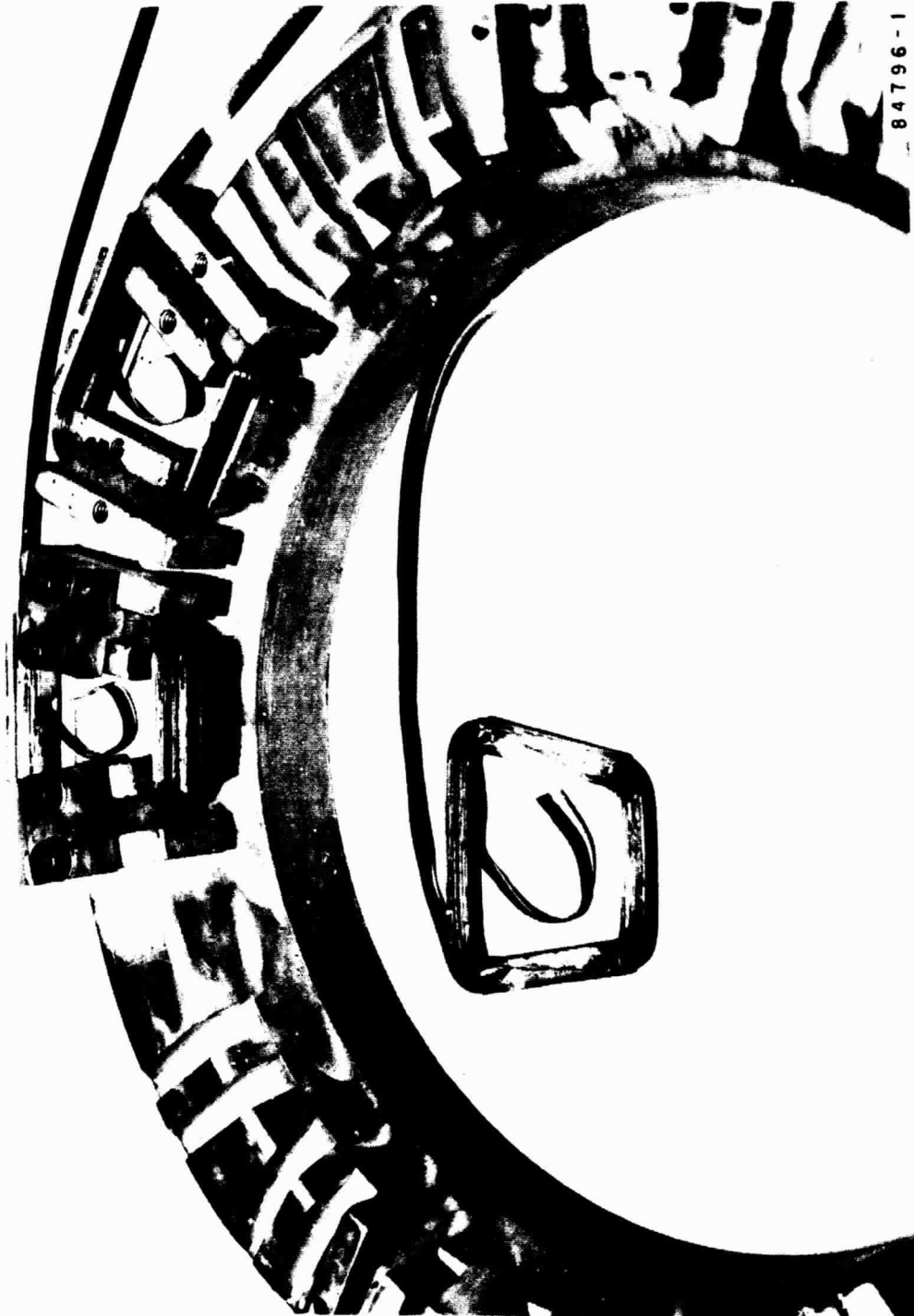




F-2910F

Figure 29.--Sample of Stator Coil for Advanced Motor, Prior to Bending.

ORIGINAL PAGE  
BLACK AND WHITE PHOTOGRAPH



84796-1

Figure 30.--Coil-bending Tooling.

The next stage of stator assembly involved aligning all 48 coils into their proper orientation and phase groups and bonding them together into the aluminum stator ring. Special tooling was designed and fabricated to accomplish this. This tooling consists of two outer aluminum rings that locate the stator coil support ring and two inner aluminum rings that register on the outer portion of the tooling and have the shape of the coils. This tooling is shown in figs. 31, 32, and 33.

Bonding was accomplished using a one-part thixotropic adhesive epoxy (ref. table 7). Two 1.63-mm-diam insulated Inconel rods were bonded in place on the i.d. to provide some structural rigidity to the assembly. The outer portions of the stator coils were bonded to the aluminum coil support ring, with the epoxy providing both electrical insulation and structural support.

After curing and removal from the alignment fixture, the stator assembly was found to have electrical shorts between phases and from phases to ground through the housing. A review of the winding and manufacturing techniques was made. It was decided that the fixture would be modified to use phenolic instead of aluminum in the portions holding the coils. This permits dielectric evaluation during all phases of construction. In addition the coils were reduced from 20 turns to 19 turns to provide increased insulation between coils, and the stator housing was modified slightly to provide more clearance to ground.

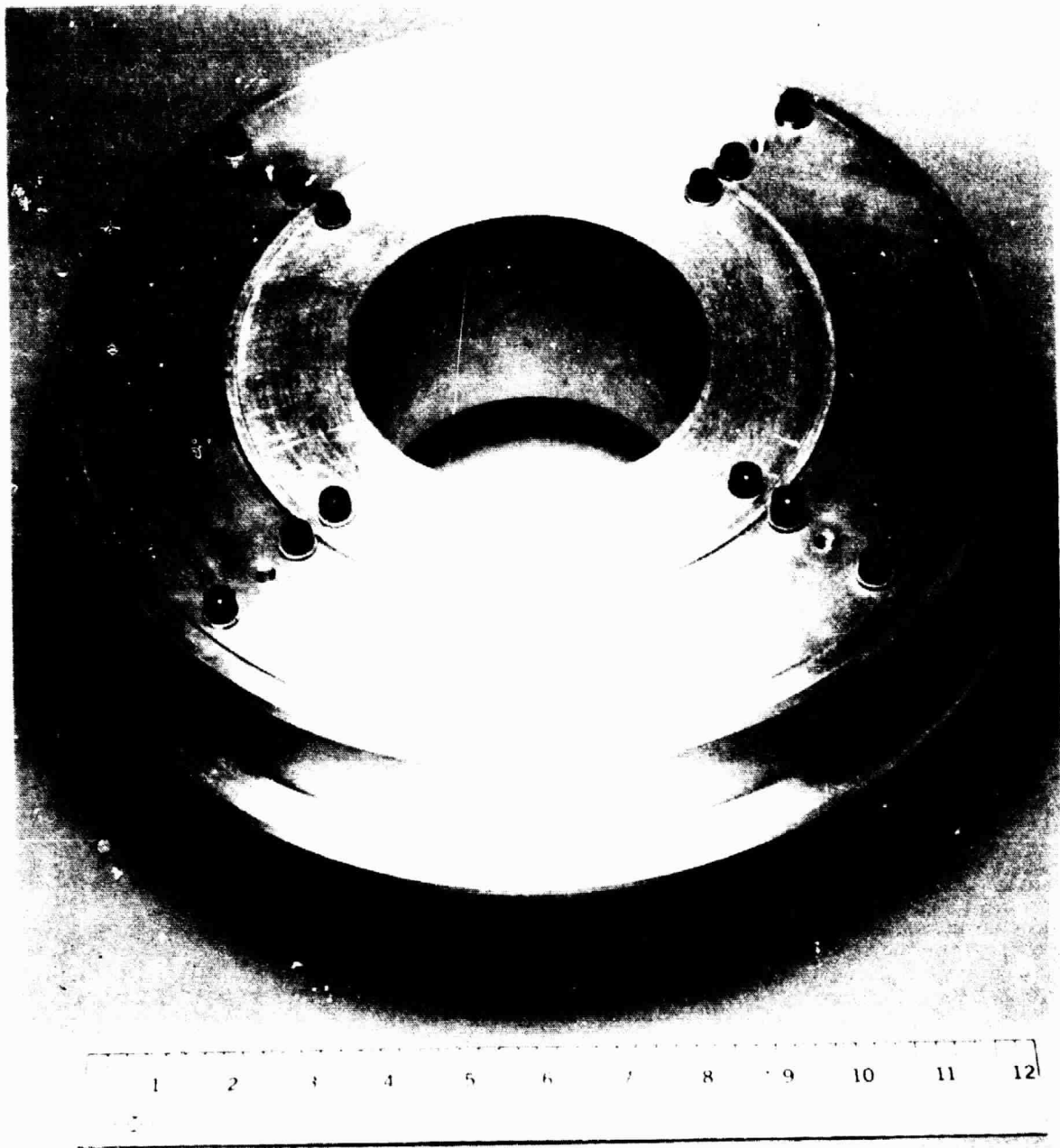
The electrically faulty stator assembly was checked for mechanical integrity. The assembly was cycled from room temperature to 205°C (400°F) and checked for cracks and mechanical shifting. After these cycles, which included a total exposure to 205°C (400°F) for 13 hr, no measurable shifting or cracking was found.

A new stator assembly was constructed using the modified tooling and hardware. During this build-up, dielectric and megger tests were used to ensure that there were no shorts between coils and phases or between the winding and ground. The winding was then potted to its support housing successfully, with no electrical faults.

The stator assembly was completed by attaching four circular bus rings to the stator-support housing through Teflon spacers and plastic screws. These bus rings, one for each of the three phases and one for the neutral, collect and distribute current from each of the eight parallel circuits in each phase (see connection diagram on drawing 2042900 in appendix E). Leads from the coils were brazed to the bus rings. Rectangular copper sections were then brazed to the bus rings and extended through holes in the end bells to provide the attachment point for electrical power from the electronic converter. A picture of the completed stator assembly is shown in fig. 34.

During testing of the proof-of-principle machine, the stator coils overheated and caused failure of the stator assembly. The failure was attributed to electrical shorts in the coils, causing excessive heating and mechanical shifting.

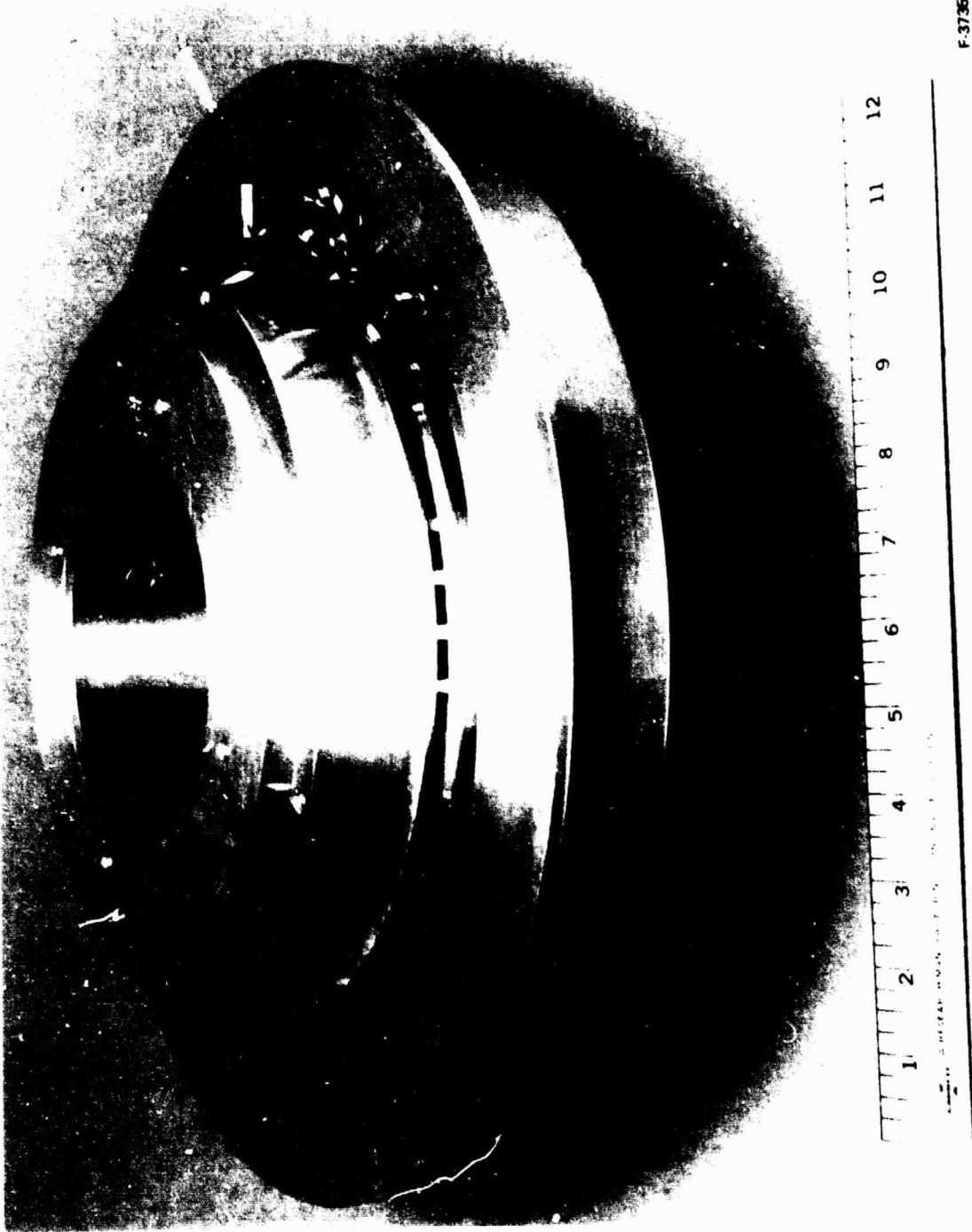
ORIGINAL PAGE  
BLACK AND WHITE PHOTOGRAPH



F 37358

Figure 31.--Stator Winding Assembly Fixture.

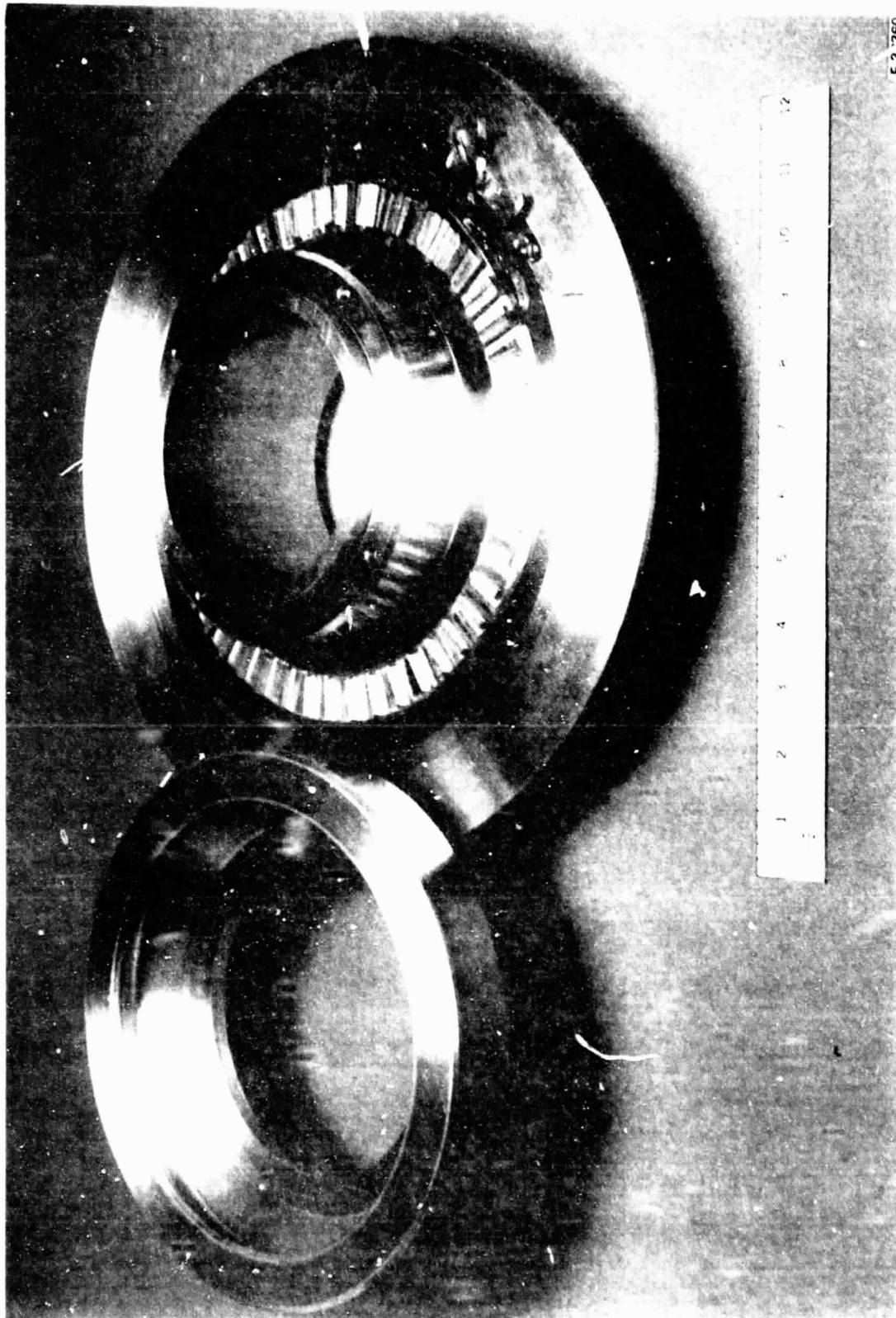
ORIGINAL PAGE  
BLACK AND WHITE PHOTOGRAPH



F-37369

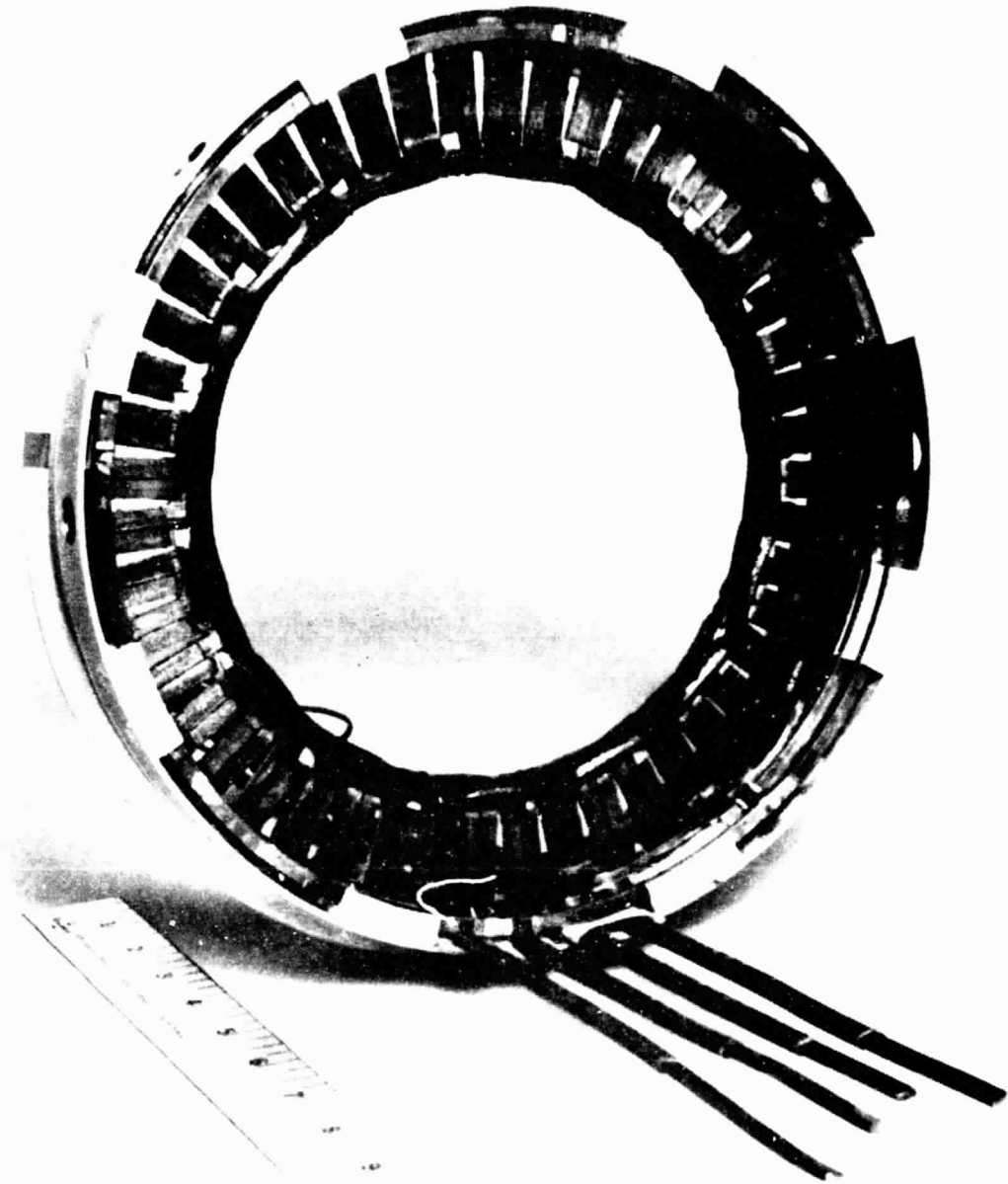
Figure 32.--Partially Assembled Stator Winding Assembly Fixture.

ORIGINAL PAGE  
BLACK AND WHITE PHOTOGRAPH



F.3.360

Figure 33.--Interior view, Stator winding Assembly Fixture.



F.37364

Figure 34.--Proof-of-Principle Model Stator Assembly.

Subsequent evaluation of the materials and techniques of the stator assembly resulted in the conclusion that a reliable stator assembly could be built only by using an enameled copper wire instead of the bare copper used previously. The concern in this approach is achieving an even coating of enamel, with sufficient thickness to achieve the desired electrical insulation and still adhere well enough on the thin edges to prevent mechanical cracking or crazing during winding of the coils. It was decided to use a coating of ML, a polyimide film with a class 220°C rating.

This led to a development period with the magnet wire vendor where various coating techniques and processes were evaluated. Initial samples had too thin a coating to achieve the proper electrical properties. Thicker coatings resulted in cracking of the insulation when the wire was flexed. The wire was tested by applying voltage to an insulated conductor submerged in salt water, with the electrically conductive salt water acting as the only return path for current. This technique provides assessment of the insulation on the full surface area of the submerged conductor.

Wire was produced successfully by using a "quad-ML" coating, that is, by coating the wire and curing the enamel four times. The total resulting insulation thickness was 0.025 to 0.030 mm. The bare wire dimensions were 0.220 +0.013 mm by 3.367 +0.178 mm. These dimensions allowed the return to the original design number of 20 turns per coil, and the coating resulted in improved electrical and mechanical properties. A new stator assembly was built using the ML-insulated wire. This stator passed all electrical tests and was tested to full current and power during the proof-of-principle motor tests.

Rotor assembly.--The rotor assembly, shown in fig. 35, mainly consists of the two identical rotor pole pieces, the magnet, the magnet containment ring, and the tiebolt/shaft. For this program, the pole pieces were machined out of a solid bar, but the design is such that they could be either forged or cast with minimal machining for purposes of economy. Each pole piece, made of 4340 steel, consists of a central section that mates with the magnet and eight "fingers" that extend radially and then bend to an axial direction. The eight steel poles plus their associated interpoles result in a 16-pole configuration.

The magnet is a pancake-shaped cylinder of material that actually is composed of several smaller pieces bonded together. The o.d. and shaft hole are precision ground and the magnet is fully magnetized in the axial direction. The magnet material used was a 15 MGO samarium-cobalt material (see drawing 2047221 in appendix E). While this is an expensive material, it is believed that a mischmetal-cobalt material with similar properties will eventually be available. Mischmetal is a term used to describe the mixed rare-earth elements as they occur in nature. Samarium is a rare earth element that must be processed or refined into its pure state because it represents only 3 to 5 percent of the rare earth elements found in nature. The use of mischmetal in place of samarium in magnets would preclude the costs associated with this extraction process. As an alternative, a samarium-enriched mischmetal-cobalt might also be developed at an intermediate cost and with intermediate magnetic properties. If in the future, the cost of samarium could be brought down through new source development or improved refining techniques, there is a cost benefit achievable by using even higher





F 37356

Figure 39.--Advanced Motor Rotor Assembly.

energy magnet materials. Presently, 22 MGO material is readily achievable. The higher the magnet energy product, the smaller the magnet will be. This represents a cost reduction in the cobalt which is a significant part of the total cost. It is felt that a low-cost magnet material with good magnetic properties will be required for permanent magnet motors to be viable candidates for propulsion on electric vehicles. The use of ferrite 8 magnets instead of samarium cobalt results in a larger motor but eliminates the availability and cost problems with the magnet materials. A preliminary design was made for this motor application using ferrite 8. See Appendix D for the comparison. Table 7 presents a comparison of properties and cost for the materials discussed above, Sm-Co 15 MGO, Sm-Co 22 MGO and ferrite 8.

Rare-earth cobalt magnets are known to be very brittle and have poor tensile properties, making them subject to damage under rotational stress or during handling and assembly. Two steps were taken to ensure that no damage occurred to the magnet in this application. First, a thin, magnetically soft, steel plate (1.8-mm thick) was bonded to the magnet on each side to prevent damage during handling and assembly to the rotor pole pieces. Tooling used for this assembly is shown in fig. 36. Secondly, an Inconel 718 shrink sleeve was fitted over the o.d. of the magnet to keep the magnet in compression under all extremes of rotational stress and temperature.

Samarium-cobalt magnets require a very high uniform magnetomotive force (greater than 30,000 oersteds) to achieve a fully charged condition. The relatively large diameter of the magnet used in the advanced motor presented problems in that conventional magnetization equipment was not capable of supplying the pulse energy necessary for magnetization. Present technology dictated that the magnet had to be made up from a number of smaller magnet sections. It was thought that magnetization of these individual smaller magnets prior to final assembly into the large disc would be a suitable procedure. Problems developed in working with these premagnetized pieces. There is an inherent high separating force between the separate pieces. Physical damage and partial demagnetization occurred during these assembly efforts.

A search revealed that equipment capable of providing a uniform field of sufficient energy to magnetize a complete magnet was available at MIT's Draper Laboratory. The magnet detail was therefore fabricated complete by the magnet vendor (Recoma Inc). AiResearch then assembled the protective surface plates and shrink sleeve and returned the assembly for magnetization. Draper Labs then successfully accomplished the magnetization.

Large magnetic forces are present when the magnet is brought near the rotor pole pieces. Rough calculations show that forces approaching 3600N (800 lbf) exist while the unit is being assembled. This represents a safety hazard to personnel as well as a danger to the integrity of the magnet (chipping and cracking is possible). Safe and successful assembly of the rotor was accomplished with the aid of special tooling. The magnet was first clamped firmly to an aluminum block. The first rotor pole piece was attached to an adapter that was held in place by the headstock of a vertical mill or other suitable machine. The table on the mill, holding the aluminum block and magnet, was then raised slowly until

TABLE 7.--PERMANENT MAGNET COMPARISON.

Property	Material		
	Samarium-Cobalt	Samarium-Cobalt	Strontium-Ferrite
Energy product, min, KJ/m <sup>3</sup> (MGO)	159 (20)	119 (15)	28 (3.5)
Residual induction, tesla (gauss)	0.90 (9000)	0.78 (7800)	0.385 (3850)
Coercive force, KA/m (oersted)	700 (8800)	600 (7600)	0.243 (3050)
Temperature coefficient, %/°C (%/°F)	-.044 (-.024)	-.044 (-.024)	-.190 (-.106)
Density, gm/cm <sup>3</sup> (lb/in. <sup>3</sup> )	8.2 (0.296)	8.2 (.296)	4.8 (.175)
Compressive strength, N/m <sup>2</sup> (psi)	3x10 <sup>8</sup> (43,500)	3x10 <sup>8</sup> (43,500)	1.5x10 <sup>9</sup> (215,000)
Approximate cost, \$/kg (\$/lb)	68.2 (150)	591 (130)	0.5 (1)
Cost per KJ, \$/KJ	17040	19470	381

ORIGINAL PAGE  
BLACK AND WHITE PHOTOGRAPH



F-37361

Figure 30.--Magnet to Side Plate Assembly Fixture.

the parts would mate, with the shaft tie bolt providing alignment. The magnet and pole piece ready for assembly are shown in fig. 37. The magnet/pole piece assembly was flipped over and screwed to the aluminum base as shown in fig. 38. The second rotor pole piece was attached to the adapter and again the mill table was raised until assembly was complete. The rotor was balanced to within 5.0 (10<sup>-5</sup>) N·m by bonding aluminum and steel plugs into axial holes in each rotor pole piece.

Final assembly.--For final assembly of the rotating machine, the rotor was partially disassembled. Index marks on the two pole pieces allowed the reassembled rotor to be in the same configuration as it was when balanced. The stator assembly was inserted between the pole pieces and then reassembled. The stator then "floated" in the air gap between the rotor poles. The total mechanical clearance was measured. End bells were installed and shims were added to center the stator between the poles. The end bells served to clamp the stator assembly in place and also contain the bearing inserts to position the rotor. The tie bolt was stretched hydraulically to a load of 31,100 N and the nuts were tightened. This also clamped the rotor assembly firmly together and also retained the drive spine adapter. Finally, a compression spring loads the rotor axially against the bearing shims to prevent the rotor from moving and rubbing the stator.

After the initial assembly of the proof-of-principle motor, it was found that there was insufficient running clearance between the rotor and stator. Since the stator assembly is nonrepairable, the rotor pole pieces were modified. Material was removed from the pole faces as well as the chamfered tips. This resulted in the successful assembly of the machine shown in fig. 39. Test data on this machine are presented later in the text.

### Motor Tests

Preliminary magnetic circuit tests.--Some preliminary tests of the magnetic circuit of the axipolar machine were conducted to compare the actual performance of the proof-of-principle machine with the performance predicted by the math model.

Fig. 40 shows the no-load waveform observed in a dynamic test where the rotor was turned at low speed (9.0 rad/s) with a pair of 19-turn coils connected in series and linking the pole flux as they would in the completed assembly. The fundamental component of no-load voltage predicted by the math model is 82.84 V, line-to-neutral (L-N) per pair of 20-turn coils in series, at 1466 rad/s. Comparison on the basis of peak-to-peak fundamental volt- per turn per Hertz shows that the actual effective flux linkage is 4.1 percent lower than predicted. Within the accuracy of the analyses, the test, and the magnetization of the magnet, this indicates that there is acceptable correlation between the math model and the hardware.

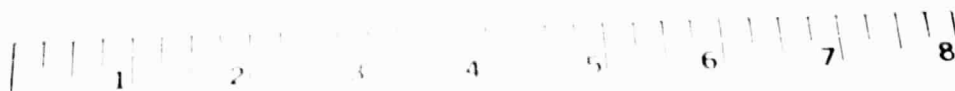
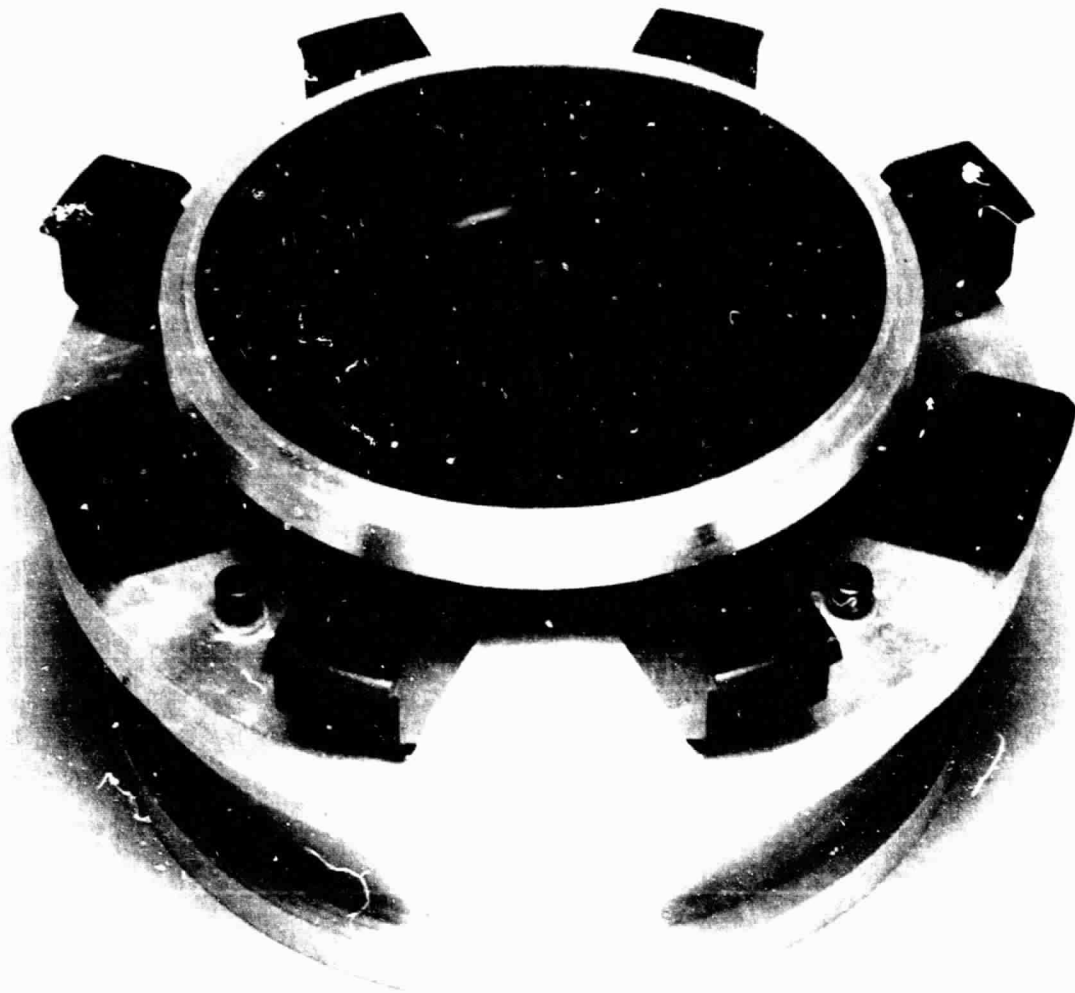
ORIGINAL PAGE  
BLACK AND WHITE PHOTOGRAPH



F.37362

Fig. 31. -- Motor Pole to Magnet Assembly Fixture.

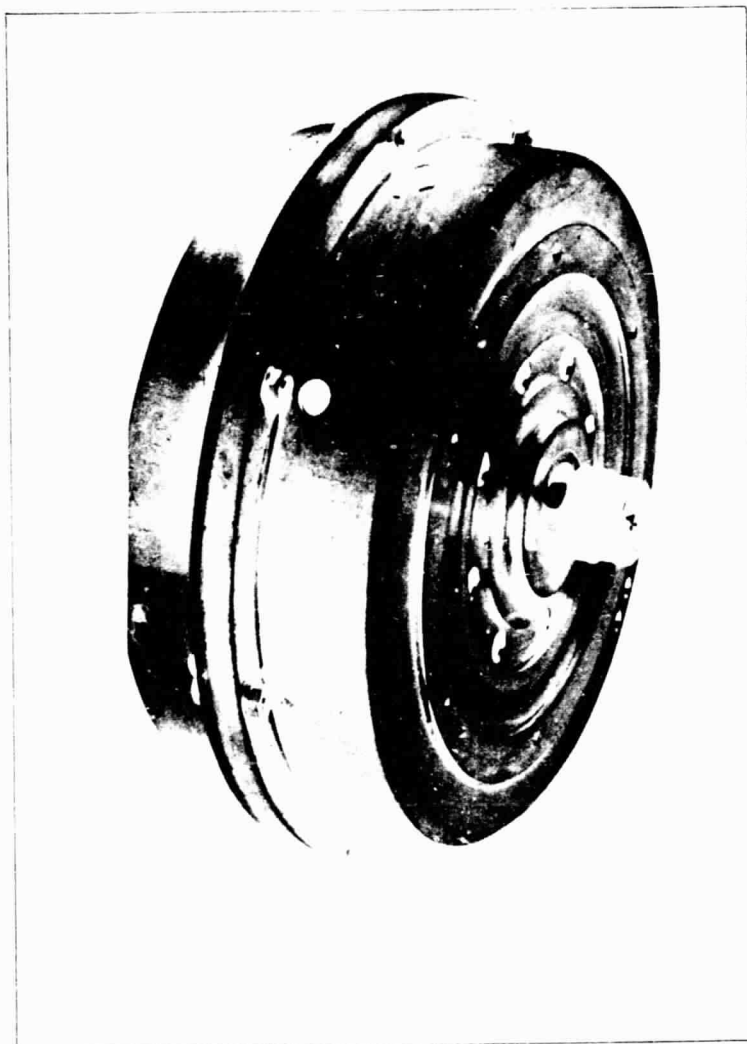
ORIGINAL PAGE  
BLACK AND WHITE PHOTOGRAPH



F-37363

FIGURE 36. Rotor Pole to Magnet Assembly Fixture.

ORIGINAL PAGE  
BLACK AND WHITE PHOTOGRAPH



F. 3/357

Figure 3.--Proof-of-Principle Motor.



ORIGINAL PAGE  
BLACK AND WHITE PHOTOGRAPH

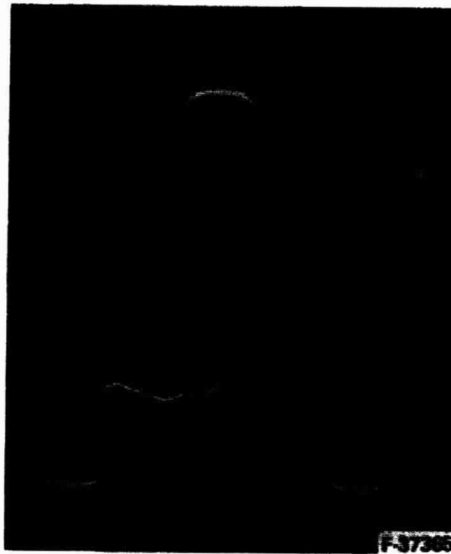


Figure 40.--No-load Voltage Waveform.

Vertical scale: 0.2 v/cm  
Horizontal scale: 20 ms/cm

NOTE:

2 series coils, 19 turns/coil

Winding factor,  $K_p \times K_d = 0.9225$

$V_{p-p} = 1.172 \text{ V}$  at 11.47 Hz

$V_{\text{fundamental, p-p}} = 1.31 \text{ V}$

$= 0.00301 \text{ V/turn/Hz, p-p}$

Math model prediction at no-load:

$82.84 V_{1-n, \text{fund}} \times 2 \times 2/40./1866.67$

$= 0.00314 \text{ V/turn/Hz, p-p}$

Per unit difference = -0.041 pu

F-37391

An independent test using a fluxmeter to read output of a single 20-turn coil when the rotor was rotated one pole pitch was conducted. The lowest flux linkage change measured was  $9.06 (10^{-3})$  Wb-turns. The effective flux swing per pole is therefore:

$$\phi = \text{Flux linkage change}/(\text{turns} \times \text{winding factor})$$

$$\phi = 9.06(10^{-3})/20 \times 0.9225 = 4.91(10^{-4}) \text{ Wb}$$

The value predicted by the math model at no-load is  $5.50(10^{-4})$  Wb

The per unit difference is:  $(4.91 - 5.50)/5.50 = -0.107$

It was not possible to obtain precisely repetitive readings from the flux meter. The highest value obtained was  $5.20 (10^{-4})$  Wb with a per unit difference of 0.055. This is more in line with the results observed in the dynamic test.

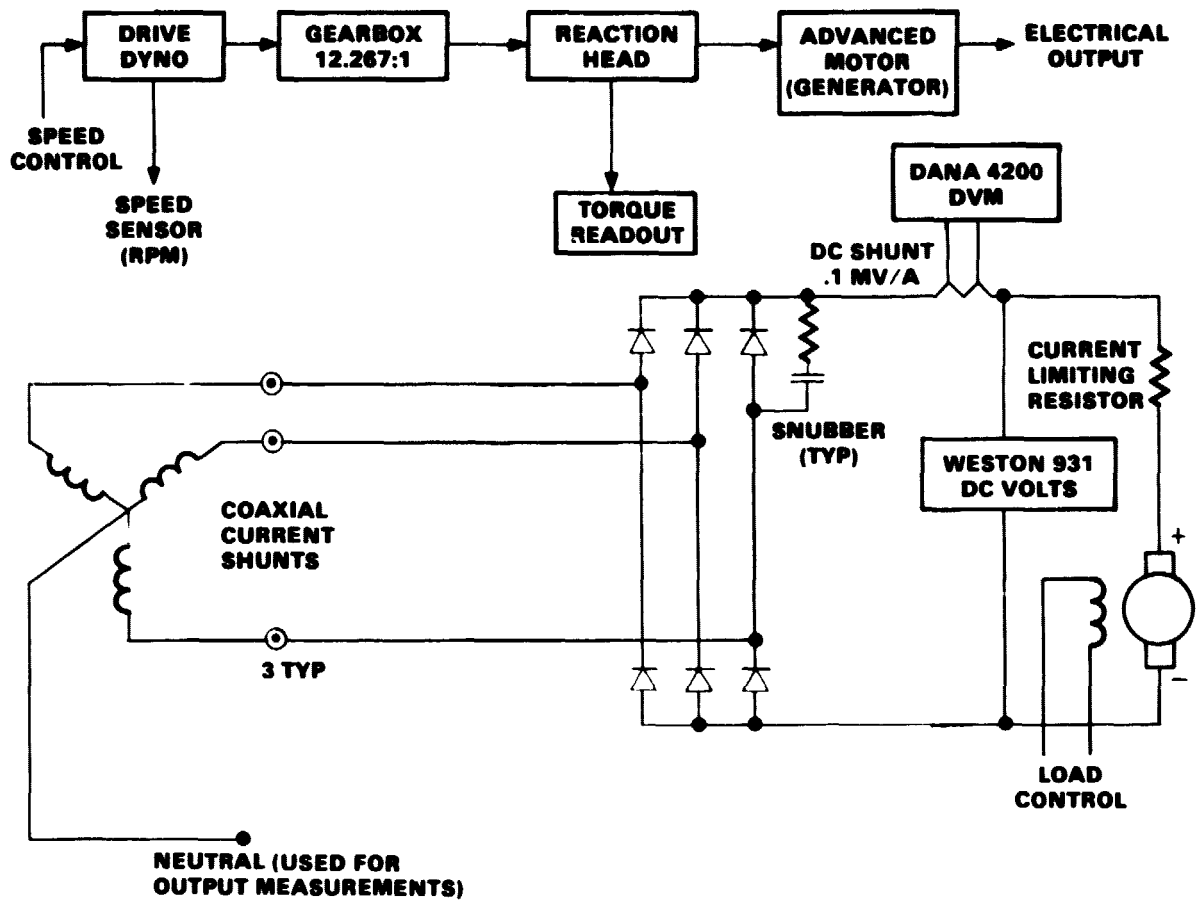
It is believed that the results of the dynamic test are more precise and more meaningful.

Low speed generator tests.--All testing of the proof-of-principle model was conducted by operating the machine as a generator. This approach eliminates the need for an electronic controller, but still provides significant data on the characteristics of the machine. The machine was mounted to a dynamometer through a gearbox and reaction-torque head. A reaction head between the dynamometer and the machine was used to measure the necessary drive torque. The electrical output from the generator was connected to a three-phase full-wave bridge rectifier, which converted the output from ac to dc. The dc output was connected through a load resistor to a bucking dc generator. The dynamometer is used to drive the proof-of-principle model to the desired speed and then the bucking generator is adjusted until the desired current is reached. Electrical parameters were monitored by the use of ac and dc voltmeters and ammeters. Torque was determined by measuring the force on the reaction head. Thermocouples were used to monitor temperatures of the winding, bearings, coil housing, and inlet and outlet air. A schematic of the test setup is shown in fig. 41.

Testing of the machine with the 19 turns per coil stator assembly was conducted up to 25 percent speed or 366 rad/s (3500 rpm) and 50 percent load current, or 70 A dc. As the speed was being raised to 50 percent, failure of the unit occurred at 702 rad/s (6700 rpm). The measured dc voltage versus dc current is plotted in fig. 42 along with the calculated curve for the 20 turns per coil machine and the estimated curve for the 19 turns per coil machine. It is seen that the regulation of the machine is quite close to the predicted value, but the no-load dc voltage is about 3.7 percent low. The precision of the electromagnetic analysis in predicting the basic flux level is therefore within the range generally achieved with permanent magnet machines on the first build.

Another important parameter of the machine that was measured was the commutating inductance of the winding. Evaluation at 25 percent speed and 25 percent load showed a commutation overlap angle of  $22^\circ$  versus the predicted value

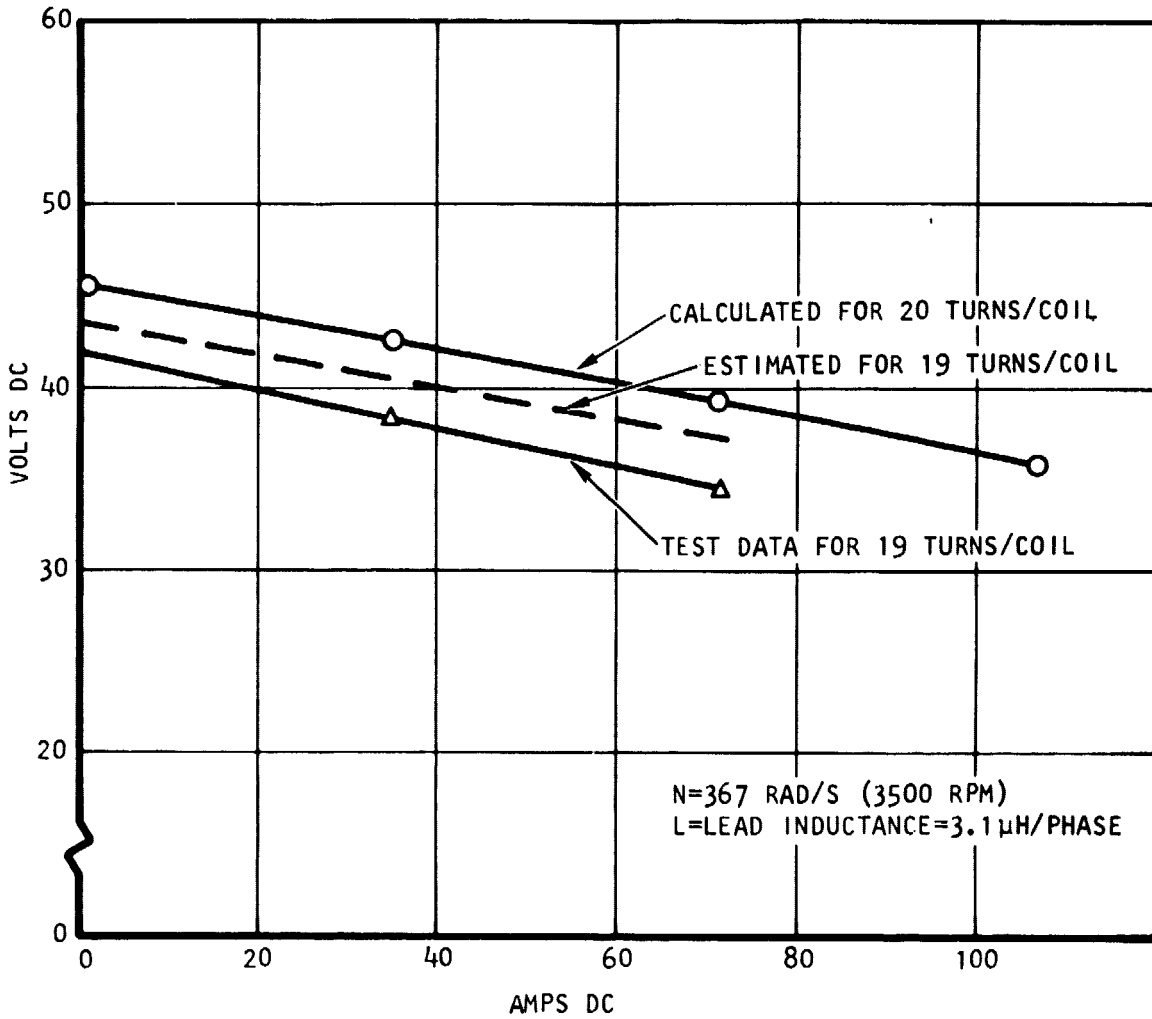
ORIGINAL PAGE IS  
OF POOR QUALITY



A-18558

Figure 41.--Advanced Motor Test Schematic.

ORIGINAL PAGE IS  
OF POOR QUALITY



A-32347

Figure 42.--Proof-of-Principle Dc-Load Regulation  
Curve at 25 Percent Speed.

of 160. This corresponds to a commutating inductance error of  $7.5 \mu\text{H}$ , with  $3.1 \mu\text{H}$  attributed to inductance of the lead wires in the test setup, a value not considered in the analysis. This parameter was evaluated further in later testing.

Fig. 43 shows the no-load losses of the system versus speed for various configurations:

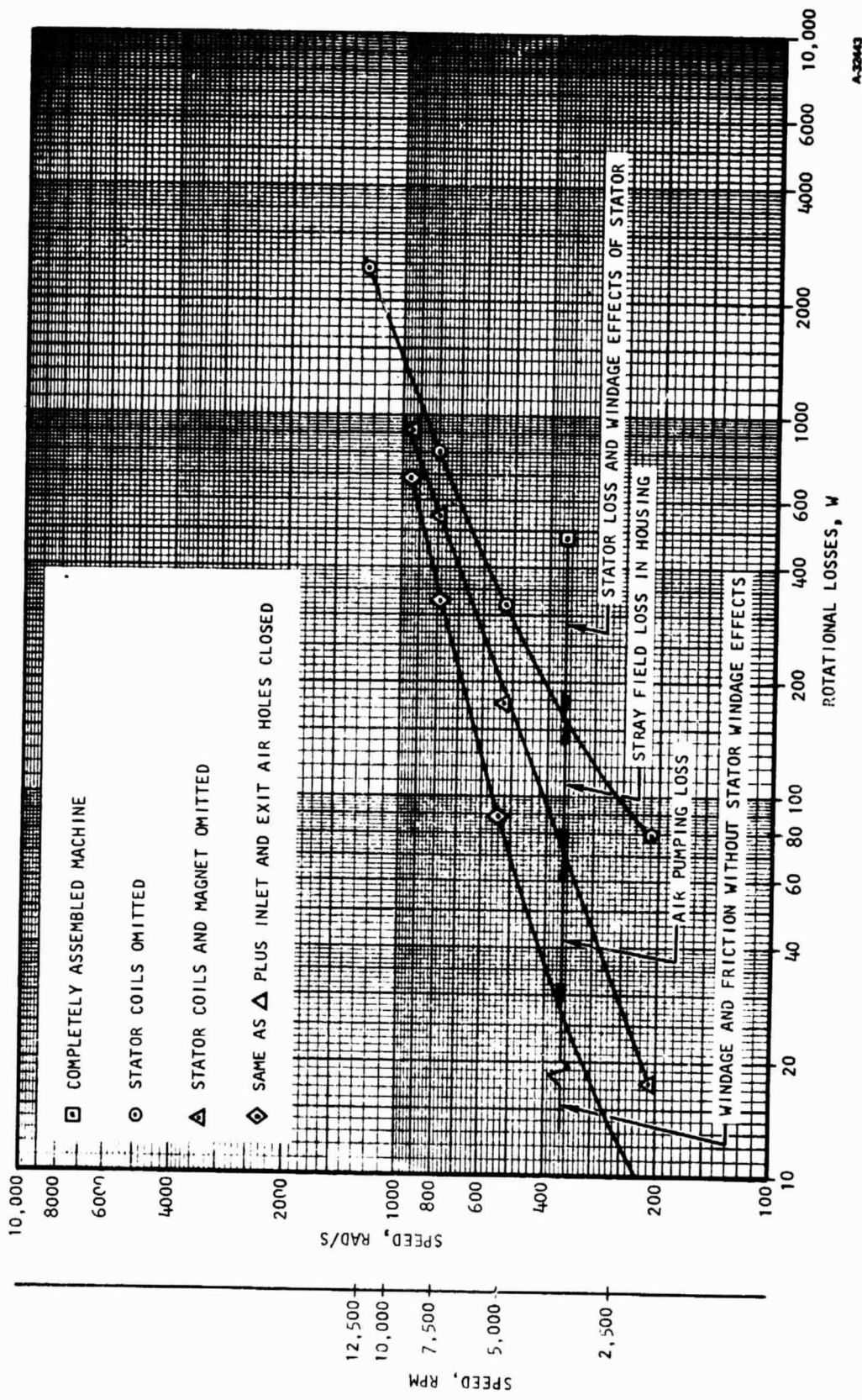
- (1) Complete assembly
- (2) Stator coils omitted to show only the losses due to windage, friction, and stray fields in the housing
- (3) Stator coils and magnet omitted to show losses due to windage and friction only, all air holes open
- (4) Same as (3) with air holes closed

The difference in the first two curves is due to circulating currents and eddy currents in the winding plus an indeterminate alteration of windage loss caused by the presence of coils in the air stream. The circulating current was likely due to a shorted turn or coil in the winding, ultimately causing the failure of the stator.

Full speed and load tests.--The construction of a new stator assembly with ML-coated conductors and 20 turns per coil resulted in testing of the proof-of-principle model to 100 percent speed and load, 1466 rad/s and 140 A dc, respectively. The laboratory test setup was the same as that used for initial testing (see fig. 41).

Ac and dc regulation at full speed is shown in fig. 44 along with the calculated values. Fig. 45 shows the regulation curves for 25 percent, 50 percent, 75 percent, and 100 percent speeds. These curves again show that the flux is low but full power would be possible with some increase in rated current. An attempt was made to verify the commutating reactance, but the bridge rectifier used diodes with a slow recovery time. This prevented the precise determination of the reactance. Faster rectifiers would be used during later testing of the functional model.

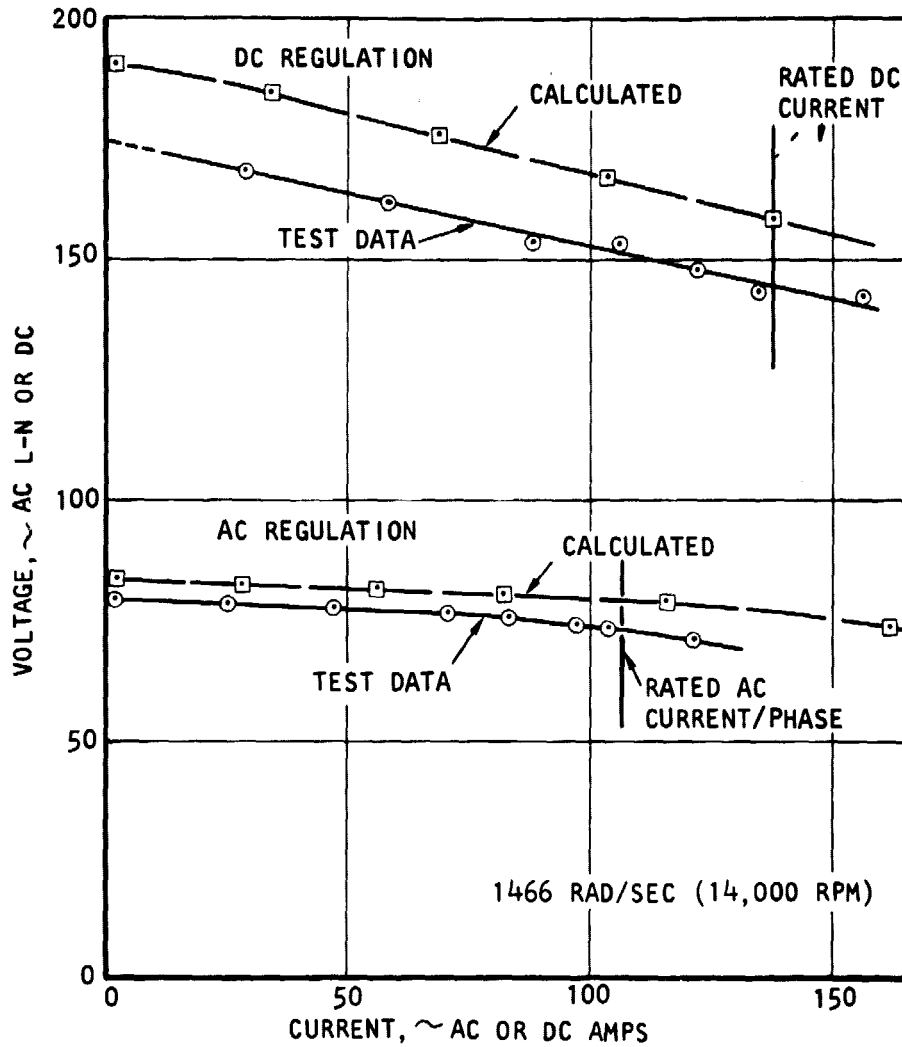
Thermal characteristics of the proof-of-principle model are shown in figs. 46 and 47. Fig. 46 shows that the stator assembly is capable of continuous operation at full current, with a resulting steady-state copper temperature of  $106^\circ\text{C}$  when the rotor speed is 733 rad/s (7000 rpm). However, fig. 47 shows that when operated at 160 A at full speed, 1466 rad/s (14,000 rpm), the stator copper temperature rises very rapidly. This is due to the copper absorbing the heat generated from high windage losses rather than copper losses. The motor losses were evaluated for different motor configurations, as seen in fig. 48. The total rotational loss at 1466 rad/s (14,000 rpm) was approximately 5500 W, versus a predicted value of 750 W. The main components of this loss are windage and pumping of air, and eddy current losses in the housings due to penetration by the



A-32843

Figure 43. ---Proof-of-Principle Losses At No-Load versus Speed.

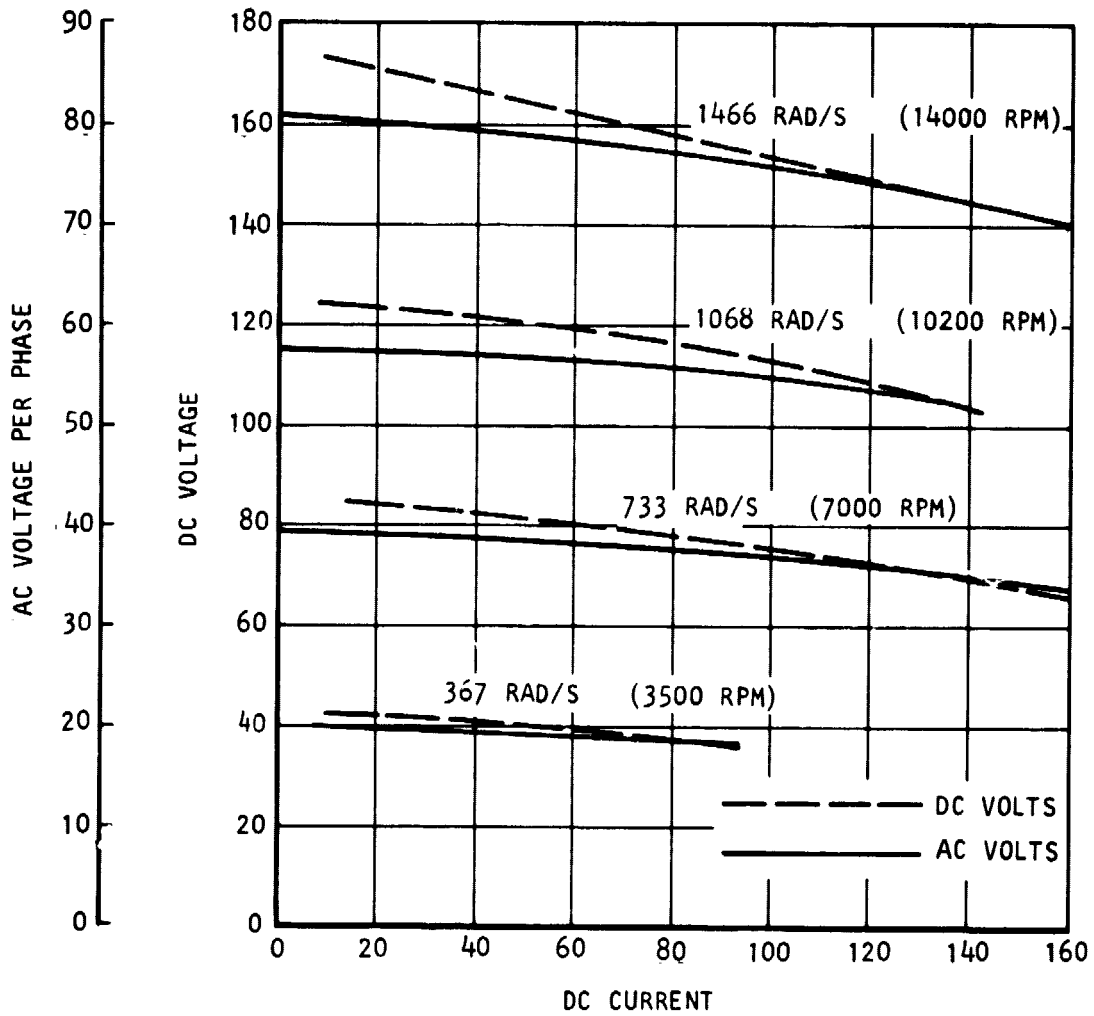
ORIGINAL PAGE IS  
OF POOR QUALITY



A-32420

Figure 44.--Proof-of-Principle dc and ac Load Regulation.

ORIGINAL PAGE IS  
OF POOR QUALITY



A-32419

Figure 45.--Proof-of-Principle ac and dc Load Regulation at Various Speeds.



ORIGINAL PAGE IS  
OF POOR QUALITY

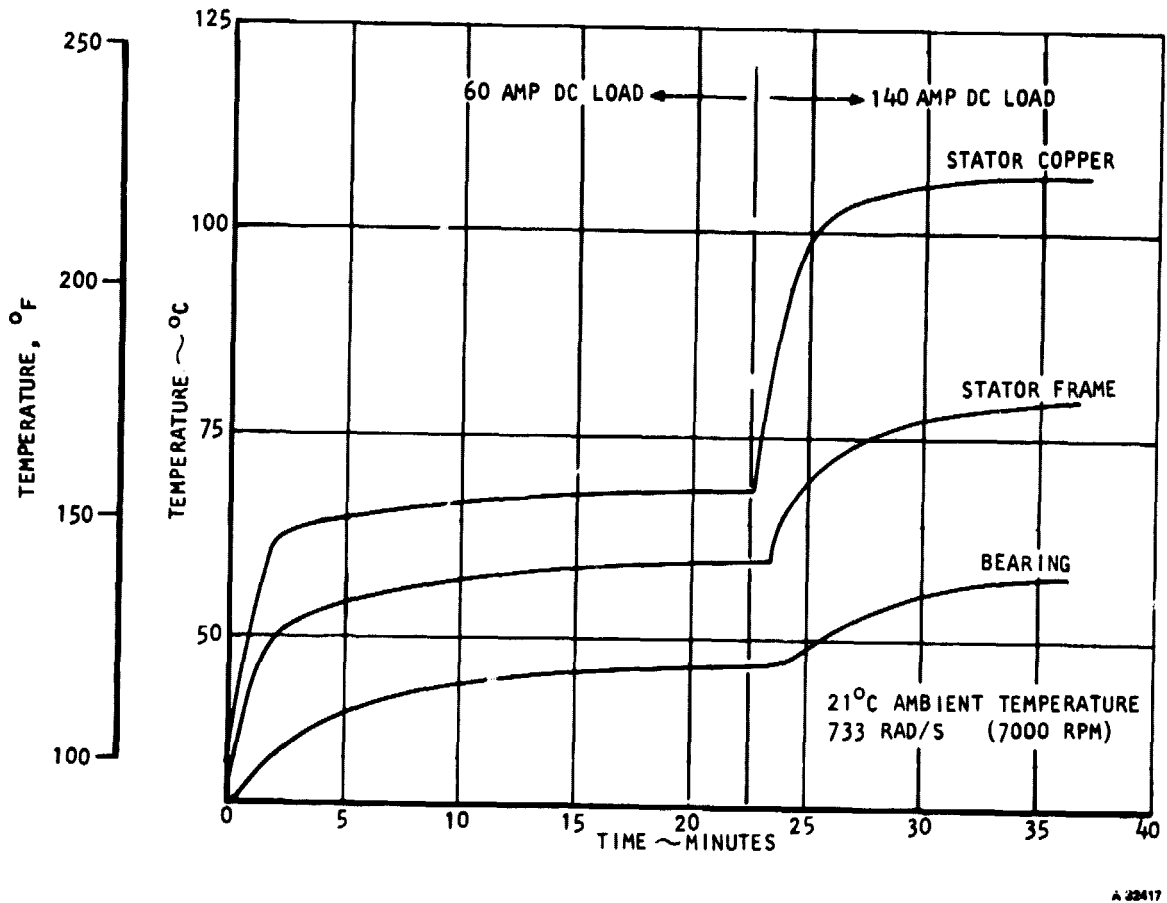
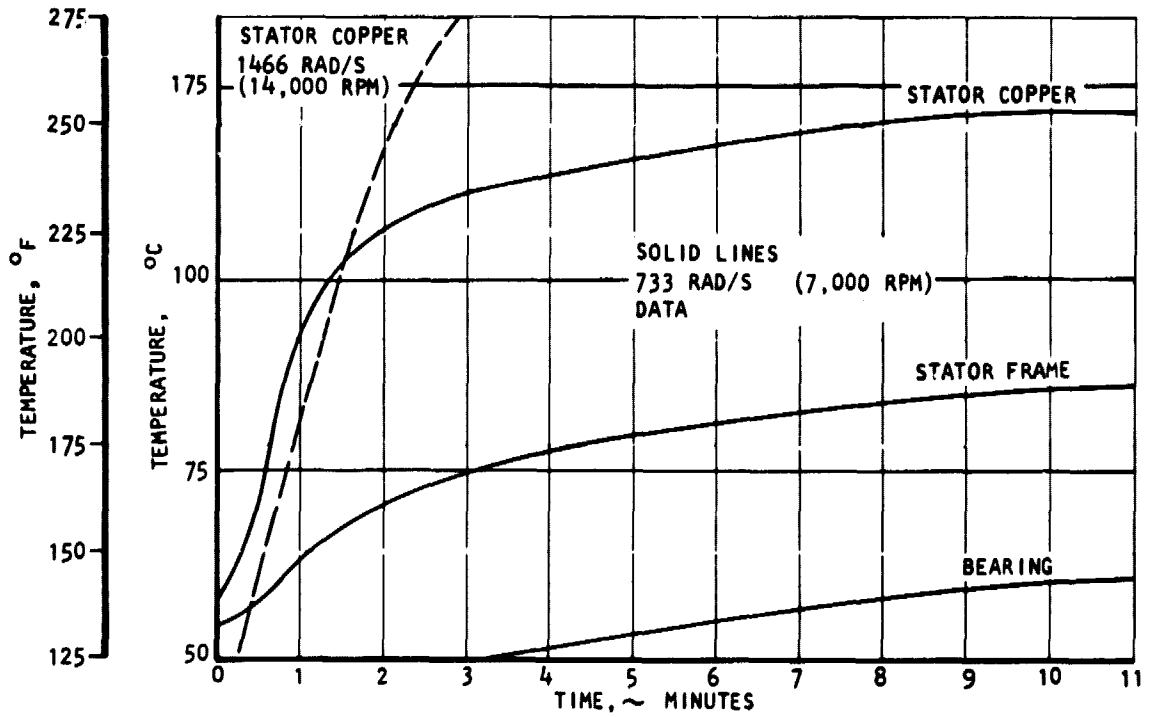


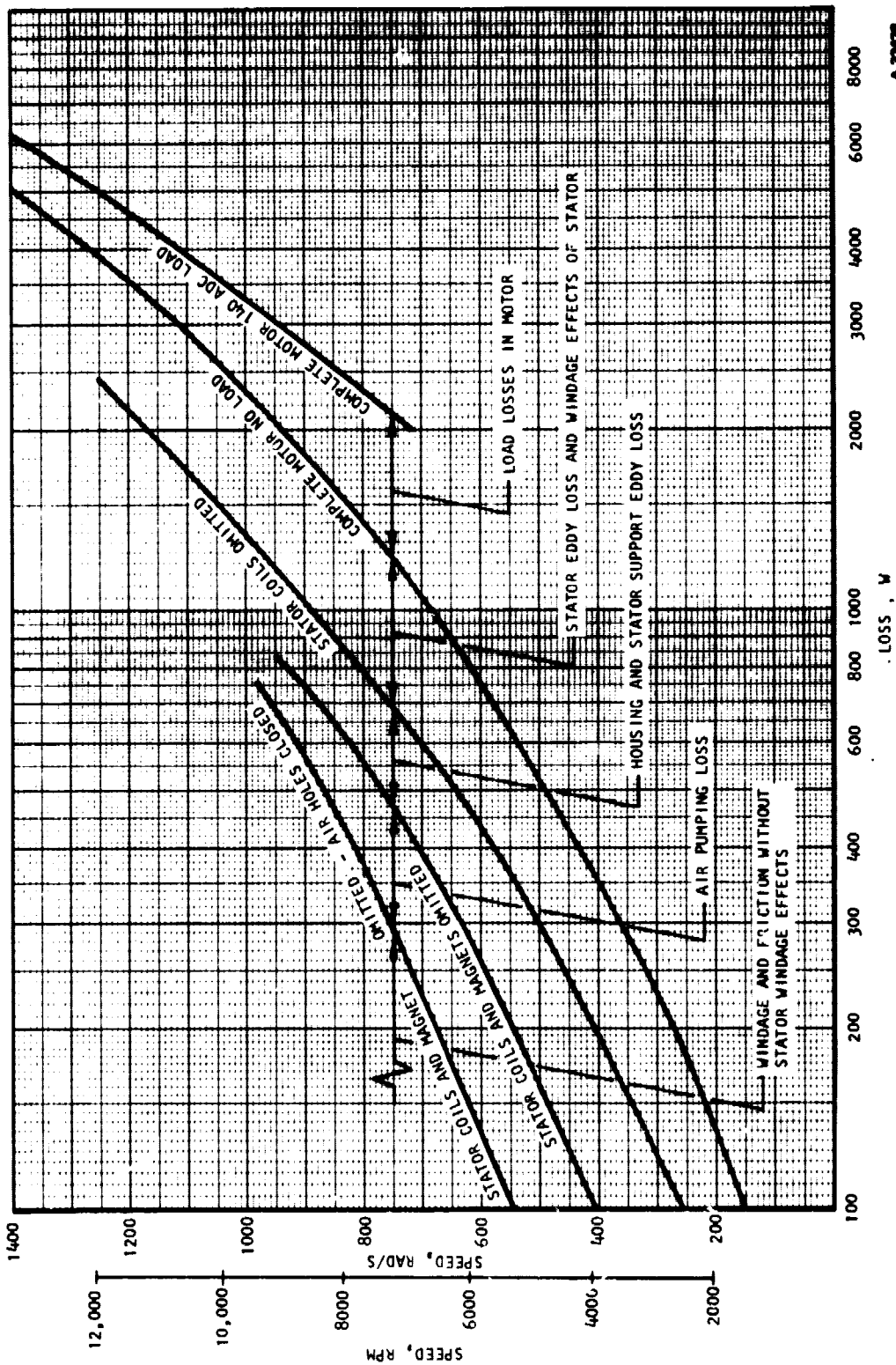
Figure 46.--Proof-of-Principle Thermal Performance at 50 Percent Speed.

ORIGINAL PAGE IS  
OF POOR QUALITY



A-32418

Figure 47.--Proof-of-Principle Thermal Performance at 160 A dc.



A-3842B

Figure 48.---Proof-of-Principle Loss Evaluation Measurements.

stray magnetic field of the rotor. Fig. 49 shows how the losses are distributed in comparison with the total predicted motor loss. The effect on efficiency is shown in fig. 50; at full speed and full current, the generator efficiency is only 75 percent as compared to a predicted value of 91 percent. In addition, the audio noise level exhibited by the machine was excessive from a subjective point of view. Efforts will be made to reduce this effect and measurements will be made during testing.

In summary:

- Power output of 26 kVA, 22 kW at 1466 rad/s (14,000 rpm) was demonstrated.
- The stator assembly demonstrated continuous operation at 160 A dc, with minimum thermal distortion and no structural damage.
- Total rotational losses were approximately 5500 W, compared with approximately 750 W predicted.
- The windage and housing eddy current components of this loss were addressed in the functional model design.
- Audio noise level of the machine was excessive and was also addressed in the functional model design.
- The commutation reactance of the machine was not fully determined and was measured more accurately during functional model test.

ORIGINAL PAGE IS  
OF POOR QUALITY

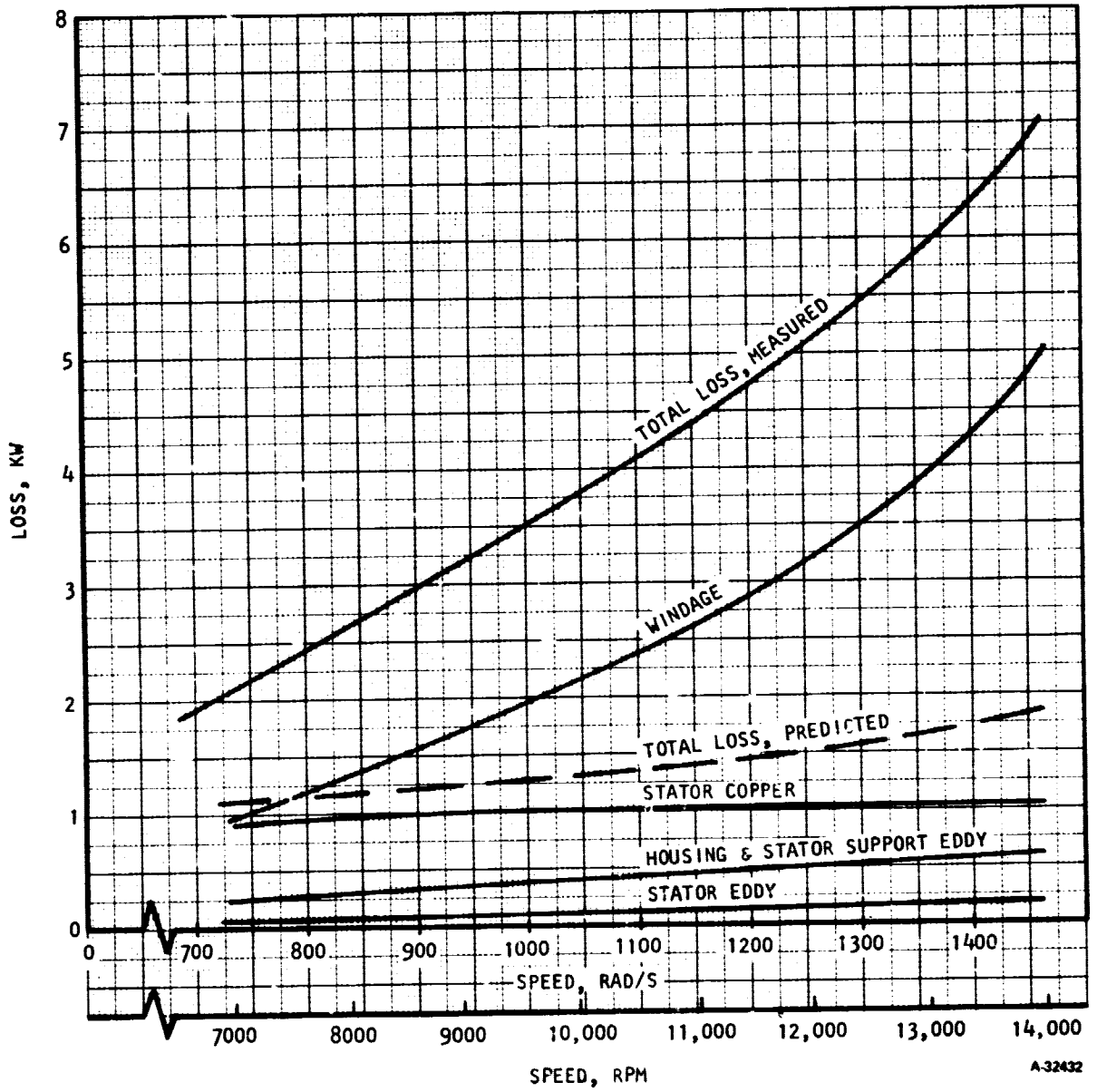
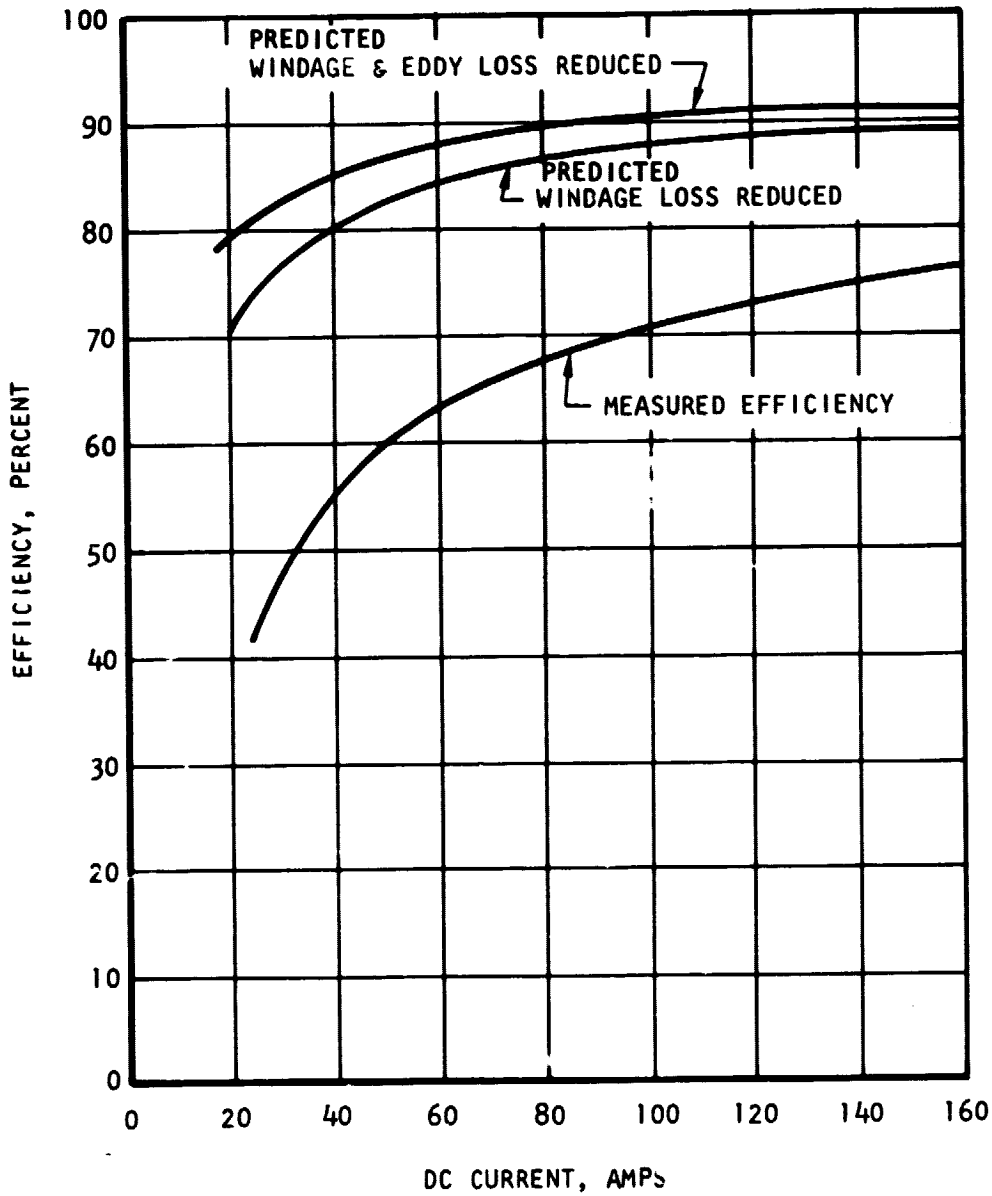


Figure 49.--Proof-of-Principle Loss Separation at 140 A dc Load.

ORIGINAL PAGE IS  
OF POOR QUALITY



A-32499

Figure 50.--Proof-of-Principle Efficiency versus Load  
at 100 Percent Speed 1466 rad/s (1400 rpm).

## FUNCTIONAL MODEL MOTOR DEVELOPMENT

Windage tests.--Due to the large rotational loss measured on the proof-of-principle model, an analytical review of the design was conducted with the aerodynamic and thermal groups. The goal was to determine the nature of the windage loss, the minimum possible loss for the configuration under ideal conditions, a realistic goal for minimum loss with actual hardware, and the thermal impact of the proposed change in configuration.

Aerodynamic analysis of a solid disk with the dimensions of the shrouded rotor, including the rim, results in a calculated windage loss of 465 W at 100 percent speed. An additional loss of 100 W can be attributed to the movement of the rotor past the stator. A flow of air sufficient to reject 1000 W of heat with a temperature rise of 85°C (necessary to cool the stator) would increase the shrouded disk loss by approximately 60 percent. Therefore, the minimum loss possible for the general machine configuration would be roughly:

$$1.6 \times 465 + 100 = 800 \text{ W}$$

However, the rotor saliency would be expected to greatly increase this loss. Tests of a shrouded radial wheel gave windage losses about six times the loss of a solid disk. Therefore, a reasonable loss for the actual configuration would be:

$$6 \times 1.6 \times 465 + 100 = 4564 \text{ W}$$

The actual loss measured on the proof-of-principle model confirms this analysis, and it can be seen that a significant improvement could be made by eliminating the saliency of the rotor assembly. A series of tests were conducted to further identify methods of windage loss reduction and quantify the potential improvement.

These tests were conducted by driving the proof-of-principle machine to a given speed by a dynamometer and measuring the torque necessary to accomplish this. The product of the torque and speed is power, which was then plotted graphically against speed. In addition, an audio sound level meter was used to measure the noise level seen with each configuration. A picture of the machine under test is shown in fig. 51 with the sound level meter in the foreground. The first configuration tested was with the stator assembly completely removed and with an aluminum disk replacing the magnet. The loss measured represents the windage loss of the rotor itself and the pumping loss due to airflow. This was repeated with the inlet and exit air holes closed to eliminate the air pumping component. A dummy stator was machined out of aluminum to simulate the "ideal" stator assembly, one with a completely smooth surface. This could be achieved with the real stator by encapsulating the assembly. Fig. 52 shows the dummy stator and magnet used during windage loss evaluation. Again, this test was repeated with the air holes closed.

ORIGINAL PAGE  
BLACK AND WHITE PHOTOGRAPH

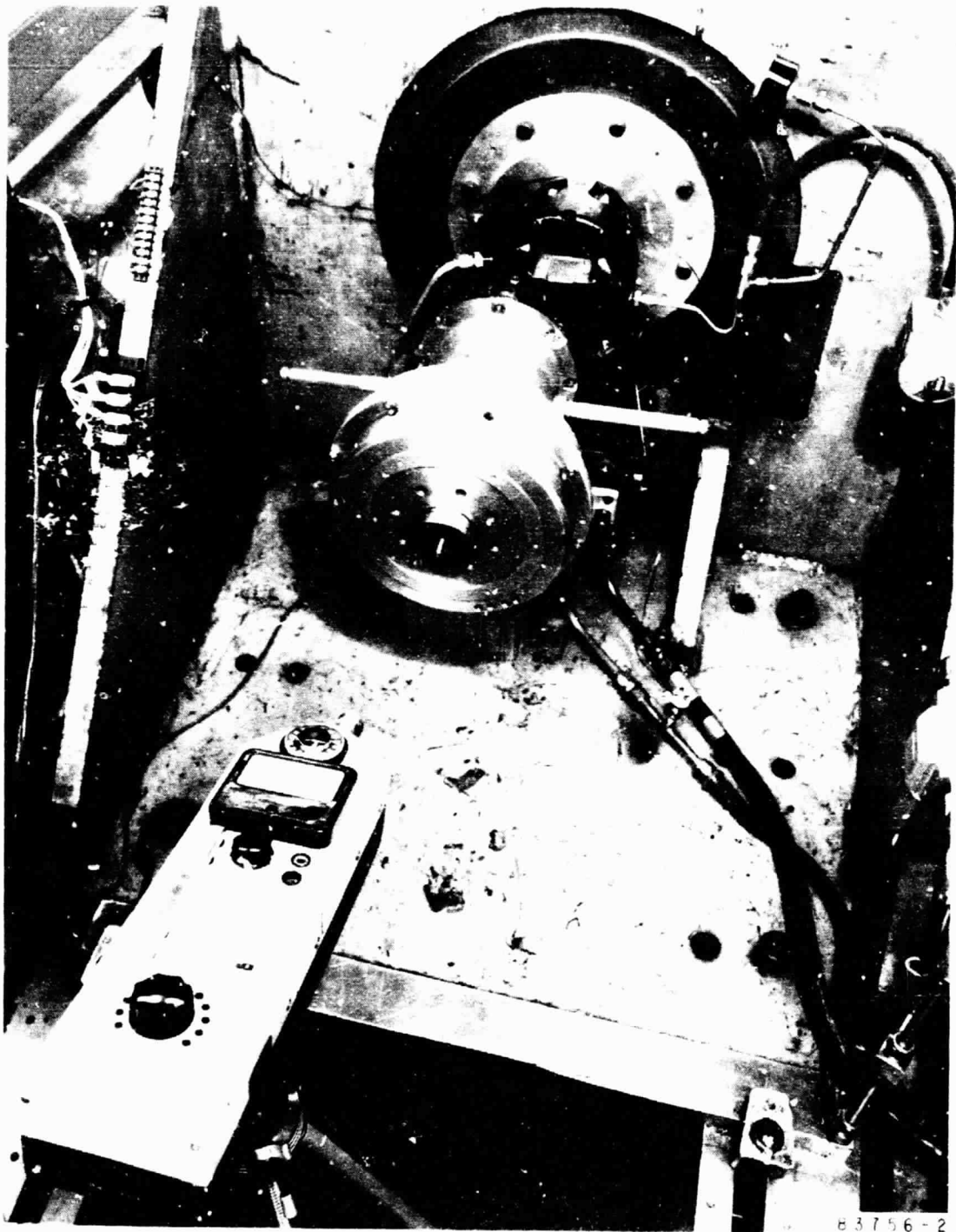
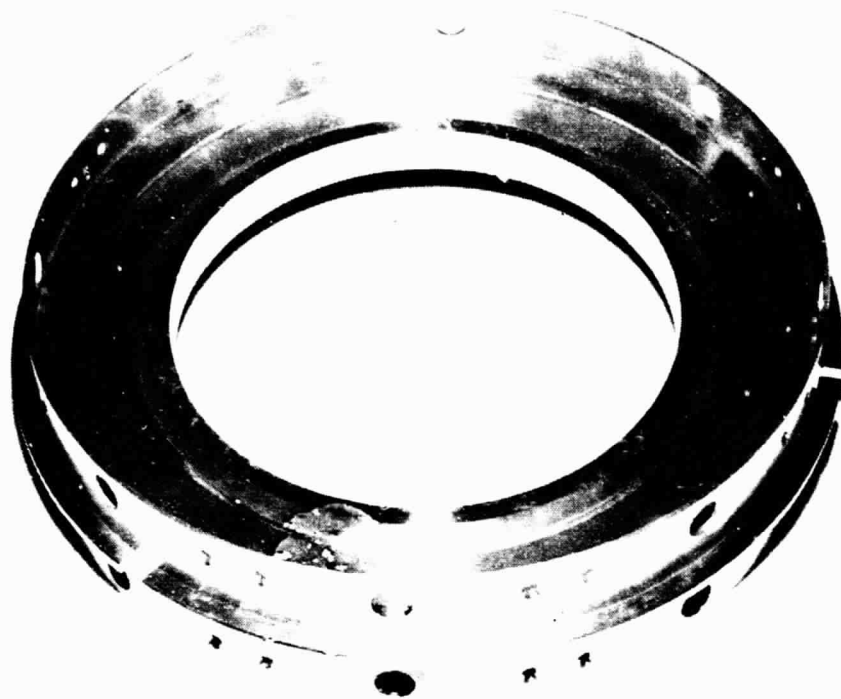


Figure 51.--Test Stand for Determining Rotational Loss.



REVERSE PAGE  
BLACK AND WHITE PHOTOGRAPH



83756-1

Figure 82.--Dummy Stator and Magnet.

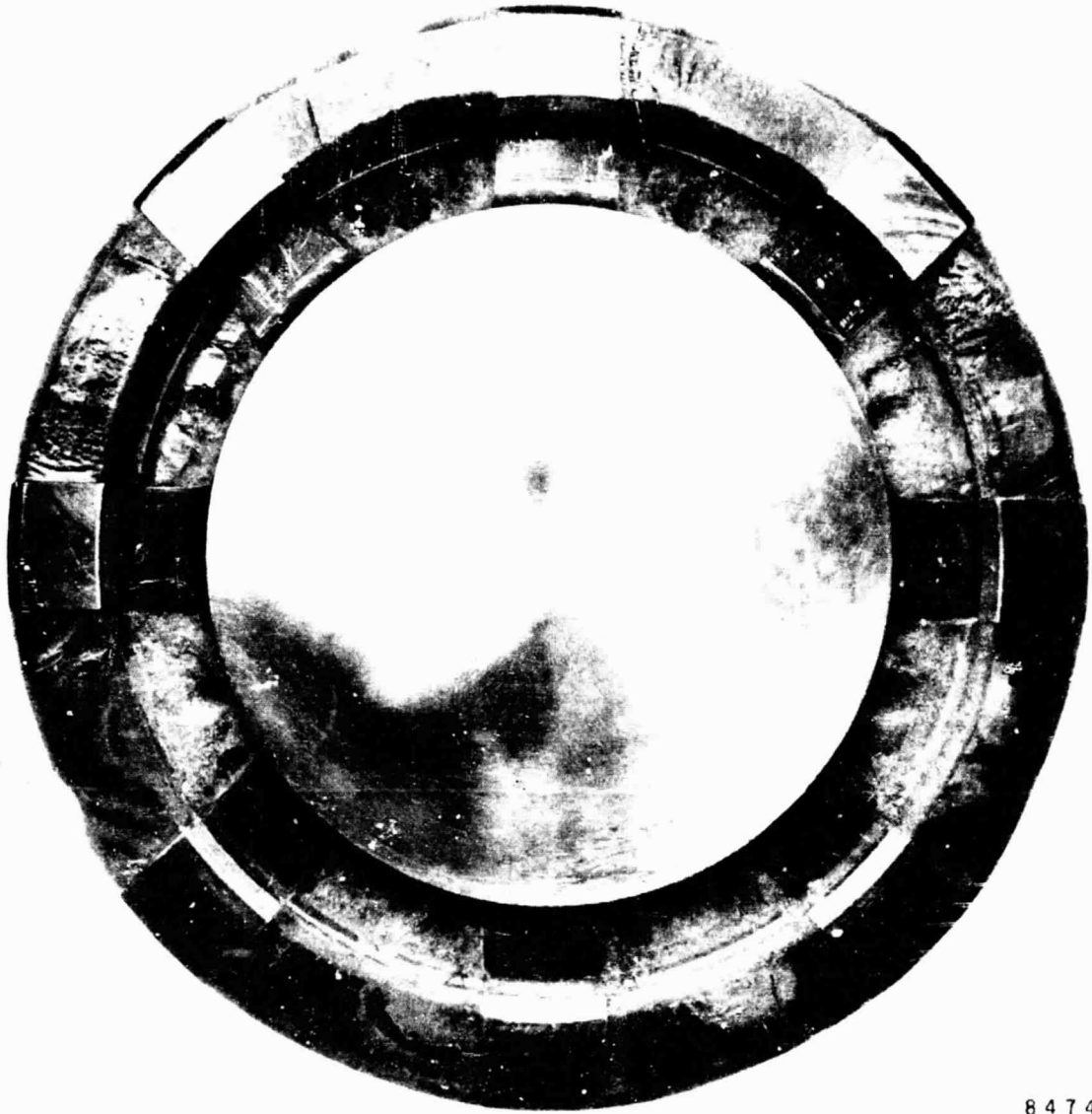
The next step involved elimination of the saliency of the rotor assembly by filling the interpoles with a light-weight material. A two-part polyurethane foam material, Stathane 6508, was used for the initial testing. This material has a  $128 \text{ kg/m}^3$  ( $8 \text{ lb/ft}^3$ ) nominal density for minimum weight increase. Some difficulties were encountered in trying to mold the chamfered pole tips and in achieving equal mold densities in the eight-rotor interpole areas. An acceptable configuration was completed, and is shown in fig. 53. Data were taken on this rotor with and without inlet and exit air holes open. Loss data for all the preceding configurations are shown in fig. 54, with the acoustical noise levels shown in fig. 55. Inspection of the loss data shows that the absolute minimum loss configuration tested uses a potted rotor, a smooth stator, a dummy magnet, and closed air holes. The loss at this condition is approximately 940 W. This, however, is not a realistically achievable loss for these reasons:

- (1) Some airflow is needed to cool the stator.
- (2) The airflow must be directed over the stator coils by drilling holes in the rotor interpoles.
- (3) The stator assembly cannot be made smooth without sacrifice of cooling capability.
- (4) The installation of the real magnet will cause additional eddy current losses in the stator and in the end bells of the motor.

Based on the results of these tests, three more configurations were tested. First, 8-mm-diam holes were drilled in the rotor interpoles to provide airflow directly over the stator coil area. Second, the aluminum end bells are spaced off from the rotor to minimize eddy current losses. This air space allows a pumping loss due to recirculation of the air. This area was filled with a nonmetallic material to reduce this loss. Finally, the effect of a non-smooth stator was evaluated by installing the actual stator assembly.

The results of these tests are best seen by inspection of table 8, which addresses the most significant configurations tested. Configuration A is the proof-of-principle data and represents the worst condition. Configuration B shows a significant benefit resulting from the use of a smooth stator when the rotor saliency exists. Configuration C is the equivalent of the proposed functional model design, with an actual stator and the potted interpoles with cooling holes added. Configuration D shows that the improvement in losses from using a smooth stator when the rotor saliency has been eliminated is minimal compared to the possible negative thermal effect. Configurations E and F have the least loss but do not provide adequate cooling for the stator. The loss with Configuration C of 2050 W is the goal for windage loss in the functional model to be built, and this would represent a loss reduction of approximately 3 kW over the proof-of-principle machine.

ORIGINAL PAGE  
BLACK AND WHITE PHOTOGRAPH



84748-1

Figure 53.--Polyurethane Rotor Encapsulation.

ORIGINAL PAGE  
BLACK AND WHITE PHOTOGRAPH

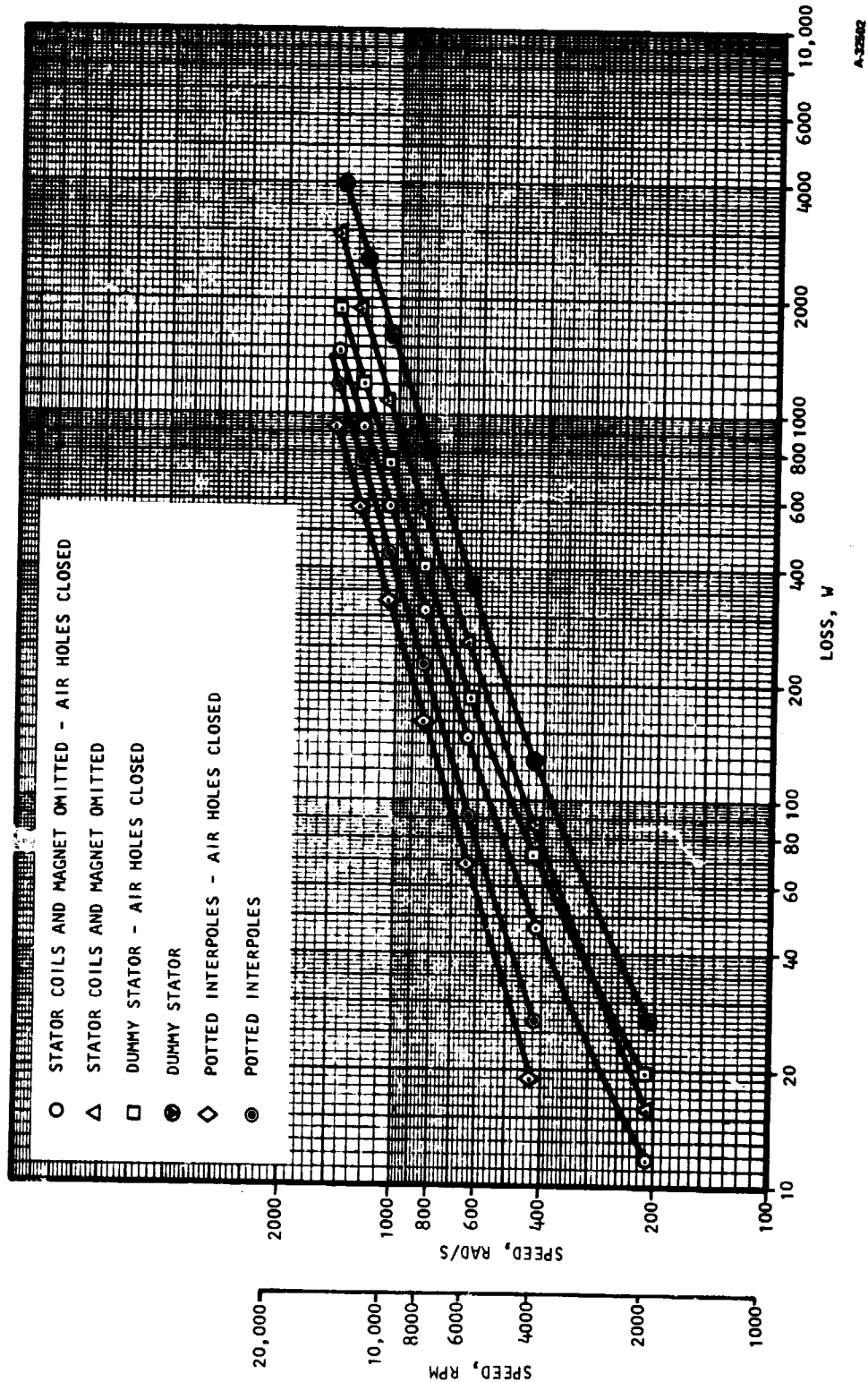


Figure 54.--Windage Losses versus Speed of Windage Evaluation Configurations.

A-32562

ORIGINAL PAGE 13  
OF POOR QUALITY

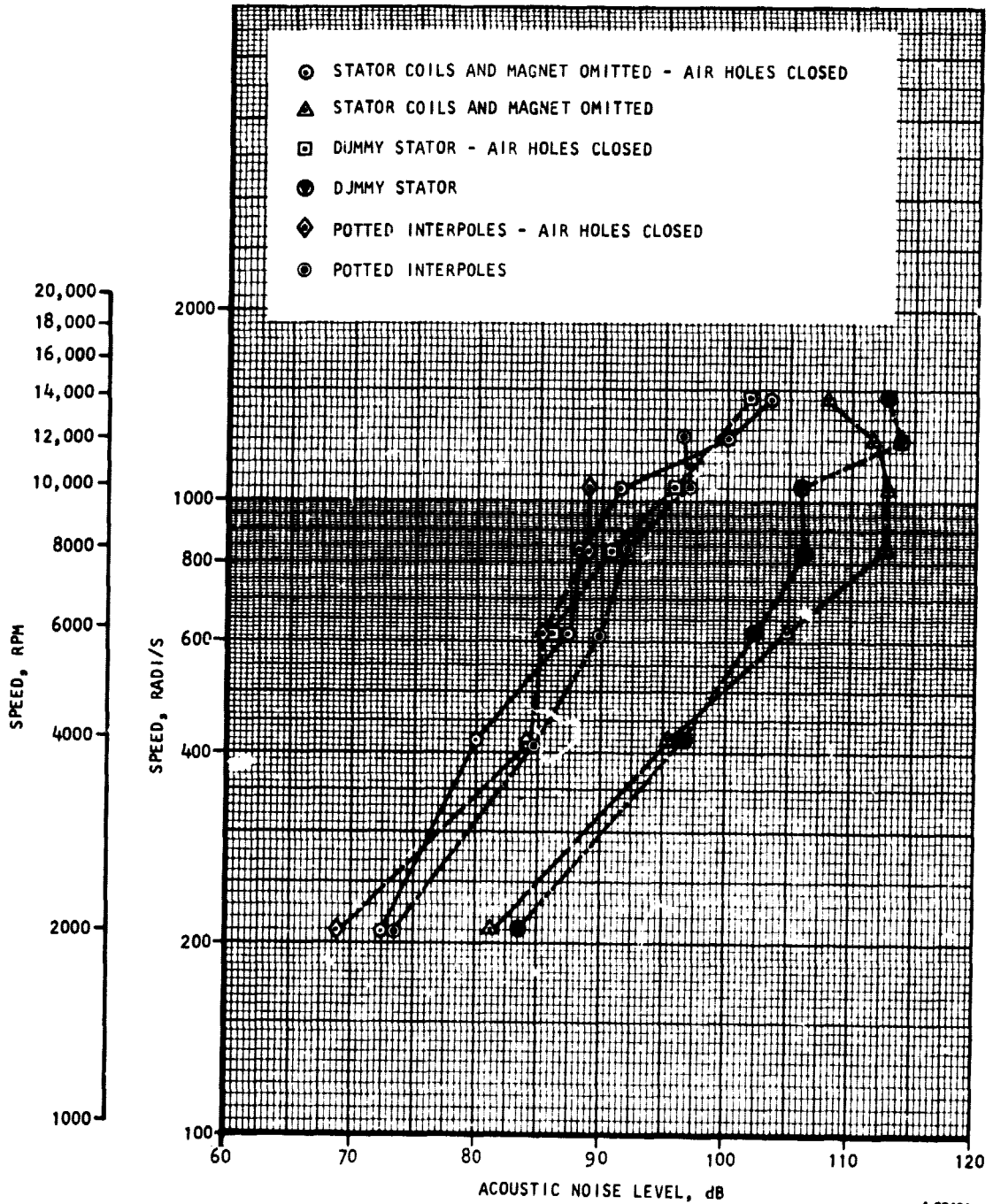


Figure 55.--Advanced Motor Windage Evaluation Configurations Acoustic Noise Level versus Speed.

TABLE 8.--WINDAGE LOSS TEST SUMMARY.

Motor Configuration	Windage loss, W	
	50 percent speed	100 percent speed
A. Actual strip copper-wound stator with no interpole fillers on rotor (proof-of-principle configuration)	910	5040
B. Smooth dummy aluminum stator with no interpole fillers on rotor	550	3950
C. Actual strip copper-wound stator with interpole filled and 8-mm cooling holes incorporated (functional model equivalent)	250	2050
D. Smooth dummy aluminum stator with interpoles filled and 8-mm cooling holes incorporated	240	1800
E. Smooth dummy aluminum stator with interpoles filled--no cooling holes	150	1180
F. Smooth dummy aluminum stator with interpoles filled--no cooling holes, closed housing	108	940

Magnetic circuit measurements.--Test results of the proof-of-principle model showed a significant rotational loss due to the presence of the magnet in the rotor. The mmf of the magnet causes a magnetic flux field distribution in the surrounding area according to the reluctance of the path. Most of the flux, therefore, travels through the iron rotor poles. However, it is unavoidable for some lines of flux to follow leakage paths through the surrounding air and perhaps other electrically conductive metal in the housing or end bells. When the rotor starts to rotate, these lines of flux move with respect to the housing and generate eddy current losses. The loss is a function of both the magnitude of the leakage flux and its rate of change (motor speed).

In the electromagnetic design of this machine, certain magnetic properties of the rotor iron were assumed. If, however, there was austenite in the iron, its magnetic reluctance would be higher than expected and cause more magnetic lines of flux to penetrate the housing and surrounding structures and create losses.

To determine some of the characteristics of the motor magnetic circuit, several search coils were installed in the unit. An excitation coil was made that simulates a permanent magnet in that it supplies mmf to the circuit. The advantage in using a wound excitation coil is that the mmf may be varied over a wide range, and a saturation curve may be plotted.

A schematic of the test setup is given in fig. 56. Pictures of the hardware test equipment are included as well. An excitation coil of 170 turns of No. 17 AWG wire was wound on a bobbin and installed between the rotor pole pieces. The i.d. of this coil is equivalent to the o.d. of the magnet that it simulates. A search coil on top of the excitation coil measures the total flux developed. Three search coils were wound around the rotor pole "fingers" at various points. An actual spare coil (fractional-pitched) from the stator assembly and a full-pitched coil were used to measure flux in the gap and between the poles. Pictures of the hardware under test are shown in figs. 57 and 58.

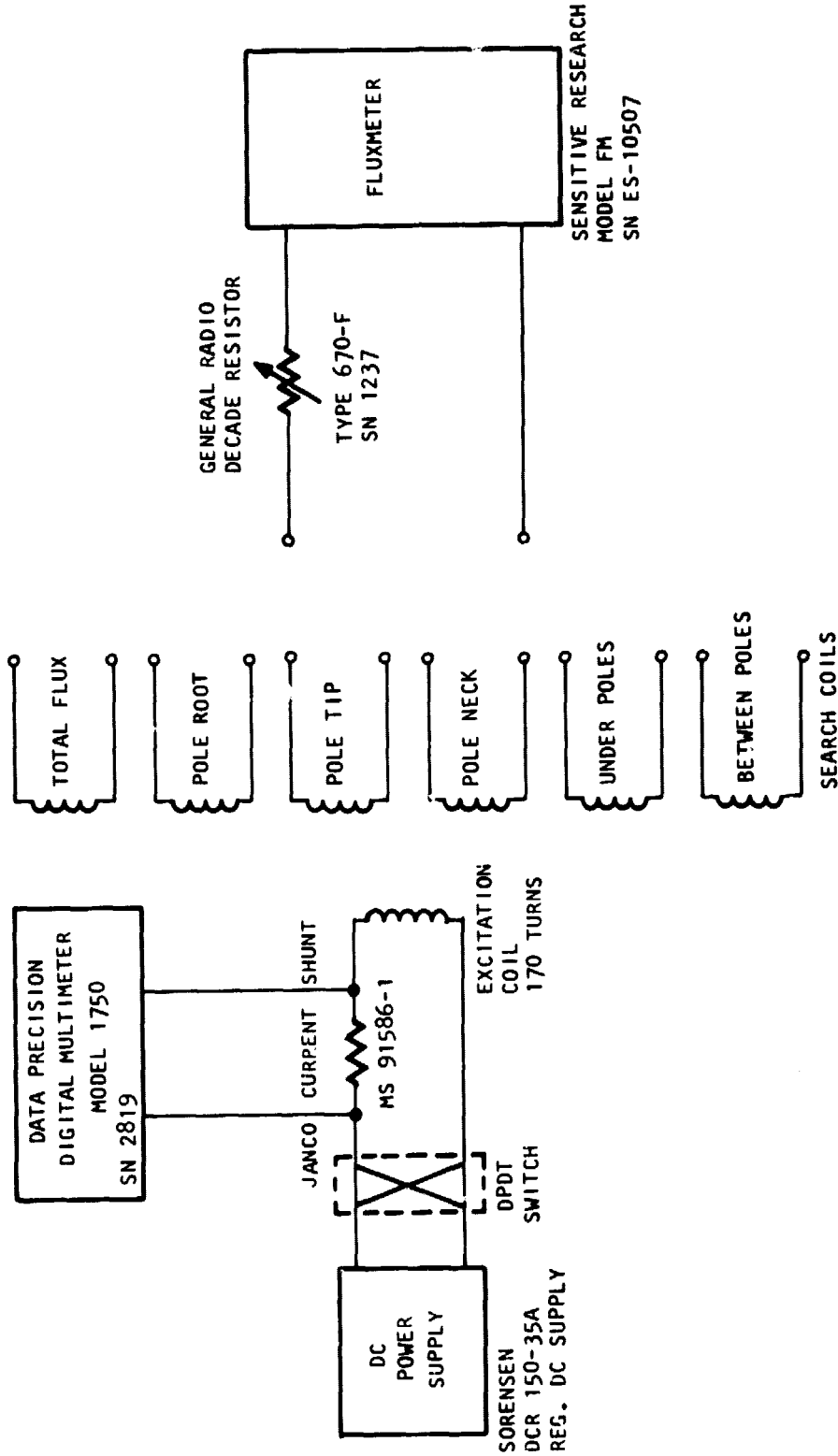
The excitation coil is supplied with current by a regulated dc power supply operated under current limit. A double-pole, double-throw switch allows a quick reversal of current in the coil. A current shunt and a digital voltmeter are used to measure the current. The search coils are connected, one at a time, to the variable resistance and the fluxmeter. The resistance is adjusted until the total resistance at the fluxmeter terminals is  $15 \pm 0.1 \Omega$ . This is a requirement for proper calibration of the fluxmeter. As the current in the excitation coil increases, the fluxmeter deflects a number of divisions proportional to the flux in the coil. The data were taken by quickly increasing the excitation current and recording this current and the deflection of the meter. The reversing switch was used to reverse the current and remove the remnant magnetism in the iron before proceeding to the next search coil. A summary of the test results is given in graphical form in fig. 59, which shows the number of lines of flux in each coil as a function of the mmf in the excitation coil:

$$\begin{aligned} \text{mmf} &= N_{\text{EXC}} I_{\text{EXC}} \\ &= 170 \times I_{\text{EXC}} \text{ A-turns} \end{aligned}$$

The flux in the excitation coil splits 8 ways into each pole "finger" so 1/8 of the total circuit flux is plotted first. The pole root and pole tip flux values are plotted next. These show that some leakage has occurred already. A full-pitched coil and a fractional-pitched coil are used to measure the flux in the gap and also between the poles. Additional data are shown with steel plates on each side of the rotor assembly, reducing the saliency of the external magnetic field. The use of the plates would attenuate any eddy current losses in surrounding support structures. Fig. 60 depicts some of the flux densities in key parts of the magnetic circuit.

The curves are essentially linear until the iron in the circuit starts to saturate. This effect becomes noticeable beyond about 2700 A-turns. Rated mmf net into the circuit is 3382 A-turns. At this point it is seen that the circuit is reaching saturation quickly. Two things can be concluded from this: (1) The flux density in the pole fingers at this point is 1.82 T indicating the proper material properties have been achieved, and (2) The higher than expected housing eddy loss is due to simplifications in modeling the rotor leakage field. A comparison of predicted versus measured values follows.

ORIGINAL PAGE IS  
OF POOR QUALITY



A-20287

Figure 56.--Advanced Motor Magnetic Circuit Test Diagram.

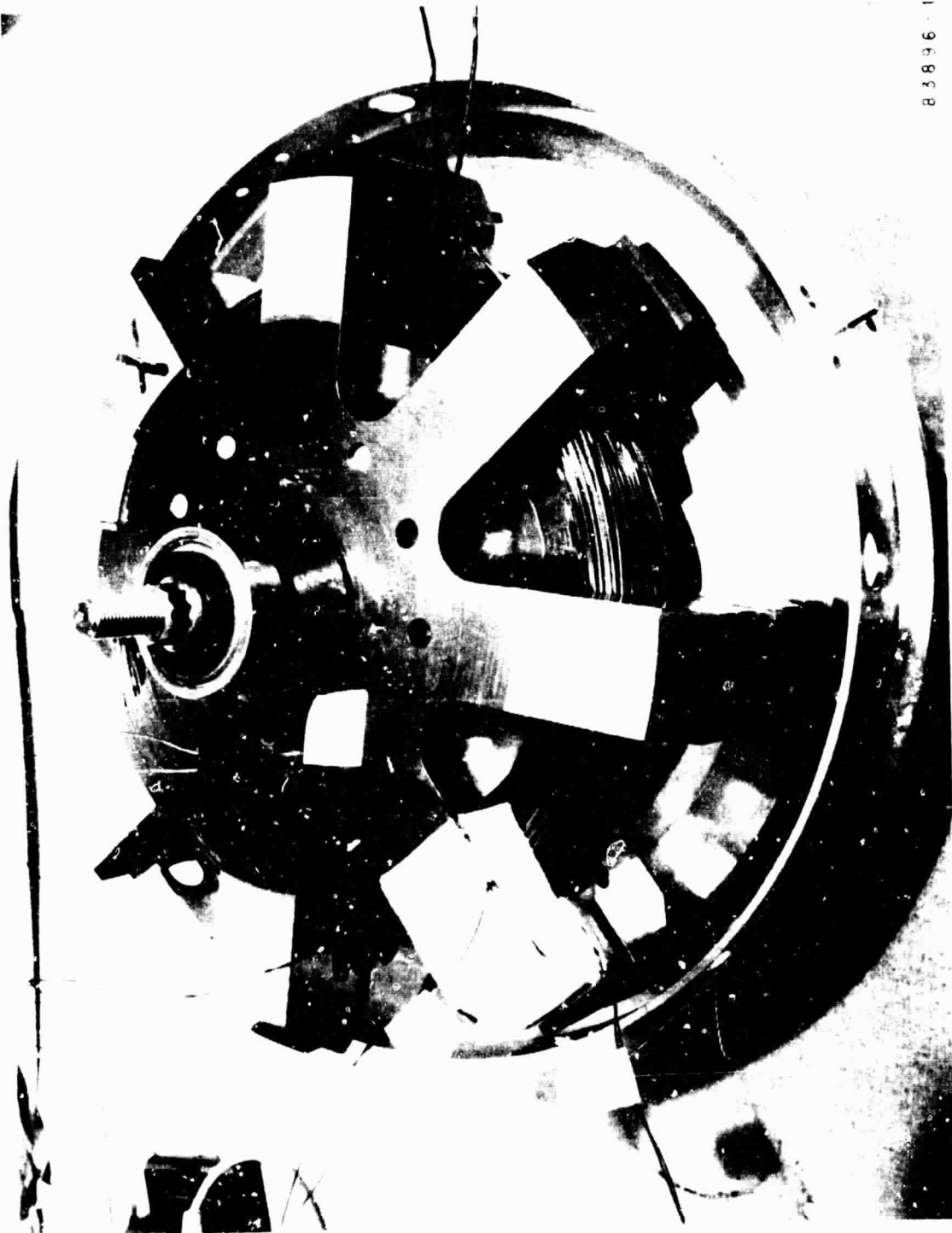


ORIGINAL PAGE  
BLACK AND WHITE PHOTOGRAPH



Figure 5/1.--Magnetic Circuit Test Setup.

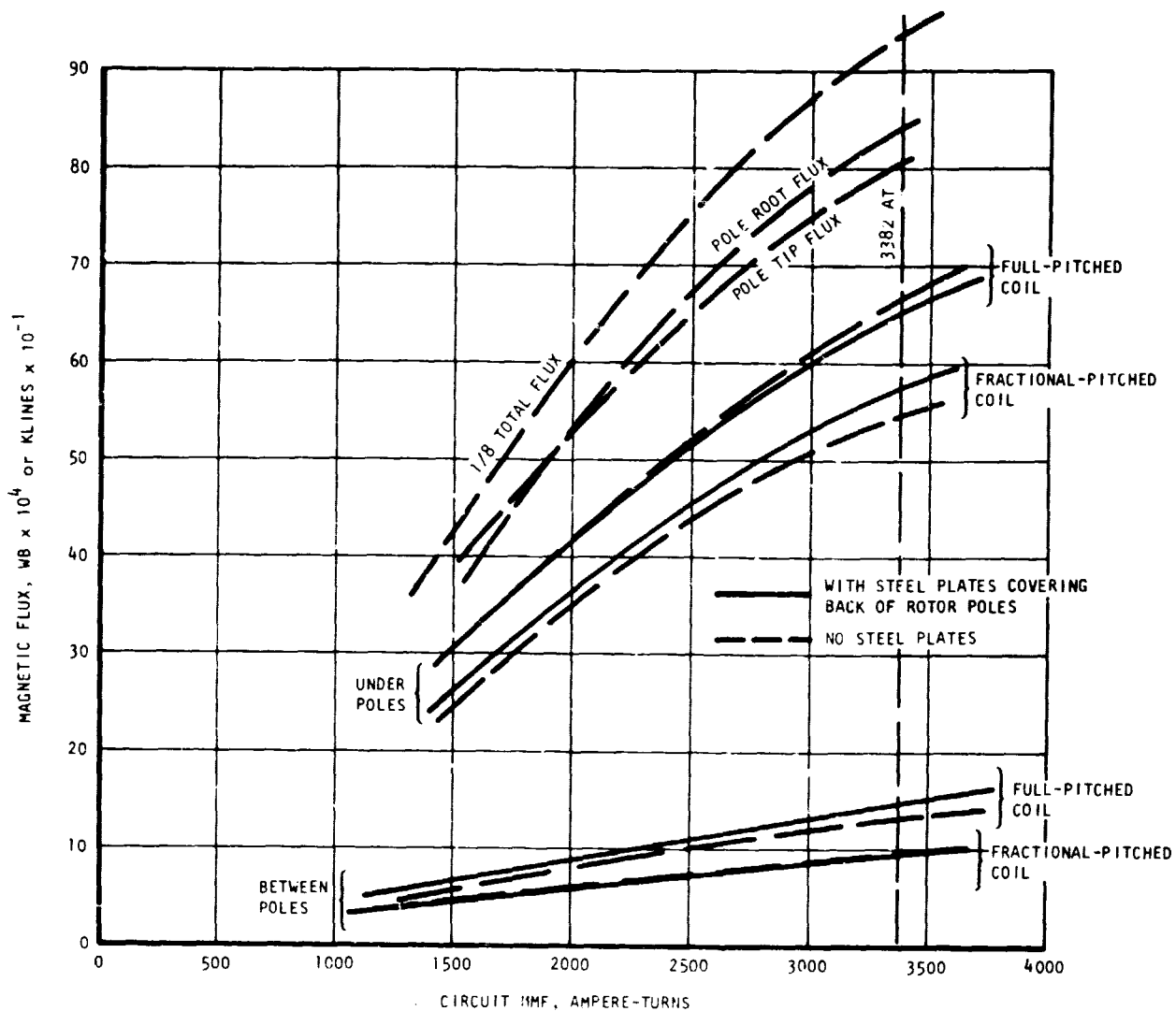
ORIGINAL PAGE IS  
OF POOR QUALITY



83896-1

Figure 58.--Advanced Motor Rotor Undergoing Magnetic Circuit Test.

ORIGINAL PAGE IS  
OF POOR QUALITY

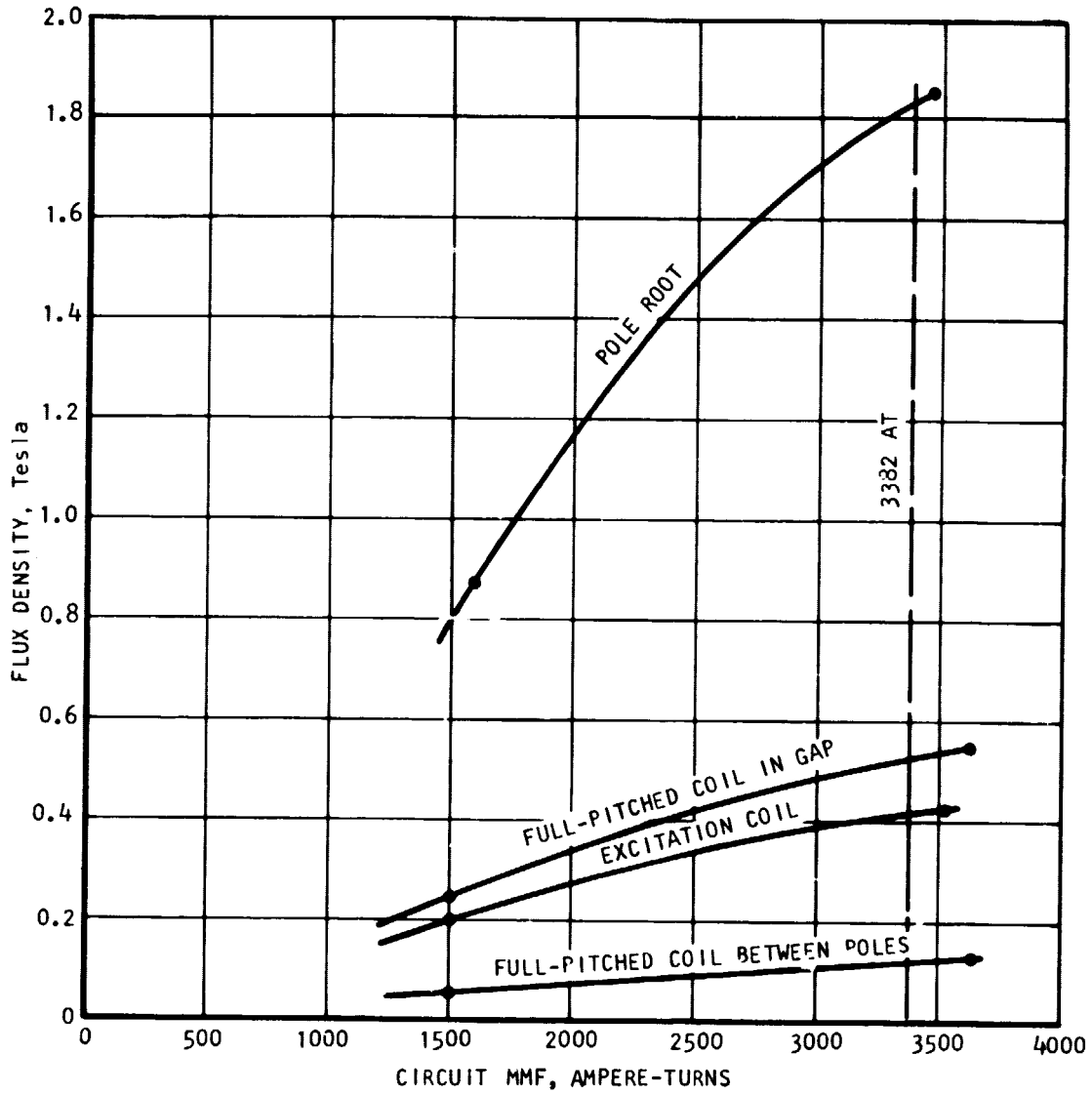


A-10810

Fig. 59.--Magnetic Circuit Flux Measurements. Magnet Simulated by Soft Iron Disk with Excitation Coil.

2

ORIGINAL PAGE IS  
OF POOR QUALITY



A-32366

Figure 60.--Magnetic Circuit Flux Density Measurements.

	Predicted	Measured
Net circuit mmf - (Ampere-turns)	3382	3382
1/8 of total flux - (Wb)	$84.5 \times 10^{-5}$	$93.5 \times 10^{-5}$
Static leakage - (Wb)	$19.5 \times 10^{-5}$	$13.0 \times 10^{-5}$
Active leakage - (Wb)	$6.1 \times 10^{-5}$	$14.5 \times 10^{-5}$
Flux per pole - (Wb)	$58.9 \times 10^{-5}$	$65.5 \times 10^{-5}$
Voltage generating flux - (Wb)	$52.8 \times 10^{-5}$	$51.0 \times 10^{-5}$

From this it is seen that for the given design point mmf, more total flux and more interpole leakage results. But the difference in these two is the voltage generating flux, and this number is quite close to the predicted value. It should be mentioned that the excitation coil does not exactly represent the permanent magnet disk. The coil itself is located in an area that is normally a leakage path for flux. The presence of the coil in this region reduces the leakage flux considerably. This may explain why the total flux is higher than predicted.

Stator assembly.--Disassembly of the proof-of-principle model after generator testing showed that some physical damage occurred to two of the stator coils and some other coil insulators. A picture of the damaged area is shown in fig. 61. This damage was unreparable; it was decided to build a new stator assembly with an improved insulation system and lower loss characteristics.

After the procurement of new ML-coated rectangular magnet wire, new stator coils were wound, varnished, and formed in the same way as was done for the proof-of-principle stator assembly. Figs. 62 and 63 show the individual coils being placed on the alignment tooling prior to bonding. At this stage, the assembly of the new stator departs from that previously used.

The coil support ring was fabricated from a phenolic material (MIL-P-15035C, Type FBE) because of its good dielectric and mechanical properties. The phenolic minimizes the eddy current losses from the stray magnetic field and also isolates the coil further from the metallic housing. This subassembly, prior to bonding on the i.d., is shown in fig. 64. New bus bar rings, insulators, and a new outer coil housing were made. The bus bars were made with increased cross section and with wire tabs brazed on to them to facilitate connection to the stator coils.

ORIGINAL PAGE IS  
OF POOR QUALITY



83596-2

Figure 51.--Delaged Proof-of-Principle Stator Assembly.

ORIGINAL PAGE IS  
OF POOR QUALITY

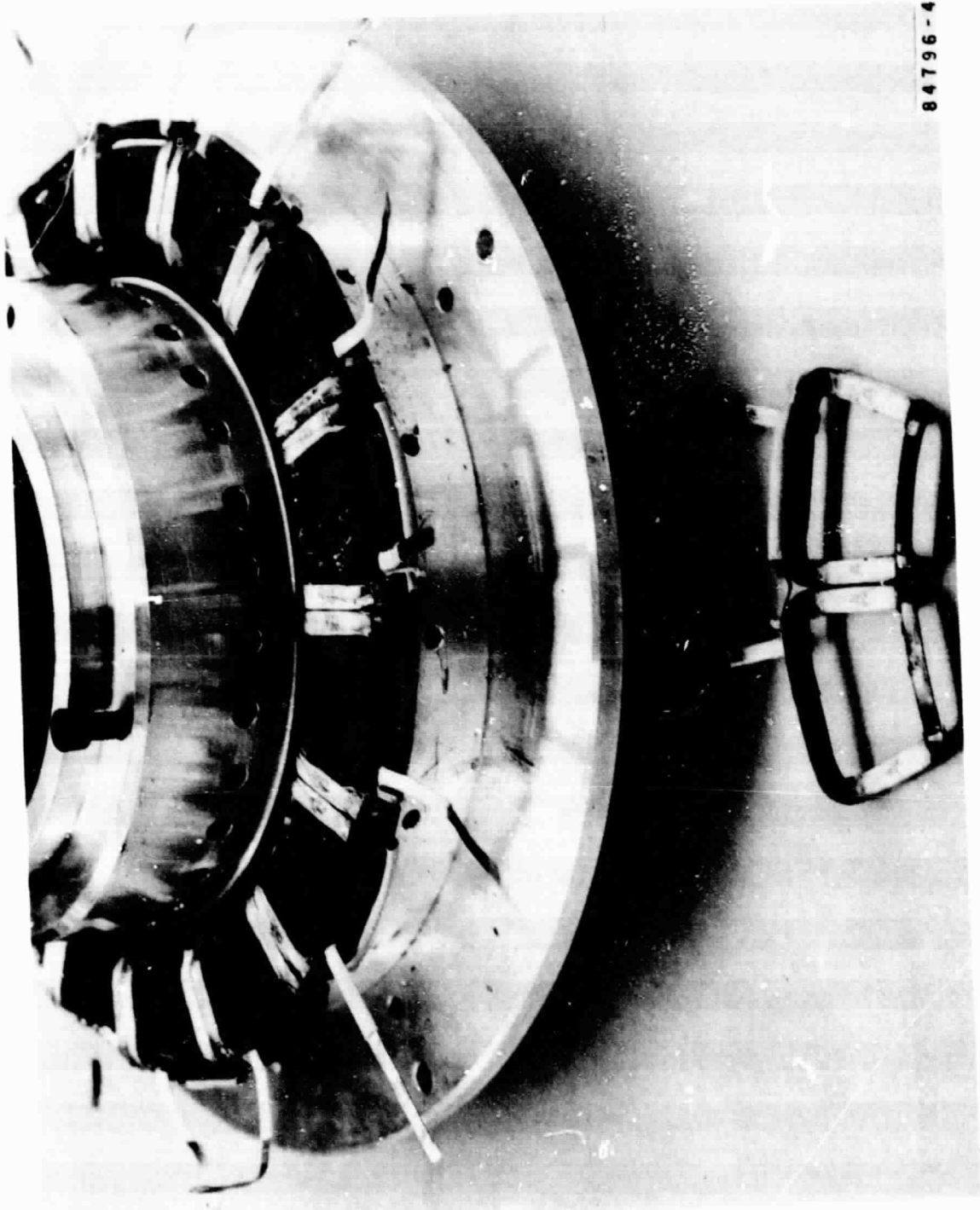


Figure 62.--Functional Model Stator During Assembly.

ORIGINAL PAGE IS  
OF POOR QUALITY

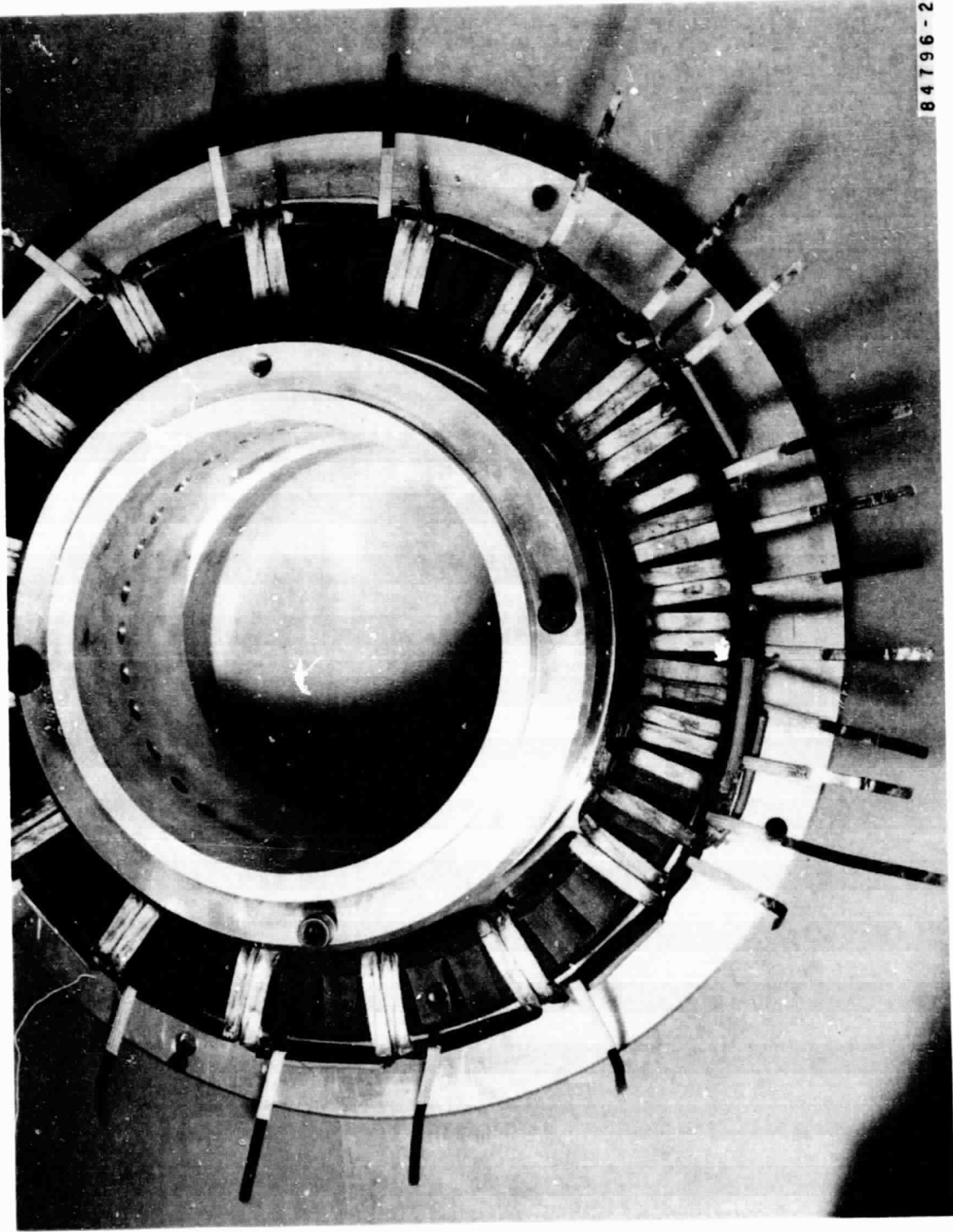
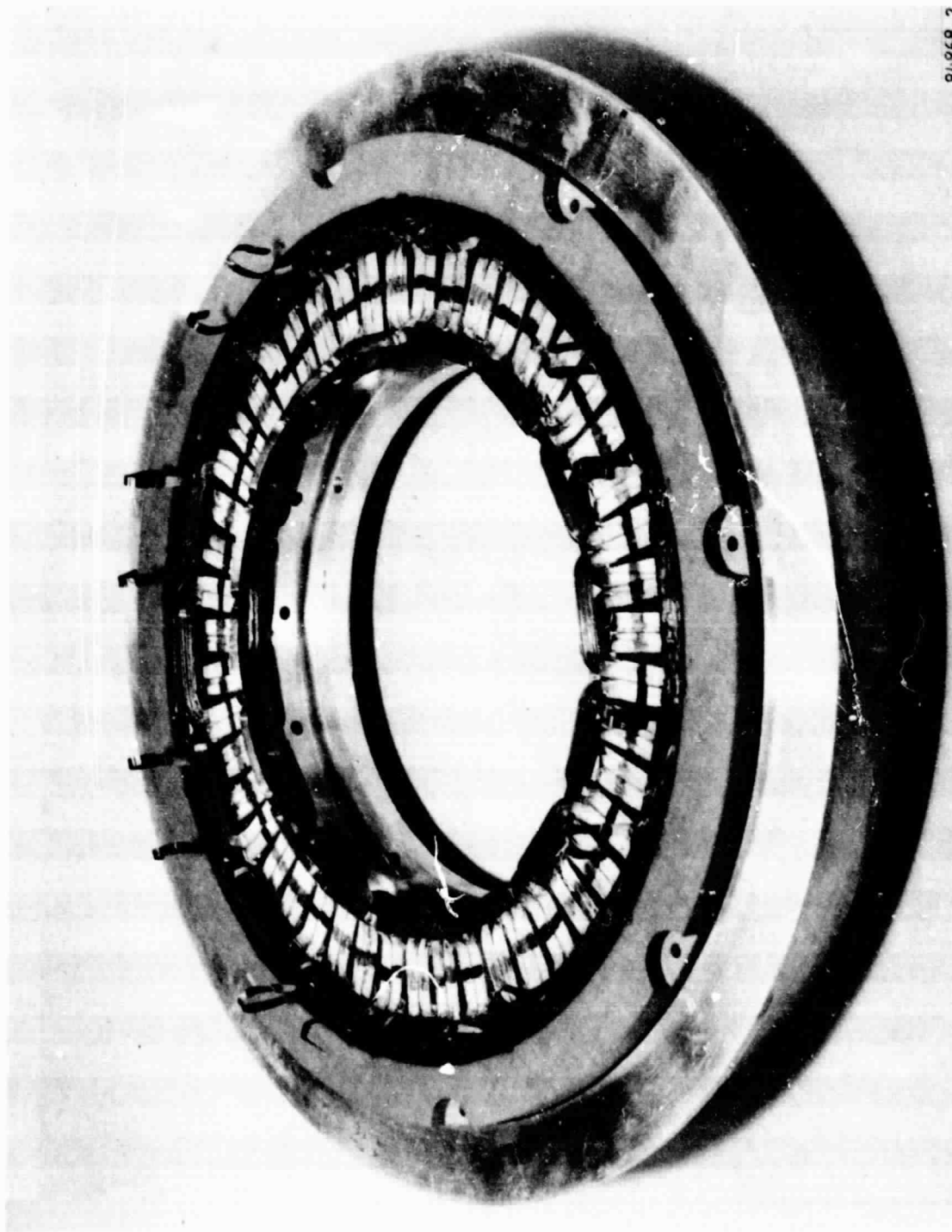


Figure 63.--Functional Model Stator Coils on Alignment Tooling.



ORIGINAL PAGE IS  
OF POOR QUALITY



84868-2

Figure 64.--Functional Model Stator Subassembly.

The coil ends and bus bar tabs were crimped together through a barrel-type terminal and then soldered to fill the voids. Again, at each level of assembly, the coils were checked for isolation from adjacent coils and ground. Flat tabs were also brazed to the bus rings to allow for attachment of the lead wires of each phase. Each phase has two No. 8 AWG color-coded wires coming out from the unit. All changes made in the stator design increased the ease of manufacturing or reliability of the assembly. In addition, two thermocouples were mounted on the stator coils on each side to monitor winding temperature during testing. The completed stator assembly is shown in fig. 65.

In summary, four stator assemblies were built during the course of the program. The method of turn-to-turn wire insulation and the design of the coil bending and alignment tooling were areas that required significant development. The stator built for the functional model was successfully built and tested, and served to prove the viability of the ironless stator concept. Table 9 summarizes the various stator assemblies built during the program.

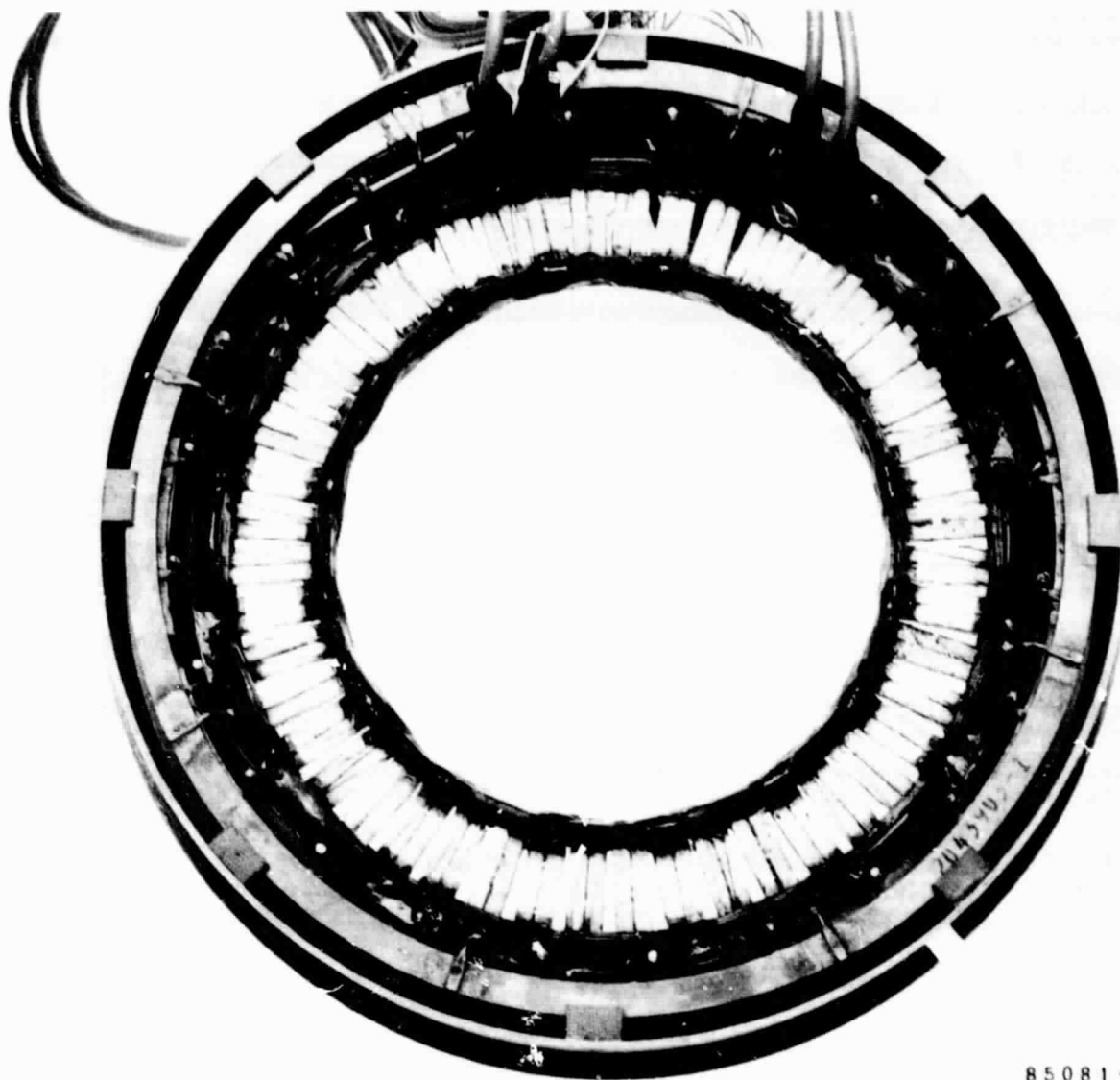
Rotor assembly.--The rotor assembly used for the windage tests was encapsulated with a polyurethane foam to minimize the saliency. This technique had a substantial effect on the windage, reducing the losses by approximately 2000 W. For the functional model rotor, this technique was improved upon in two ways.

First, further review of the material properties of the polyurethane indicated that its thermal expansion coefficient may be too high (compared to the steel rotor) for successful operation at full speed and moderate temperatures. Substantial damage to the stator assembly could result if one of the interpole sections were to break loose at the bond line. Investigation of alternate materials resulted in the selection of a polyester foam material. This material was developed specifically to retain a high percentage of its ambient temperature physical properties when exposed to elevated temperatures. It has outstanding characteristics for compressive strength and can be used at temperatures from -60°C to 150°C, showing little growth and good retention of its physical properties, when properly cured. In addition, the system produces excellent molded parts, picking up small details and intricate patterns.

Second, the quality of the molded shape was improved by the use of better molding tooling. Aluminum rings were made to form the shape of the inner portion of the rotor. An open mold technique was used instead of the semiclosed method used previously. A picture of one rotor pole piece ready for molding is shown in fig. 66. After removal of the molding tooling, the open portion of the mold is machined to blend in with the rotor pole faces. A picture of the first encapsulation of a rotor is shown in fig. 67. Subsequent improvements in the mold-release process resulted in rotors with significantly better mold contours at the outer pole tips. The 8-mm-diam cooling holes were drilled in each pocket as shown in fig. 68. Other than the molding of interpoles, the rotor assembly was identical to that used in the proof-of-principle model.

End bells.--New end bells were made to accommodate the large diameter stator housing built for the functional model. Other changes were also made to improve the characteristics of the system. These improvements address problems that fall into three categories:

ORIGINAL PAGE IS  
OF POOR QUALITY



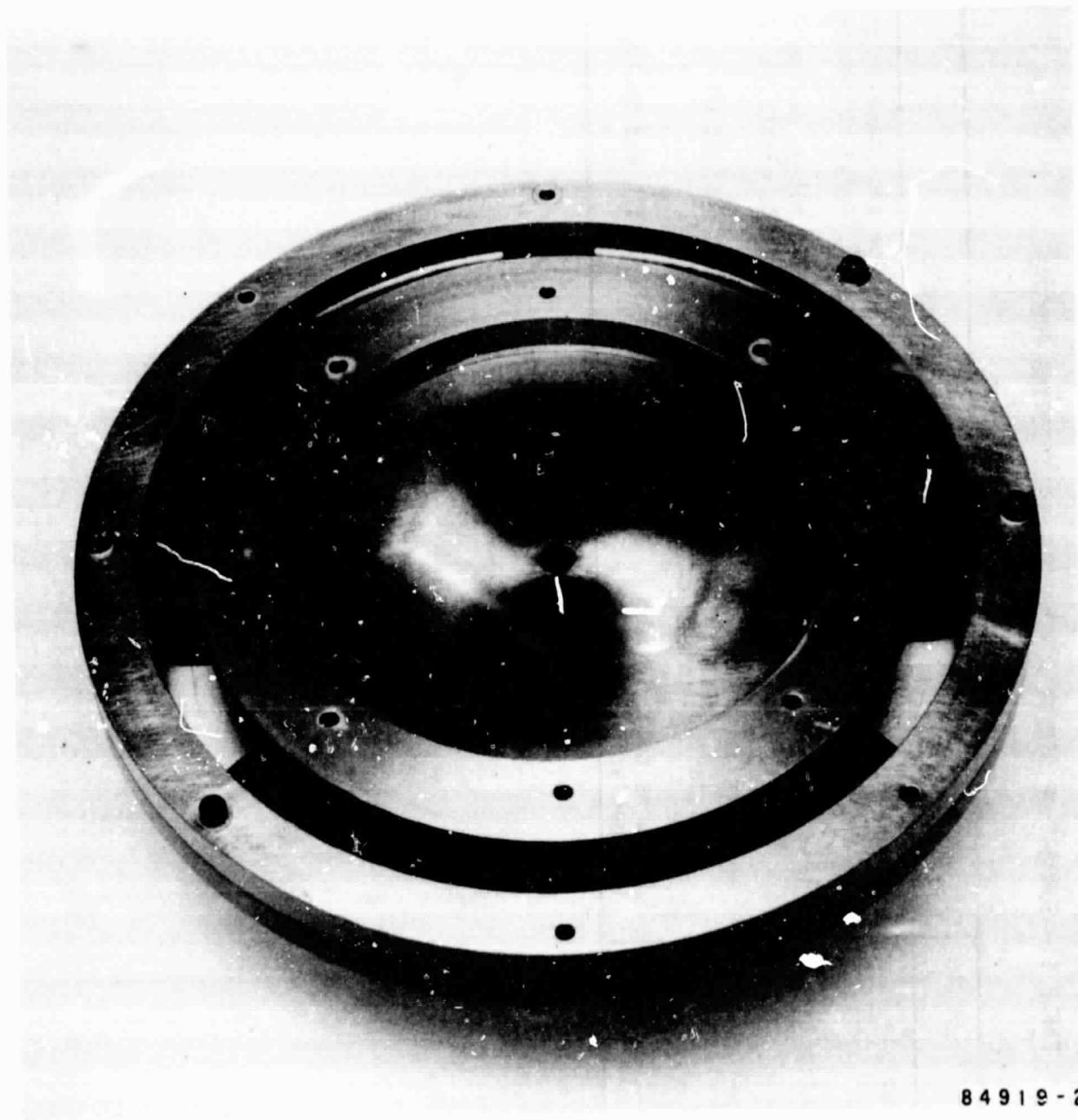
85081-2

Figure 65.--Completed Functional Model Stator Assembly.

TABLE 9.--SUMMARY OF STATOR ASSEMBLIES BUILT DURING PROGRAM.

No.	Model	Description	Result
1	Proof-of-Principle	20 turns/coil, 0.05 mm Kapton strip insulation	Phase-to-phase and phase-to-ground electrical faults before testing
2	Proof-of-Principle	19 turns/coil, 0.05 mm Kapton strip insulation	Overheated and failed during testing due to electrical faults
3	Proof-of-Principle	20 turns/coil, ML wire insulation	Damaged during testing or disassembly
4	Functional	20 turns/coil, ML wire insulation	Successfully built and tested

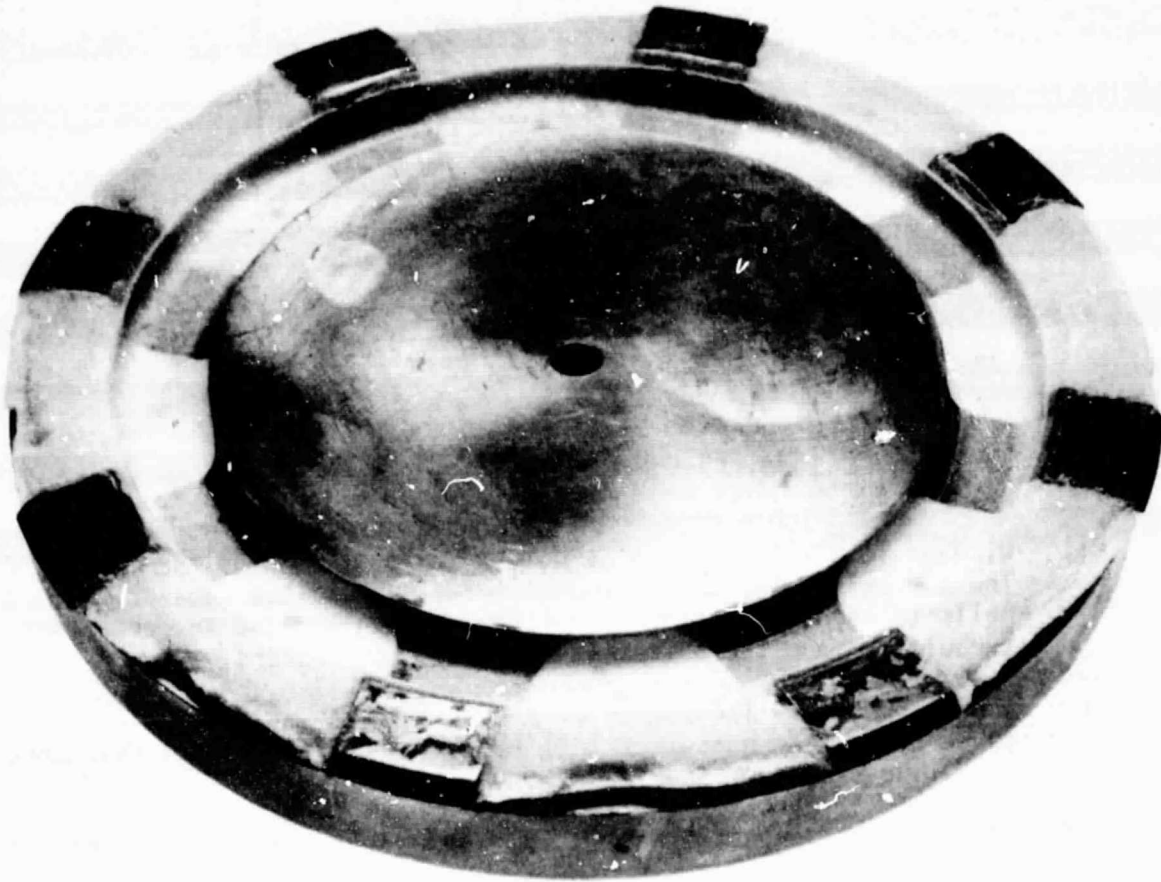
ORIGINAL PAGE  
BLACK AND WHITE PHOTOGRAPH



84919-2

Figure 66.--Rotor Pole Piece With Molding Tooling.

ORIGINAL PAGE IS  
OF POOR QUALITY



84938-3

Figure 67.-- Initial Polyester Rotor Molding.

ORIGINAL PAGE IS  
OF POOR QUALITY

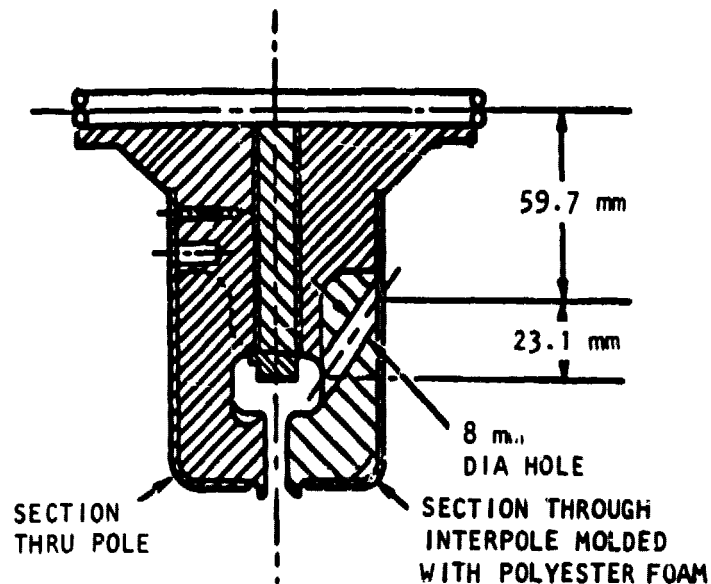


Fig. 68.--8-mm-diam Cooling Holes.

A-32286

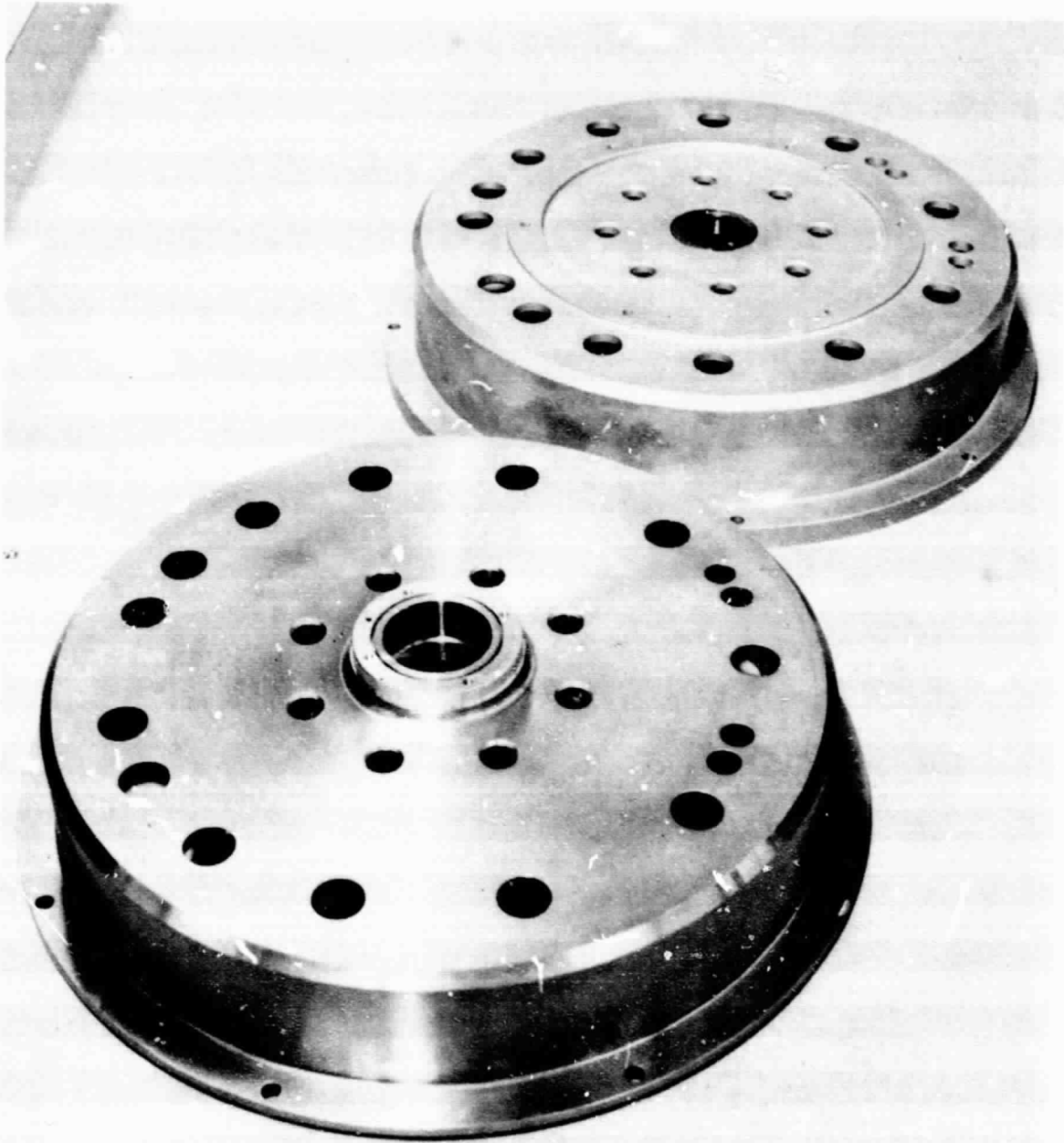
- (1) Windage loss - The air inlet holes were chamfered on the leading edge. The air exit holes were moved from the o.d. to the face of the end bells to reduce the diameter of the exiting air and to reduce air turbulence from the bus rings and insulator spacers.
- (2) Acoustic noise - The number of air exit holes was changed and their pattern was made nonsymmetrical to reduce the acoustical resonance resulting from even spacing.
- (3) Eddy current losses - The end bells were spaced axially and radially farther away from the rotor assembly to minimize penetration by the stray magnetic field. This loss could be eliminated in later designs by using high-strength plastic end bells, assuming the immediate space around the motor is free of sensitive parts (electrically conductive materials).

Instrumentation was added to the end bells to provide information on the air flow characteristics of the functional model. Pressure taps were added near the inlet and exit air holes. Thermocouples were installed to measure the inlet and exit air temperatures and also the bearing temperatures. The completed end bells are shown in figs. 69 and 70.

Final assembly.--Final assembly followed the same procedures as were used for the proof-of-principle machine. Installation of the new stator assembly between the rotor pole pieces showed that there was again a clearance problem between the parts. To provide sufficient clearance two steps were taken:

- (1) The inside and outside pole tips were modified slightly.

ORIGINAL PAGE  
BLACK AND WHITE PHOTOGRAPH

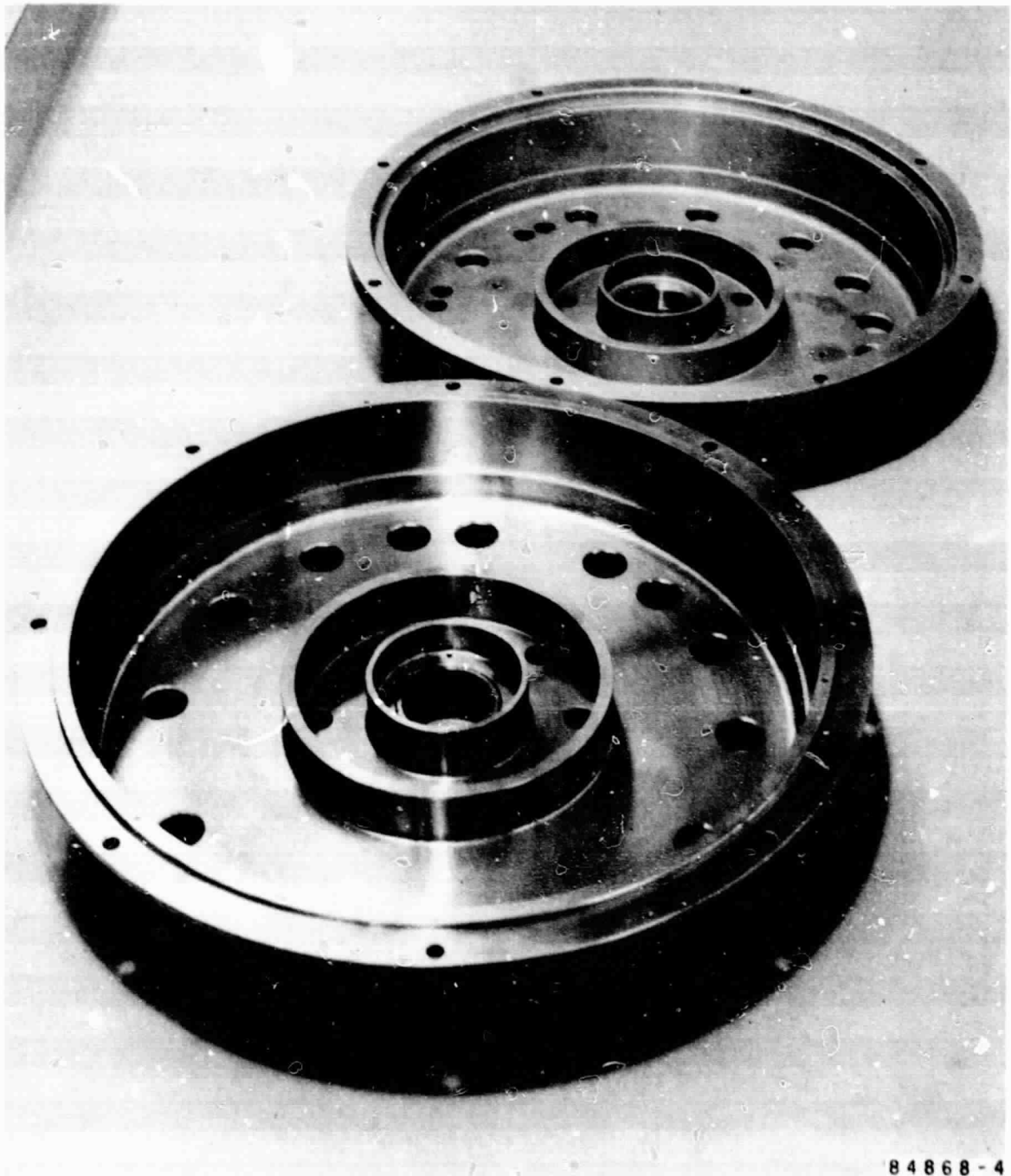


84868-3

Figure 69.-- Functional Model End Bells.



ORIGINAL PAGE  
BLACK AND WHITE PHOTOGRAPH



84868-4

Figure 70.--Functional Model End Bells.

- (2) A 0.200-mm soft-steel shim was added to each side of the magnet, increasing the magnetic air gap by 0.40 mm and resulting in a net decrease in flux level as discussed in detail later in the text.

The completed functional model, including instrumentation pressure taps and thermocouples, is shown in fig. 71. The significant materials used in manufacturing the functional model are shown in table 10.

### Rotating Machine Tests in Generator Mode

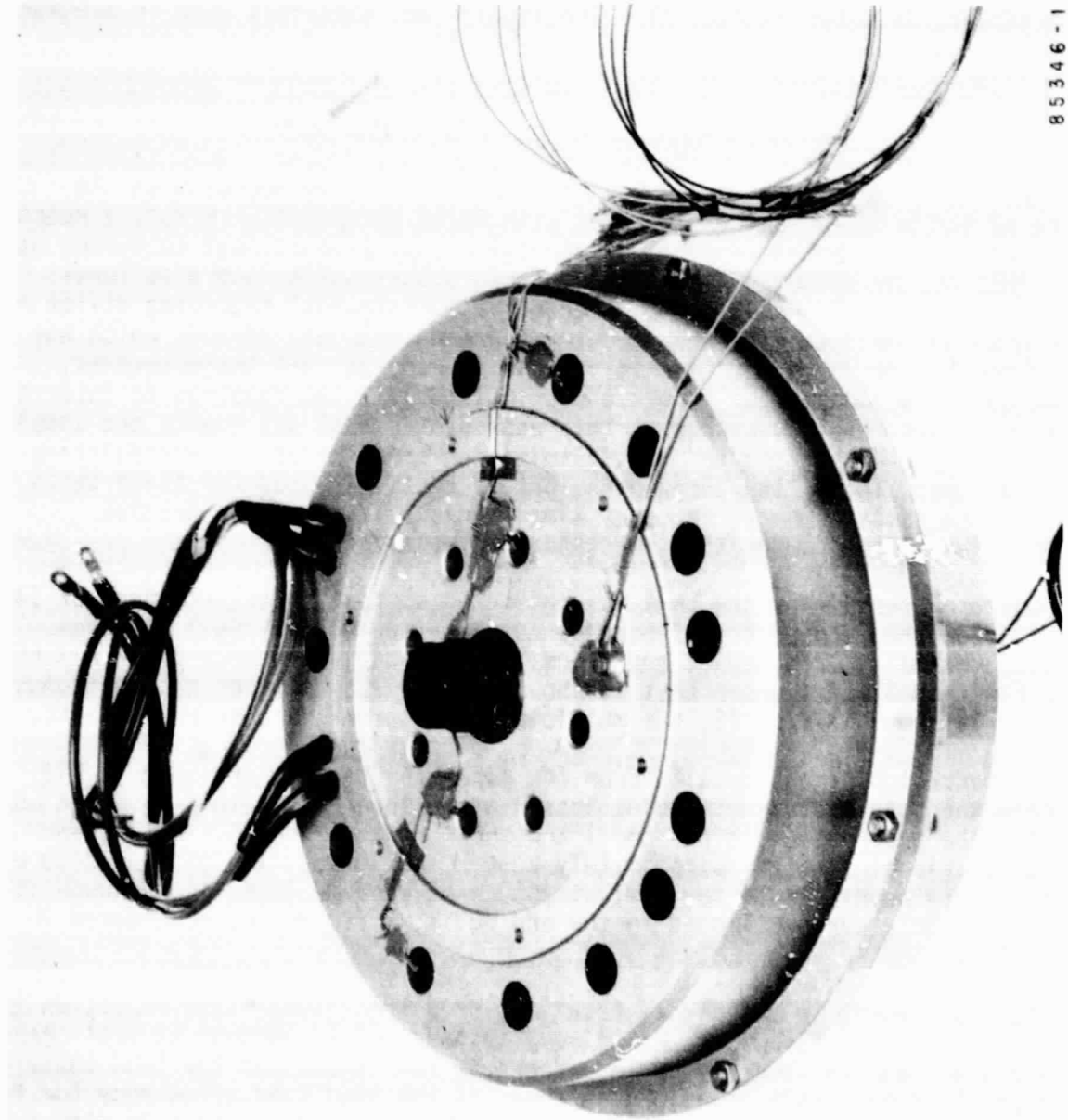
Functional model testing was conducted under the same approach as the testing of the proof-of-principle model with three exceptions. First, a reaction torque head that generates a small electrical signal proportional to torque was used. This device produced accurate and repeatable results, and also lends itself well to signal conditioning. Second, a multichannel recording device with built-in signal conditioning was used to record data. This device, which was used to monitor dc volts, dc amperes, torque, speed, and all thermocouples, accepts up to 16 independent inputs and prints out digital readings in intervals as small as 10 s. The advantage of this approach is that all inputs are sampled simultaneously and then printed out, eliminating time delays in interpolating meter readings. Third, the three-phase bridge rectifier used for these tests had diodes with a faster reverse recovery time. This allowed a more precise determination of the commutating reactance of the machine.

Generator testing of the unit was conducted up to 100 percent speed of 1466 rad/s (14,000 rpm) and up to 115 percent current (160 A dc). Full electromagnetic, thermal, aerodynamic, and acoustic noise data were recorded. A picture of the functional model under test is shown in fig. 72. Some of the instrumentation used is shown in fig. 73; the multichannel recorder is seen on the left.

The most significant results from the generator testing are seen in fig. 74, where the total rotating machine losses at no load and at full load are compared for the proof-of-principle model and the functional model. This graph shows a rotational loss of approximately 2350 W, or a reduction of over 3000 W. This loss very nearly meets the goal of 2050 W of windage loss, even though it includes the eddy current losses in the end bells, a factor not considered in the windage loss goal.

The improvement in efficiency resulting from the windage loss reduction is seen in fig. 75, which shows an efficiency increase of 10 percent at full speed and full load, and an increase of 15 percent at full speed and low load compared to the proof-of-principle model. Also shown is the predicted efficiency for the "ideal" case, where the windage is reduced to level that would be seen with a completely smooth rotor and stator with no air pumping losses. Fig. 76 shows the functional model efficiency at various speeds and loads.

ORIGINAL PAGE  
BLACK AND WHITE PHOTOGRAPH



85346-1

Figure 71.--Functional Model Motor Assembly.

TABLE 10.--FUNCTIONAL MODEL MOTOR MATERIALS.

Item	Functional Model
Magnet	Sm-Co; 16 MGO energy product
Magnet plates	1020 sheet metal
Rotor poles	4130 steel
Support sleeve	Inconel 718
Tie bolt	Inconel 718
Bearings	SAE 52100; shielded
Lubrication	MIL-G-81322
Magnet wire	3.37 mm x 0.22 mm copper; ML coated
Stator potting	Eccobond 281
Varnish (coil)	Sterling Y338
Varnish (stator)	PD George 433-75VT
Coil support ring	Phenolic
Stator housing	AL2024-T351
End bells	AL2024-T351
Interpole filler	Stafoam AA606

ORIGINAL PAGE  
BLACK AND WHITE PHOTOGRAPH

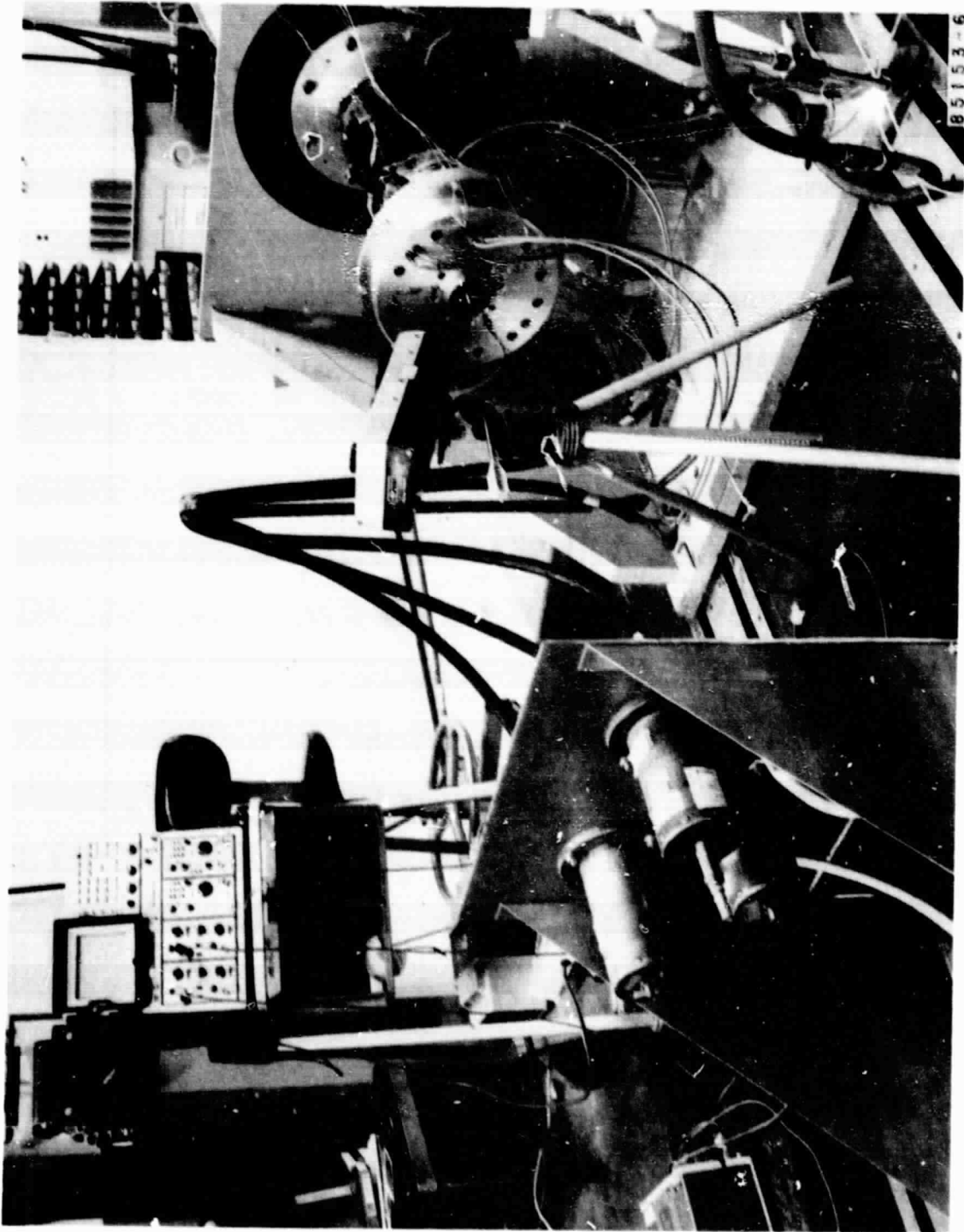


Figure 72.---Functional Model Rotating Machine During Testing.

ORIGINAL PAGE  
BLACK AND WHITE PHOTOGRAPH

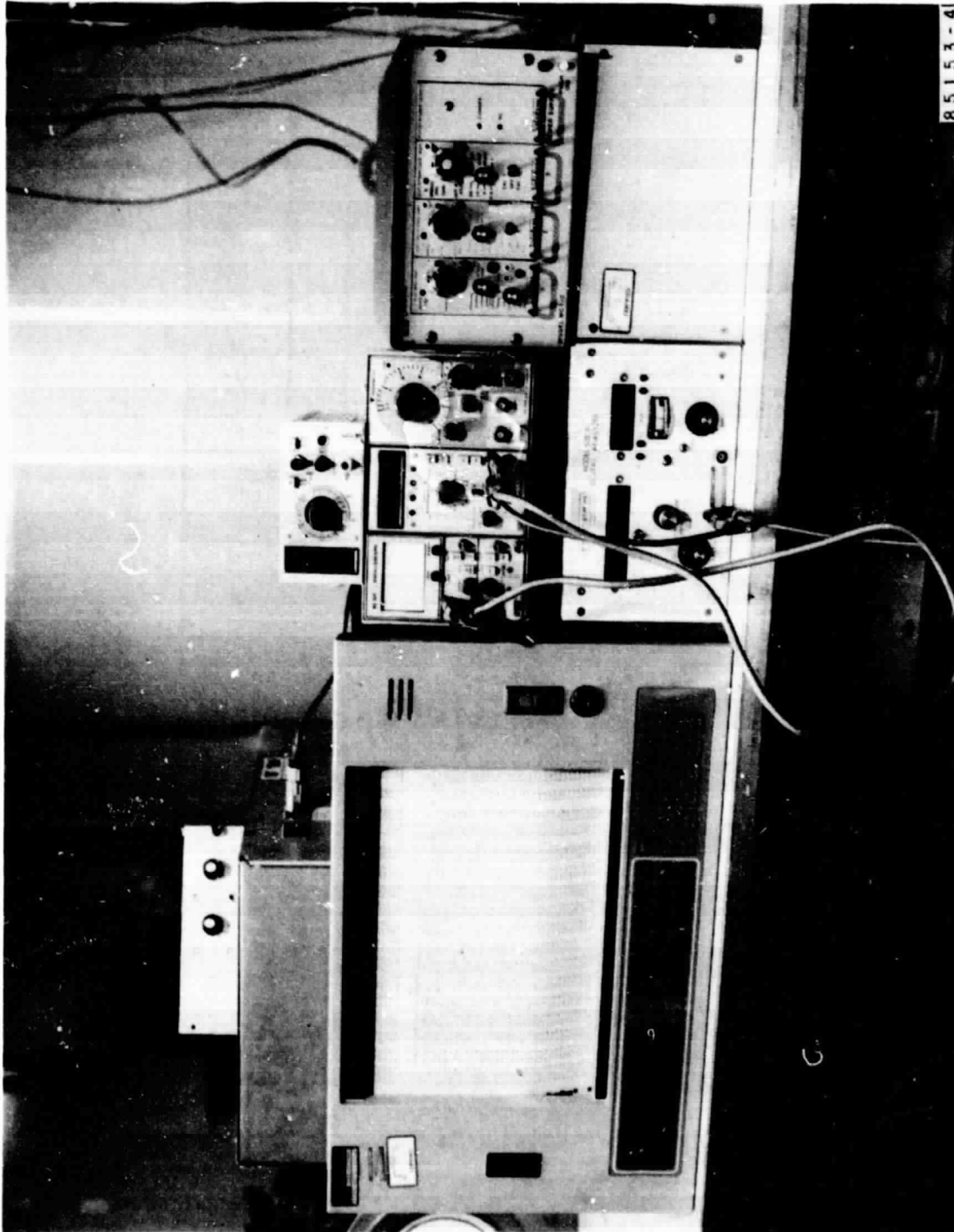
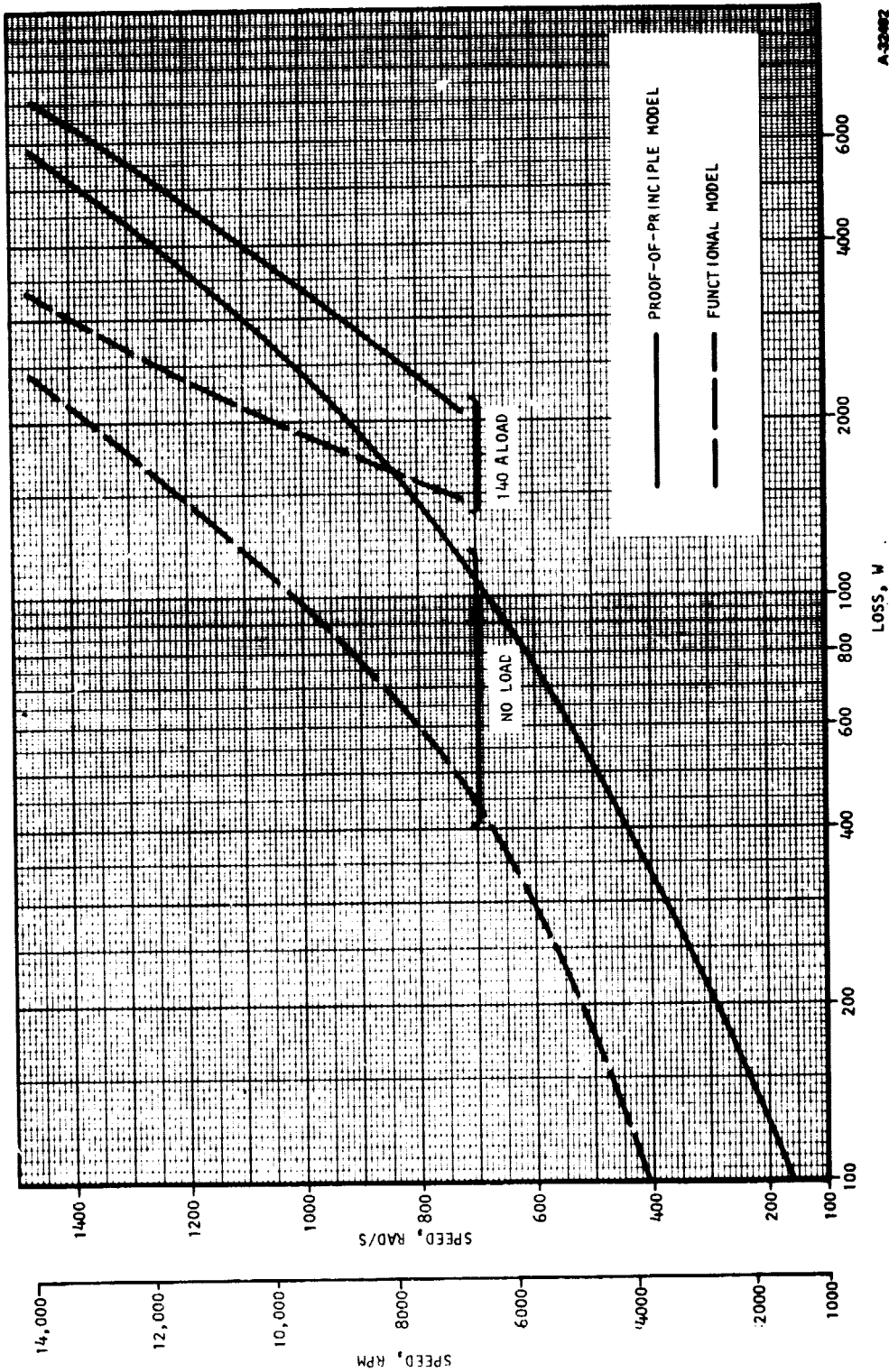


Figure 73.---Functional Model Rotating Machine Test Instrumentation.

ORIGINAL PAGE IS  
OF POOR QUALITY



A-32462

Figure 74.--Comparisons of Total Rotating Machine Loss versus Speed, Functional vs. Proof-of-Principle Model Rotating Machines.

ORIGINAL PAGE IS  
OF POOR QUALITY

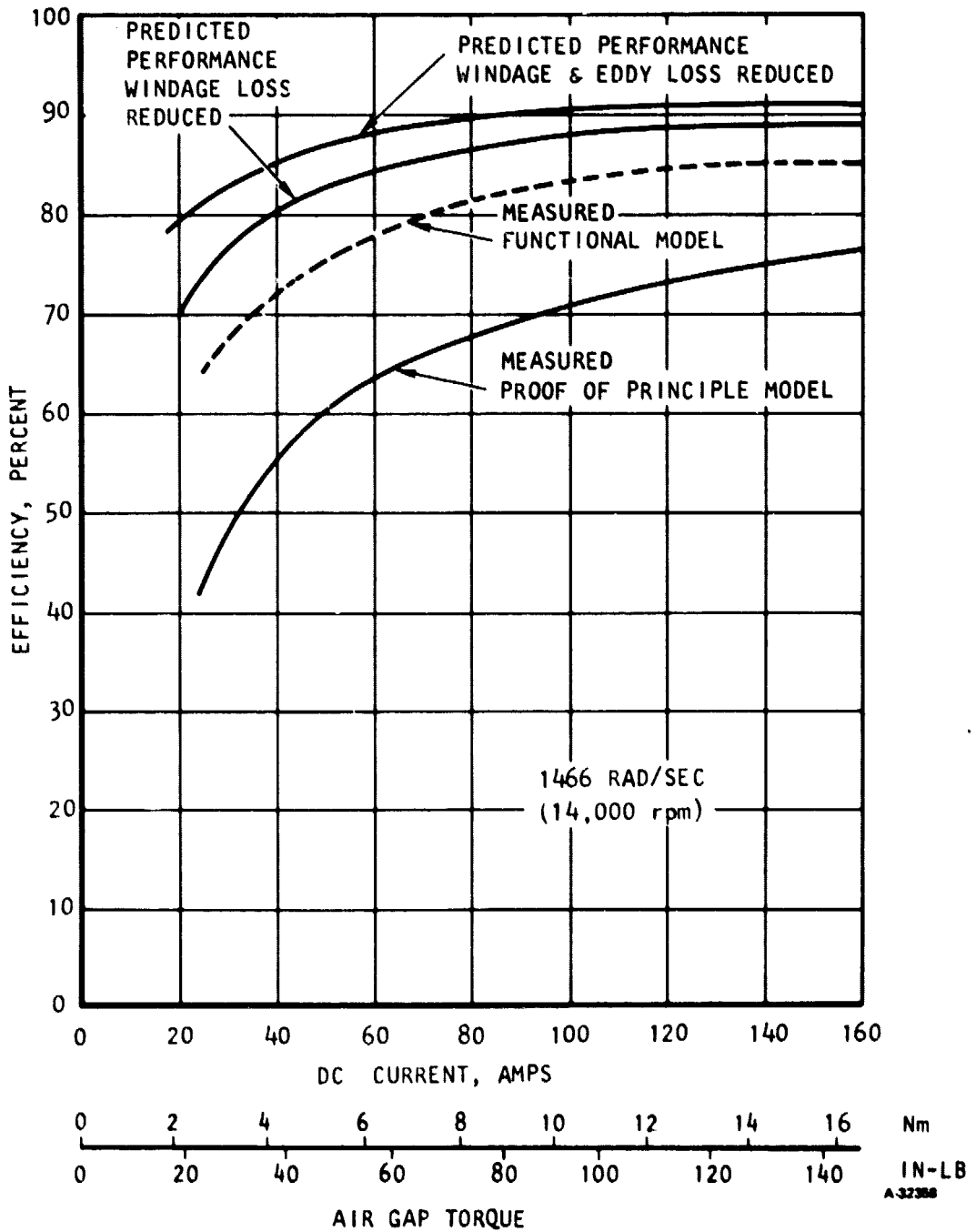


Figure 75.--Predicted and Actual Performance Comparison of Rotating Machines in Generator Mode.



ORIGINAL PAGE IS  
OF POOR QUALITY

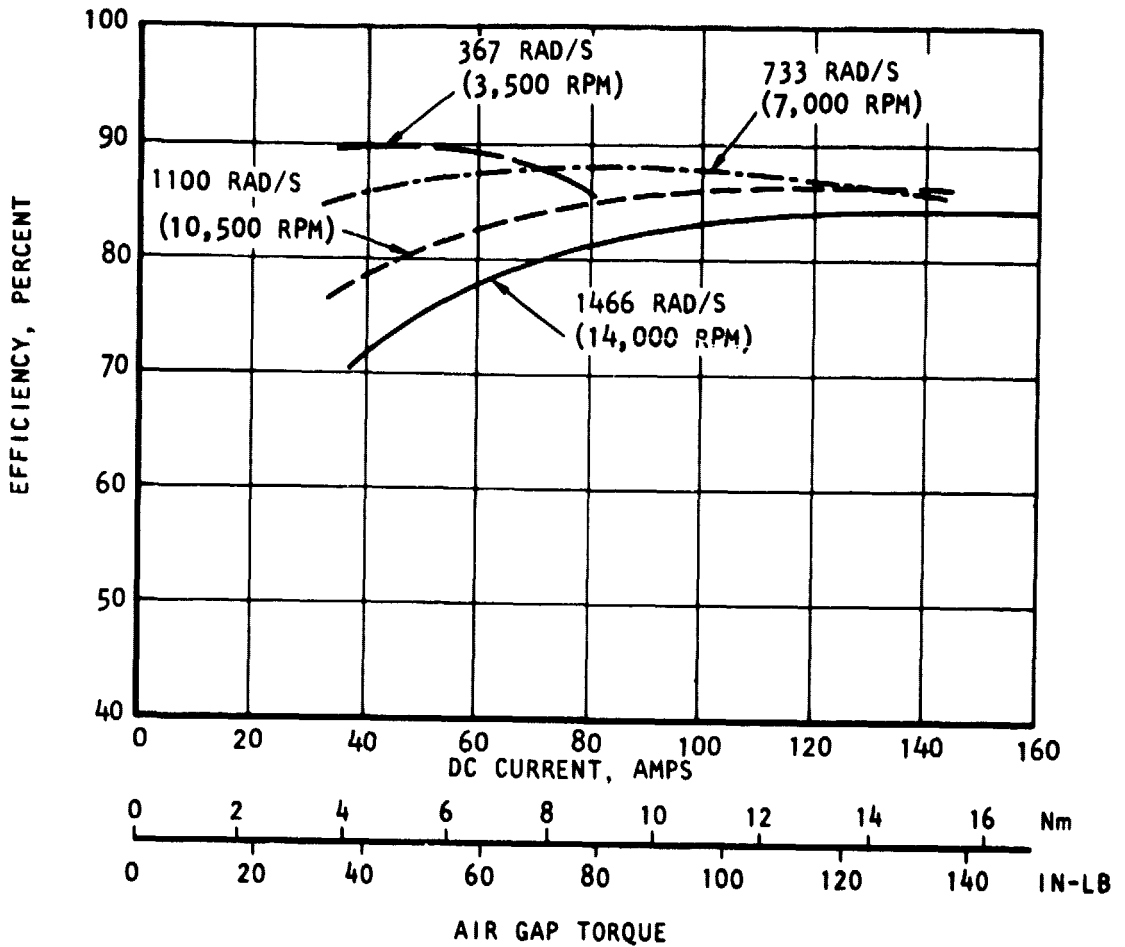


Figure 76.--Functional Model Rotating Machine Performance.

A.32360

Though the windage loss was reduced significantly, there was still sufficient air pumping through the unit to cool the stator assembly coils with a substantial thermal margin. Figs. 77 and 78 compare the results of the proof-of-principle model and the functional model. Steady-state copper temperature at 100 percent speed and 115 percent load is only 106°C, while the rating of the insulation system is 177°C. This indicates that a reduction in airflow might increase the system efficiency if the reduced windage losses offset the increased copper losses due to the temperature increase.

Airflow through the unit was calculated by two approaches. First, the pressure taps installed in the end bells at the inlet and exit air holes were monitored during testing. The pressure drop across the machine and the size and number of holes were used to calculate airflow. These data are presented in fig. 79. Second, a rough calculation of flow was made by assessing the temperature rise of the air through the machine and the total loss. This analysis gave air flow results that were approximately 50 percent higher than those derived from the first method, but it is felt that the pressure drop calculations are more accurate.

The effect of opening the magnetic air gap to achieve running clearance is seen by inspection of fig. 80. The no-load voltage is down by approximately 10 percent from the proof-of-principle model and by approximately 15 percent from the original predicted value. This reduces the power capability as discussed later in the text.

The audio noise level exhibited by the machine was also monitored during the generator testing and is shown in fig. 81. No data of this type were recorded for the proof-of-principle model, so a direct comparison with the functional model cannot be made. However, data from various configurations were recorded during the windage loss testing, and this information is included in fig. 80. Noise levels were measured with a portable audio analyzer mounted on a tripod and located at a distance of approximately 300 mm directly in front of the unit. From the subjective point of view, the noise levels were still quite high in the functional model. The motor noise could be reduced to an acceptable level by some straightforward noise damping techniques if the motor was mounted in an electric vehicle.

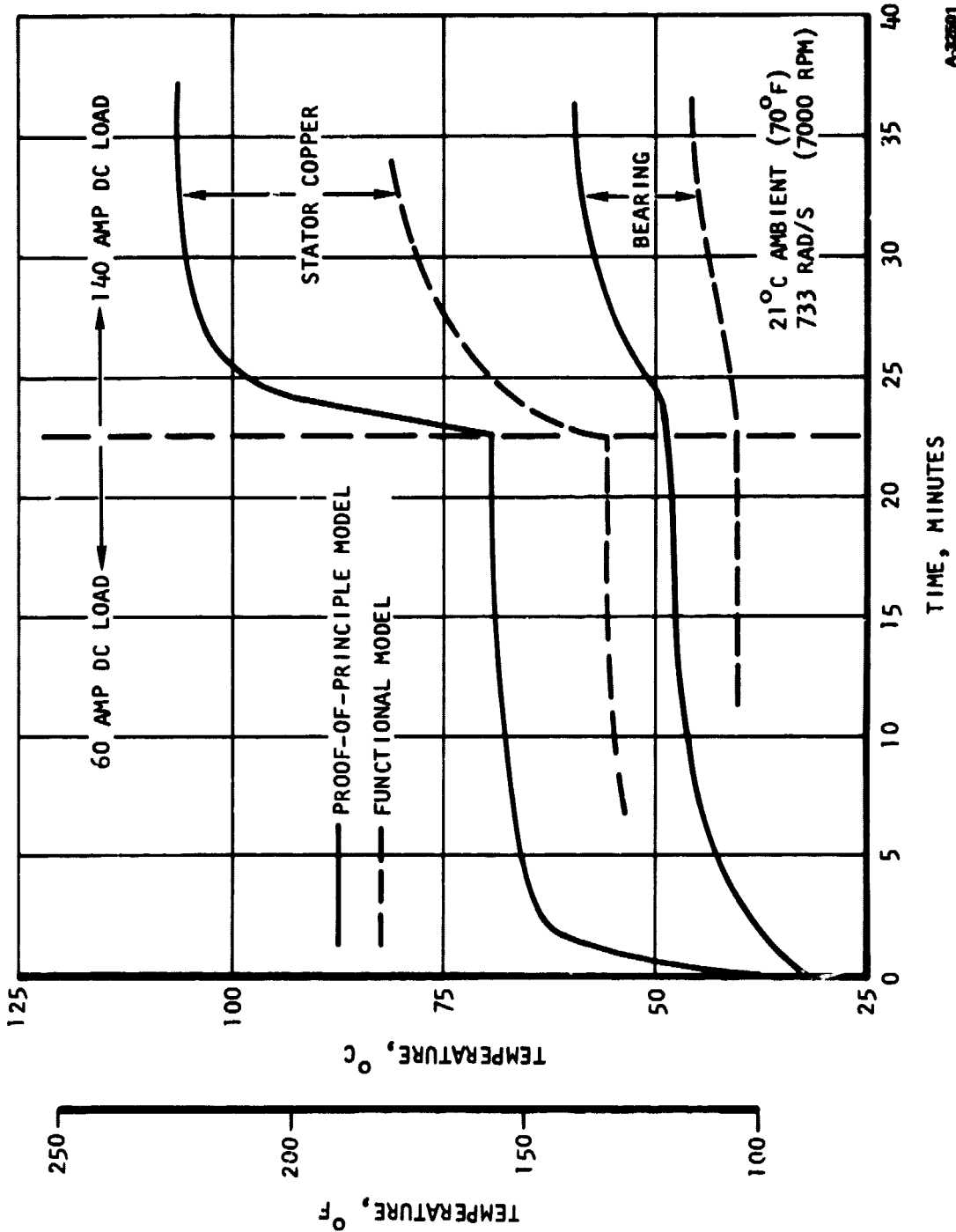


Figure 77.--Comparison of Thermal Performance of Rotating Machines at 50 Percent Speed.

ORIGINAL PAGE IS  
OF POOR QUALITY

A-32590

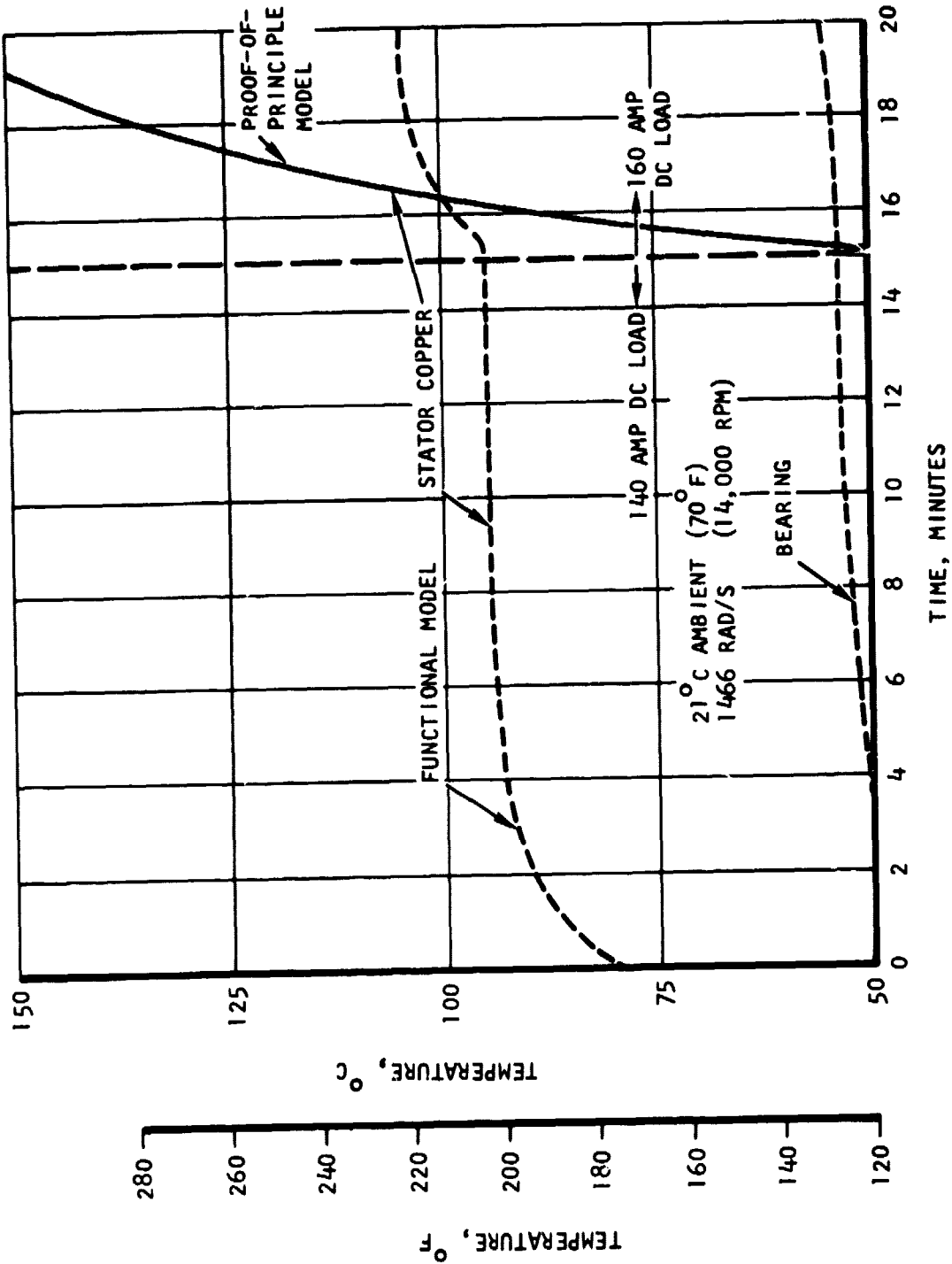


Figure 78.--Comparison of Thermal Performance of Rotating Machines at 100 Percent Speed.

ORIGINAL PAGE IS  
OF POOR QUALITY

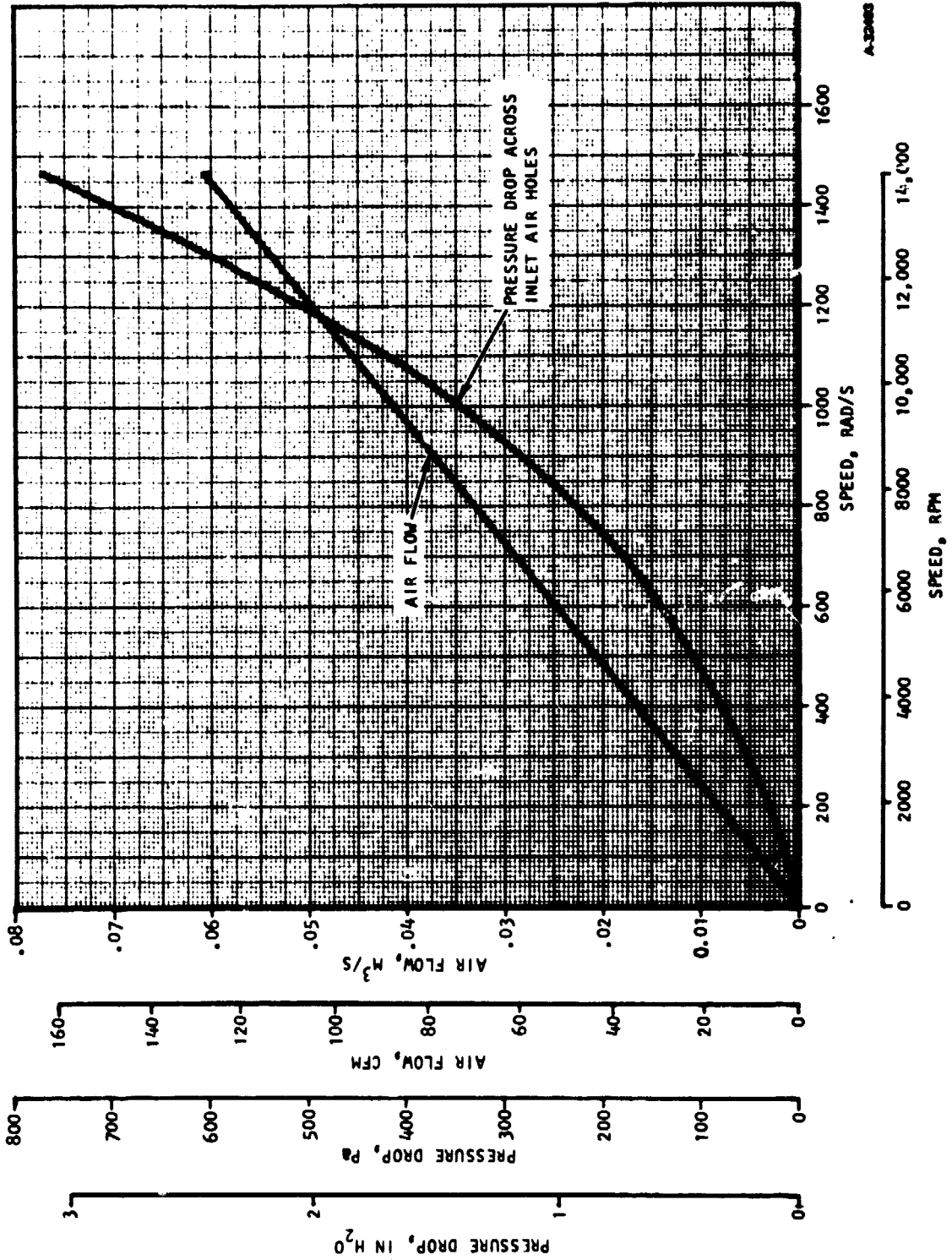
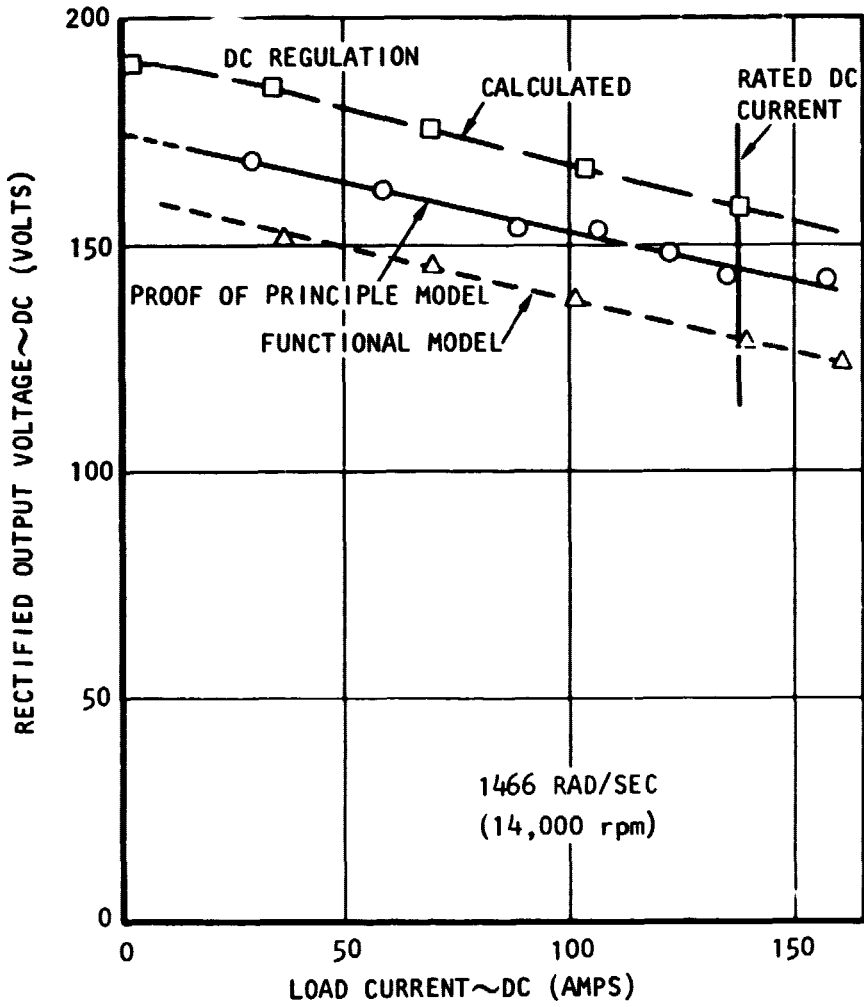


Figure 79.--Functional Model Rotating Machine Airflow versus Speed.

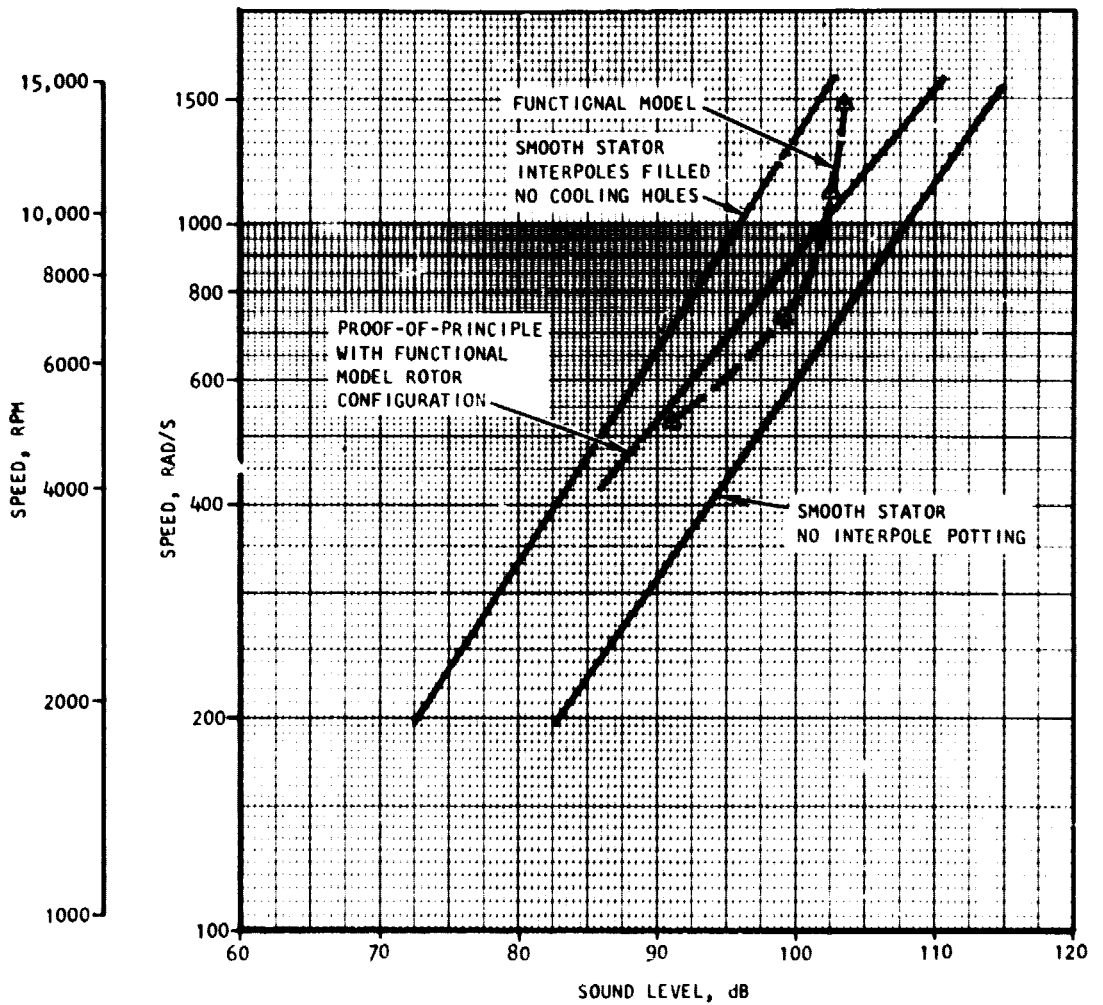
ORIGINAL PAGE IS  
OF POOR QUALITY



A 32346

Figure 80.--Comparison of dc Load Regulation of Rotating Machines.

ORIGINAL PAGE IS  
OF POOR QUALITY



A 32488

Figure 81.--Comparison of Audio Noise Level versus Speed for Various Configurations.

## FUNCTIONAL MODEL MOTOR TEST CONSIDERATIONS IN MOTOR MODE

### Functional model system analysis

Due to the problems encountered in the fabrication of the PM motor stator assembly, further development of the converter was de-emphasized. It was felt that it would be most judicious to establish the viability of the rotating machine before completing a converter design and proceeding with its development.

Early in 1982, with the performance constraints of the rotating machine alleviated and the necessary constraints established, an analysis of the available controller options suitable for motor testing was conducted. This analysis considered the funding and schedule constraints as well as the technical suitability of the options. It was decided that the best approach would be to utilize the improved electronically commutated motor (IECM) breadboard controller developed under NASA contract DEN 3-64. Fig. 82 is the basic block diagram of the IECM controller.

Similar to the advanced motor (AM) converter, the function of the IECM converter is to commutate and control the IECM over its full range of speed. The converter provides the controls for the drive and the brake modes of operation, which includes a regenerative switching scheme that returns energy to the battery during braking.

The major power elements of the converter are the upper and the lower transistor choppers,  $Q_U$  and  $Q_L$ , respectively, freewheeling diodes,  $D_1$  and  $D_2$ , and a thyristor inverter  $Q_1$  through  $Q_6$ . The primary devices used on the functional converter are listed in table 11. The lower (main) chopper  $Q_L$  controls the motor current by modulating the fixed dc voltage (battery volts). The freewheeling diodes  $D_1$ ,  $D_2$  maintain a continuous motor current by providing a path for this current when the chopper is off. During this period, the current is sustained by the system inductances in the chopper, the inverter, and the motor loop. The freewheeling diodes are also a part of the regenerative scheme. The thyristor (SCR) inverter acts as a solid-state commutator for the motor.

In the drive mode, the inverter is a load-commutated type, in which the thyristors are turned off by the back EMF (voltage) of the motor. Since the motor is a permanent-magnet, fixed-field type, the back EMF is proportional to speed. Thus, at low motor speeds (less than 10 percent of rated speed), when the back EMF is relatively low and is not sufficient to ensure turnoff of the thyristors, the transistorized choppers provide the means for thyristor turnoff. At motor speeds greater than 10 percent rated, the upper chopper ( $Q_U$ ) is bypassed by the automatic closure of its associated contactor ( $SW_2$ ). The upper chopper ( $Q_U$ ) is required only during the initial start-up; the converter losses are minimized by bypassing the upper chopper at higher speeds.

In the brake mode, by opening contactor  $SW_2$  and changing the SCR phase angle control, the inverter is operated as a conventional phase-delayed rectifier (PDR), which acts to control the current or energy returned to the battery. The current path is through  $D_2$ ,  $SW_1$ , the battery,  $D_1$  and  $L_1$  as shown in fig. 82. For



ORIGINAL PAGE IS  
OF POOR QUALITY

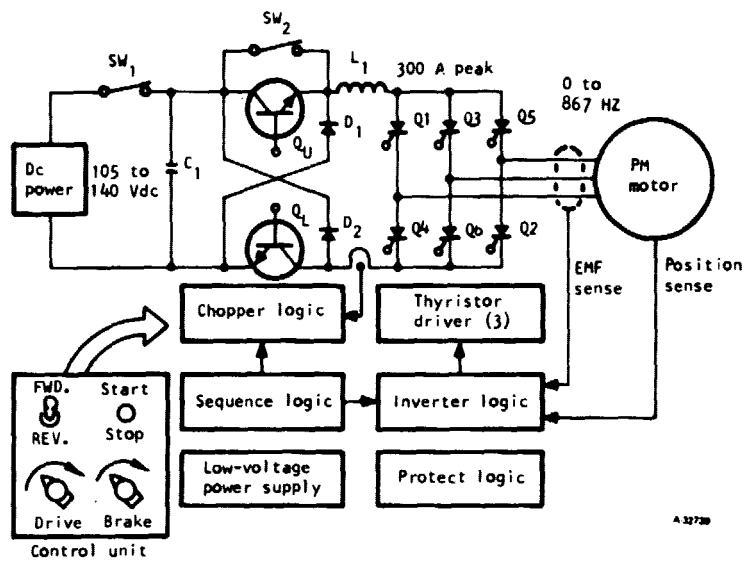


Fig. 82.--Functional Model Converter Basic Schematic.  
(Designed for IECM Motor Drive)

TABLE 11.--FUNCTIONAL MODEL CONVERTER DEVICES.

Component	Type
Thyristors, Q1-Q6	GE 434S, 600 V, 500 A, 14 s
Transistors, QU, QL (12 parallel, each)	Motorola MJ10015, 400 V, 50 A
Diodes (FW), D1, D2 (8 parallel, each)	Motorola MR874, 400 V, 50 A
Capacitors, C1 (12 parallel)	Sprague 36D type, 6000 F, 300 V
Interrupt contactor, SW1	Siemens 3TC74, 400 A dc single pole
CFO contactor, SW2	Hartmann 300 A dc double break
Logic cards	216 by 152 mm (8.5 by 6 in.), CMOS, 43 pin, +15 Vdc power
Current sensor	Hall effect, 5000:1 current ratio
EMF sensor	Step-down control transformer
Position sensor	Photo-optical with slotted disc

conditions wherein the motor back-EMF is not sufficient to provide brake or regenerative energy to the battery, the motor voltage is boosted by the operation of the lower chopper ( $Q_L$ ). The chopper allows for the build-up of current through  $D_1$  and  $L_1$ , which is then transferred to the battery when  $Q_L$  turns off.

The converter is described in more detail in the final report entitled, "A Lightweight Electronically Commutated DC Motor for Electric Passenger Vehicles," DOE/NASA/0064-82-1, NASA Contractor Report No. 165601, AiResearch Report No. 81-18266.

To conduct the required tests, several temporary breadboard modifications need to be implemented. These changes are necessary to accommodate the 2 to 1 difference in system voltages, and permit the chopper/thyristor-type converter to operate with the advanced motor (designed for a transistor converter).

1. The windings of the advanced motor need to be reconnected from a "wye" to a "delta" configuration. This reduces the motor terminal voltage from 140 V rms at 1867 Hz to 81 V rms at 1867 Hz. This modification creates a better electrical match between the advanced motor and the 120 Vdc link inverter associated with the IECM converter.
2. The inverter transient suppression networks may have to be modified because the maximum inverter operating frequency increases from 887 Hz to 1867 Hz for the advanced motor.
3. The inverter-thyristor firing angle must be modified to provide adequate thyristor turn-off time margin, while producing as high a power factor as possible for the motor.
4. The motor position sensor interface must be reviewed and possibly changed so that the advanced motor position sensor outputs are compatible with the inverter control logic.
5. The current regulator should be modified to provide the proper current magnitudes for a given command input. The transfer function should be compatible with the advanced motor current requirements.
6. A series inductor needs to be added to the dc link. Proper IECM chopper operation is based on a predetermined value of inductance in the chopper circuit. Total inductance is the sum of the dc link and PM motor inductance. Since the advanced motor has substantially less inductance than the improved motor, a dc link inductor is required. Note that the dc link inductor is not part of the inverter thyristor circuit loop inductance, and hence does not interfere with normal inverter operation.

Prior to a review of the existing IECM converter, the advanced motor was investigated using AiResearch computer modeling. The results showed that only 11.59 kW of motor output power could be achieved; 23 to 26 kW was the desirable motor output. The reasons for the limited output power are discussed in the following paragraphs.

The functional model motor was tested in the generator mode and the commutation inductance was measured using the overlap angle while operating into a three-phase full-wave rectifier to a dc load. The functional model motor commutation inductance was higher than predicted and in addition, the increased air gap resulted in a lower voltage available to commute the inductance. The lower voltage and higher inductance both act to reduce the power rating of the motor. Of these, the commutation inductance has the greater adverse effect on the IECM thyristor-inverter that was planned to be used to provide the motor excitation.

The reason for this is the fact that as the inverter commutates or transfers the motor current from phase-to-phase, the current in the preceeding phase must be reduced to zero and remain at zero for sufficient time to allow the conducting thyristor(s) to turn off. The forcing factor for the reduction of the thyristor current is the motor voltage.

Therefore, for a given motor voltage, the greater the motor inductance, the longer it takes to reduce the phase current to zero. Comparison of the original motor design versus the functional model motor parameters shows an inductance increase of 58.2 percent and a voltage decrease of 19 percent, both of which are in an adverse direction.

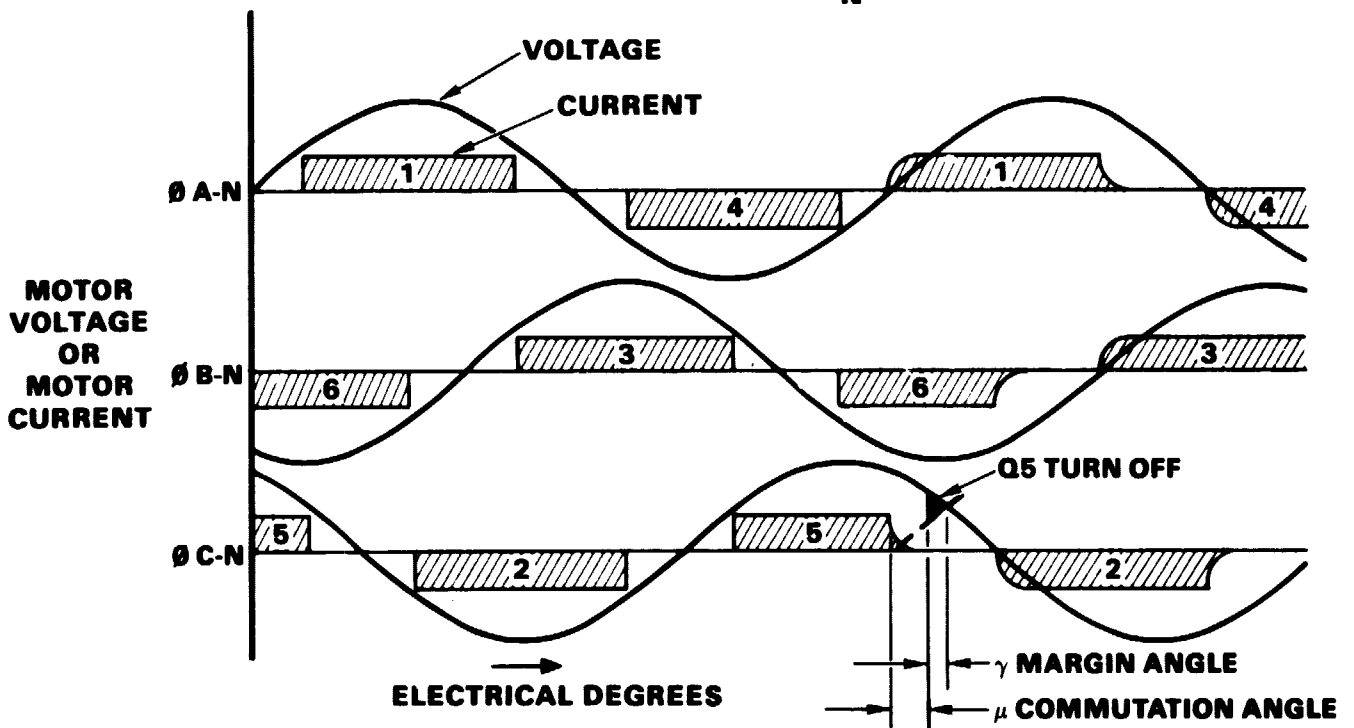
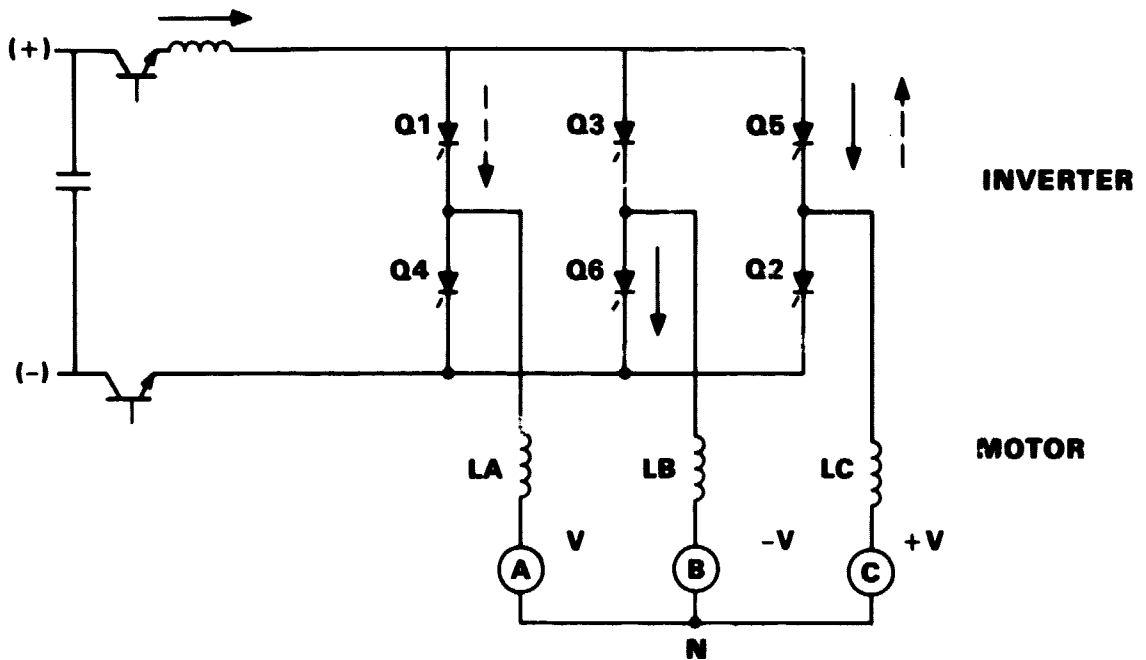
Functionally, this means that the inverter firing angle must be limited to a greater extent for the functional model motor compared to the original motor design, i.e., the inverter thyristor current conduction electrically leads the motor voltage by a greater amount.

Fig. 83 illustrates the affect of the leading current as compared to prior ideal in-phase current waveform. Initially current is flowing through thyristor Q<sub>5</sub>, motor line inductances LC and LB, and thyristor Q<sub>6</sub>. By turning-on thyristor Q<sub>1</sub> at an earlier than ideal time, a circulating current is caused to flow by the polarity difference between the PM-motor phase C and A EMF-voltages. Thus, the current through Q<sub>1</sub> will increase and the current through Q<sub>5</sub> will decrease. The time for the current in Q<sub>5</sub> to decrease to zero is defined as the commutation angle,  $\mu$ .

After the current through Q<sub>5</sub> has reached zero, the PM-motor phase C voltage must be greater than the phase A voltage, so that thyristor Q<sub>5</sub> can remain reverse-biased for sufficient time for turn-off. This time is defined as the margin angle,  $\gamma$ . The sequence then continues, with thyristors Q<sub>1</sub> and Q<sub>6</sub> conducting the motor current.

Fig. 84 shows the results of the computer model wherein the leading motor current causes a low motor power factor and low real output power. The relationship between the commutation and margin angle for a given motor kVA rating is shown in fig. 85. Since the thyristor current and motor voltage are not in-phase, an effective power factor exists for which a given current and voltage reduces the real power (kW) available to drive the motor. Analysis has shown the reduction to be from 20 kW to 14.8 kW for the design to functional model.

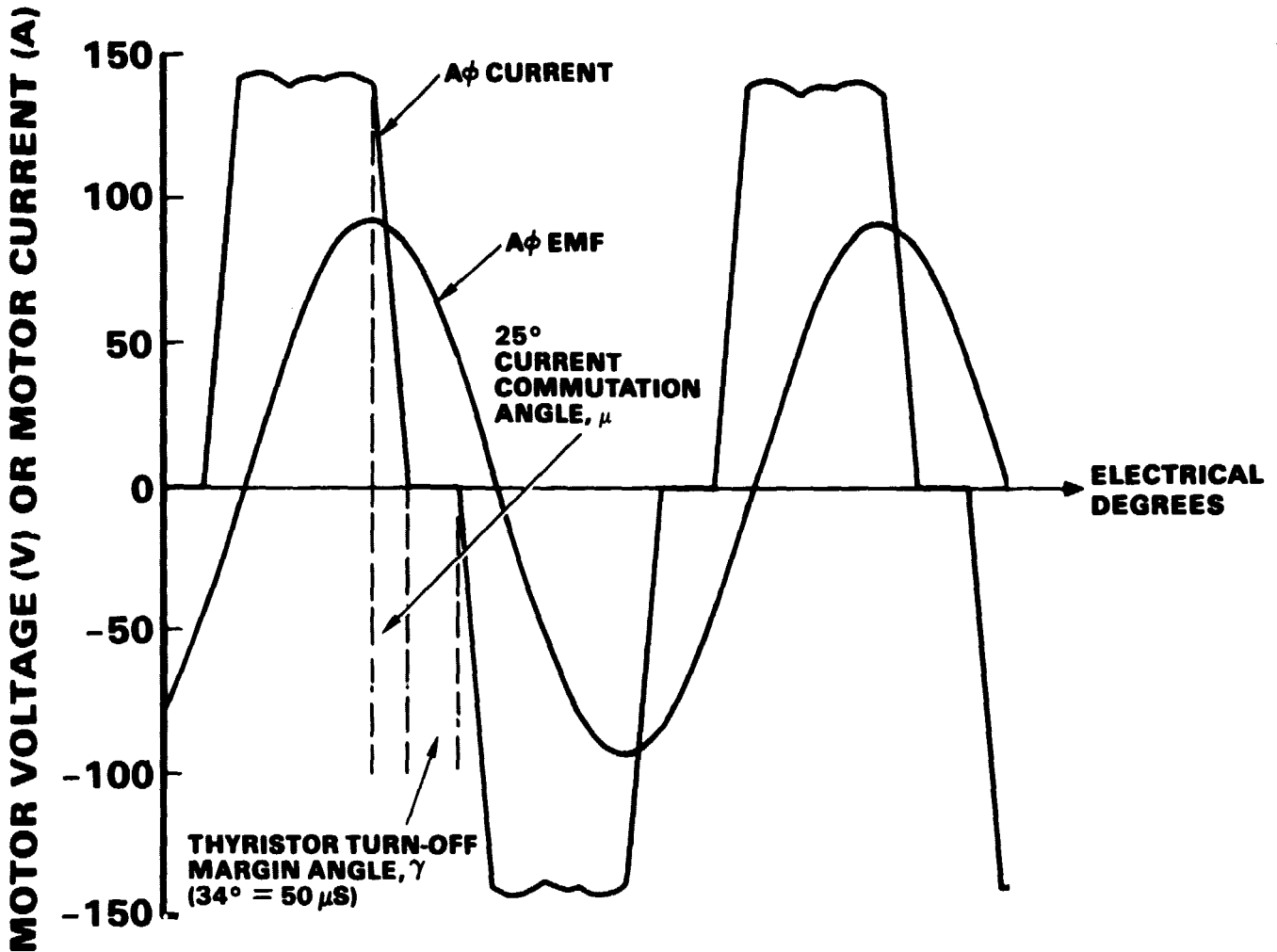
ORIGINAL PAGE IS  
OF POOR QUALITY



A-31508

Figure 83.--Thyristor Line Commutation

ORIGINAL PAGE IS  
OF POOR QUALITY



**MOTOR VOLTAGE = 65.6 VRMS L-N; 1,867 Hz**

**AVERAGE DC CURRENT = 140 ADC**

**INPUT DC POTENTIAL = 106 VDC**

**MOTOR REAL INPUT POWER = 14.84 KW**

**MOTOR INPUT POWER FACTOR =  $\cos(34^\circ + 25^\circ)$   
=  $\cos(59^\circ)$   
= 0.52**

**MOTOR OUTPUT POWER = 14.84KW - MOTOR LOSSES**

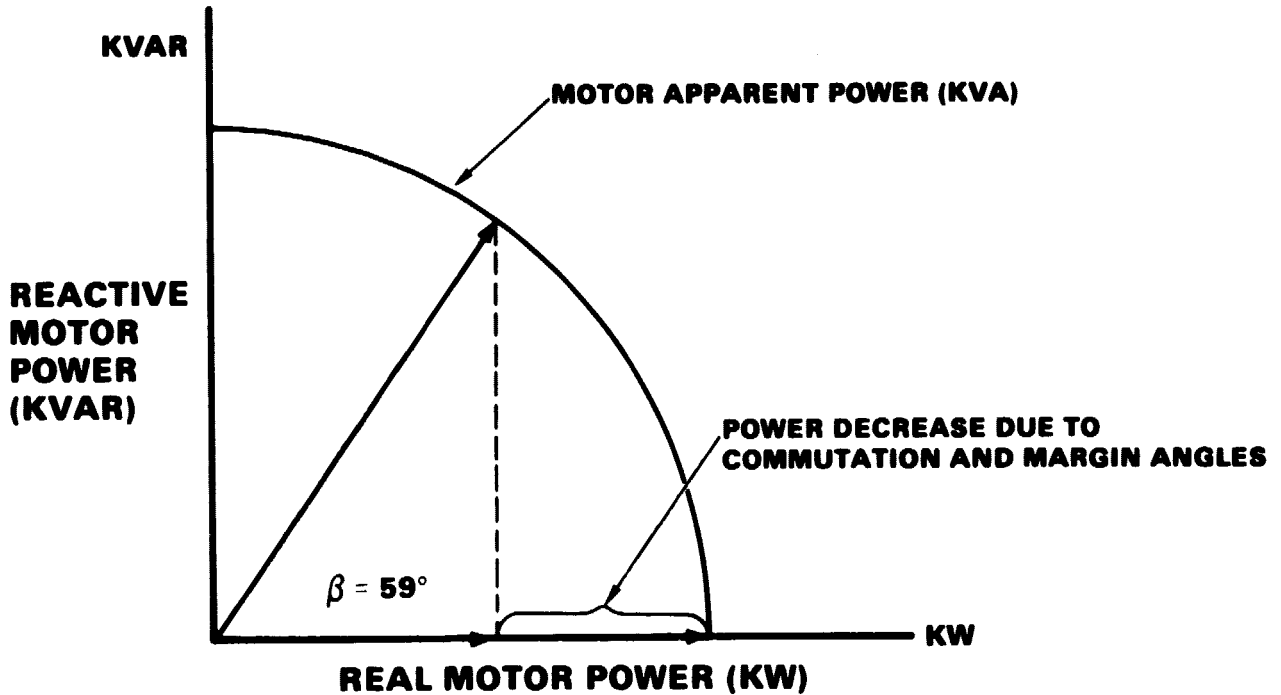
**= 14.84 KW - 3.25 KW**

**= 11.59 KW**

A-31509

Figure 84.--Thyristor Inverter, Functional Model Motor.

ORIGINAL PAGE IS  
OF POOR QUALITY



$$\text{KW} = \text{KVA} \cos \beta = \text{KVA} \times \text{MOTOR POWER FACTOR}$$

$$\begin{aligned} \text{MOTOR POWER FACTOR} &= \cos \beta \\ &= \cos 59^\circ \\ &= 0.52 \end{aligned}$$

WHERE:

$$\beta = \mu + \delta \quad \text{DEGREES (59}^\circ\text{)}$$

$$\mu = \text{COMMUTATION ANGLE (25}^\circ\text{)}$$

$$\delta = \text{MARGIN ANGLE (34}^\circ\text{)}$$

A-31598

Figure 85.--Motor Input Power Factor (Thyristor Inverter).

In contrast, using a transistor inverter as envisioned for the advanced motor converter, the motor current could be controlled to within the ideal conditions, so that near-unity power factor could be delivered to the motor. Fig. 86 shows the computer model results, with the functional model motor output rated at 23.63 kW. Note that since the transistor inverter turn-off is controlled solely by its base drive, the transistor inverter does not require a margin angle analogous to the thyristor inverter, hence, can operate at a much higher motor power factor. Figure 87 shows a system efficiency map for this configuration, assuming 192 vdc input to the system. This map considers the losses in both the rotating machine and the electronics.

Table 12 shows the key parameters of the functional model rotating machine. Table 13 shows the comparative predicted performance of the functional model motor using transistor or thyristor inverter circuits. Based on the predicted 11.59 kW output using the thyristor inverter IECM converter, it was mutually agreed between AiResearch and NASA that actual testing with this converter need not be performed.

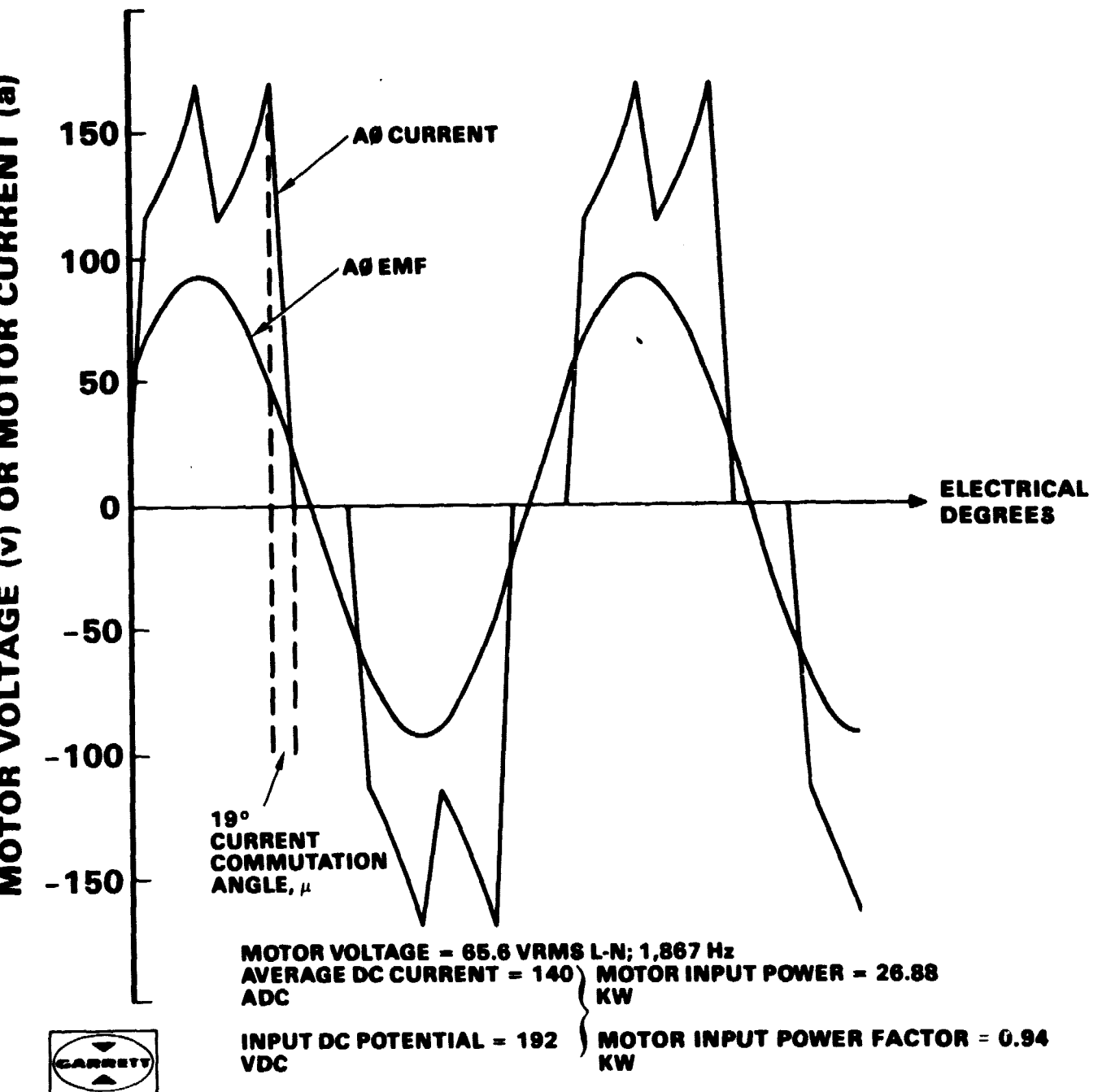


Figure 86.--Transistor Inverter, Functional Model Motor.



ORIGINAL PAGE IS  
OF POOR QUALITY

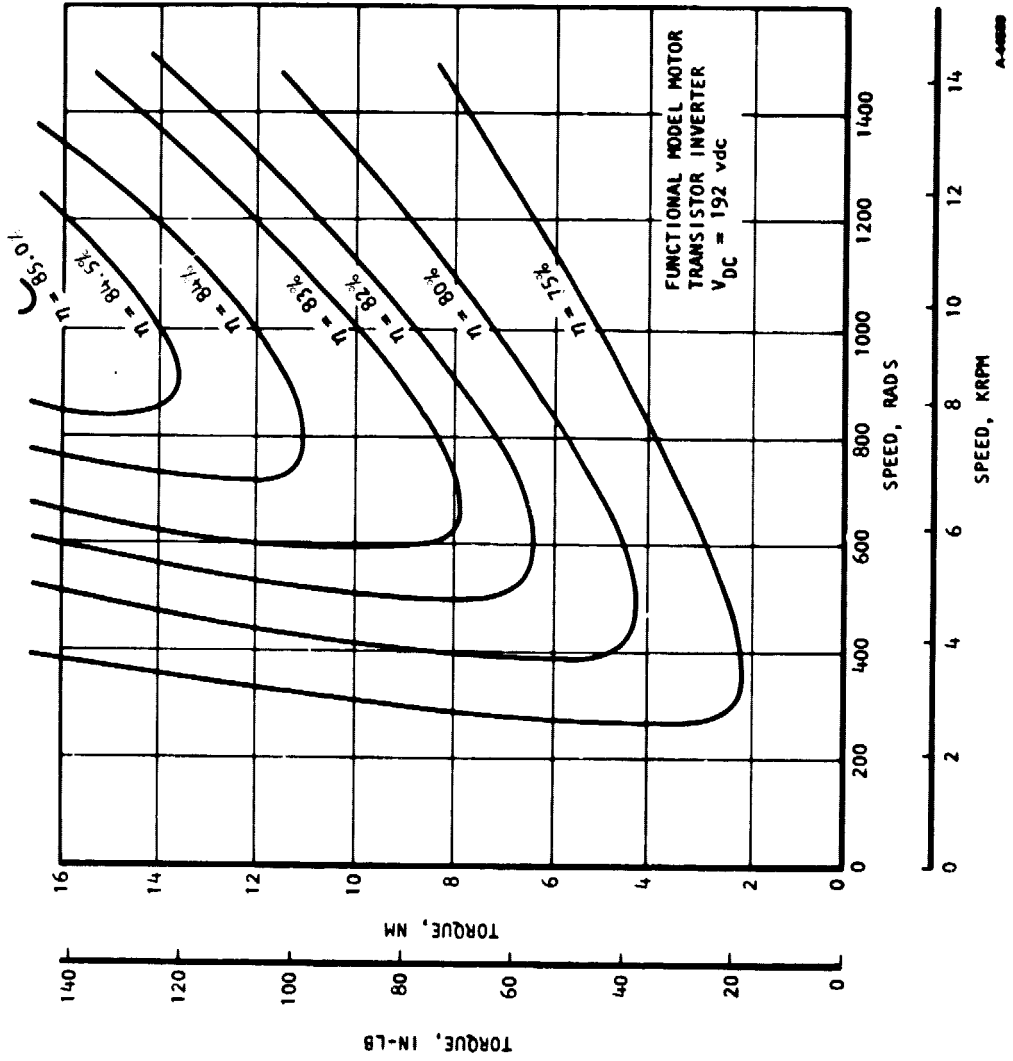


Figure 87.--Predicted Efficiency Map of Functional Model Motor  
with Transistor Inverter

TABLE 12.--ADVANCED MOTOR FUNCTIONAL MODEL ROTATING MACHINE PARAMETERS.

Parameter	Value
Resistance per phase, (ohms)	0.0205
Commutating inductance per phase, ( $\mu$ H)	14.92
Commutating reactance per phase, (pu)	0.294
Ac volts per phase, (V rms)	65.6
Ac current per phase, (A rms)	110.0
Motor speed, (radis)	1466
Motor speed, (rpm)	14,000

TABLE 13.--ADVANCED MOTOR FUNCTIONAL MODEL PREDICTED PERFORMANCE.

Parameter	Converter Type	
	Transistor	Thyristor
Dc voltage, (Vdc)	192	106
Dc current, (Adc)	140	140
Firing angle, $\alpha$ (deg)	180	121
Commutation angle, $\mu$ (deg)	19	25
Margin angle, $\delta$ (deg)	-	34
Input power, (kW)	26.88	14.84
Output power, (kW)	23.63	11.59
Motor efficiency, (percent)	87.9	78.1

## CONCLUSIONS

This report presents the analytical and test results of the advanced axipolar ironless stator ac motor. The design, fabrication, testing, and data reporting for this advanced motor and controller concept were accomplished under Contract DEN 3-77 with NASA Lewis Research Center.

The motor is a unique design, using permanent magnet excitation, homopolar flux path concepts, axial air gap design, and ironless stator construction. This effort was directed toward the goal of providing a low-cost motor for electric passenger vehicle propulsion that would operate at a high efficiency and acceptable weight. In conjunction with the rotating machine, a controller was designed to achieve optimum system performance.

The major determinations made during the program are summarized below.

- (1) Stator fabrication was a major problem on both the proof-of-principle and functional model machines. Special thin-strip multiple-coated polyimide magnet wire had to be developed to successfully build the stator. Program funding was not of a magnitude to permit design and fabrication of full-scale coil forming and assembly tooling; thus, the stators were built with tooling that required many hand forming and dimensional control operations. With the constraints of this approach on stator fabrication, the dimensional tolerances achieved necessitated modifications to the rotor poles. This limited the motor performance capability and increased the machine per unit reactance. The analytical design predicted 26 kW, however, the actual functional model hardware would have been capable of operating up to 23 kW as a motor. It is felt that this problem would not be present in a properly tooled production stator.
- (2) The windage losses of the rotating machine were higher than originally predicted. The homopolar pole arms of the rotor design were intended to act as a pump to provide cooling air for the stator assembly. The proof-of-principle motor used shrouds on the rotor poles to control the flow. This proved to be inadequate, so, on the functional model, the interpole areas were filled with a foam encapsulant. Small holes were provided to pump the air to the stator assembly. The windage/pumping losses were reduced from 5 kW to 2 kW, and the rotating machine operated successfully in the generator mode with thermal stability achieved at rated current with considerable thermal margin. The pumping power could be reduced still further in a subsequent design, but it appears from the windage analysis test data that a design completely restricting cooling airflow would still have approximately a 1-kW aerodynamic loss.

- (3) As a corollary to the windage consideration, audible noise control is required. If not muffled, the air noise at high speeds would be unacceptable in a passenger vehicle. This would not represent a significant problem in the suitability of this motor. Internal combustion engines require exhaust mufflers to make them usable.
- (4) One other area of higher losses developed in the testing of the rotating machine. The nature of the axial gap homopolar rotor is such that a stray magnetic field exists behind and above the rotor poles. The extent of this field is increased to some degree when operated with an ironless or high-reluctance stator. This stray magnetic field is an ac field (1867 Hz at full speed), which attempts to penetrate any metal support structures in close proximity. Machined aluminum housings were used on the motor to reduce weight and cost, thus some eddy current losses were developed by the stray field at the higher rotating speeds. The functional model motor made some adjustments in this area, increasing the separation between the magnetic poles and any surrounding metal structure. This would not be a limiting constraint on the use of this motor. The magnitude of this loss was not prohibitive, and with proper spacing and the use of some nonmetallic components, this loss would be controlled.
- (5) The inertia of the rotating assembly in this axipolar design is inherently high. On the positive side, this will smooth any torque ripple seen by the drivetrain; however, it does present some concern regarding the time and energy required to accelerate the rotor when accelerating the vehicle, and the time required to decelerate the rotor when shifting gears. The extent of the problem is evident when considering that 28 percent of the total energy required to accelerate a 1350-kg (3000-lb) vehicle system to 56 km/hr (35 mph) would be used to accelerate the motor rotor. To decelerate the rotor while shifting from first to second gear would require 2.3 s.
- (6) Magnet fabrication presented some difficulty. Although the magnet is basically a single piece, the present industry capability limits the size of samarium cobalt blocks that can be made. The bonding of a number of magnet sections together, then grinding and magnetizing, somewhat defeats the purpose of the single magnet design. Further development in rare-earth cobalt magnet fabrication techniques or use of a ferrite material option would seem to be required to realize the full cost potential of the axipolar design.
- (7) An interesting design constraint developed when consideration was given to driving the rotating machines with a thyristor inverter rather than a transistor type. In order to limit program costs, modification of an existing thyristor controller was considered. The motor reactance was such that when the thyristor firing angle was set to provide for the switching or commutation event, the effective power factor became so low that motor output power would be limited to 11.6 kW. With that power constraint making thyristor inverter operation impractical and with insufficient funds available to fabricate the intended transistor inverter, the program activities were concluded after fully testing the

functional model in the generator mode. This evaluation reinforced the point that for power outputs up to 100 kW, transistor inverters are favored. If a thyristor inverter were to be used, the machine reactance control would necessitate a physically larger rotating machine.

- (8) The axipolar machine is easily adapted to the use of the very low cost and easily fabricated ferrite magnet material. Due to the lower energy level of those magnets when compared to rare-earth cobalt, the motor would have to be approximately 30 percent larger and 2 percent lower in efficiency.

The axipolar ironless motor operated at its design power level with considerable thermal margin. Maximum full-power efficiency was down from the predicted 91 percent to 85 percent. This was a result of the not-fully-optimized windage losses and some additional stray field losses. Improvements can be made, but based on the characteristics of the machines tested, an efficiency goal of 87 percent now appears to be more realistic. The last few years have not brought the technical progress in the rare-earth cobalt magnet industry necessary to fabricate at low cost the single magnet type needed for this motor. The utilization of ferrite magnets would thus be preferred for the mass market even with some weight and efficiency penalty. The inherent motor rotor inertia and its effect on vehicle system performance would need a full evaluation before further development is undertaken on the axipolar ironless motor.

AiResearch Manufacturing Company  
A Division of The Garrett Corporation  
Torrance, California 90509  
June, 1983

## REFERENCES

1. Adapted from Knowlton, A. E.: Standard Handbook for Electrical Engineers. Eighth Edition, Sec. 2-81. McGraw-Hill, New York, 1949.

APPENDIX A  
LEAKAGE INDUCTANCE OF IRONLESS STATOR

The material below is for the calculation of the leakage inductance of an ironless stator as shown in fig. 88.

The inductance of an isolated rectangular coil of fig. 89 (ref. 1).

$$A: L_{SELF} = 2.303 \times K/10^9 \times d \times (a + b) \times \log_{10} (2a/(p + q))$$

$$-4 \times a \times \log_{10} ((a + d)/b)$$

$$-4 \times b \times \log_{10} ((b + d)/b) +$$

$$K/10^9 \times 8 \times d \times 2 \times (a + b) + 1.79 \times (p + q) \times H$$

$$\text{where } K = 2.54 \times N^2$$

N = Turns in a rectangular section, p x q

$$d = (a^2 + b^2)^{.5}$$

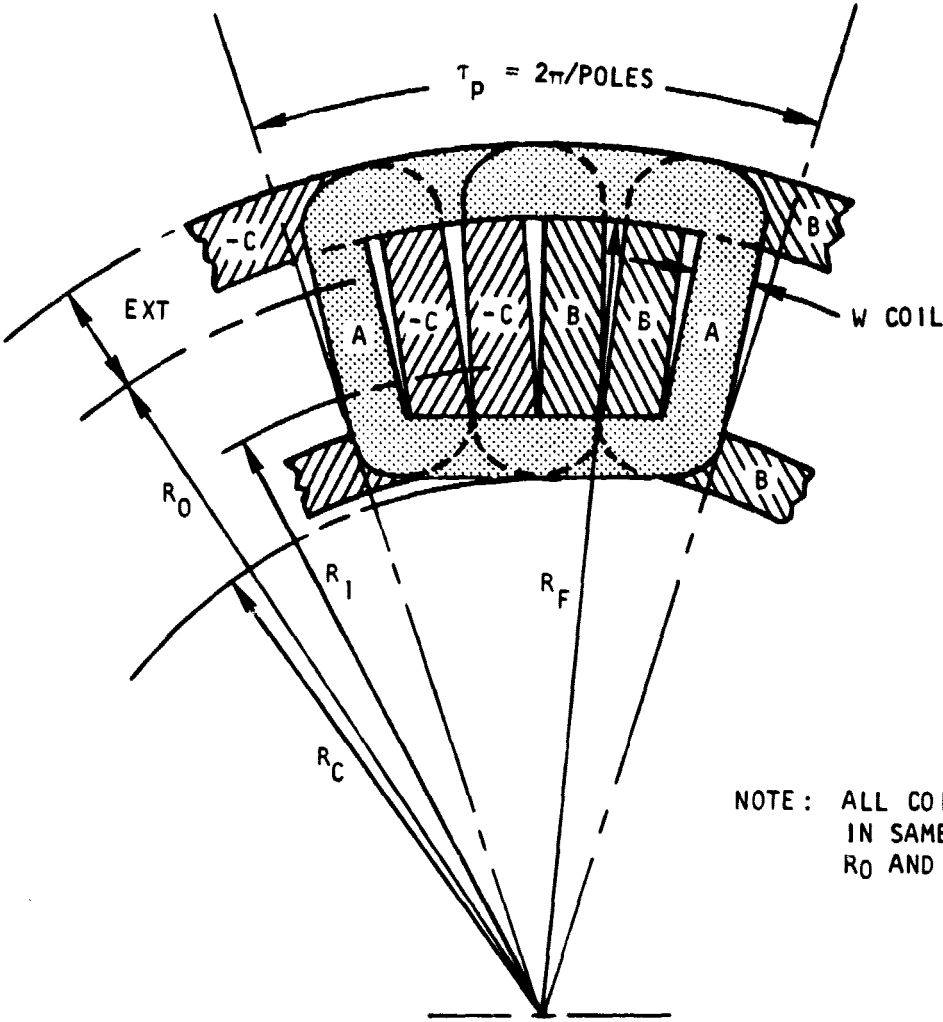
Dimensions are in inches. For dimensions in millimeters, use k = 0.1 N<sup>2</sup>.

Assume this expression is approximately correct for the trapezoidal coil model shown in fig. 90, if the average value of dimension b is used in expression A.

For a string of rectangular coils, the mutual inductance may be roughly estimated by inspection of fig. 91:

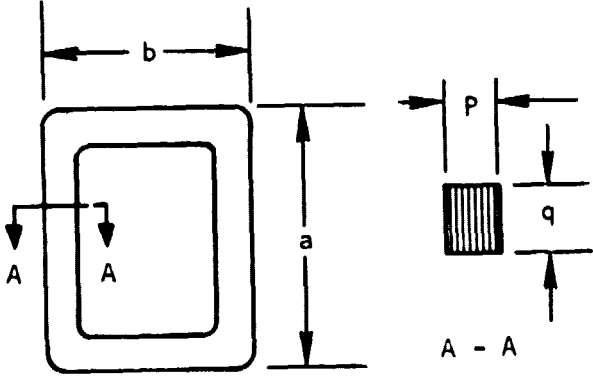
- (a) All coils are electrically in series and mutually aiding.
- (b) If the abutting coil sides occupied the same space (i.e., perfectly coupled), the mutual induction due to linkage of  $\Phi_{MI}$  of a coil pair X and Y would be  $\frac{1}{4}$  of the self induction of an isolated coil. This is inherent from the geometry regardless of coil proportions.
- (c) Since the coil sides do not occupy the same space, a coupling factor must be determined. From inspection of the ironless stator, the coupling factor between adjacent coils of the same phase group is estimated to be  $\frac{5}{6}$  when the width of a coil side p is about  $\frac{1}{6}$  of coil width b (see fig. 92).
- (d) Arrangement of a number of trapezoidal coils in a closed circular pattern is essentially equivalent to a long linear string of rectangular coils as far as self and mutual linkages are concerned.

ORIGINAL PAGE IS  
OF POOR QUALITY



A-32640

Figure 88.--Ironless Stator Model.

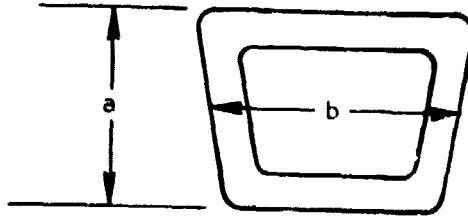


A-32641

Figure 89.--Rectangular Coil for Inductance Calculation.

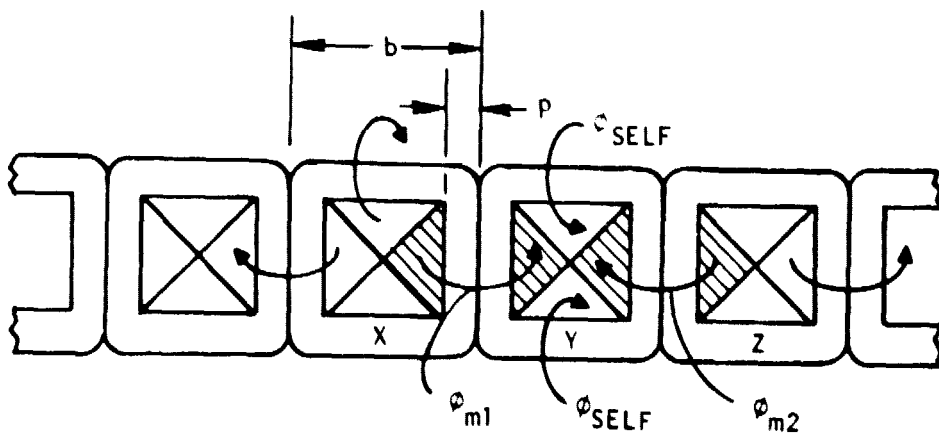


ORIGINAL PAGE IS  
OF POOR QUALITY



A-44956

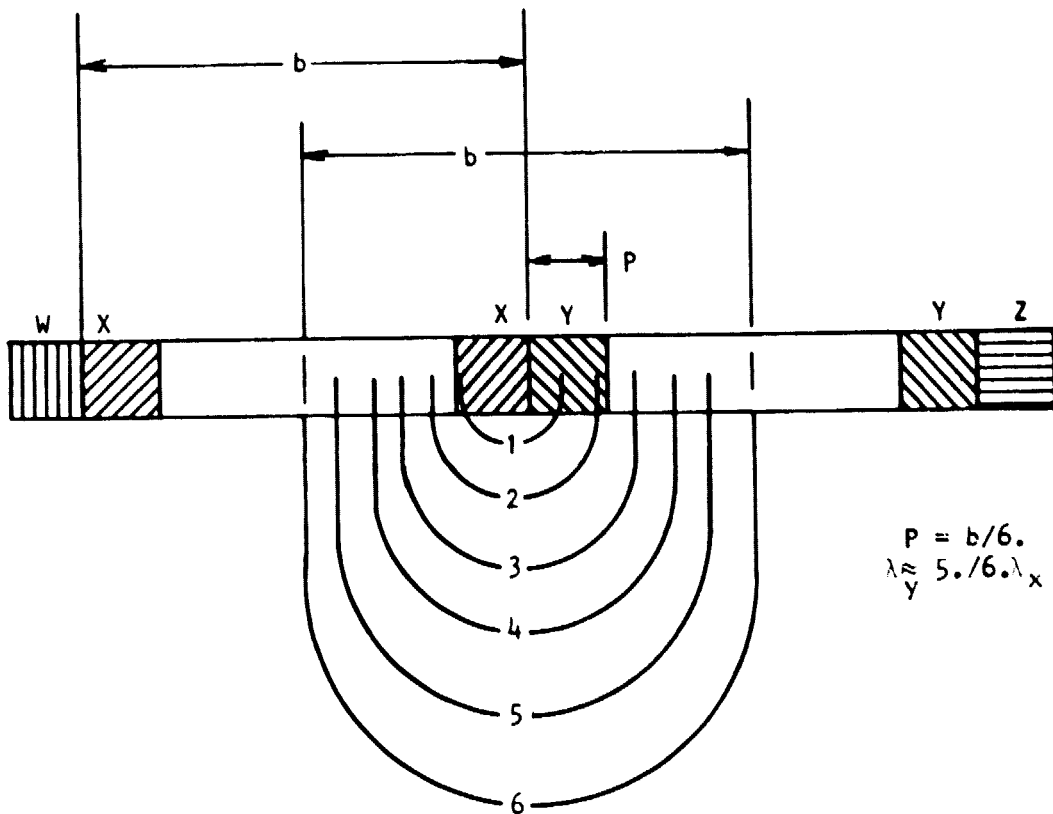
Fig. 90.--Trapezoidal Coil Model.



A-32639

Fig. 91.--Linear String Model of Phase "A" Coils.

ORIGINAL PAGE IS  
OF POOR QUALITY



A-32647

Figure 92.-- Section Through Coil String Showing Linkage  
Through Coil "Y" Due to Excitation of Coil "X".

**ORIGINAL PAGE IS  
OF POOR QUALITY**

Considering only the coils of a given plane A, the inductance  $L_{A1}$  of a single coil, Y, will be:

$$B: \quad L_{A1} = L_{SELF} + M_{YX} + M_{YZ}$$

where:  $L_{SELF}$  = the self inductance of the isolated coil Y given by expression A.

$M_{YX} = M_{YZ}$  = Mutual inductance contributed to coil Y due to excitation of adjacent coils X and Z.

$$C: \quad M = M_{YX} + M_{YZ} \approx 2 \times (L_{SELF}/4 \times K)$$

where:  $K$  = coupling factor  $\approx 5/6$

Combining B and C:

$$D: \quad L_{A1} = L_{SELF} + M = 17/12 \times L_{SELF}$$

Coil Y is also coupled with coils of phases B and C of the ironless stator. With balanced three-phase load, current vectors are equal but displaced 120 degrees in time. Also, each coil group is circularly displaced 120 electrical degrees. From inspection of fig. 88 it was concluded that when current in A is 1 pu and current in B and C is 0.5 pu, the total inductance of any stator coil is:

$$\begin{aligned} L_T &= L_{A1} + L_{C1} \times 0.5/\underline{60^\circ} - L_{B1} \times 0.5/\underline{120^\circ} \\ &= 1.5 \times L_{A1} \\ &= 2.125 \times L_{COIL} \end{aligned}$$

The above expression is valid only in the absence of iron. When the iron inductor poles are added, the demagnetizing flux must be accounted for by  $X_{AD}$  and  $X_{AQ}$ ; so  $L_T$  must be reduced to eliminate the direct and quadrature linkage that exists due to an entirely different magnetic circuit comprised of rotor pole iron, the magnet, and rotor leakage paths. Considering this, the inductance of a stator coil due to stator leakage paths in air and excluding iron paths is defined as follows:

$L_L = L_T \times (1 - \alpha/2)$  where  $\alpha$  is the pu unit pole embrace of the inductor rotor pole.

Expressing stator leakage as a pu unit reactance for a multipole, multi-circuit, three-phase winding:

$$X_{LPU} = \omega \times L_L \times I_{COIL}/V_{COIL}$$

where:  $\omega = 2 \times \pi \times f$

$$I_{COIL} = I_{BASE}/C$$

$$V_{COIL} = V_{BASE} \times C/POLES$$

C = No of parallel stator circuits

$$\text{Therefore: } X_{LPU} = \omega \times L_L \times POLES/C^2/Z_{BASE}$$

$$\text{where: } Z_{BASE} = V_{BASE}/I_{BASE}$$

It is believed that the estimated value of  $X_{LPU}$  is somewhat higher than actual because reduction of mutual linkage in the formed-end regions of the ironless stator coils was not taken into account. Furthermore, the presence of an electrically conductive housing around the stator o.d. will reflect and constrain stator leakage flux. Since the fundamental positive-sequence component of stator leakage flux is synchronous with the rotor hub and magnet located at the stator i.d., the latter are inhibitory only to non-synchronous components of stator flux. Leakage due to rotor hubs and poles is separately accounted for in the analysis of the excitation circuit of the machine.

## APPENDIX B THERMAL ANALYSIS OF THE ADVANCED ELECTRIC VEHICLE MOTOR

Note: The following thermal analysis was conducted during the preliminary design phase and does not represent the actual configuration of the functional model. It is presented here to indicate the type of cooling scheme intended and to give some feel for the portions of the duty cycle that are thermally critical.

### Analysis

A complete steady-state and transient thermal analysis has been performed on the salient pole propulsion motor for the advanced electric vehicle. A thermal nodal diagram of the motor appears in fig. 93. Flow enters the center of the unit by means of holes in the rotor shroud near the center shaft. The flow is pumped through the vertical rotor-stator gap by the centrifugal pumping effect created by the rapidly rotating, multipoled motor. A thermally actuated bimetallic choke (or similar flow-restricting mechanism) limits the amount of cooling flow in order to minimize the pumping losses of the motor, while at the same time providing adequate cooling. A small amount of the outlet cooling flow passes over a bimetallic actuation device for the choke and causes the choke to open somewhat for high outlet temperatures and to close somewhat for low outlet temperatures. This type of mechanism provides a nearly uniform outlet-coolant temperature, and thus, a nearly uniform motor temperature. The flow is therefore varied on demand depending on both the ambient temperature and the power level of the motor. The amount of air horsepower consumed by the pumping power of the motor is represented as follows:

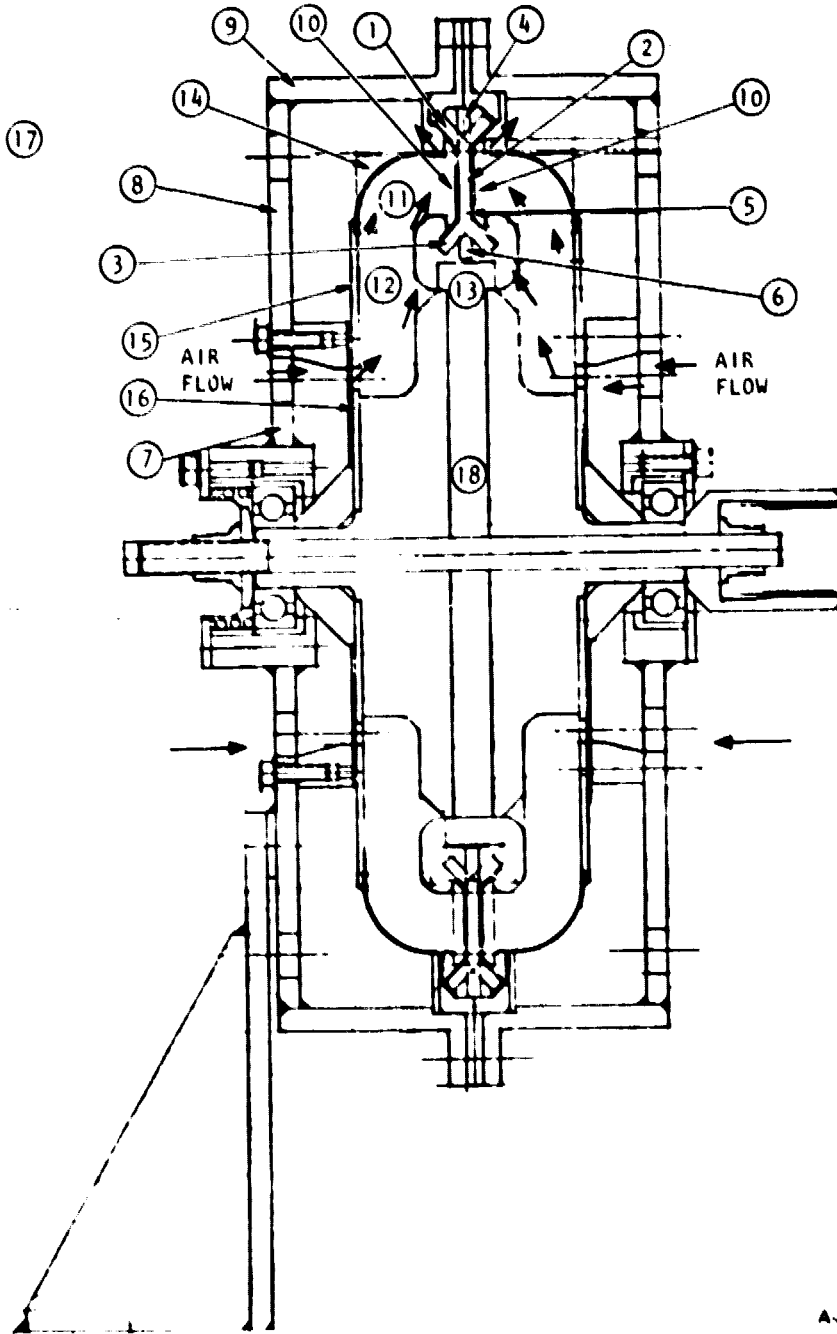
$$\text{Air Hp} = \text{flow (M}^3/\text{S)} \times \Delta P \text{ (Pa)} / 746.7$$

The pressure rise of the air,  $\Delta P$ , is a function of the motor speed. Thus, for any given speed, the pumping air horsepower consumed is directly proportional to the amount of cooling flow passing through the motor. Minimizing this flow by means of a bimetallic choke (or similar flow-restricting mechanism) is very important. For very low motor speeds, when the pumping power of the motor is extremely small, a vaneaxial centrifugal fan aids in cooling the motor (fig. 94).

The stator, which is a thin disk of copper windings, is insulated by a 0.05 mm-thick (0.002 in.) kapton tape and is held in place by external body structures. Nodes 1-6 represent the copper stator and nodes 7-9 are the external motor housing. Nodes 10-16 and 18-19 generally represent the rotor. Specifically, nodes 14-16 are the rotor windage shroud, nodes 10-12 are the iron salient poles, node 18 is the permanent magnet, node 13 is an Inconel ring, and node 19 is a solid iron center rotor section. Node 17 is a constant-temperature ambient boundary condition at 50°C (122°F).

For the worst steady-state operating condition, the electric vehicle climbs a 10 percent grade hill at 56.3 km/hr (35 mph) with 26 kW output power. The rotor speed is 1466 rad/s (14,000 rpm), and the total copper losses are 1.16 kW at 149°C (300°F). At this worst case steady-state condition, the unit is assumed to be cooled by 0.019 m<sup>3</sup>/s (40 cfm) of hot ambient air at 50°C (122°F).

ORIGINAL PAGE IS  
OF POOR QUALITY



A-32843

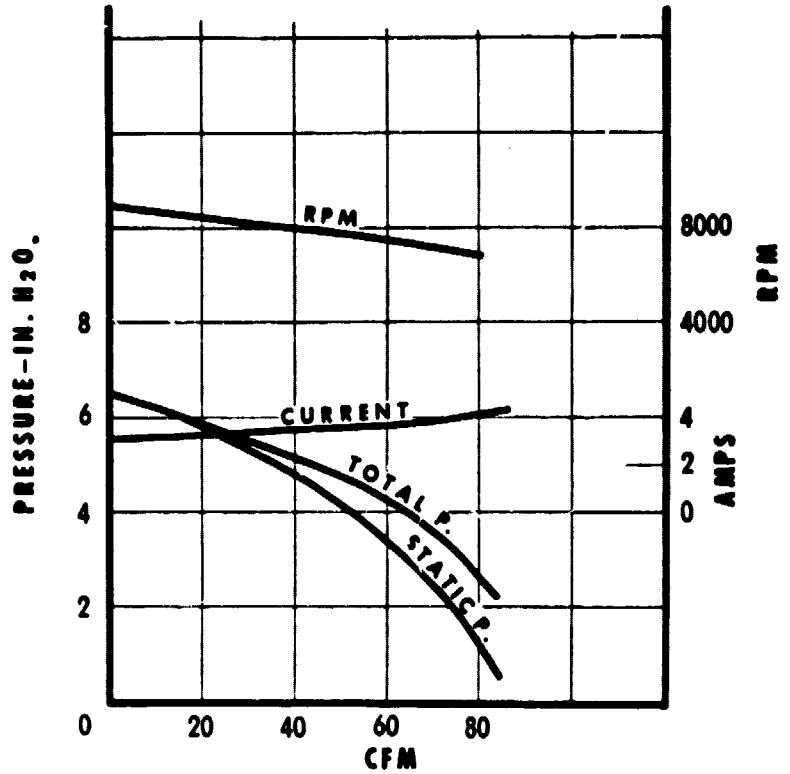
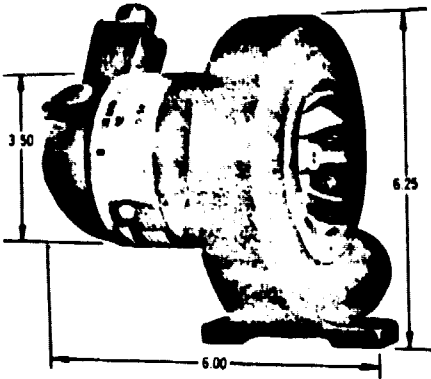
Figure 93.-- Thermal Nodal Diagram of the Advanced Electric Vehicle Motor.

ORIGINAL PAGE IS  
OF POOR QUALITY

**PERFORMANCE CURVE**

**CENTRIFUGAL FAN**

27 VDC  
SERIES WOUND



**DESIGN POINT:**

50 CFM @ 4" H<sub>2</sub>O  
STATIC PRESSURE

WEIGHT 4.75 lb.

**MODEL NO. M125Q-9C**

A-32842

Figure 94.-- Auxiliary Fan for Advanced Electric Vehicle Motor.

As a worst-case transient condition, the cycle shown in fig. 95 was applied using initial conditions from the uphill steady-state case. The cycle consists of a 15-s initial acceleration to 56.3 km/hr (35 mph) followed by an 11-s upshift acceleration to 72.4 km/hr (45 mph). The vehicle then cruises at 72.4 km/hr (45 mph) for 53 s and coasts down to 62.8 km/hr (39 mph) for 9 s. The final 11 s of the run consists of a downshift and braking to a full stop. Thus, the full cycle lasts approximately 99 s.

## Results

Steady-state climb.--A computer printout of the steady-state thermal results for the hot day 56.3 km/hr (35 mph), 10 percent grade climb appears in table 14. The hottest temperature of 208°C (407°F) appears at copper node 4. This region is cooled almost solely by conduction, since it is surrounded by an insulation support. However, even this temperature is safely below the maximum allowable temperature limit of 220°C (428°F). The weight-averaged copper temperature is somewhat less at 165°C (329°F).

The magnet, node 18, is at a safe 99°C (211°F), which is below its maximum allowable limit of 121°C (250°F). The iron pole temperature is running at a safe temperature of approximately 110°C (230°F), and the external housing has a maximum temperature of approximately 126°C (258°F).

A summary of the motor losses for the 56.3 km/hr (35 mph), 10 percent grade climb is given in table 15. The largest is the 1158 W of copper resistance heat. The second largest loss is a 310-W windage loss associated with the 1466 rad/s (14,000 rpm) rotor spinning inside the stationary housing. This could be decreased by approximately 25 percent by using somewhat more optimum rotor-to-housing gaps and by rounding all corners to minimize eddy flow losses. In addition, the rotor-to-stator internal windage loss of 25 W could be cut in half if some type of filler was used between the salient rotor poles, i.e., if the rotor disk was cylindrically smooth instead of consisting of eight distinct poles.

The amount of power consumed by the pumping action of the salient pole rotor is 135 W for 0.019 m<sup>3</sup>/s (40 cfm) at 1466 rad/s (14,000 rpm). This value is expected to be significantly less for lower speeds and/or lower flow rates as determined by the flow-restricting mechanism of the bimetallic choke. At any point in the duty cycle, however, use of no more than 0.019 m<sup>3</sup>/s (40 cfm) of cooling air is anticipated.

Transient duty cycle.--For the transient case that is assumed to follow immediately after the 56.3 km/hr (35 mph), 10 percent grade climb, the hottest temperature appears at the end of the initial 15-s acceleration (table 16). At this time, the maximum copper temperature has climbed an additional 80°C to 214°C (417°F). This is well below the maximum allowable short-term copper temperature of 250°C (482°F). All other iron, housing, and magnet temperatures are essentially the same as those found during the steady-state climb.

A plot of the maximum copper temperature versus time for this worst case, hot day transient appears in fig. 96. After the initial acceleration, the copper power decreases significantly, and the higher speed of the rotor helps to cool the copper more efficiently. A constant flow of 0.19 m<sup>3</sup>/s (40 cfm) cooling air



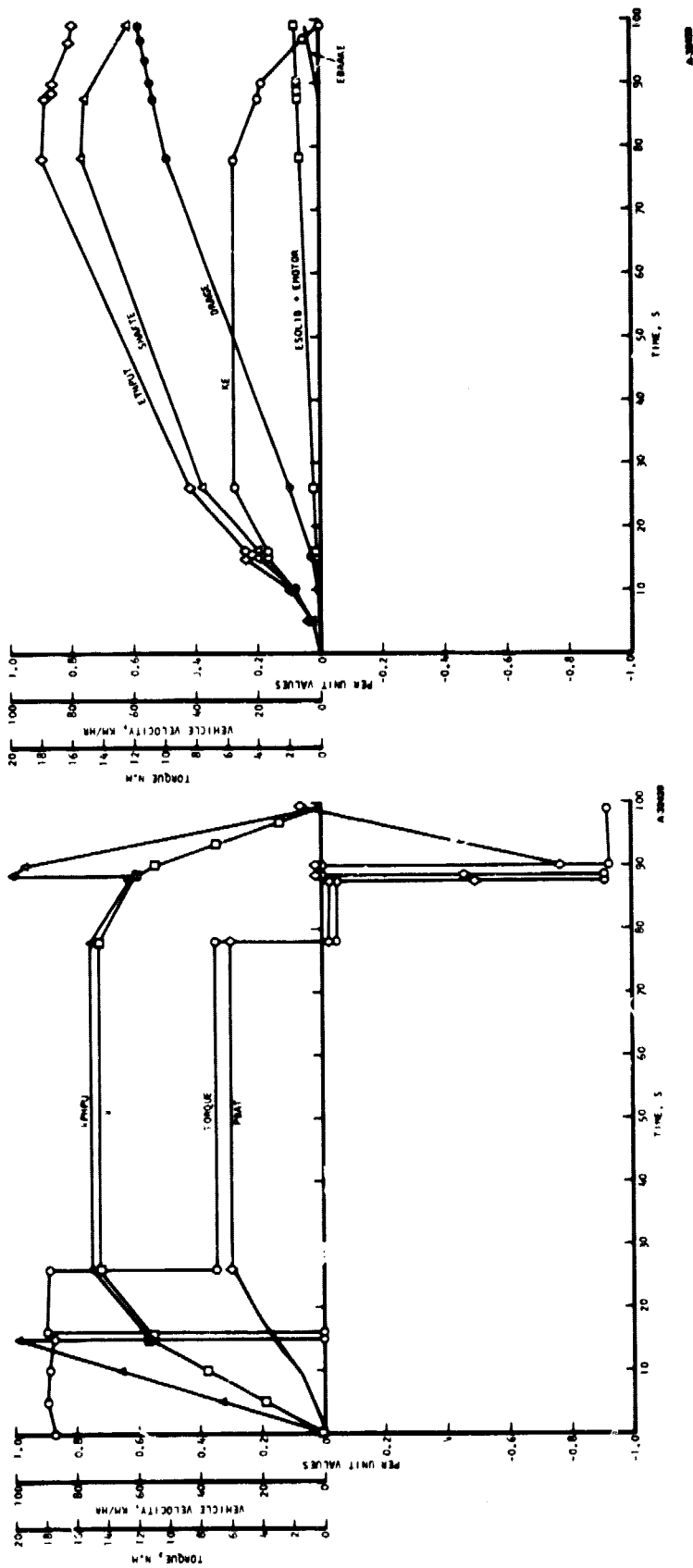


Figure 95.--Vehicle and Motor Performance Versus Time.

NOTE:

- V = Vehicle speed, km/hr
- RPM/PU = Motor speed per unit, 1 pu = 1466 rad/s.
- EMPUT = Energy delivered at the battery terminals per unit, 1 pu = 1000 kJ.
- SHAFT = Energy at the motor shaft per unit
- DRAG = Total vehicle drag energy (aerodynamic, rolling resistance, gear loss) per unit
- KE = Vehicle kinetic energy ( $\frac{1}{2} MV^2$ ) per unit. Kinetic energy due to wheels, drive train, and motor is ignored.
- ESOLID = Total energy loss due to solid state converter and its auxiliary devices (cooling fan, controls, and choke) per unit
- EBRAKE = Energy loss due to mechanical braking per unit
- EMOTOR = Total energy loss due to motor (copper loss, eddy loss, stray loss, pole head loss, bearing loss and windage) per unit
- EMBAT = Power at battery terminals per unit, 1 pu = 30 kW.
- TORQUE = Motor torque, N·m

A-10000

ORIGINAL PAGE IS  
OF POOR QUALITY

TABLE 14.--ADVANCED ELECTRIC VEHICLE MOTOR THERMAL RESULTS FOR STEADY STATE,  
56.3 km/hr (35 mph), 10 PERCENT GRADE CLIMB.

NO.OF ITER.= 8      DTEMP= .5000      ACCEL= 1.0000

NODE NO.	TEMP.	HEAT IN.	RHOV	CPN	KN	TEMPC.
1	334.15	270.3594	.453440	.1000	200.00000	167.85
2	305.45	336.5689	.582160	.1000	200.00000	151.90
3	279.85	175.5185	.318560	.1000	200.00000	137.68
4	406.94	149.1219	.226816	.1000	200.00000	208.29
5	354.31	180.2600	.294048	.1000	200.00000	179.05
6	340.98	95.8554	.159264	.1000	200.00000	171.65
7	205.11	.0000	.655741	.1200	25.00000	96.16
8	256.42	.0000	6.210610	.1200	25.00000	124.67
9	258.12	.0000	3.121200	.1200	25.00000	125.61
10	232.25	.0000	.817870	.1200	25.00000	111.24
11	232.49	.0000	4.580650	.1200	25.00000	111.37
12	219.16	.0000	4.907220	.1200	25.00000	103.96
13	174.92	.0000	.897975	.1300	8.00000	79.39
14	247.70	.0000	.980577	.1200	25.00000	119.82
15	245.90	.0000	.871624	.1200	25.00000	118.82
16	226.26	.0000	1.334602	.1200	25.00000	107.91
17	122.00	.0000	-1.000000	1.0000	.01600	49.99
18	210.70	.0000	3.508400	.1000	4.85000	99.26
19	212.48	.0000	3.861040	.1200	25.00000	100.26

TOTAL WEIGHT IS 33.7878 LBS.

FLUID CAPACITY RATE ELEMENTS

STREAM NO.= 1      NODE NO.= 100      INLET TEMP.= 122.00

SECTION	NODE NO.	TOUT	FLOW	RHOV	HEAT IN.
1	101	126.86	163.7000	.0679	.472598
2	102	138.18	163.7000	.0670	.000000
3	103	174.08	163.7000	.0644	46.359074
4	104	192.73	163.7000	.0617	71.755592
5	105	269.06	163.7000	.0574	177.946375
6	106	286.34	163.7000	.0538	110.632318
7	107	264.58	163.7000	.0540	212.926889

A-32844

TABLE 15.--ADVANCED ELECTRIC VEHICLE MOTOR LOSSES FOR 56.3 km/hr (35 mph),  
10 PERCENT GRADE CLIMB.

Source	Loss, W
Copper	1158
Rotor to Housing Windage	310
Rotor to Stator Windage	250
Coolant Flow Pumping	133
Total	1851

NOTE: Copper loss based at 1490C (3000F)  
Motor speed - 1466 rad/s (14,000 rpm)  
Coolant flow - 0.019 m<sup>3</sup>/s (40 cfm) at 500C (1220F)

at 500C (1220F) is assumed to flow through the motor during the entire transient. At higher speeds, the flow is restricted by a bimetallic choke in order to limit pumping losses, and at a slower speeds, the cooling flow is aided by the auxiliary fan.

Pressure drops.--At 1466 rad/s (14,000 rpm), the total expected velocity head at the outer rotor diameter is 6970 Pa (28in. H<sub>2</sub>O). This is half of the velocity head corresponding to a flow with the full tangential velocity of the rotor. The anticipated pressure drop across the rotor mechanism itself is about 747 Pa (3 in. H<sub>2</sub>O) at this flow and rotor speed. Therefore, an additional 6220 Pa (25 in. H<sub>2</sub>O) pressure drop must be applied across the butterfly bimetallic choke for this 56.3 km/hr (35 mph) climb condition. The preferred diameter of a butterfly valve choke for this application is about 29.2-mm (1.15 in.) i.d. With 1466 rad/s (14,000 rpm), the valve would close about 40° from the center line to provide the above additional 6220 Pa (25 in. H<sub>2</sub>O) pressure drop. With the valve fully opened, approximately 1240 Pa (5 in. H<sub>2</sub>O) pressure drop would be incurred in the system, thus meeting the specification curve for vaneaxial fan no. M125Q-9C at 0.019 m<sup>3</sup>/s (40 cfm) (fig. 94).

ORIGINAL PAGE IS  
OF POOR QUALITY

TABLE 16.--ADVANCED ELECTRIC VEHICLE MOTOR THERMAL RESULTS FOR WORST-CASE  
TRANSIENT ACCELERATION CONDITION.

TIME= 15.000    DTHETA= .99999999    NODE NO.= 0

NODE NO.	TEMP.	HEAT IN.	RHOV	CPN	KN	TEMPC.
1	340.07	286.8767	.453440	.1000	200.00000	171.14
2	314.93	372.2500	.588160	.1000	200.00000	157.17
3	293.30	201.5000	.318960	.1000	200.00000	145.16
4	416.50	143.9867	.226816	.1000	200.00000	213.60
5	367.66	186.0767	.294048	.1000	200.00000	186.66
6	359.37	100.8000	.159264	.1000	200.00000	181.86
7	206.31	.0000	.655741	.1200	25.00000	96.83
8	253.64	.0000	6.210610	.1200	25.00000	123.12
9	255.06	.0000	3.121200	.1200	25.00000	123.91
10	230.04	.0000	.817870	.1200	25.00000	110.01
11	231.37	.0000	4.580650	.1200	25.00000	110.75
12	218.96	.0000	4.907220	.1200	25.00000	103.85
13	175.11	.0000	.897975	.1300	8.00000	79.49
14	240.48	.0000	.980577	.1200	25.00000	115.81
15	239.00	.0000	.871624	.1200	25.00000	114.99
16	223.31	.0000	1.334602	.1200	25.00000	106.27
17	122.00	.0000	-1.000000	1.0000	.01600	49.99
18	210.84	.0000	3.508400	.1000	4.85000	99.34
19	212.67	.0000	3.861040	.1200	25.00000	100.36

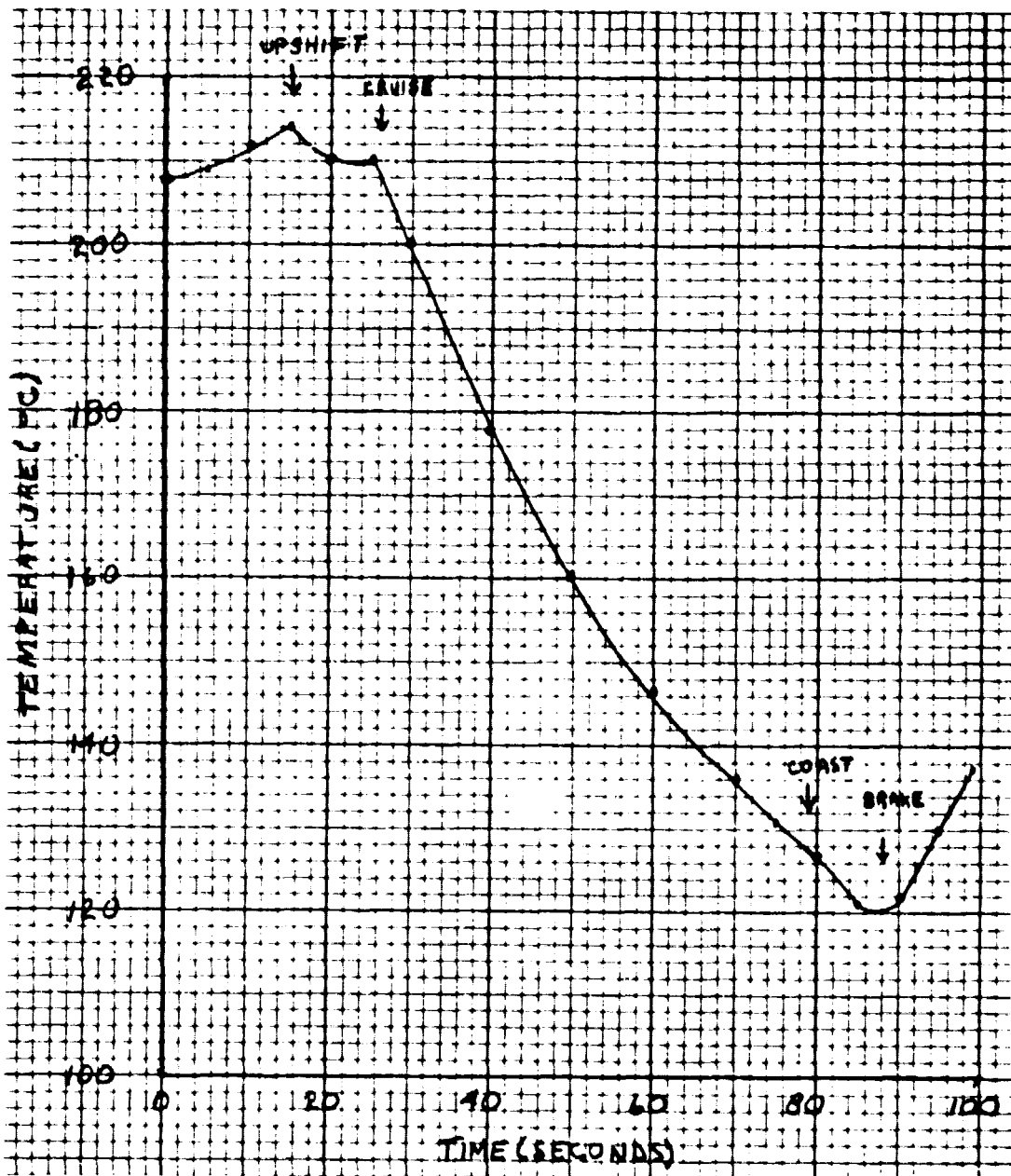
TOTAL WEIGHT IS 33.7878 LBS.

FLUID CAPACITY RATE ELEMENTS

STREAM NO.= 1    NODE NO.= 100    INLET TEMP.= 122.00

SECTION	NODE NO.	TOUT	FLOW	RHOV	HEAT IN.
1	101	126.73	163.7000	.0679	.270526
2	102	137.70	163.7000	.0670	.000000
3	103	173.86	163.7000	.0645	25.076421
4	104	191.16	163.7000	.0619	43.499998
5	105	262.29	163.7000	.0579	43.499998
6	106	276.03	163.7000	.0546	43.499998
7	107	255.78	163.7000	.0547	114.574678

A.32648



NOTE: Initial Conditions are from 35 MPH, 10% Grade, Steady-State

A32648

Figure 96.--Maximum Stator Winding Temperature for Worst Case Operation, 50°C Ambient.

## APPENDIX C

### ADVANCED ELECTRIC MOTOR

The motor, as defined by layout L518950-1, was analyzed for the following conditions:

- (1) Maintain magnet disk tensile stress below 27.58 MPa (4000 psi) at 1774 rad/s (16,940 rpm).
- (2) Size hoop ring and shrink fit required to obtain (1) above.
- (3) Estimate shaft preload required to maintain clamp-up under all loading conditions.
- (4) Calculate the critical speed of the rotating mass.
- (5) Calculate stresses at the junction of the rotor poles to the disk.

The results of the analysis showed the following:

- (1) For a hoop ring of 8.12-mm (0.32 in.) thickness, the required radial shrink fit is 0.36 mm (0.0143 in.) to maintain a tensile stress of less than 27.58 MPa (4000 psi) in the magnet disk when rotating at 27.58 MPa (16,940 rpm).
- (2) The shaft preload required is 31,100 N (7000 lb).
- (3) The critical speed of the rotating mass is 3030 rad/s in comparison with 1466 rad/s operating speed.
- (4) The maximum stress at the junction of the rotor poles and disk is 436 MPa (63,180 psi), which contains a 1.37 stress-concentration factor. The maximum stress in the rotor disk at the shaft hole is 198 MPa (28,765 psi).
- (5) A preliminary study of plan strain fracture,  $K_{IC}$  versus flaw size, indicates that this mode of failure will not be a problem.
- (6) The diameter of the steel rotor disk at the o.d. of the magnet disk must be maintained at a 0.15-mm (0.006 in.) smaller diameter than the magnet disk in order for the shrink fit forces to be transmitted to the magnet disk.
- (7) The hoop ring must be heated to 400°C (750°F) minimum to enlarge the ring diameter prior to assembly onto the magnet disk.

The stress analysis was based upon the following criteria:

Normal Operating Speed: 1466 rad/s (14,000 rpm)

Maximum Overspeed: 1774 rad/s (16,940 rpm)

Temperature Range: -30°C to 150°C in magnet  
150°C maximum in rotor poles

Acceleration (Lateral to Shaft): 10 g assumed

Rotor Imbalance: Based on 0.030 N·m (4.3 in. oz)  
0.25 mm (0.010 in.) offset and WT - 12.3kg (27 lb)

Magnet Material:

$F_{tu}$  27.58 MPa (4 ksi)  $t$  = 11.4 mm (0.4493 in.)  
 $F_{cu}$  0.241 GPa (35 ksi) o.d. = 151.3 mm (5.957 in.)  
 $E$  117.2 GPa ( $17 \times 10^6$  psi)  
0.3  
8580 kg/m<sup>3</sup> (0.31 lb/in.<sup>3</sup>)  
 $9.59 \times 10^{-6}$  mm/(mm·°C) ( $5.33 \times 10^{-6}$  in./in./°F)

Hoop Material: Inconel 718

$F_{tu}$  = 1.24 GPa (180 ksi)  
 $F_{ty}$  = 1.03 GPa (150 ksi)  
 $E$  = 204.1 GPa ( $29.6 \times 10^6$  psi)  
= 8221 kg/m<sup>3</sup> (0.297 lb/in.<sup>3</sup>)  
=  $12.78 \times 10^{-6}$  mm/(mm·°C) ( $7.1 \times 10^{-6}$  in./in./°F)

Shaft and Rotor Material: 4340 steel

$F_{tu}$  = 0.86 GPa (125 ksi)  
 $F_{ty}$  = 0.71 GPa (103 ksi)  
 $F_{su}$  = 0.52 GPa (75 ksi)  
 $E$  = 200.0 GPa ( $29 \times 10^6$  psi)  
=  $11.3 \times 10^{-6}$  mm/(mm·°C) ( $6.3 \times 10^{-6}$  in./in./°F)

where:

$F_{tu}$  = Ultimate tensile strength

$F_{cu}$  = Ultimate compressive strength

$E$  = Young's modulus of elasticity

$\mu$  = Poisson's ratio

$\rho$  = Material density

$\alpha$  = Coefficient of thermal expansion

$F_{ty}$  = Tensile yield strength

$F_{su}$  = Ultimate shear strength



## APPENDIX D

### DESIGN COMPARISON: RARE-EARTH COBALT MAGNETS VERSUS STRONTIUM FERRITE

Although rare-earth cobalt magnets exhibit the highest energy per unit volume of all currently existing magnet materials, they are also considerable more expensive than other magnet options. To evaluate the impact of using a lower-cost magnet material, a preliminary design comparison was made between a rare-earth magnet machine (15 MGO) and one using strontium ferrite (3.3 MGO). This ferrite magnet material has the highest cost efficiency on a dollars per energy product basis. The result of this analysis is presented in table 17.

The use of this lower energy product material results in a larger diameter machine, necessitating a reduction in rated rotational speed to keep the rotor-tip speed at the same level. The resulting weight penalty is about 28 percent and the efficiency penalty is about 2 percent. The magnet cost, however, is substantially lower for the ferrite version, even though a larger volume and weight is required. Another advantage of the ferrite is its lower density, resulting in a thinner section shrink ring to maintain magnet containment. This characteristic also makes it better suited to scaling in power and size.

This analysis is intended to indicate trends in comparative size and efficiency for a given power level. It is not intended to be an optimized design for this application, which would require a more intensive design analysis.

**ORIGINAL PAGE IS  
OF POOR QUALITY**

TABLE 17.--COMPARISON OF AXIPOLAR MACHINES USING 15 MGO AND 3.3 MGO MAGNETS

Magnet material	15 MGO, Sm-Co	3.3 MGO, ceramic 8
Magnet weight, kg (lb)	1.67 (3.68)	4.73 (10.41)
Magnet density, kg/m <sup>3</sup> (lb/in. <sup>3</sup> )	8300 (0.300)	4844 (0.175)
Estimated magnet cost, dollars	478	10.41
Magnet operating point, kg/koe	3.73/3.73	1.75/1.75
Motor diameter, mm (in.)	255.5 (10.06)	308.6 (12.41)
Speed, rad/s (rpm)	1466 (14,000)	1152 (11,000)
Volts, ac	81	81
Amperes, ac	110	110
Shaft power, kW	25.8	25.4
Electromagnetic weight, kg (lb)	11.18 (24.6)	14.32 (31.5)
Estimated total weight, kg (lb)	14.55 (32.0)	18.64 (41.0)
total motor losses, kW	1.91	2.51
motor efficiency, percent	93.1	91.0

APPENDIX E  
KEY COMPONENT DRAWING LIST  
FUNCTIONAL MODEL

Motor

Drawing No.	Drawing Title
518950	Motor outline
518951	Motor assembly
2043900	Stator assembly
2043901	Stator subassembly
2047243	Coil assembly
2047247	Rotor assembly
2047231	Multipole hub
2047240	Disc assembly
2047221	Disc, magnet
2043910	End bell assembly
2043911	End bell assembly

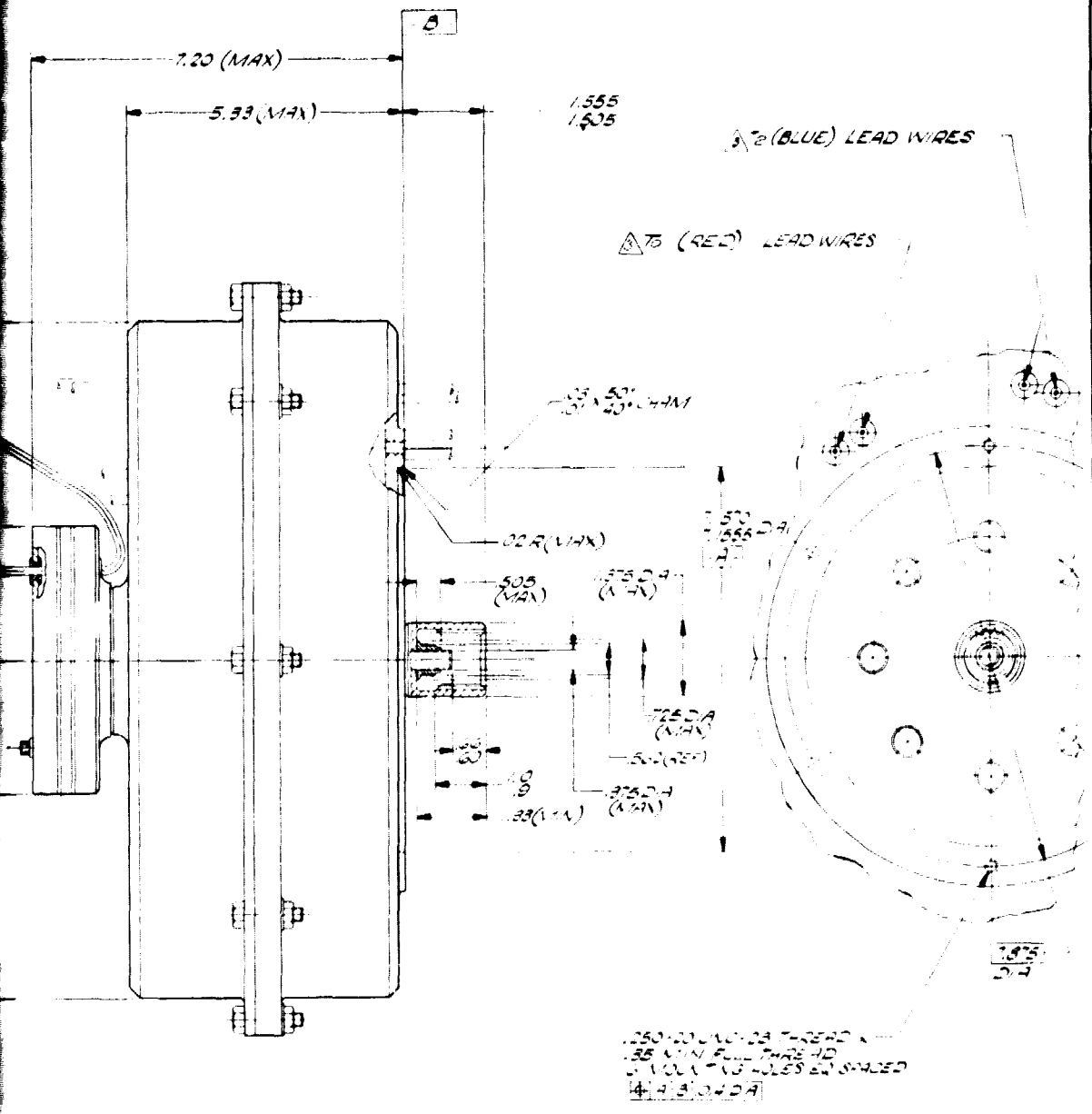
Power Converter

Drawing No.	Drawing Title
2001564	Inverter
2001592	Sync and speed decoder logic
2001566	Current sense and comparator
2001556	Drive-brake direction and tractive effort pause
2001558	Fault protection and tractive effort pause
2001570	Base drive power supply logic
2001560	Power supply
SKPW820910	Interface

Note: This list contains only the key components and is not a complete parts list for the motor. Further details must be determined by reviewing the complete parts list.



REVISIONS			
NO.	DESCRIPTION	DATE	BY

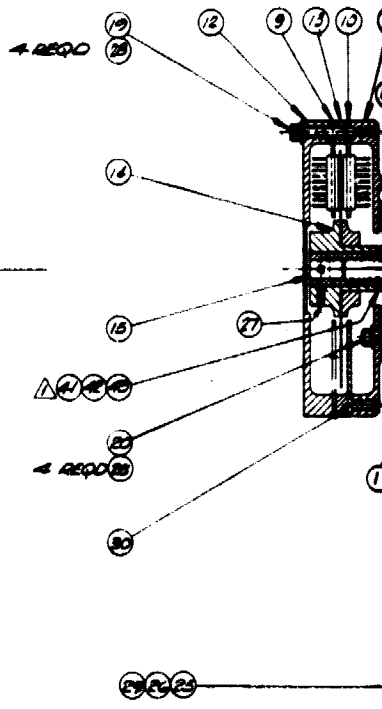
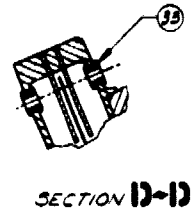
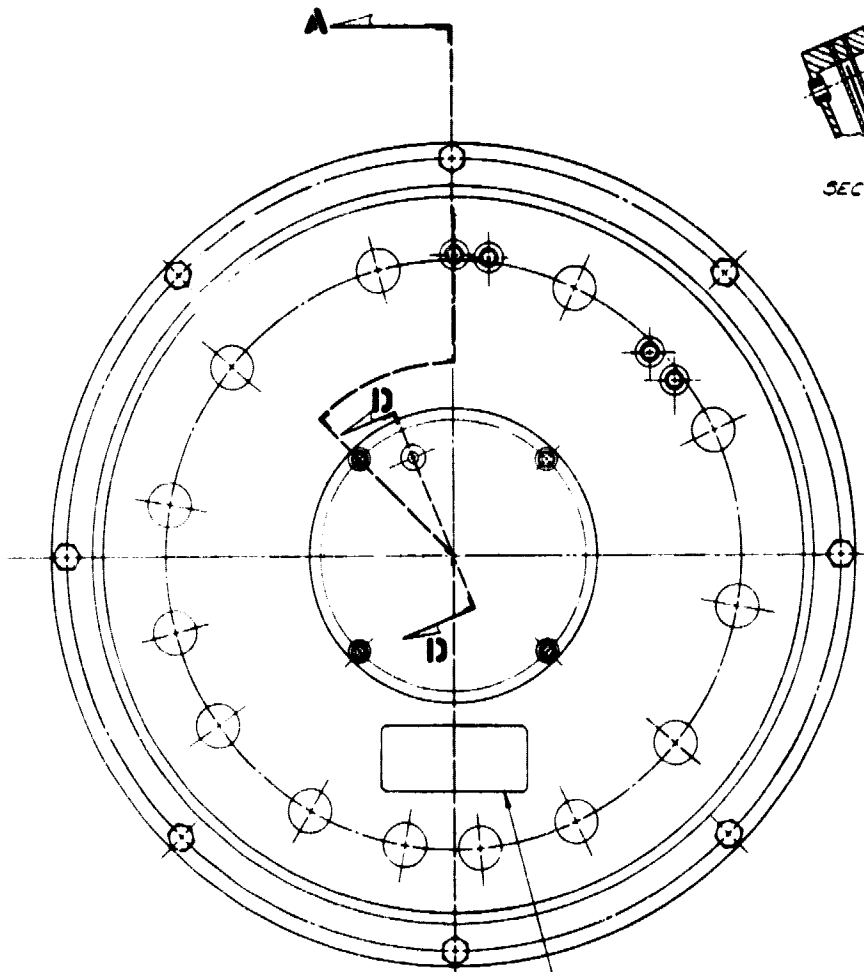
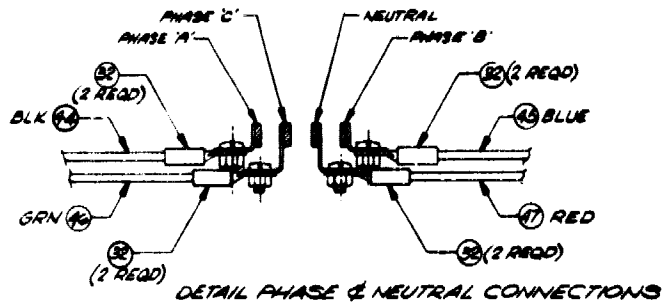


2 FOLDOUT FRAME

ORIGINAL PAGE IS OF POOR QUALITY

SEE PER SPEC MIL-W-18879.5  
 LINE DATA  
 1892, 1870 16 TEETH 1.00 DIAMETRAL  
 PRESSURE ANGLE, FILLET ROOT SIDE .5 T  
 FACE WIDTH .09955 ON STANDARD 1000  
 WITH DATA 1 WITH 200 TA  
 Wires FOR INSTALLATION PURPOSES ONLY  
 NOTES UNLESS OTHERWISE SPECIFIED

518950-1		518950-1	
PART NO.		ASSEMBLY NO.	
UNLESS OTHERWISE SPECIFIED DIMENSIONS ARE IN INCHES DIMENSIONS IN PARENTHESES ARE IN MILLIMETERS FINISH: UNLESS OTHERWISE SPECIFIED		MORGAN MANUFACTURING COMPANY 1000 S. GATEWAY AVENUE TORRANCE, CALIF. 90503	
MOTOR OUTLINE BRUSHLESS DC 4-4-3-0-0-0-0		E 70210 518950	
SCALE: 1/2"		SHEET 01 OF 01	



ORIGINAL PAGE IS  
OF POOR QUALITY

1	2	3	4	5	6	7	8	9	10	11	12	13	14	15	16	17	18	19	20	21	22	23	24	25	26	27	28	29	30	31	32	33
---	---	---	---	---	---	---	---	---	----	----	----	----	----	----	----	----	----	----	----	----	----	----	----	----	----	----	----	----	----	----	----	----

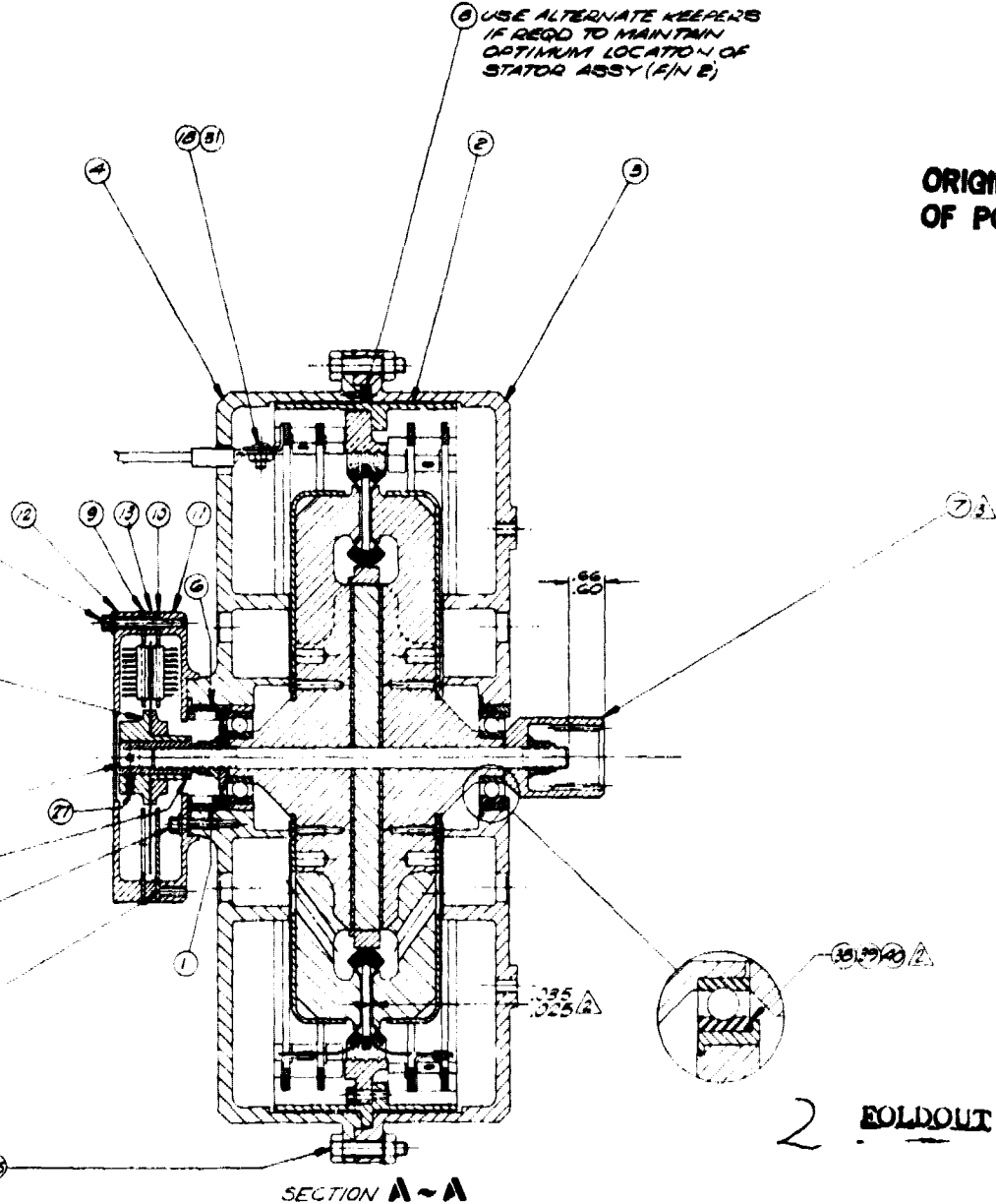
- ▲ APPLY PER AIRSEARCH
- ▲ WHEN RE-ASSEMBLING USE HYDRAULIC LOADER 7000 LBS AXIAL LOAD (APPLY BEFORE & AFTER LOADING)
- ▲ SHIM IF REQD. TO OBTAIN ROTOP ASSY (FIND NOT)
- ▲ SHIM AS REQUIRED TO OBTAIN SHUTTER ASSY (FIND NOT)
- ▲ SOURCE ASSY (FIND NOT)

NOTES: UNLESS OTHERWISE SPECIFIED

REVISIONS	
NO.	DESCRIPTION

⑨ USE ALTERNATE KEEPERS IF REQD TO MAINTAIN OPTIMUM LOCATION OF STATOR ASSY (F/N E)

ORIGINAL PAGE IS OF POOR QUALITY



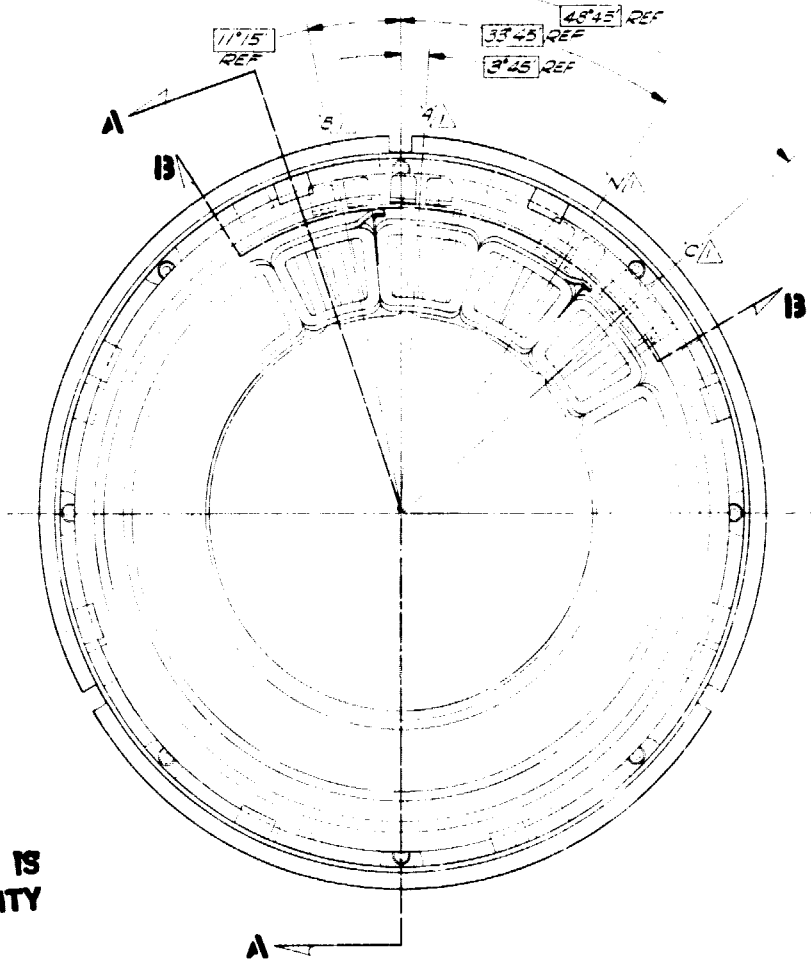
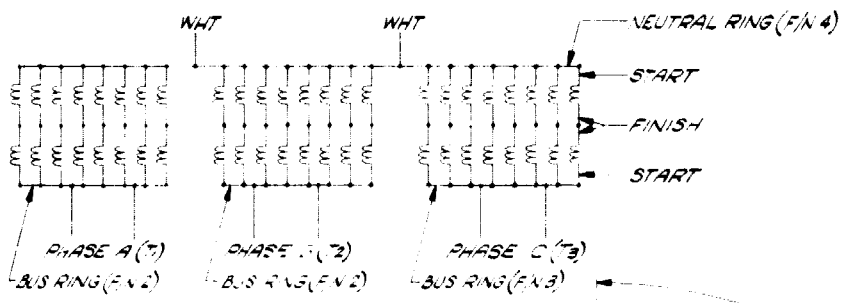
PRECEDING PAGE BLANK NOT FILMED

APPLY PER AIRSEARCH SPEC MC 9A  
 WHEN RE-ASSEMBLING ROTOR ASSY (FIND NO.7)  
 USE HYDRAULIC LOADER TOOL NO T70932 TO APPLY  
 7000 LBS AXIAL LOAD (REF) BOLT LENGTH TO BE MEASURED  
 BEFORE & AFTER LOADING. BOLT STRETCH .010-.014  
 SHIM IF REQD TO OBTAIN .090 REF CLEARANCE BETWEEN  
 ROTOR ASSY (FIND NO.7) & STATOR ASSY (FIND NO.2)  
 SHIM AS REQUIRED TO CENTRALIZE SHUTTER OF  
 SHUTTER ASSY (FIND NO.4) BETWEEN  
 SOURCE ASSY (FIND NO.10) & SENSOR ASSY (FIND NO.9)  
 NOTES: UNLESS OTHERWISE SPECIFIED

PART NO SEE SEPARATE PARTS LIST

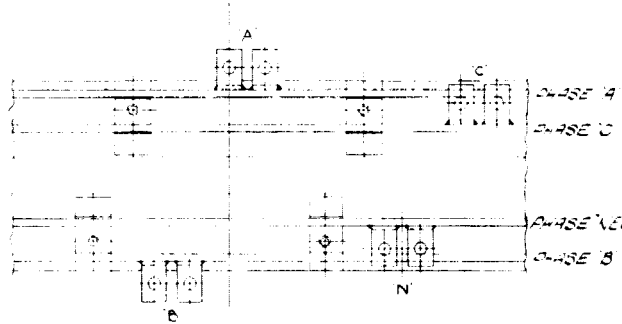
ADVANCED CONCEPT, INC. 1500 S. GARDEN AVENUE GARDEN CITY, CALIF. 92345	MOTOR ASSEMBLY ADVANCED CONCEPT, BRUSHLESS, DC	PART NO. E 70210	DRAWING NO. 518951
		SCALE: 1/1	SHEET: 1 OF 1

518951



ORIGINAL PAGE IS OF POOR QUALITY

FOLDOUT FRAME



SECTION B-B

3. WINDING RESISTANCE SHALL  
 4. WINDING ISOLATION RESISTANCE  
 5. THE INSULATION RESISTANCE  
 6. BUS RING (FN 2, 3 OR 4) & THE HOUSING  
 7. MIN. OF 2000 MEGOHMS AT 50  
 8. EACH PHASE OF THE WINDING SHALL  
 9. 2000 VOLT SURGE TEST FOR 1/2 S  
 10. THE WINDINGS SHALL WITHSTAND  
 11. VOLTAGE OF 500 VOLTS RMS OF  
 12. 10 TO 100 HOURS LESS THAN 2  
 13. CURRENT BETWEEN ANY BUS  
 14. & SOLDER (FN 4) FOR ONE SECON  
 15. 100 WATT POWER & NEUTRAL LEAD  
 16. OF EACH PHASE GROUP TO BUS RIN  
 17. AS SHOWN & SOLDER PER WBS 21 US  
 18. 100 WATT POWER TEST IN ALL OF BUS R  
 19. CORRESPONDING INDEX MARKS  
 20. HOUSING (FN 5) AS SHOWN  
 NOTES: UNLESS OTHERWISE SPECIFIED

FORM											
LET	AA	AB	AC	AD	AE	AF	AG	AH	AJ	AK	AL
LETTER ASSIGNMENT AND LOCATION RECORD FOR DATUMS, SECTIONS, VIEWS AND TABULATIONS											



4

3

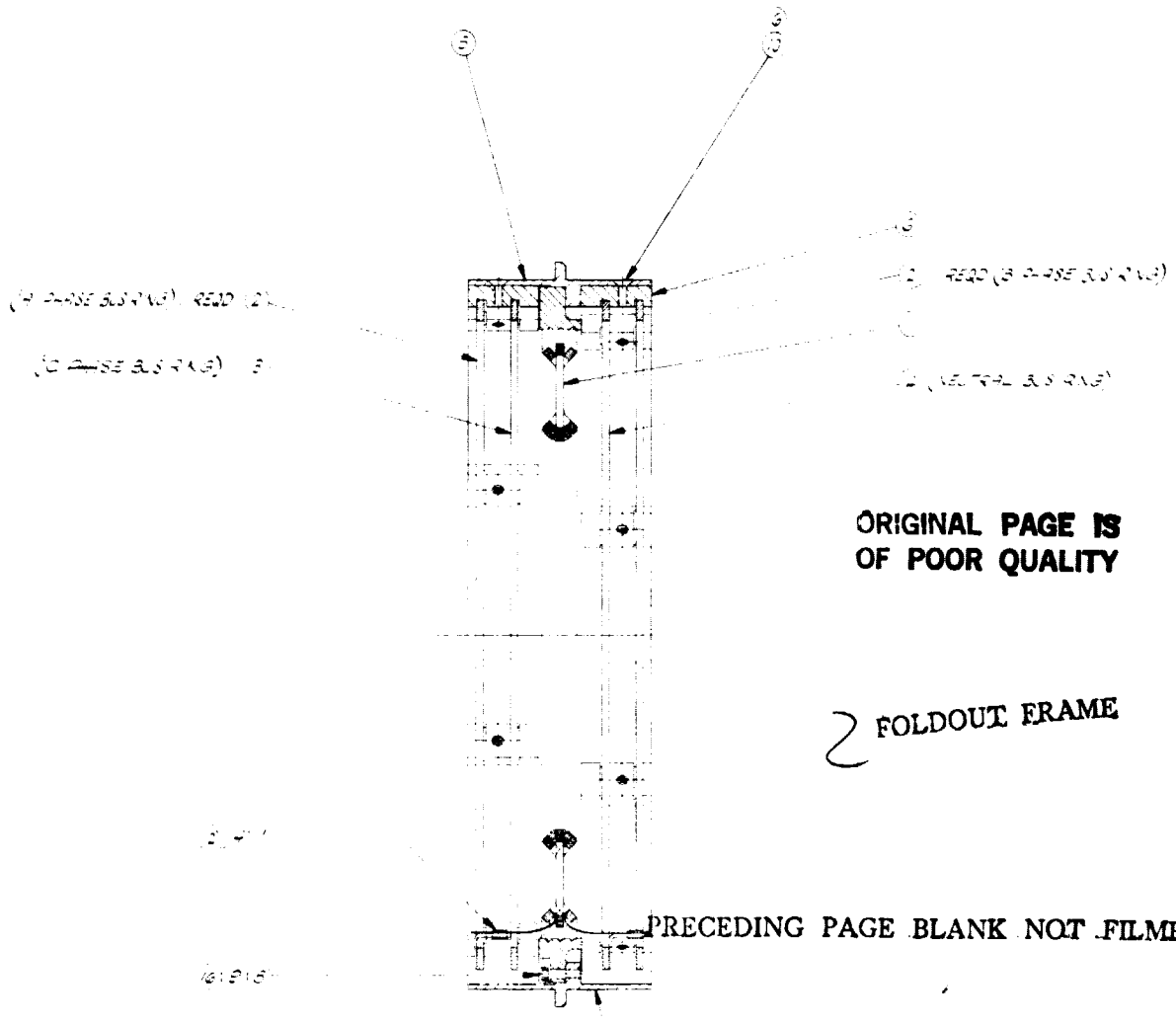
2

1

REVISIONS			
LTN	DESCRIPTION	DATE	APPROVED

000000

D  
H  
G  
F  
E  
D  
C



ORIGINAL PAGE IS OF POOR QUALITY

2 FOLDOUT FRAME

PRECEDING PAGE BLANK NOT FILMED

PART NO. THIS SURFACE

SECTION A-A

- 4. WINDING RESISTANCE SHALL BE 0.000023 OHMS PER PHASE
  - 5. THE INSULATION RESISTANCE BETWEEN ANY BUS BAR (A, B, OR C) & THE GROUND (G, EN) SHALL BE A MIN. OF 2000 MEGOHMS AT 500 VDC
  - 6. EACH PHASE OF THE WINDING SHALL BE TESTED AT 2000 VOLTS AC TEST FOR 10 SECONDS (10)
  - 7. THE WINDING SHALL BE TESTED AT 500 VOLT AC TEST VOLTAGE OF 500 VOLTS RMS OF 60 HZ FREQ. (60 HZ)
  - 8. THE WINDING SHALL BE TESTED AT 500 VOLT AC TEST CURRENT BETWEEN ANY BUS BAR (A, B, OR C) & GROUND (G, EN) FOR 10 SECONDS (10)
  - 9. EACH PHASE & NEUTRAL LEAD (COIL STARTS) OF EACH PHASE GROUP TO BUS BAR TERMINALS AS SHOWN ON DRAWING SHALL BE USING 30 AWG
  - 10. EACH PHASE & NEUTRAL LEAD OF BUS BAR ASSYS. AT STATOR END TO INLET MARKS ON STATOR HOUSING (FINS) AS SHOWN
- NOTES: UNLESS OTHERWISE SPECIFIED

PART NO. SEE SEPARATE PARTS LIST

UNLESS OTHERWISE SPECIFIED DIMENSIONS ARE IN INCHES DIMENSIONS IN PARENTHESES ARE IN MILLIMETERS IDENTIFICATION MARKING PER MIL-STD-130	PROPERTY: <i>Altek Corp</i> DATE: <i>1/10/61</i> BY: <i>Johnston</i>	AIRSEARCH MANUFACTURING COMPANY 1000 W. 10TH AVENUE DENVER, COLORADO 80202
STATOR ASSEMBLY MOTOR		
REV: E	QTY: 70210	IMP. NO. 2043900
SCALE: 1/2" = 1"		DATE: 1/10/61

4

3

2

1

A

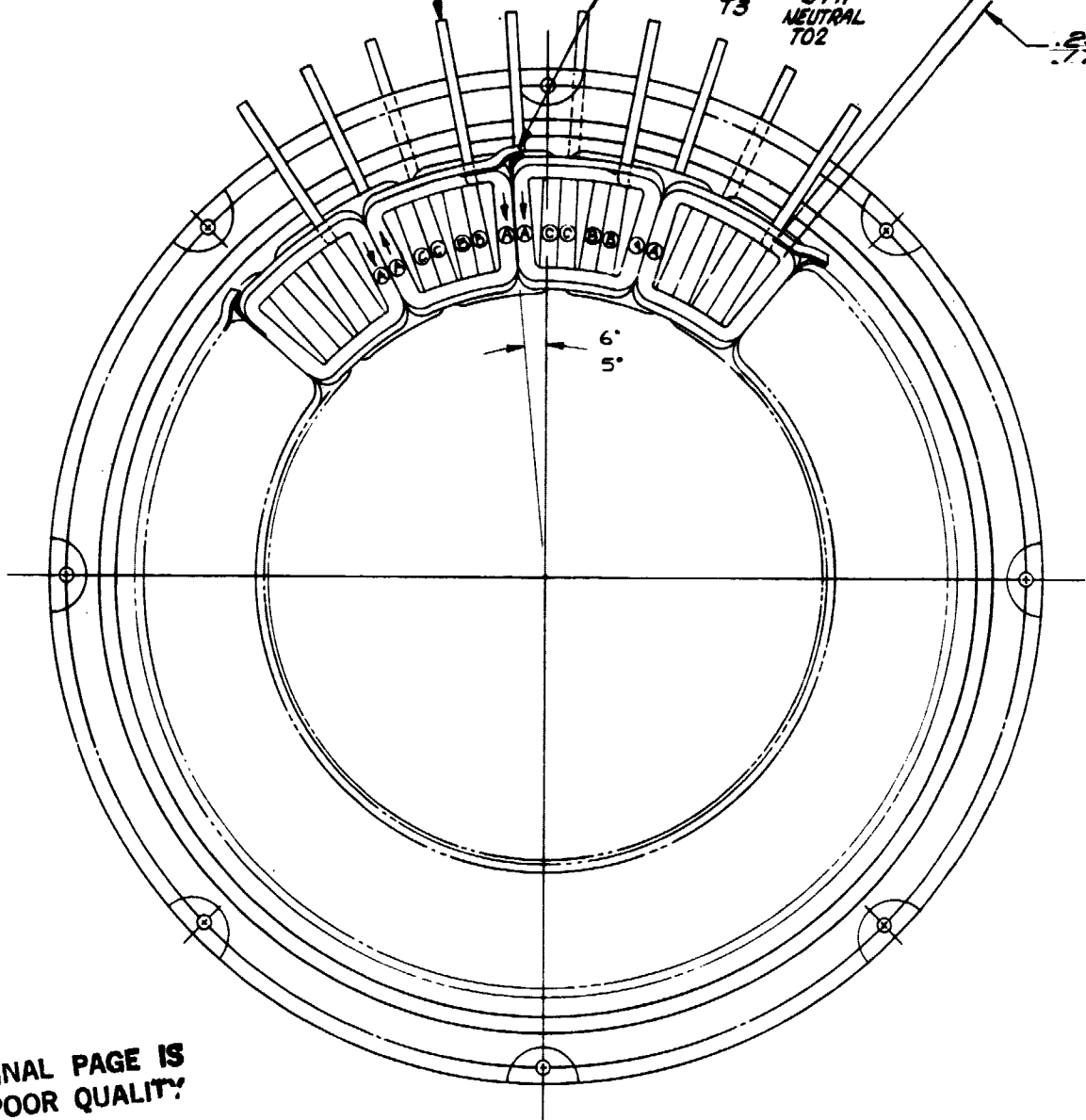
IDENTIFY EACH LEAD AS SHOWN. PATTERN REPEATS 8 TIMES

'A' PH POWER T1  
'C' PH NEUTRAL T03  
'B' PH POWER T2  
'A' PH NEUTRAL T01  
'C' PH POWER T3  
'B' PH NEUTRAL T02

(TYP) 8 FLC'S EACH PHASE ②

23 (TYP)  
77

1.5 MIN - PHASE L THIS SIDE

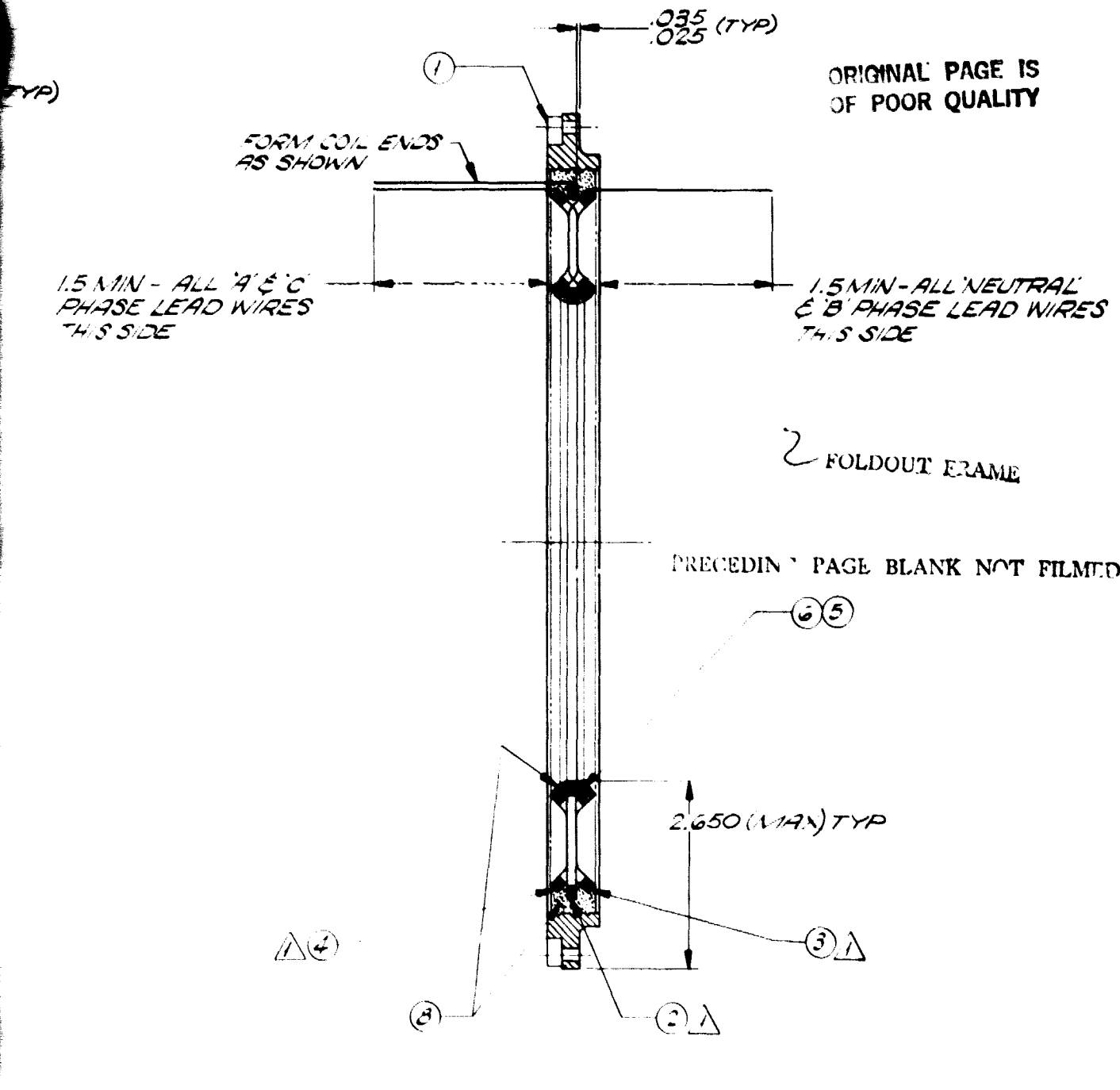


ORIGINAL PAGE IS OF POOR QUALITY

FOLDOUT FRAME

3. HI POT TEST TO ASSURE ISOLATION BETWEEN COIL PAIR & ADJOINING COILS AT 1000 VOLTS R.M.S. SOLDER PER SPEC WBS 21 USING ⑨
- ②. DIRECTION OF WIND OF EACH COIL AS SEEN IN LEFT VIEW CW WITH START (INNER TURN) & FINISH (OUTER TURN) EACH COIL POSITIONED AS SHOWN
- ①. NOTES: UNLESS OTHERWISE SPECIFIED

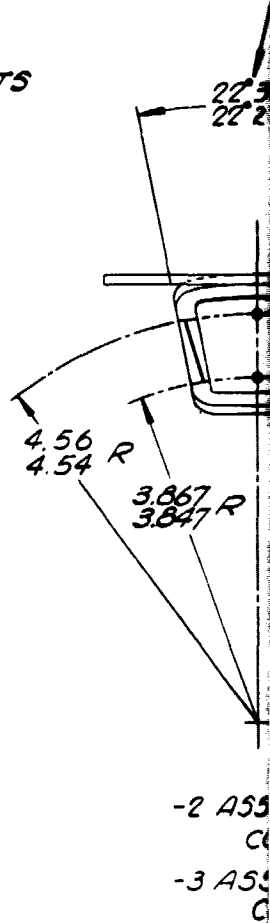
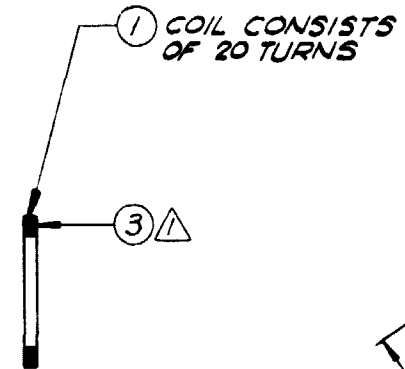
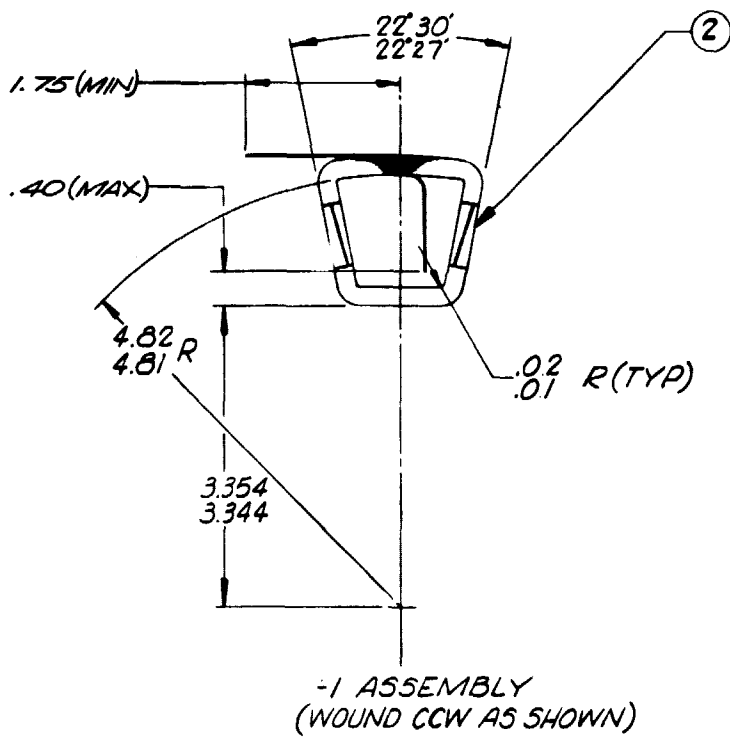
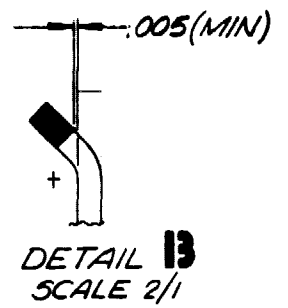
2043901		REVISIONS	
ZONE	LTR	DESCRIPTION	DATE



PART NO SEE SEPARATE PARTS LIST

UNLESS OTHERWISE SPECIFIED: BURR CONTROL PER SCS STD INTERPRETATIONS PER PMS IDENTIFICATION MARKING PER MCS	CONTRACT NO	AIRESEARCH MANUFACTURING COMPANY OF CALIFORNIA A DIVISION OF THE BARRETT CORPORATION TORRANCE, CALIFORNIA
	DESIGNED BY <i>[Signature]</i> CHECKED BY <i>[Signature]</i> DATE <i>8/25/51</i>	
MATERIAL	VALVE ENGR	<b>STATOR SUB-ASSY, MOTOR</b>
FINISH PROCESS	MAYL	
RECYCLE TREATMENT	APPROVED BY <i>[Signature]</i>	DESIGNED BY <i>[Signature]</i> PROJECT ENGINEER CHECKED BY <i>[Signature]</i> DATE <i>8/25/51</i>
APPLICATION	GOVERNMENT USE	D 70210 2043901 SCALE // SHEET / OF /

...TION BETWEEN EACH  
... AT 100 VOLTS RMS SO HE  
... NG (9)  
... H COILS AS SEEN IN  
... ER TURN FINISH OF  
... OWN  
... SPECIFIED



ORIGINAL PAGE IS  
OF POOR QUALITY

REOLDOUT FRAME

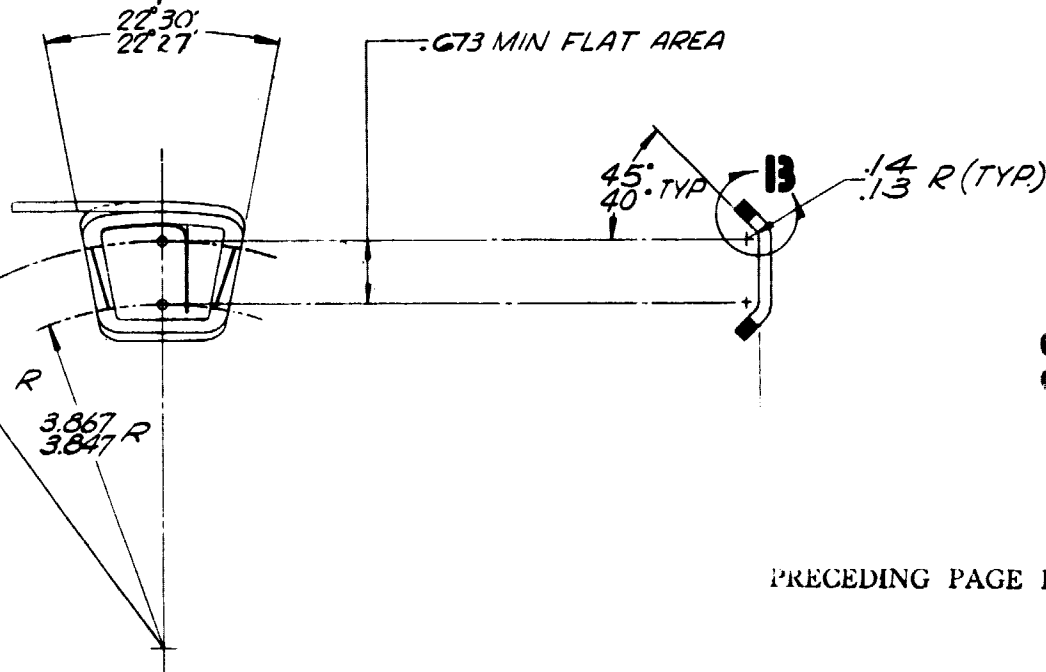
4. COIL INDUCTANCE .029 MH (APPROX)
3. COIL RESISTANCE SHALL BE .072-
2. THE COIL SHALL WITHSTAND A 1000 VDC SURGE TEST BETWEEN EACH COIL & STD FOR 2 SEC USING A G.E. NO. 1 SURGE TESTOR OR EQUIV. A SINGLE TRACE IS REQD

$\triangle$  PROCESS -1 COIL ASSY PER  
AIRESEARCH SPEC RS 154-01  
NOTES: UNLESS OTHERWISE SPECIFIED

JOB NO. 2047243		REV. A	1	
REVISIONS				
ZONE	LTR	DESCRIPTION	DATE	APPROVED
A		SEE ENGRG ORDER	02-05-79	W. [Signature]

5(MIN)

TO BE MAINTAINED  
ON FULL EXTENT OF  
THESE SURFACES  
AFTER FORMING



ORIGINAL PAGE IS  
OF POOR QUALITY

PRECEDING PAGE BLANK NOT FILMED

-2 ASSEMBLY (MAKE FROM -1 ASSY.) FORM AS SHOWN WITH  
COIL POSITIONED FOR CCW WIND.

-3 ASSEMBLY (MAKE FROM -1 ASSY.) FORM AS SHOWN WITH  
COIL POSITIONED FOR CW WIND

2 FOLDOUT FRAME

SEE SEPARATE PARTS LIST

0 MH (APPROX)

ALL BE .072-.082 OHMS

AND A 1000 VOLT  
EACH COIL & A  
A G.E. NO. 112CB206  
W. A SINGLE

PER  
154-01  
UNLESS OTHERWISE SPECIFIED

PART NO 2047243-1

UNLESS OTHERWISE SPECIFIED: SURF CONTROL PER SCS STD INTERPRETATION PER PMS IDENTIFICATION MARKING PER MCS, CLVI		CONTRACT NO	AIRESEARCH MANUFACTURING COMPANY OF CALIFORNIA A DIVISION OF THE BARRETT CORPORATION TORRANCE, CALIFORNIA	
MATERIAL		DESIGNED BY D. S. [Signature]	COIL ASSEMBLY, STATOR, MOTOR	
FINISH PROCESS		VALVE ENGR D. S. [Signature]	PROJECT ENGINEER K. [Signature]	
READY/READYED		DATE 5-4-79	REV	DATE/ISSY NO
RECD		DESIGN SUPERVISOR K. [Signature]	D	70210
NEXT ASSY		GOVERNMENT APP	2047243	
APPLICATION		SCALE // 1		SHEET / OF /

16(3)	2047242-1	5/1950-1
16(2)	2047242-1	5/1950-1
16(4)	2047242-1	5/1950-1
REQD	NEXT ASSY	USED ON

4

3

2

1

8

7

6

5

D

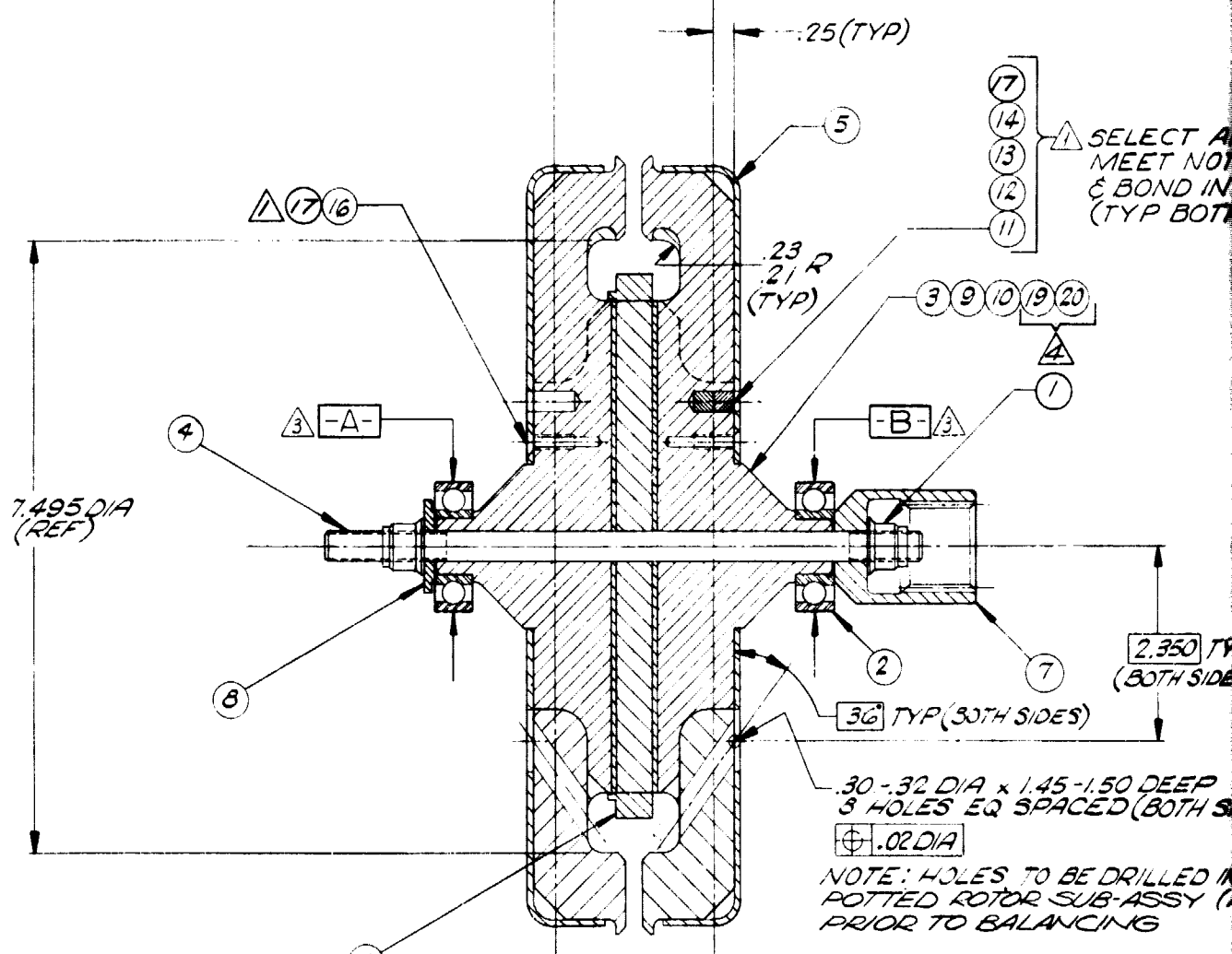
C

B

A

BALANCE PLANE NO.1

BALANCE PLANE NO.2



CAUTION:  
ROTOR ASSY IS HIGHLY MAGNETIC

FOLDOUT FRAME

ORIGINAL PAGE IS  
OF POOR QUALITY

- 1. EACH MULTIPOLE HUB (FIN 3) TO BE POTTED BETWEEN POLES USING ROTTING CMPD (FIN 1) & PRIMER (FIN 20). CURE AT 250°F FOR 2 HRS & MACHINE AS SHOWN
  - 2. ROTOR ASSEMBLY TO BE SUPPORTED ON BEARINGS (DATUMS A & B) WHEN MEASURING & CHECKING UNBALANCE.
  - 3. DYNAMIC UNBALANCE TO BE NO GREATER THAN .20 GRAM INCHES IN PLANES 1 & 2
  - 4. PROCESS PER AIRESEARCH SPEC R5 42
- NOTES: UNLESS OTHERWISE SPECIFIED

R

7

6

5

4

3

DWG NO 2047247

REV

1

REVISIONS

LTR	DESCRIPTION	DATE	APPROVED

D

ORIGINAL PAGE IS OF POOR QUALITY

NO. 2

SELECT APPROPRIATE WEIGHTS TO MEET NOTED BALANCING REQUIREMENTS & BOND IN PLACE USING FINO. 17 (TYP BOTH ENDS)

20  
1

7  
DES)

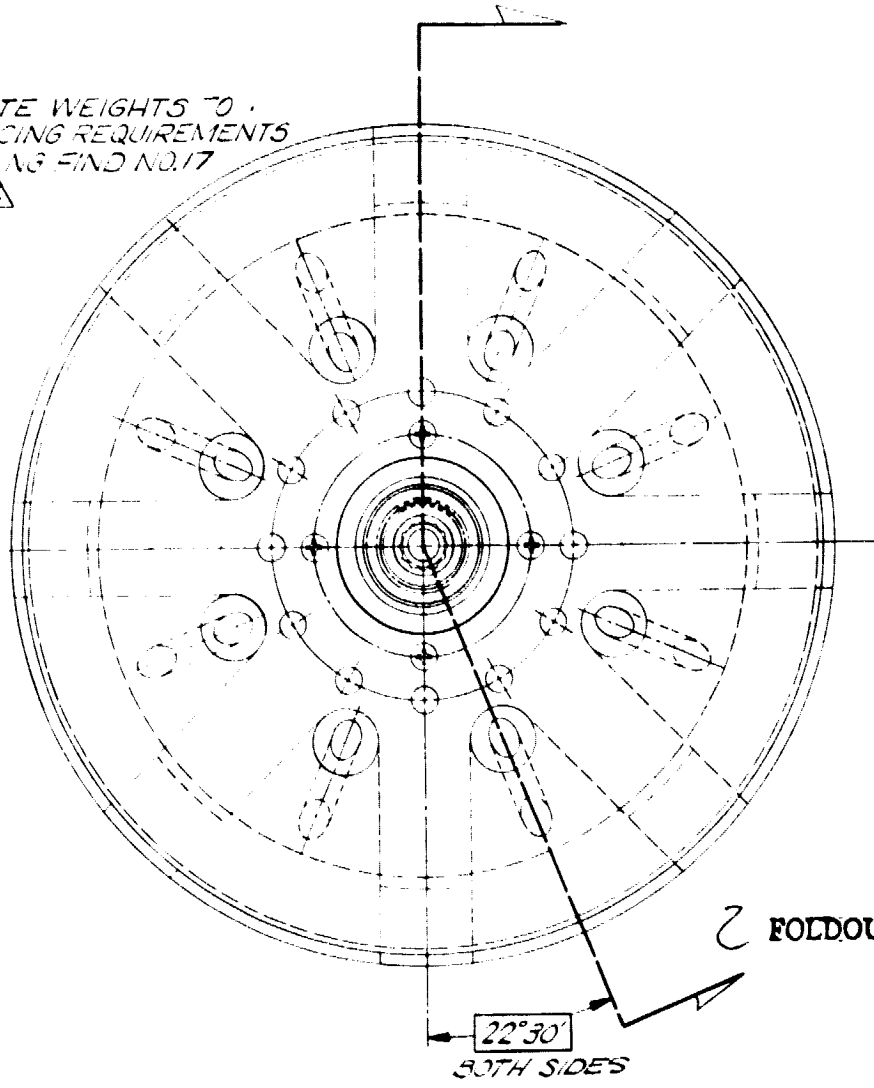
45-150 DEEP SPACED, (BOTH SIDES)

TO BE DRILLED INTO SUB-ASSY (FIN 10) BALANCING

TO BE POTTED MOUNTING COMPD (FIN 19) @ 250°F FOR 2 HOURS

PORTED ON BEARINGS MOUNTING & CHECKING

GREATER THAN 2 SEC R5 42 SPECIFIED



FOLDOUT FRAME

22°30'  
BOTH SIDES

PRECEDING PAGE BLANK NOT FILMED

C

B

PART NO SEE SEPARATE PARTS LIST

UNLESS OTHERWISE SPECIFIED: SURF CONTROL PER DOWS STD INTERPRETATIONS PER FIGS IDENTIFICATION MARKING PER MC16, CL VI	CONTRACT NO	AIRESEARCH MANUFACTURING COMPANY OF CALIFORNIA A DIVISION OF THE GARRETT CORPORATION TORRANCE, CALIFORNIA
	PREPARED BY ENGR. <i>Nick...</i>	
MATERIAL	DESIGN <i>...</i>	ROTOR ASSEMBLY, BALANCED, MOTOR
FINISH PROCESS	VALVE SNGR MATEL SYNTH	
TREATMENT	APPROVED BY PROJECT ENGINEER <i>...</i>	SCALE V1
REQD. NEXT ASSY USED ON APPLICATION	GOVERNMENT AND	D 70210 2047247

A

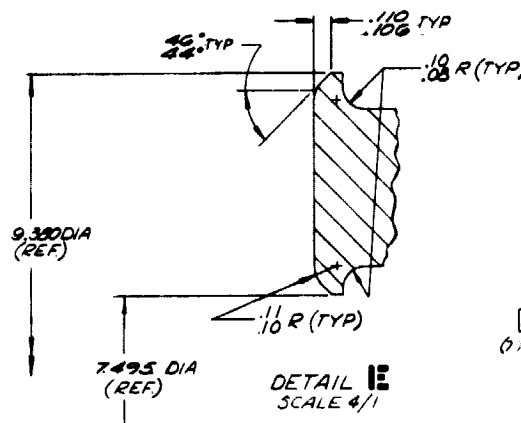
4

3

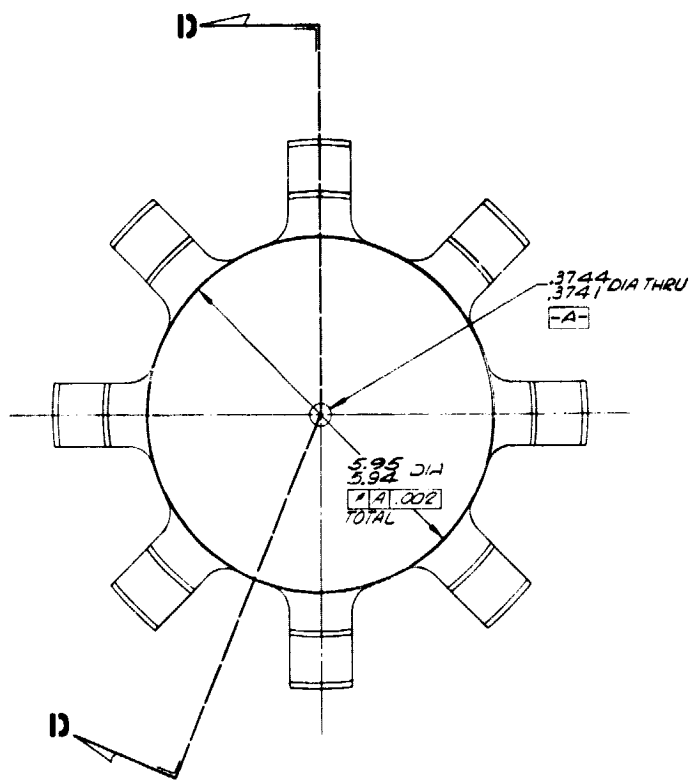
2

1

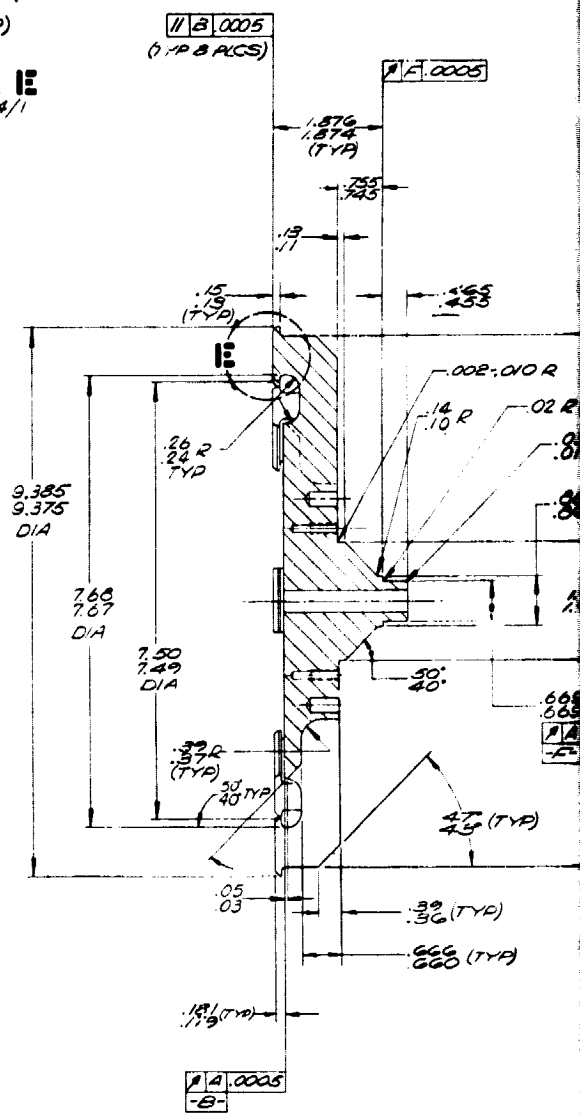
ORIGINAL PAGE IS  
OF POOR QUALITY



DETAIL E  
SCALE 4/1



EOLDOUT FRAME



SECTION D-D

REV	DATE	BY	CHK	APP	DESCRIPTION
1					
2					
3					
4					
5					
6					
7					
8					
9					
10					

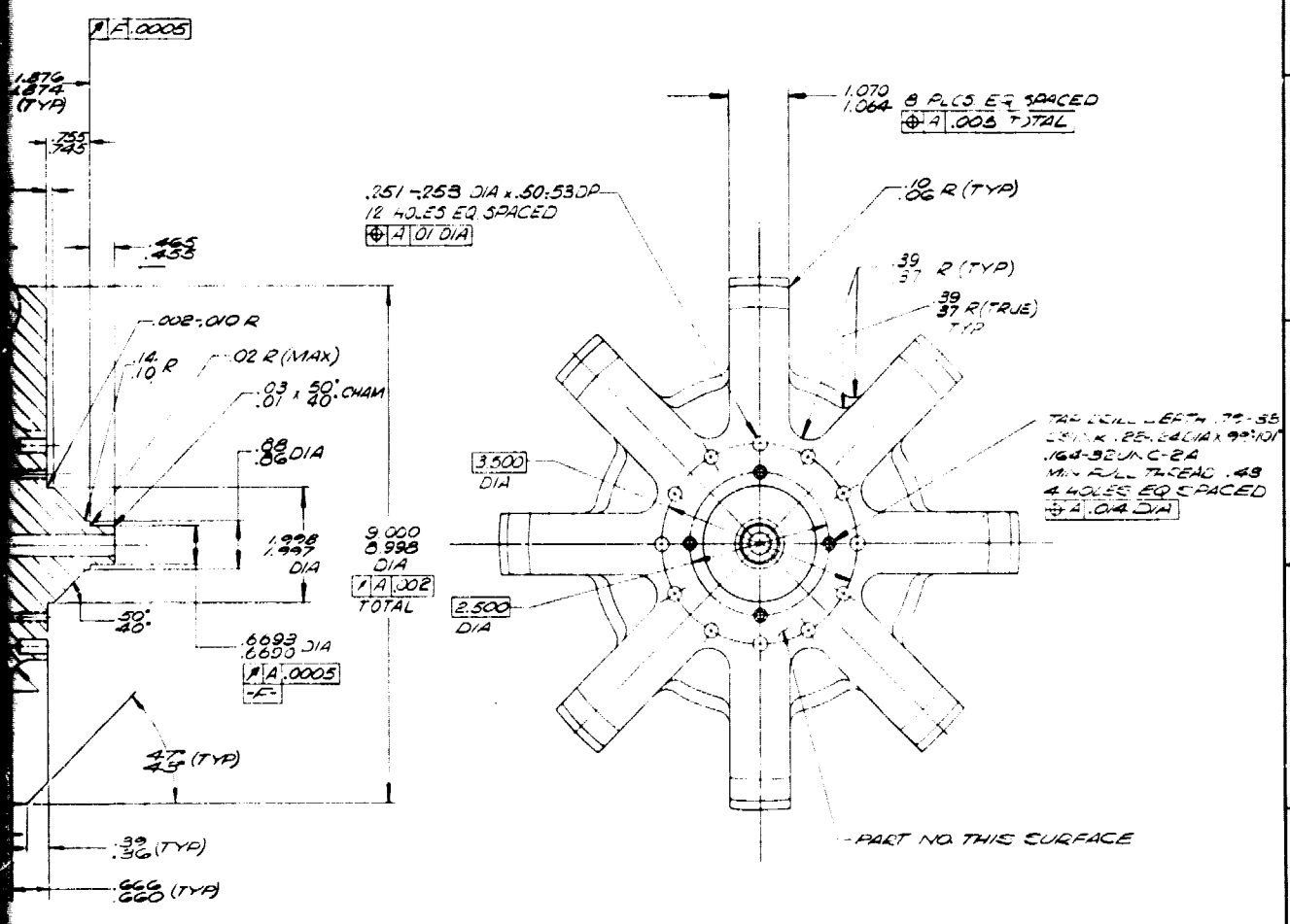
1. BLACK OXIDE PER MIL-C-15  
DO NOT APPLY SUPPLEMENTARY  
2. MAGNETIC PARTICLE INSPECT  
SPEC MIL-I-6868  
1. ALL SURFACES TYP

NOTES: UNLESS OTHERWISE



REVISIONS			
REV	DATE	BY	APP
A	5-14-77	...	...
B	6-2-77	...	...
C	8-27-78	...	...

ORIGINAL PAGE IS  
OF POOR QUALITY



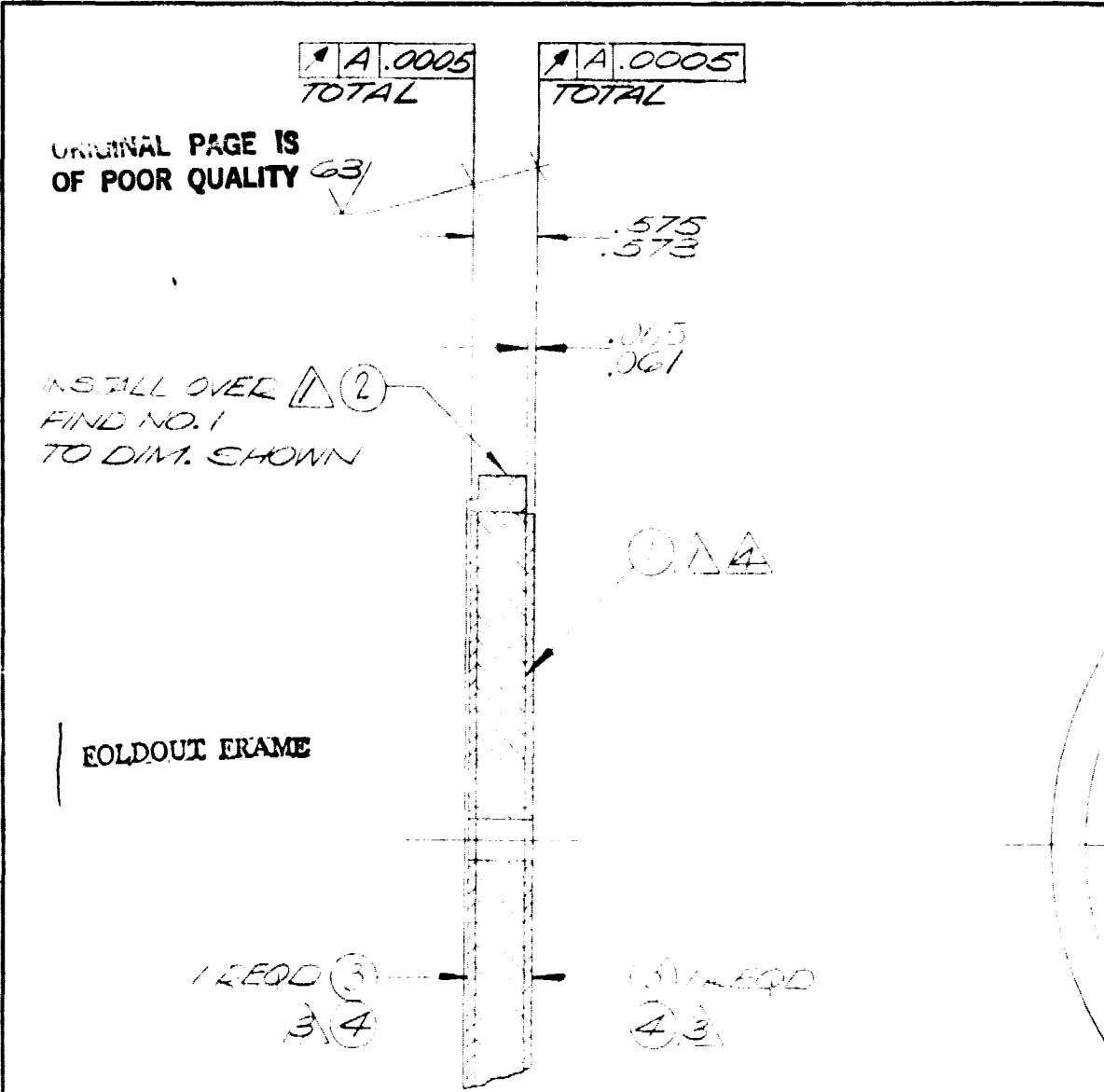
PRECEDING PAGE BLANK NOT FILMED

2 FOLDOUT ERAM

OXIDE PER MIL-C-13924, CL 1  
APPLY SUPPLEMENTAL PRESERVATIVE  
PARTICLE INSPECT PER  
MIL-I-6868  
SURFACES ONLY

NOTES UNLESS OTHERWISE SPECIFIED

PART NO 2047251		REVISIONS	
UNLESS OTHERWISE SPECIFIED DIMENSIONS ARE IN INCHES DIMENSIONS ARE TO BE HONED AND FINISHED TO THE TOLERANCES SHOWN		SEARCHED MANUFACTURING COMPANY OF CALIFORNIA A DIVISION OF THE HARBETZ COMPANY TORRANCE, CALIFORNIA	
MIL-I-6868 EG-54 HRC		MULTI-POLE HUB, ROTOR, MOTOR	
E 70210 2047251		SCALE 1/1 CAL WT 116.65 SHEET 001	



④ DISC (FIND NO. 1) TO BE MAGNETIZED AFTER INSTALLATION OF SIDE PLATES (FIND NO. 3) & RING (FIND NO. 2) TO FULL ENERGY LEVEL  
 ③ CLEAN & DRY MATING SURFACES OF FIND NO'S. 1 & 3. APPLY FIND NO. 4 TO FIND NO. 1 ONLY & BOND IN PLACE AS SHOWN. HEAT CURE ASSEY. FOR 45 MIN AT 200°F  
 2. CAUTION: CHILLING MULTI-PIECE MAGNET MAY RESULT IN FRACTURES AT BOND LINES  
 ① FOR ASSEMBLY PURPOSES, HEAT RING (FIND NO. 2) TO 700°-750°F. MAINTAIN MAGNET (FIND NO. 1) AT ROOM TEMP  
 NOTE: QUICKLY REMOVE COMPLETED ASSY FROM HEAT SINK FIXTURE & COOL BY IMMERSION IN WATER  
 NOTES: UNLESS OTHERWISE SPECIFIED.

REQD	NEXT ASSY	USED ON
APPLICATION		

PART NO	SEE
UNLESS OTHERWISE SPECIFIED: BURR CONTROL PER SC663 STD INTERPRETATIONS PER FIG IDENTIFICATION MARKING PER MC16, CL 1-AAA	
MATERIAL	
FINISH PROCESS	
HEAT TREATMENT	

REVISIONS				
ZONE	LTR	DESCRIPTION	DATE	APPROVED
	A	SEE ENGRG ORDER	6-14-79	<i>[Signature]</i>
	B	SEE ENGRG ORDER	80-03-18	<i>[Signature]</i>

R  
R  
R

ORIGINAL PAGE IS  
OF POOR QUALITY


PART NO. THIS SURFACE

2 HOLDOUT BRAMM

.374-.3744 DIA -A-  
TO BE MAINTAINED  
BY ALIGNMENT OF  
FIND NO'S 1 & 3  
DO NOT MACHINE

PRECEDING PAGE BLANK NOT FILMED

PART NO SEE SEPARATE PARTS LIST

UNLESS OTHERWISE SPECIFIED BURR CONTROL PER BC863 STD INTERPRETATION'S PER PIB6 IDENTIFICATION MARKING PER MC16, CL VAA	CONTRACT NO	 <b>AIRESEARCH MANUFACTURING COMPANY OF CALIFORNIA</b> A DIVISION OF THE GARRETT CORPORATION TORRANCE, CALIFORNIA
	PREPARED BY <i>[Signature]</i> CHK <i>[Signature]</i> DESIGN VALUE ENGR <i>[Signature]</i> DATE APPROV <i>[Signature]</i> DRG'G SUPERVISOR PROJECT ENGINEER GOVERNMENT APPROV	
MATERIAL	DATE	SIZE <b>C</b> CODE IDENT NO <b>70210</b> DWG NO <b>2047240</b>
FINISH SYMBOL	DATE	SCALE    SHEET / OF /
USED ON	DATE	

DWG NO 2047240  
 15 B


ORIGINAL PAGE IS  
OF POOR QUALITY

DWG NO. 2047221

REVISIONS			
LTR	DESCRIPTION	DATE	APPROVAL
A	SEE ENGRG ORDER	3-21-79	<i>[Signature]</i>
B	SEE ENGRG OLDER	3-21-79	<i>[Signature]</i>

NOTES: UNLESS OTHERWISE SPECIFIED

- PART NUMBER CHANGES AND/OR DESIGN CHANGES AFFECTING ITEM INTERCHANGEABILITY REQUIRE PRIOR AIRESEARCH APPROVAL AND AUTHORIZATION BY REVISION TO THIS DRAWING.
- PACKAGING AND SHIPPERS SHALL INCLUDE THE AIRESEARCH CODE IDENTIFICATION NUMBER AND ITEM IDENTIFYING NUMBER.
- ITEM TO BE PERMANENTLY MARKED WITH THE FOLLOWING MINIMUM IDENTIFICATION IN ACCORDANCE WITH MIL-STD-130:  
 AIRESEARCH CODE IDENT NUMBER "70210"  
 AIRESEARCH ITEM IDENTIFICATION NUMBER 2047221-1  
 VENDOR CODE IDENT NUMBER OR TRADEMARK
- ONLY THE ITEM DESCRIBED ON THIS DRAWING WHEN PROCURED FROM THE VENDOR(S) LISTED HEREON IS APPROVED BY AIRESEARCH MFG CO. OF CALIFORNIA, TORRANCE, CALIFORNIA, FOR USE IN THE APPLICATION(S) SPECIFIED HEREON. A SUBSTITUTE ITEM SHALL NOT BE USED WITHOUT PRIOR TESTING AND APPROVAL BY AIRESEARCH MANUFACTURING CO.
- PURCHASING: SHEET 4 CONTAINS APPROVED VENDOR INFORMATION ONLY, AND SHALL BE REMOVED FROM COPIES TRANSMITTED OUTSIDE AIRESEARCH.
- IDENTIFICATION OF THE APPROVED SOURCE(S) HEREON IS NOT TO BE CONSTRUED AS A GUARANTEE OF PRESENT OR CONTINUED AVAILABILITY AS A SOURCE OF SUPPLY FOR THE ITEM DESCRIBED ON THE DRAWING.

SHEET INDEX	REVISION LTR	B	B																		
	SHEET NO	1	2	3	4																
SOURCE CONTROL DRAWING	CONTRACT NO																				
	DFT	<i>[Signature]</i>	 <b>AIRESEARCH MANUFACTURING COMPANY OF CALIFORNIA</b> A DIVISION OF THE GARRETT CORPORATION TORRANCE, CALIFORNIA																		
	CHK	<i>[Signature]</i>	DISC, MAGNET, ROTOR, MOTOR																		
	APVD	<i>[Signature]</i>																			
	AIRESEARCH APVD	<i>[Signature]</i> 2-19-79	SIZE	CODE IDENT NO	DWG NO																
OTHER ACTIVITY APVD		A	70210	2047221																	
SCALE		NONE		SHEET 1		OF 4															

FORM 2347-2 (9-78)

PRECEDING PAGE BLANK NOT FILMED

6.0 SCOPE

6.1 THIS SPECIFICATION COVERS THE DETAIL REQUIREMENT FOR FABRICATION OF A RARE-EARTH-COBALT PERMANENT MAGNET ROTOR DISC.

7.0 MATERIAL

7.1 THE DISC SHALL BE FABRICATED FROM A SUITABLE MATERIAL TO MEET THE FOLLOWING TYPICAL MAGNETIC PROPERTIES

7.2 MULTIPLE MAGNET SECTIONS MAY BE USED TO FABRICATE MAGNET DISC AT OPTION OF VENDOR.

8.0 MAGNETIC PROPERTIES

8.1 RESIDUAL INDUCTION ( $B_r$ ): 8000 GAUSS (NOMINAL)

8.2 COERCIVE FORCE ( $H_c$ ): 8000 OERSTEDS (NOMINAL)

8.3 ENERGY PRODUCT ( $B_d H_d$ ):

MAGNETIZE DISC TO OBTAIN  $16 \pm .3$  MGO AT A MAGNET DENSITY OF 3.75 KG.

9.0 PHYSICAL PROPERTIES

9.1 DENSITY: 8.3 G/CC (APPROX)

9.2 COMPRESSIVE STRENGTH: 33,000 PSI (APPROX)

10.0 VENDOR ACCEPTANCE TESTS

10.1 PERFORM VISUAL AND DIMENSIONAL INSPECTION PER DRAWING REQUIREMENTS.

10.2 'B-H' CURVES MEASURED ON EACH MAGNET SHALL BE SHIPPED WITH EACH ORDER.

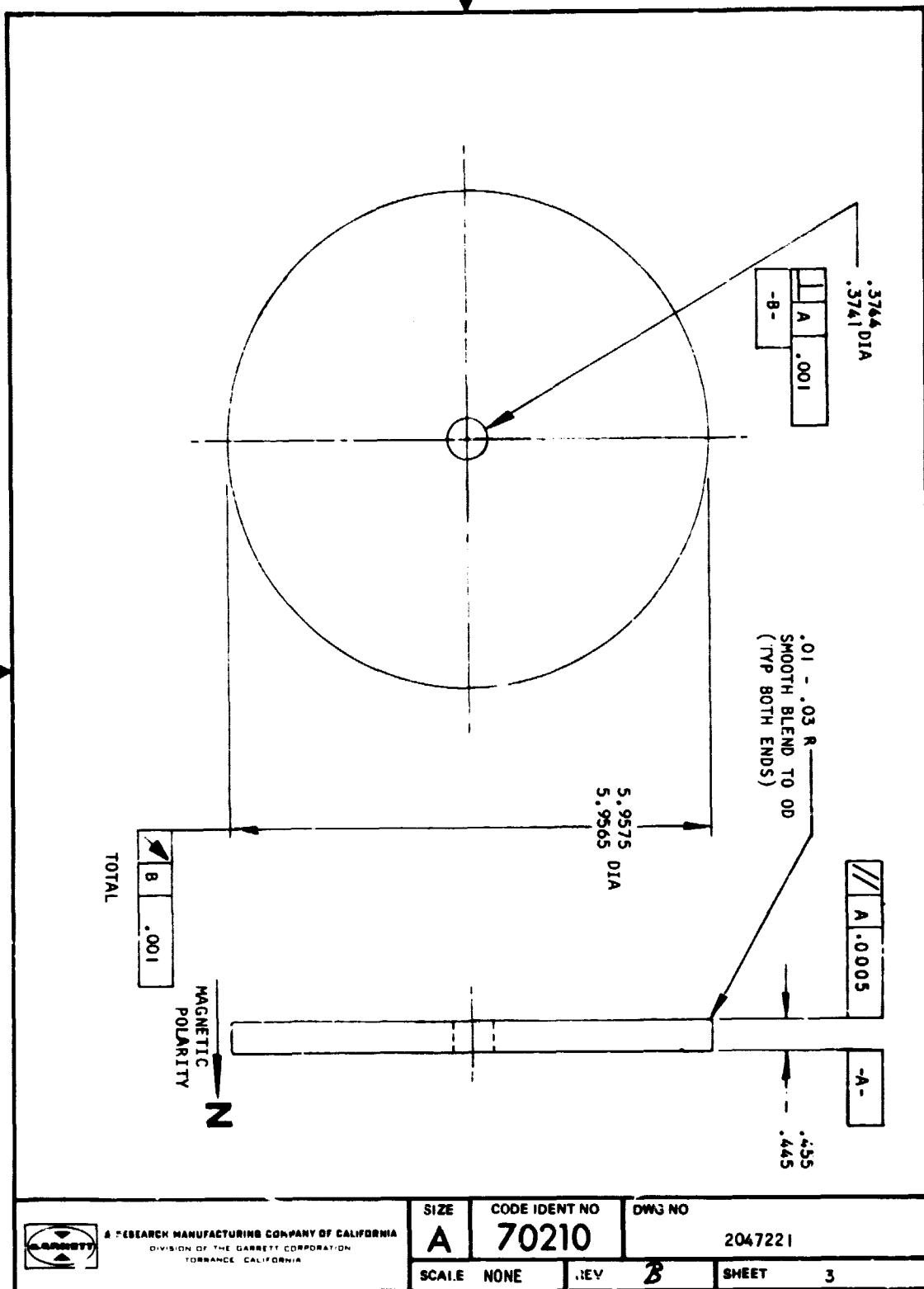


AMERSBACH MANUFACTURING COMPANY OF CALIFORNIA  
A DIVISION OF THE SABBETT CORPORATION  
TERRANCE, CALIFORNIA

SIZE <b>A</b>	CODE IDENT NO <b>70210</b>	DWG NO <b>2047221</b>
SCALE NONE	REV	SHEET <b>2</b>

FORM 2247-4 (1-74)

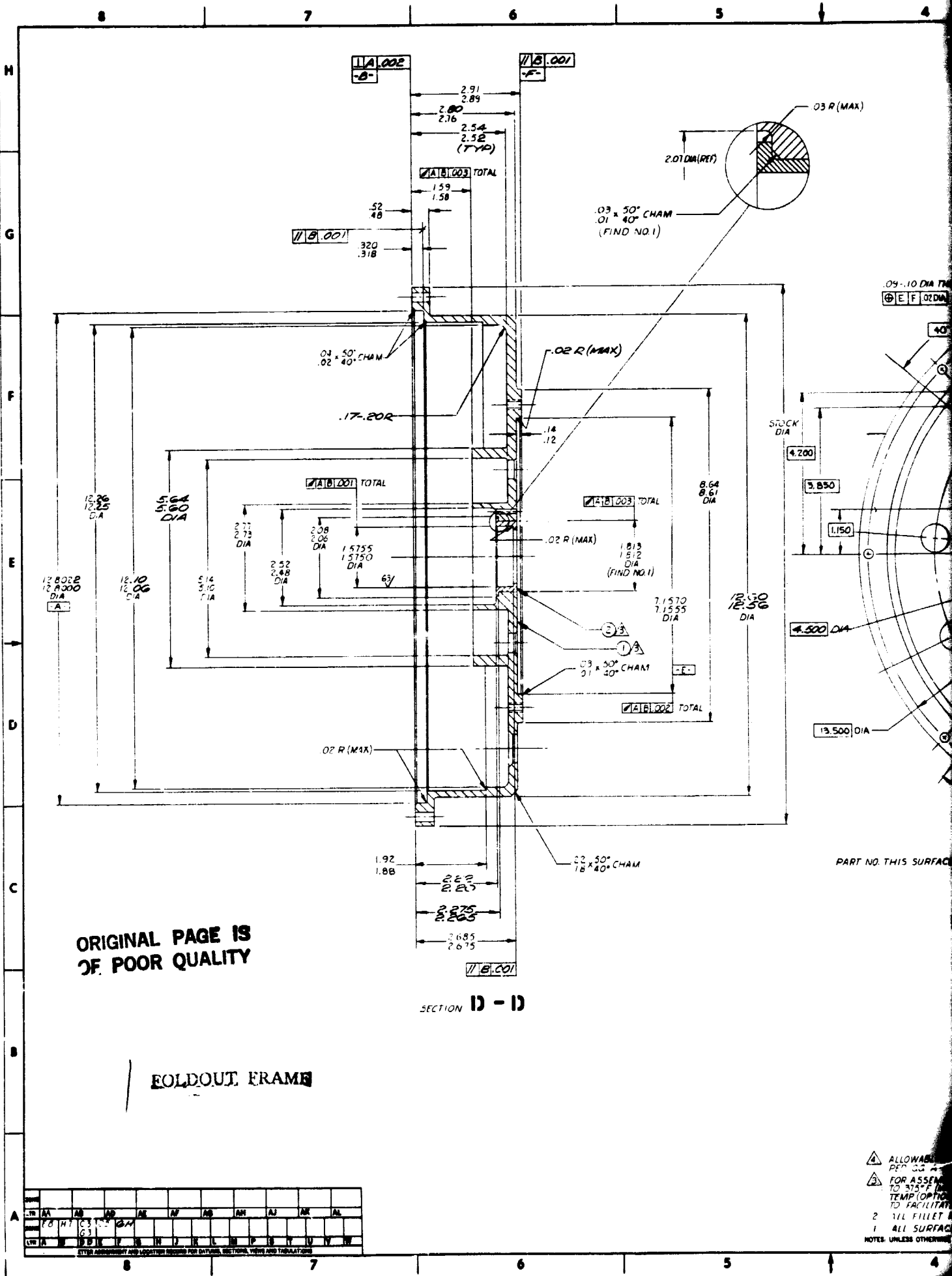
ORIGINAL PAGE IS  
OF POOR QUALITY



A RESEARCH MANUFACTURING COMPANY OF CALIFORNIA  
DIVISION OF THE GARRETT CORPORATION  
TORRANCE, CALIFORNIA

SIZE <b>A</b>	CODE IDENT NO <b>70210</b>	DWG NO <b>2047221</b>
SCALE NONE	REV <b>B</b>	SHEET <b>3</b>

FORM 2347-4 (1-74)



ORIGINAL PAGE IS  
OF POOR QUALITY

SECTION D - D

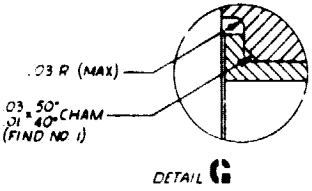
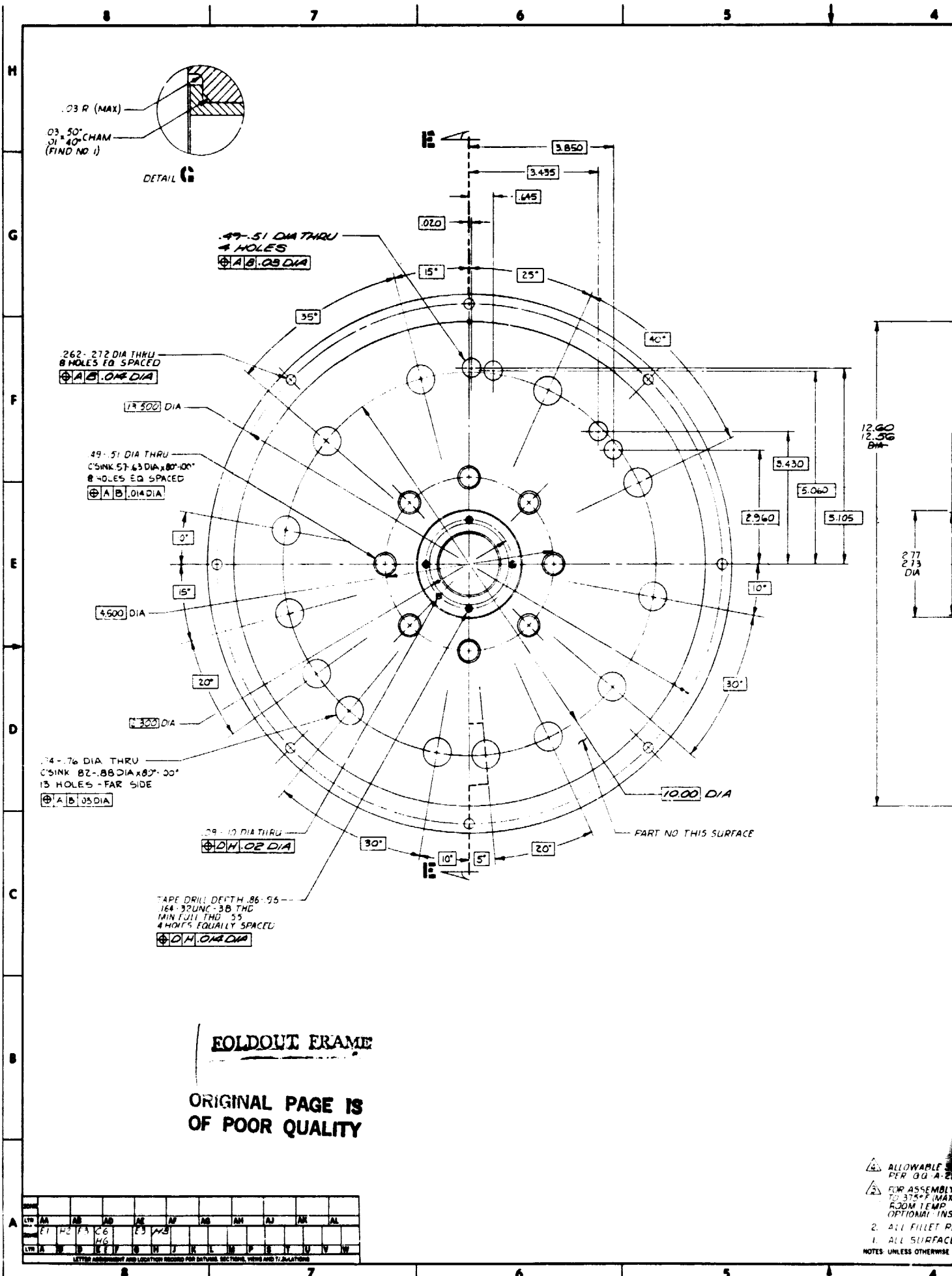
REOLDOUT FRAME

A	AA	AB	AC	AD	AE	AF	AG	AH	AI	AJ	AK	AL
1	2	3	4	5	6	7	8	9	10	11	12	13

ALLOWABLE  
PER 33 4  
FOR ASSEMBLY  
TO 375°F IN  
TEMP (OPTIC)  
TO FACILITATE  
2 1/4 FILLET  
1 ALL SURFACE  
NOTES: UNLESS OTHERWISE







.49-.51 DIA THRU  
4 HOLES  
⊕ A | B | .03 DIA

.262-.272 DIA THRU  
8 HOLES EQ SPACED  
⊕ A | B | .04 DIA

.49-.51 DIA THRU  
C/SINK .57-.63 DIA x .80 x .00"  
8 HOLES EQ SPACED  
⊕ A | B | .04 DIA

.74-.76 DIA THRU  
C/SINK .82-.88 DIA x .80 x .00"  
13 HOLES - FAR SIDE  
⊕ A | B | .05 DIA

.09-.10 DIA THRU  
⊕ D | M | .02 DIA

TAPE DRILL DEPTH .86-.95  
164-37 UNC - 3B THG  
MIN FULL THG .55  
4 HOLES EQUALLY SPACED  
⊕ D | M | .04 DIA

**FOLDOUT FRAME**

**ORIGINAL PAGE IS  
OF POOR QUALITY**

REV	1	2	3	4	5	6	7	8	9	10	11	12	13	14	15	16	17	18	19	20
BY	AA	AB	AC	AD	AE	AF	AG	AH	AJ	AK	AL	AM	AN	AO	AP	AQ	AR	AS	AT	AU
DATE	21	22	23	24	25	26	27	28	29	30	31	32	33	34	35	36	37	38	39	40

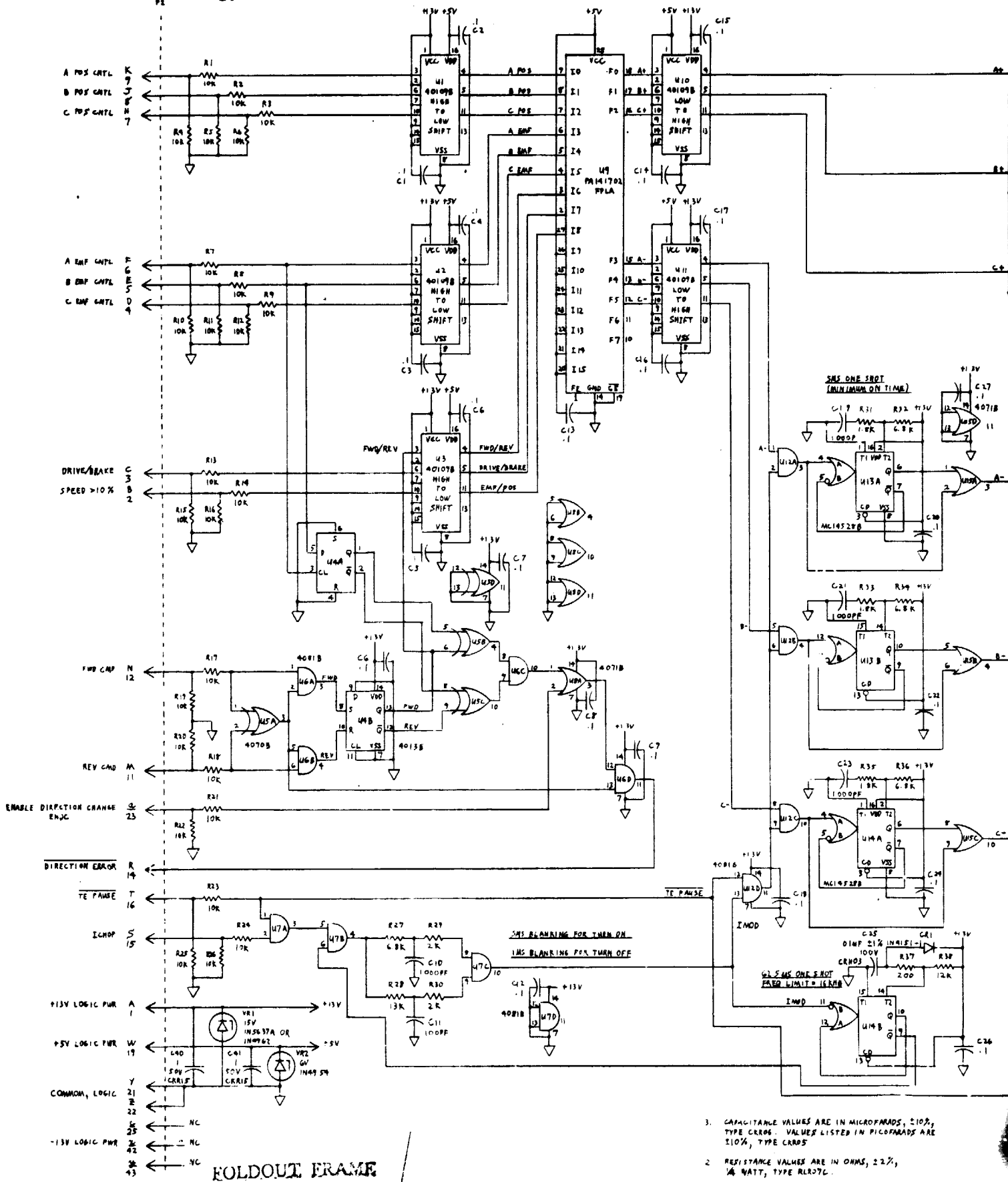
12.360  
BIM

2.77  
2.73  
DIA

ALLOWABLE PER GD-A-23  
FOR ASSEMBLY TO 375°F (MAX) & ROOM TEMP. OPTIONAL INSEAL  
2. ALL FILLET RADIUS  
1. ALL SURFACES  
NOTES: UNLESS OTHERWISE SPECIFIED



ORIGINAL PAGE IS  
OF POOR QUALITY



FOLDOUT FRAME

- CAPACITANCE VALUES ARE IN MICROFARADS, 50%, TYPE CR05. VALUES LISTED IN PICOFARADS ARE 10%, TYPE CR05.
- RESISTANCE VALUES ARE IN OHMS, 2%, 1/4 WATT, TYPE RL07C.
- PARTIAL REFERENCE DESIGNATORS ARE SHOWN, FOR COMPLETE DESIGNATION PREFIX WITH UNIT NUMBER AND SUBASSEMBLY DESIGNATORS.

1 HIGH REL PARTS ARE NOT TO BE SPECIFIED ON THIS PMA P/L.

NOTES: UNLESS OTHERWISE SPECIFIED

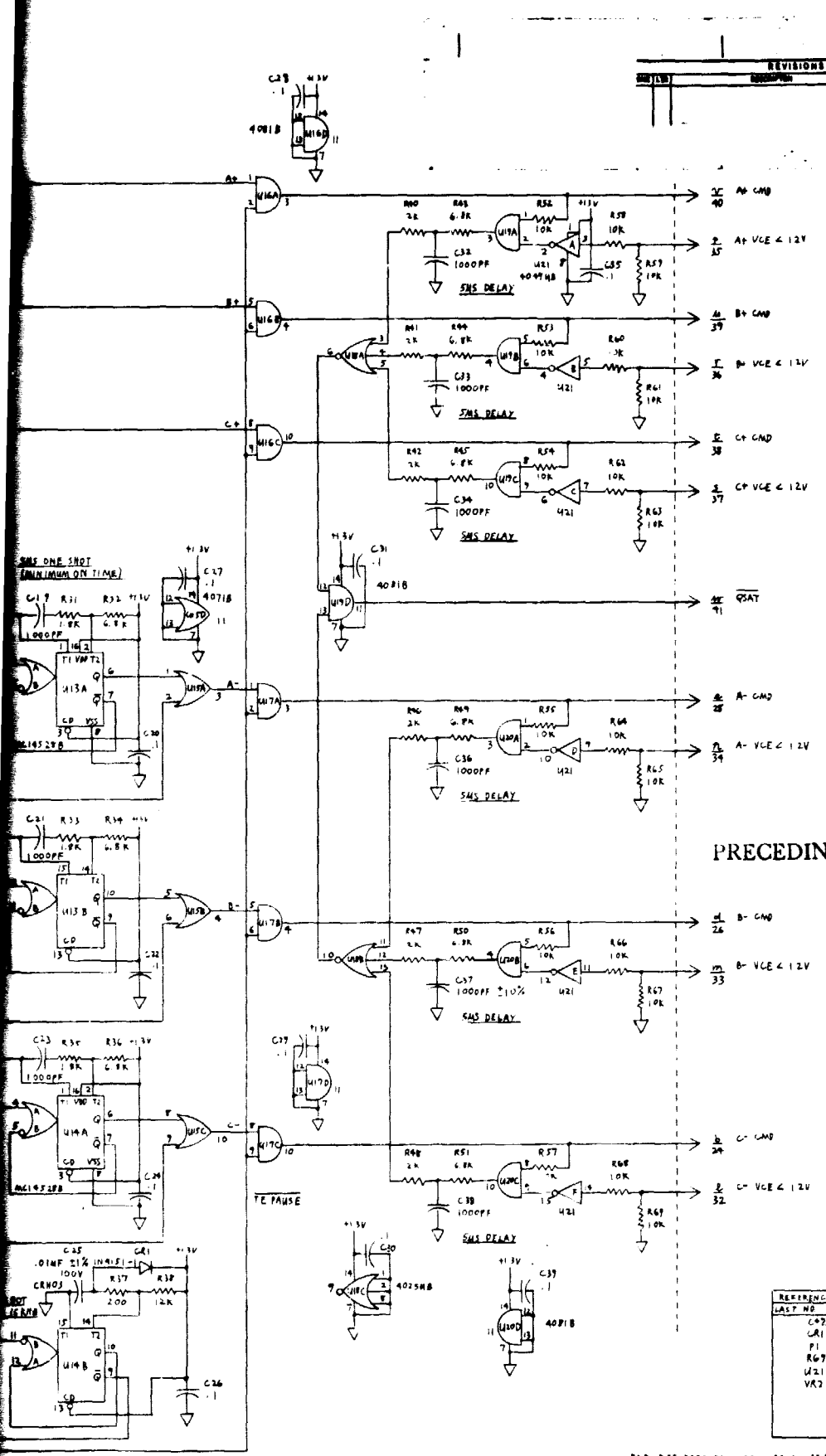
REVISIONS			
NO.	DESCRIPTION	DATE	APPROVED

**ORIGINAL PAGE IS OF POOR QUALITY**

PRECEDING PAGE BLANK NOT FILMED

~~ORIGINAL PAGE IS OF POOR QUALITY~~

2 **EXOLDOUT FRAME**



REFERENCE DESIGNATION BLOCK	
LAST NO. USED	NO. NOT USED
C02	
U01	
P1	
R69	R39
U21	
VR2	

REF DES PREFIX: LOGIC PACK - ASAZ

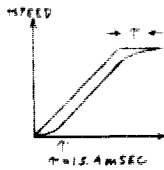
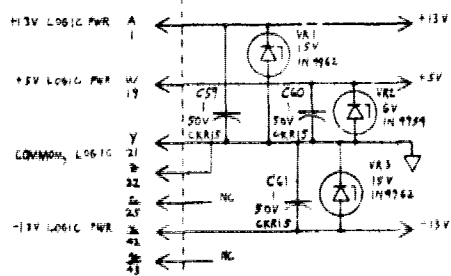
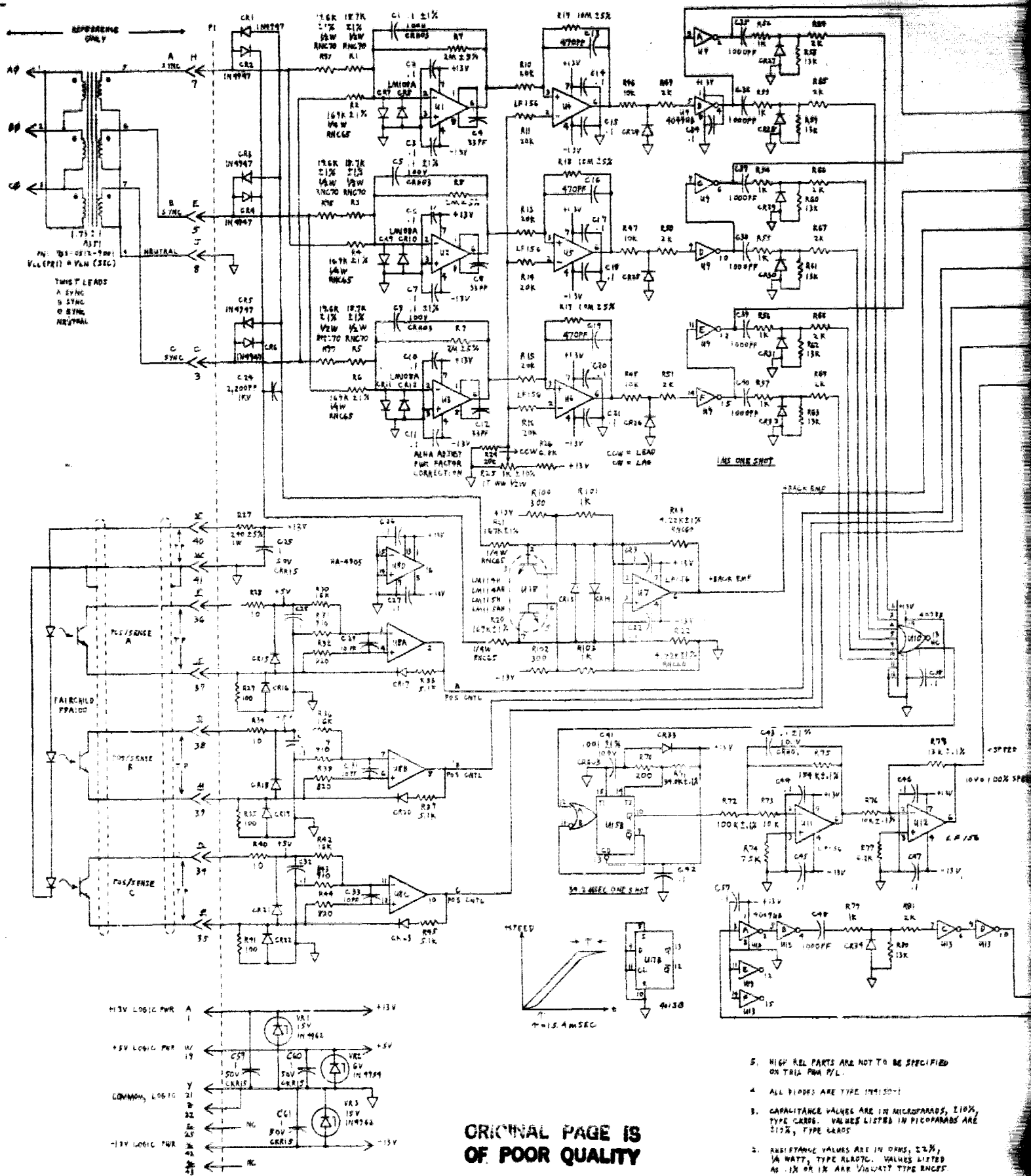
RESISTORS IN MICROFARADS, 5%, LISTED IN PICOFARADS ARE

RESISTORS IN OHMS, 2%, 1/4W

DESIGNATIONS ARE SHOWN IN BRACKET WITH UNIT PREFIX

UNLESS SPECIFIED OTHERWISE

TITLE ELECTRICAL SCHEMATIC DIAGRAM VUEVER LOGIC PROGRAMS ADVANCED NASA DRIVE	PROJECT NO. 720210	DRAWING NO. 2001564
	DATE 1/11/62	SCALE 1:1
DESIGNED BY R.A. KUSTICH	CHECKED BY J.E. BROWN	APPROVED BY J.E. BROWN
AUTHORITY ADVANCED NASA DRIVE	ORGANIZATION NASA	PROJECT TITLE ADVANCED NASA DRIVE



ORIGINAL PAGE IS  
OF POOR QUALITY

5. HIGH REL PARTS ARE NOT TO BE SPECIFIED ON THIS PWA P/L.
4. ALL DIODES ARE TYPE 1N4947.
3. CAPACITANCE VALUES ARE IN MICROFARADS, 10%, TYPE CAPS. VALUES LISTED IN PICOFARADS ARE 10%, TYPE LEADS.
2. RESISTANCE VALUES ARE IN OHMS, 1%, 1/4 WATT, TYPE ALDTC. VALUES LISTED AS .1K OR 1K ARE 1/10WATT TYPE RNC65.
1. PART(A) REFERENCE DESIGNATIONS ARE SHOWN FOR COMPLETE DESIGNATION PREFIX WITH UNIT NUMBER AND SUBASSEMBLY DESIGNATORS.

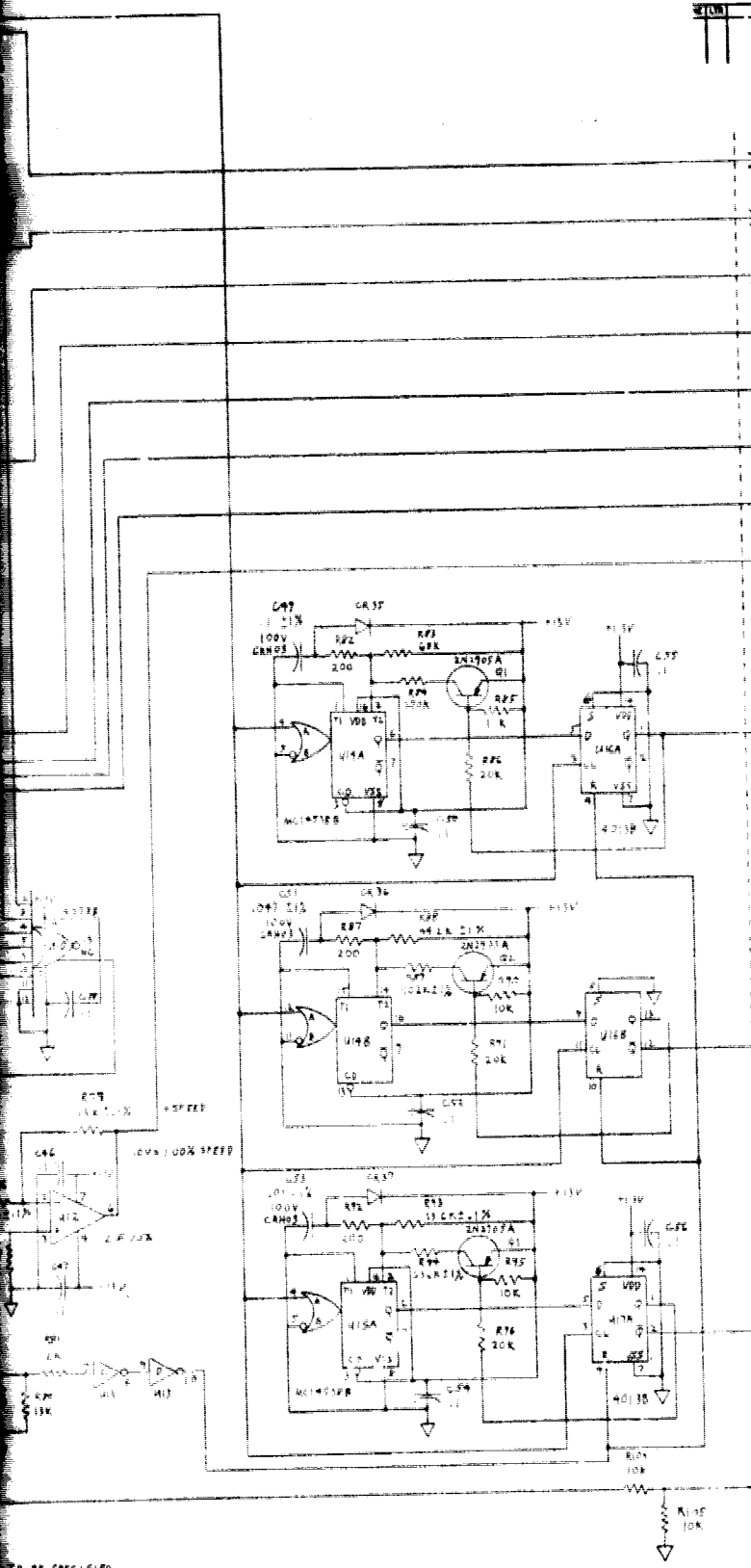
NOTED: UNLESS OTHERWISE SPECIFIED

EOLDOUT FRAME

REVISIONS		
NO.	DESCRIPTION	DATE

- P A EMP CTRL
- R B EMP CTRL
- S C EMP CTRL
- T + BACK EMP
- HL A POS CTRL
- A B POS CTRL
- K C POS CTRL
- V + SPEED  $\frac{100\% \text{ SPEED}}{10V}$

**FOLDOUT FRAME**



SPEED > 10%



SPEED	VREF	VREF	RPM	M.P.
P	149.7	6.075	111K	2.7
R	184.7	5.976	14K	3.5
S	190.1	2.023	2.1K	9
T	223.4	1.875	4K	10
HL	189.7	3.366	14K	3.5
A	189.4	4.967	15K	3.8

\* SPEED IN RPM FOR FIRST GEAR

SPEED < 10%



**ORIGINAL PAGE IS OF POOR QUALITY**

**PRECEDING PAGE BLANK NOT FILMED**

OVER-TEMP



REFERENCE DESIGNATION BY SYMBOL	
PART NO.	USED   NO. NOT USED
C1	
C17	
F1	
Q1	
R105	R12
U1C	
VK3	

TO BE SPECIFIED

180-1

IN MICRO-AMPS, 100K, 100M IN MICROFARADS ARE

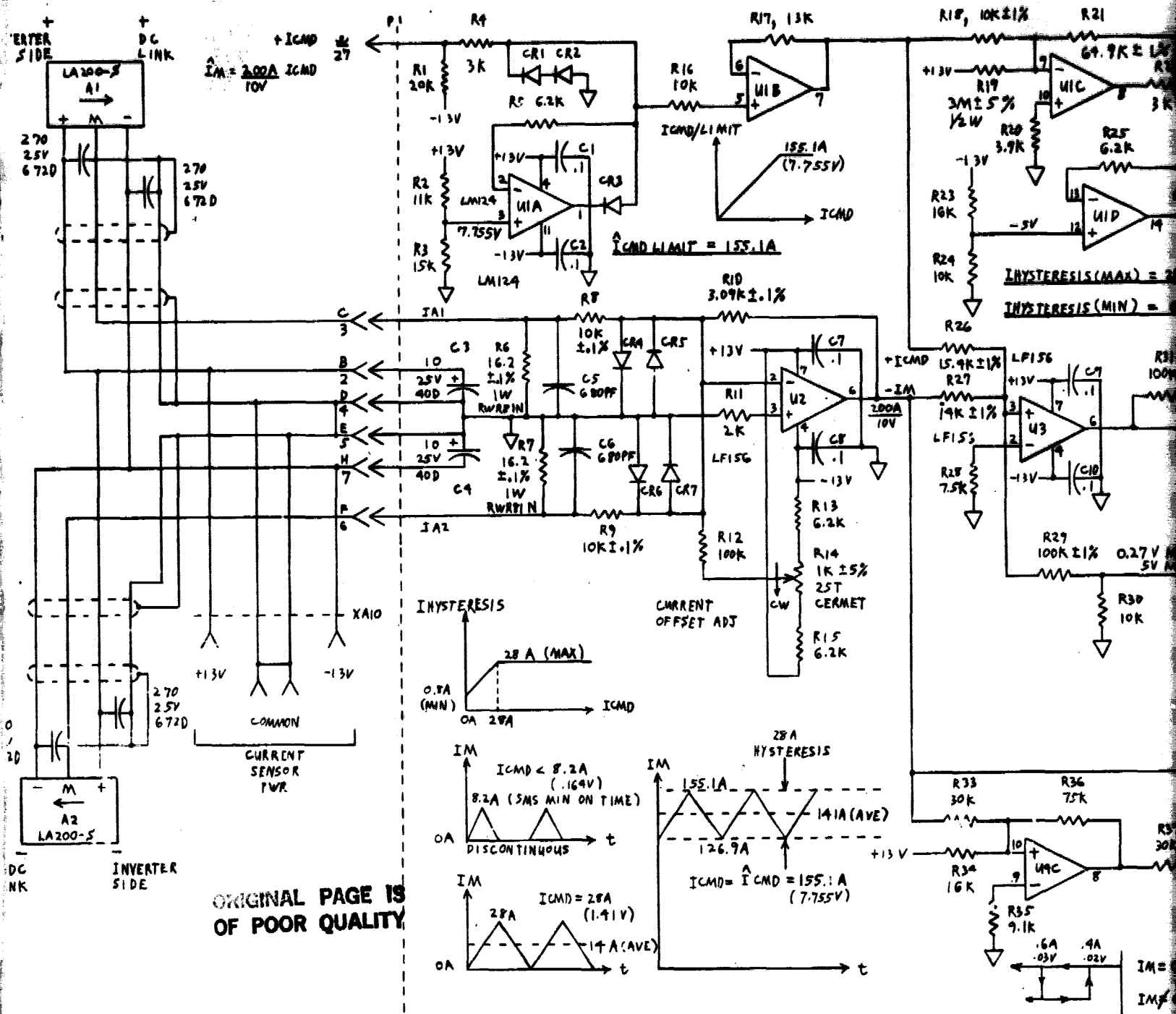
IN OHMS, 2.2%, VALUES AVOIDED PART TYPE RULES

NOTATIONS ARE WITH UNLESS SPECIFIED WITH UNLESS DESIGNATORS.

SPECIFIED

REF DES PREP: LOGIC PACK-A1A2

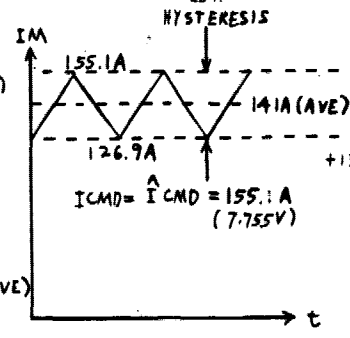
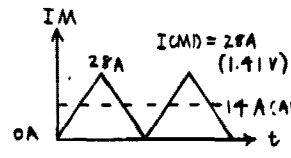
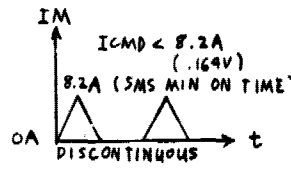
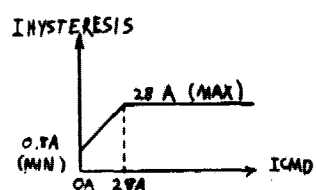
DESIGNED BY CHECKED BY DATE	DRAWN BY DATE	APPROVED BY DATE	PROJECT NO. 70210	DRAWING NO. 2001592
TITLE ELECTRICAL SCHEMATIC DIAGRAM SYNC AND SPEED ORDER LOGIC PROGRAM ADVANCED DATA DRIVE		SHEET NO. 2001592		



DC LINK  
INVERTER SIDE



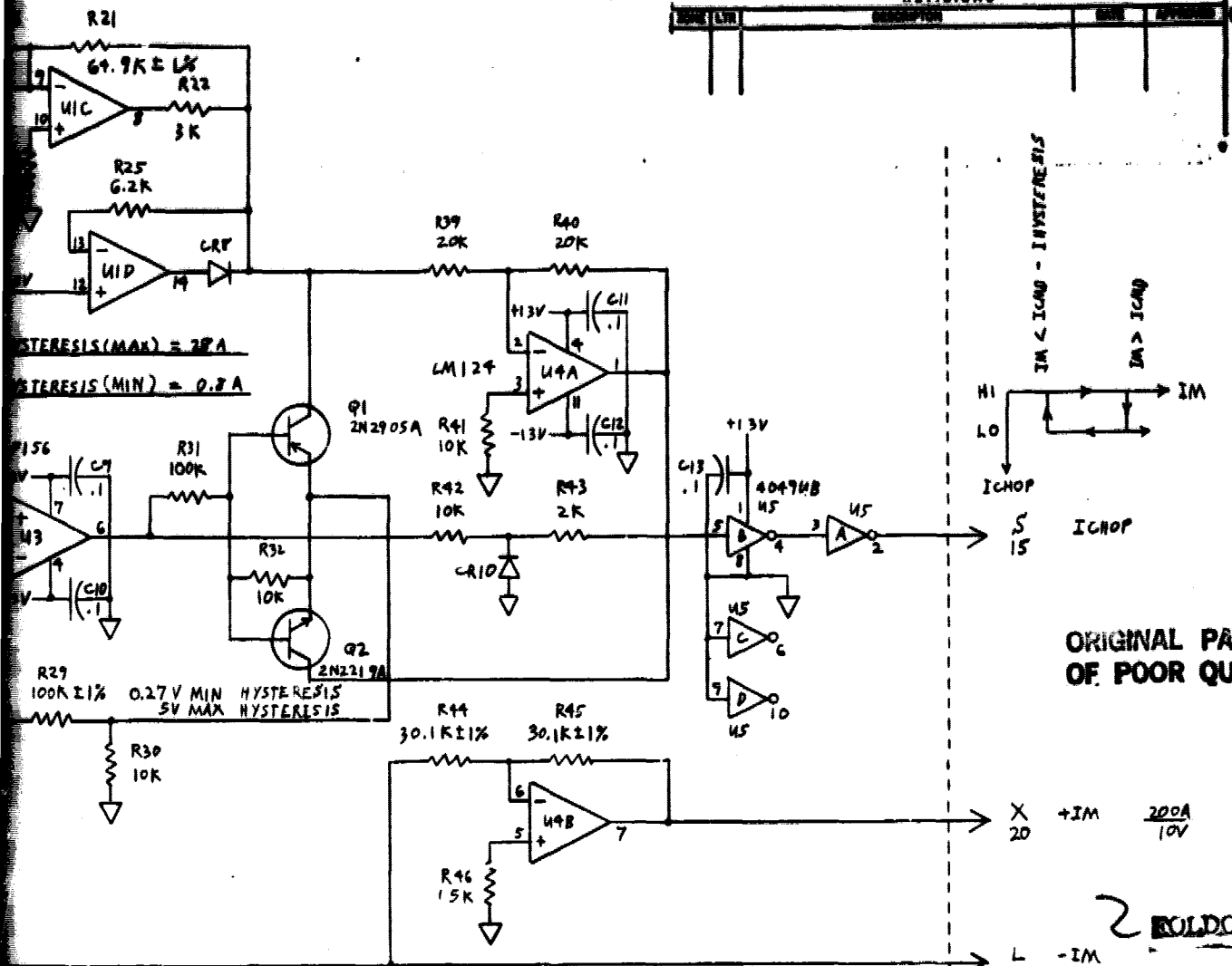
ORIGINAL PAGE IS OF POOR QUALITY



5. HIGH REL PARTS ARE NOT TO BE SPECIFIED ON THIS PWA P/L.
4. ALL DIODES ARE TYPE IN4150-1.
3. CAPACITANCE VALUES ARE IN MICROFARADS, ±10%, TYPE GRK06. VALUES LISTED IN PICOFARADS ARE ±10%, TYPE CR05.
2. RESISTANCE VALUES ARE IN OHMS, ±2%, ¼ WATT, TYPE ALR07C. VALUES LISTED AS ±.1% OR ±1% ARE ¼ WATT TYPE RNCC0.
1. PARTIAL REFERENCE DESIGNATIONS ARE SHOWN, FOR COMPLETE DESIGNATION PREFIX WITH UNIT NUMBER AND SUBASSEMBLY DESIGNATORS.

NOTES: UNLESS OTHERWISE SPECIFIED

REVISIONS			
NO.	DATE	DESCRIPTION	BY



HYSTERESIS (MAX) = 28 A  
 HYSTERESIS (MIN) = 0.8 A

0.27 V MIN HYSTERESIS  
 5V MAX HYSTERESIS

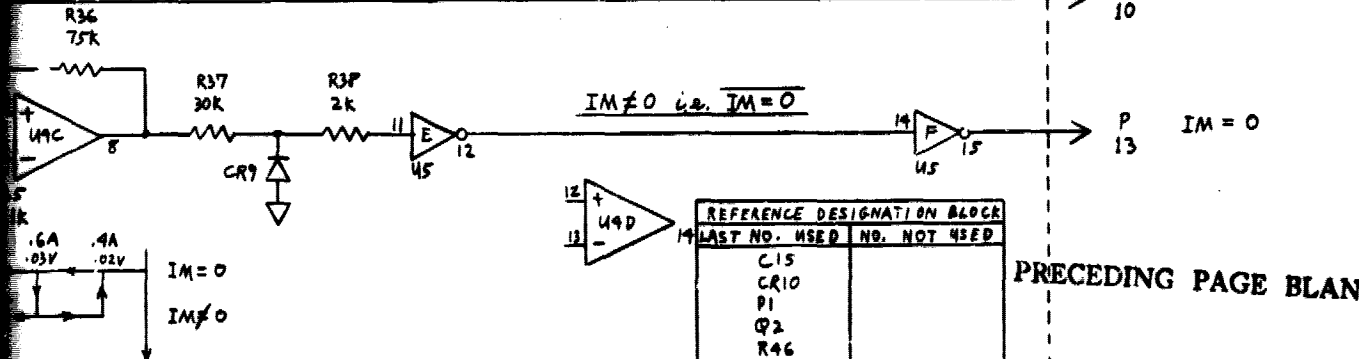
ORIGINAL PAGE IS  
 OF POOR QUALITY

X +IM 200A / 10V

L -IM 10

P IM = 0 13

**BOLDOUT FRAME**



REFERENCE DESIGNATION BLOCK	
LAST NO. USED	NO. NOT USED
C15	
CR10	
Q1	
Q2	
R46	
U5	
VR2	

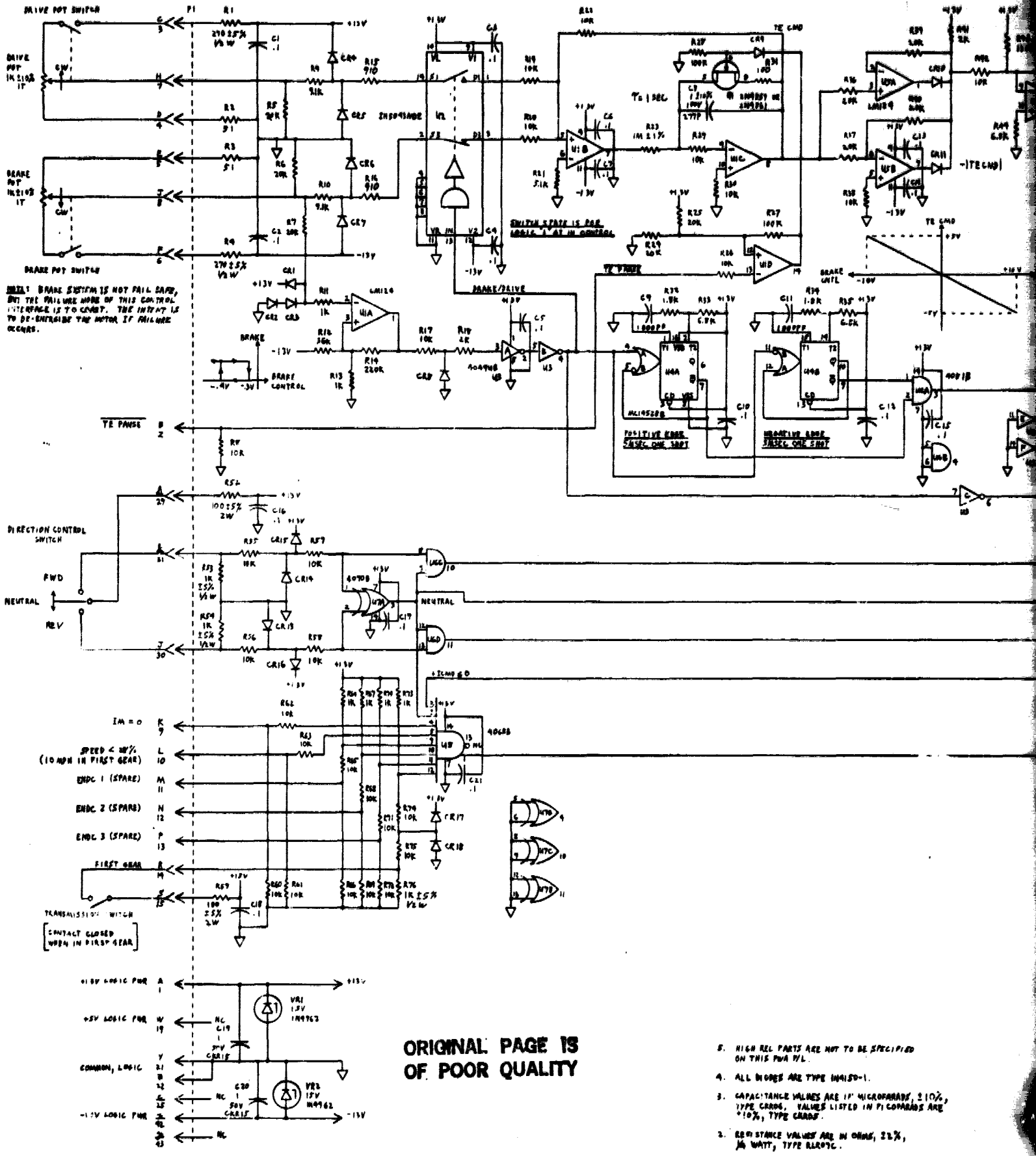
PRECEDING PAGE BLANK NOT FILMED

REF DES PREFIX: LOGIC RACK - A3A4

SHOWN, UNIT

UNLESS OTHERWISE SPECIFIED: DIMENSIONS PER BOSS AND INTERPRETATIONS PER FIG IDENTIFICATION MARKING PER MSC10	DESIGNED BY: <b>ICR KUSTICH</b>	AERSEARCH MANUFACTURING COMPANY OF CALIFORNIA A DIVISION OF THE SABERTY CORPORATION YORBA LINDA, CALIFORNIA
	DRAWN BY: <b>W. J. GORIO</b>	
CHECKED BY: <b>W. J. GORIO</b>	DATE: <b>7/25/66</b>	ELECTRICAL SCHEMATIC D. AGRAM ISENSE AND COMPANATOR LOGIC PROGRAM: ADVANCED NASA DRIVE
PART NUMBER: <b>70210</b>	DRAWING NUMBER: <b>2001566</b>	
REVISION: <b>1</b>	SCALE: <b>-</b>	SHEET: <b>1</b> OF <b>1</b>





IF THE BRAKE SWITCH IS NOT FAIL SAFE, BUT THE FAILURE MODE OF THIS CONTROL INTERFACE IS TO CAUSE THE INPUT IS TO DE-ENERGIZE THE MOTOR IF FAILURE OCCURS.

SWITCH STATE IS FOR LOGIC AT ALL TIMES CONTROL

POSITIVE EDGE 5/16 SEC ONE SHOT

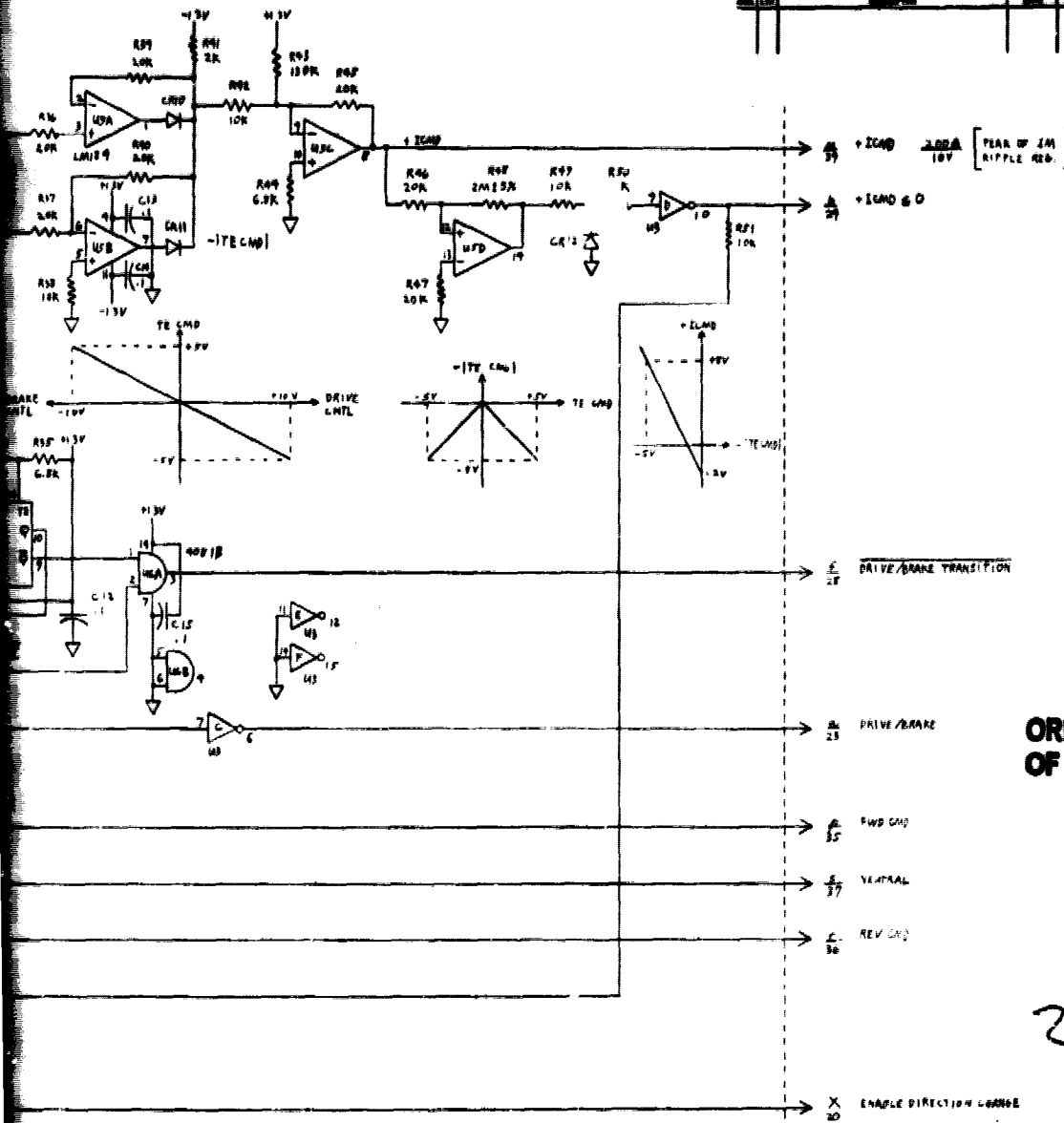
NEGATIVE EDGE 5/16 SEC ONE SHOT

ORIGINAL PAGE IS OF POOR QUALITY

1. PARTIAL REFERENCE DESIGNATIONS ARE SHOWN FOR COMPLETE DESIGNATION PREPARE WITH UNIT NUMBER AND SUBASSEMBLY DESIGNATIONS
  2. RESISTANCE VALUES ARE IN OHMS, 1%, 1/4 WATT, TYPE RL00TC.
  3. CAPACITANCE VALUES ARE IN MICROFARADS, 5%, TYPE CAPS.
  4. ALL INDUCTORS ARE TYPE M15D-1.
  5. HIGH REL PARTS ARE NOT TO BE SPECIFIED ON THIS PWA P/L.
- NOTES: UNLESS OTHERWISE SPECIFIED

**SOLDOUT FRAME**

REVISIONS	



**ORIGINAL PAGE IS OF POOR QUALITY**

**2 BOLDOUT FRAME**

**PRECEDING PAGE BLANK NOT FILMED**

REFERENCE DESIGNATION	
LAST NO.	REV.
C11	
C12	
C13	
U5A	
U5B	
U5C	

TO BE SPECIFIED

RES-1

IN MICROSECONDS, ±10%,  
SERVED IN MICROSECONDS ARE

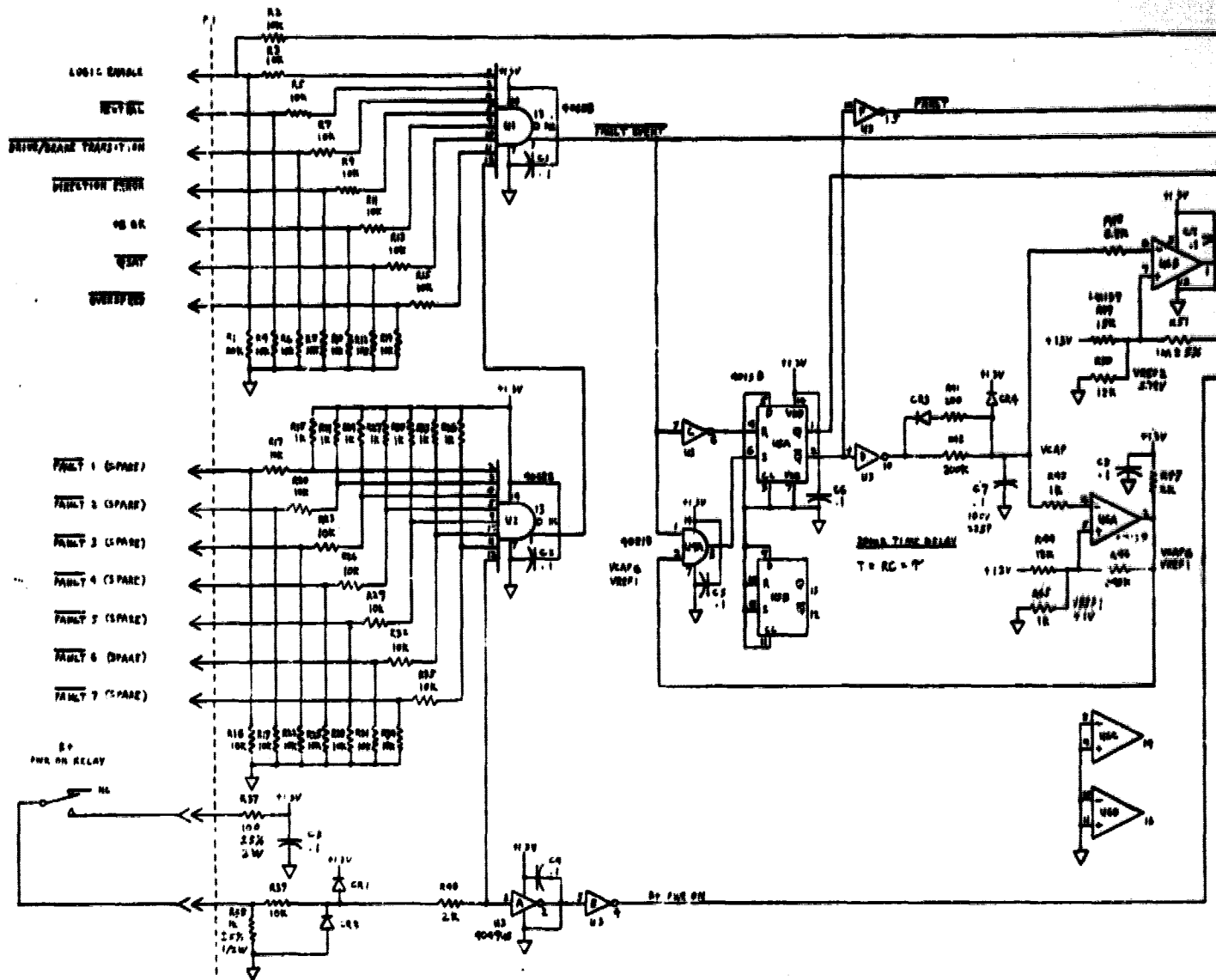
IN OHMS, ±1%,

VALUES ARE SHOWN,  
UNLESS PRECISE WITH UNIT  
DESIGNATORS

SPECIFIED

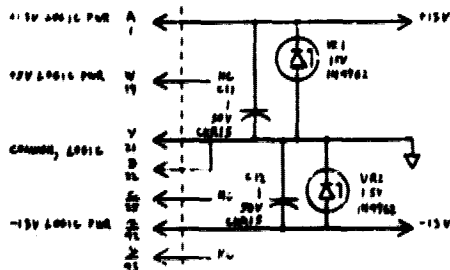
REF DES PREFIX: LOGIC RATE- ADAS

PROJECT NO. DRAWING NO. REV. NO.	DATE BY CHECKED BY	APPROVED BY TITLE	ELECTRICAL SCHEMATIC DIAGRAM DRIVE/BRAKE, DIRECTION AND TE CONTROL LOGIC PROGRAM: ADVANCED MORA DRIVE
PART NO. QUANTITY UNIT	PART NO. QUANTITY UNIT	PART NO. QUANTITY UNIT	E 70210 200156



**BOLDOUT FRAME**

**ORIGINAL PAGE IS OF POOR QUALITY.**

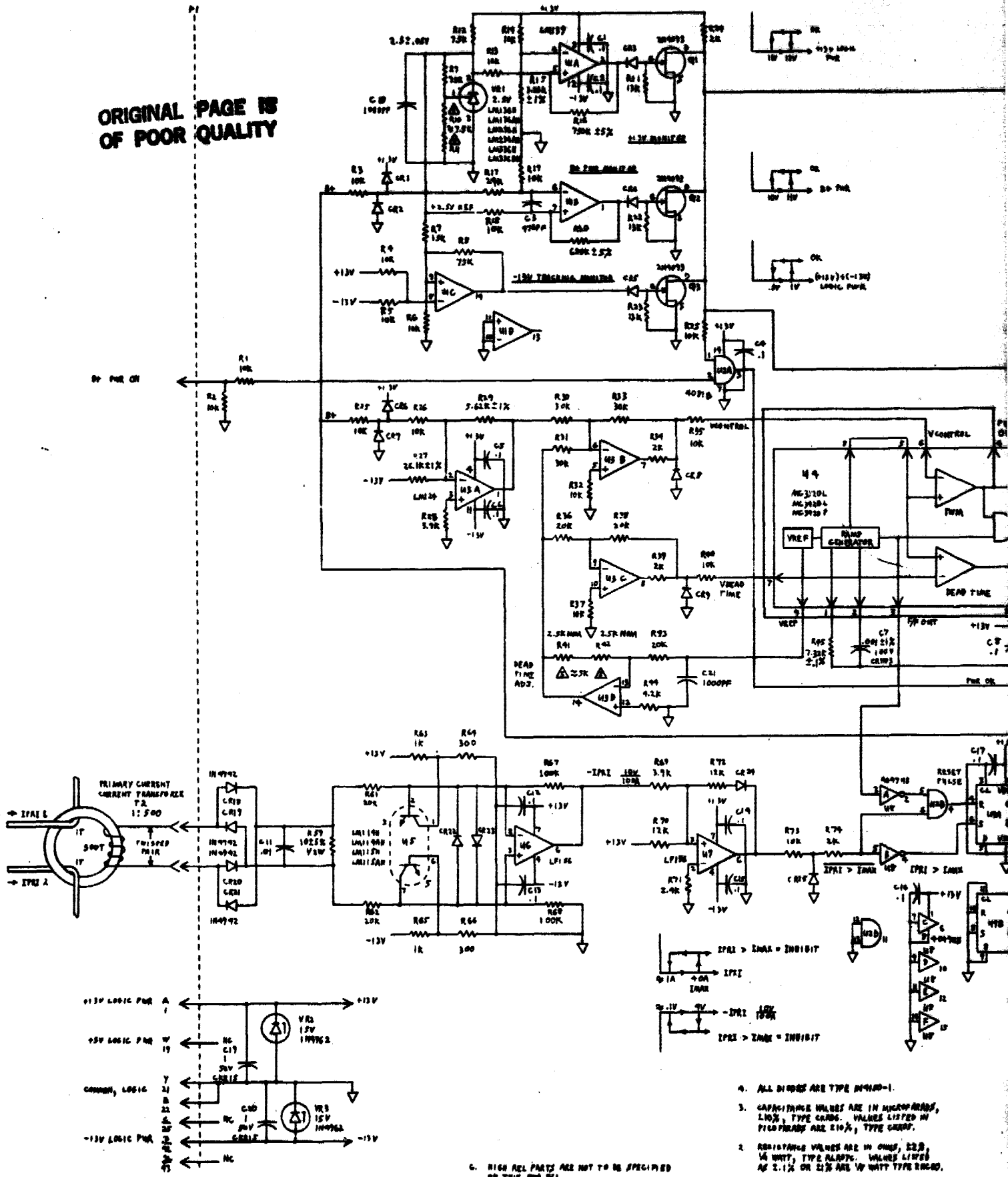


7. HIGH REL PARTS ARE NOT TO BE SPECIFIED ON THIS PWR SUP.
  8. ALL DIODES ARE TYPE 1N4100-1.
  9. CAPACITANCE VALUES ARE IN MICROFARADS, SIZE 5 TYPE CAPS.
  10. RESISTANCE VALUES ARE IN OHMS, 1/4W, 1/2W, 1W TYPE RESIST.
  11. PARTIAL REFERENCE DESIGNATIONS ARE GIVEN FOR COMPLETE DESIGNING PURPOSES WITH ONLY NUMBER AND SYMBOLIC DESIGNATIONS.
- NOTES: UNLESS OTHERWISE SPECIFIED



# OLDOUT FRAME

ORIGINAL PAGE IS OF POOR QUALITY



C. HIGH REL PARTS ARE NOT TO BE SPECIFIED ON THIS PWA I/A.

▲ SELECT IN TEST RING.

1. PARTIAL COMPONENT DESIGNATIONS ARE SHOWN FOR COMPLETE DESIGNATION PURPOSE WITH PART NUMBER AND MANUFACTURER DESIGNATION.
2. RESISTANCE VALUES ARE IN OHMS, 10K, 100K, 1M OHMS, TYPE CARDS. VALUES LISTED IN FIGS PARAGRAPH ARE 10%, TYPE CARDS.
3. CAPACITANCE VALUES ARE IN MICROFARADS, 100K, TYPE CARDS. VALUES LISTED IN FIGS PARAGRAPH ARE 10%, TYPE CARDS.
4. ALL DIODES ARE TYPE 1N4001-1.

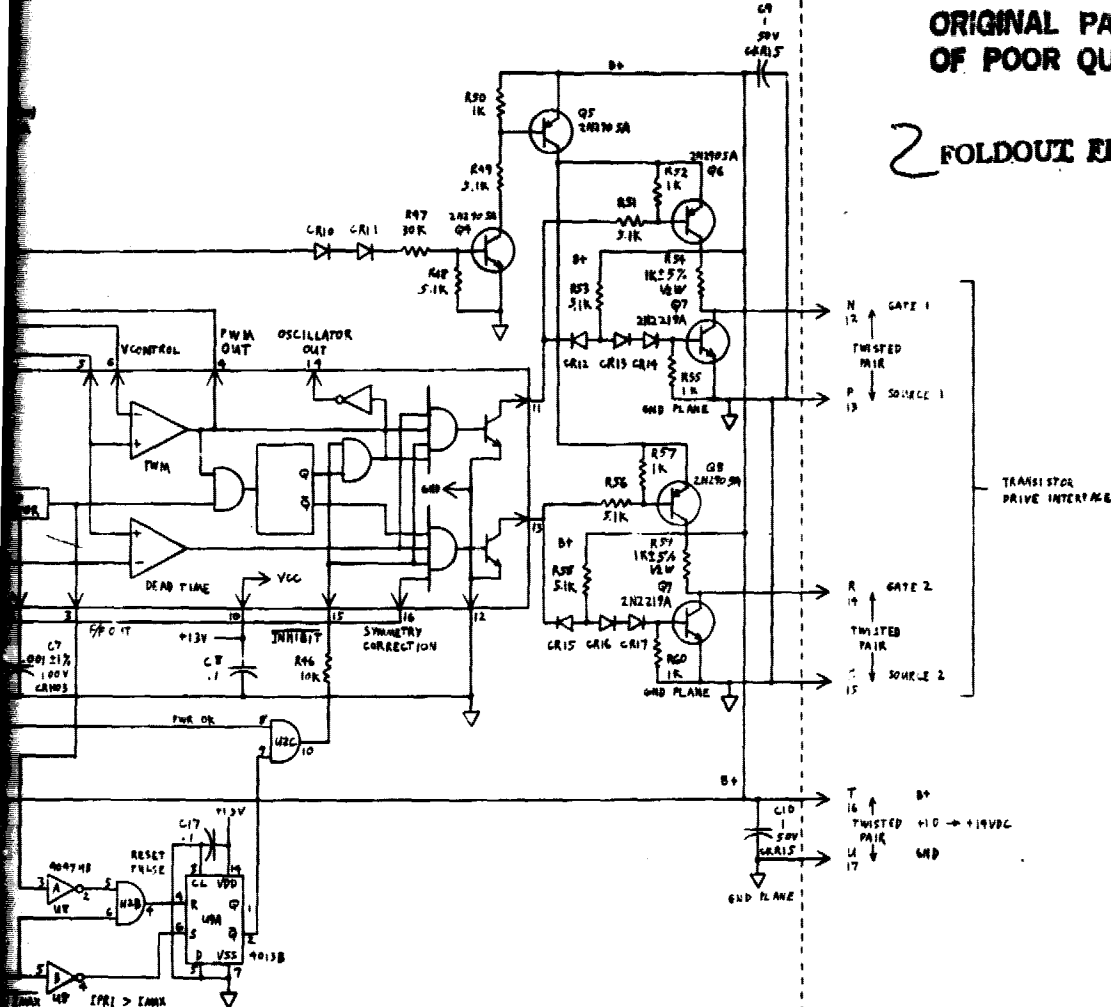
NOTE: UNLESS OTHERWISE SPECIFIED

REVISIONS	
NO.	DESCRIPTION

B4 OK

ORIGINAL PAGE IS OF POOR QUALITY

2 FOLDOUT FRAME



PRECEDING PAGE BLANK NOT FILMED

REFERENCE DESIGNATION ALPHABET	
USED	NOT USED
C10	
C11	
C12	
C13	
C14	
C15	
C16	
C17	
Q5	
Q6	
Q7	
Q8	
R47	
R48	
R49	
R50	
R51	
R52	
R53	
R54	
R55	
R56	
R57	

REF DES PREPARE: LOGIC PAGE-ABAT

VALUES LISTED IN TYPE CRAFT.  
 IN OHMS, 220, VALUES LISTED IN WATT TYPE RFLCO.  
 DIMENSIONS ARE SHOWN UNLESS OTHERWISE SPECIFIED.  
 SPECIFIED

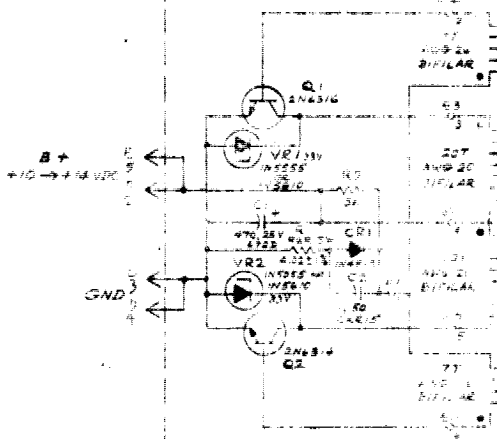
PROJECT NO. DRAWING NO. REV. NO.	DATE TIME	APPROVED BY DESIGNED BY CHECKED BY	ELECTRICAL SCHEMATIC DIAGRAM MADE DRIVE POWER SUPPLY LOGIC PROGRAM ADVANCED MESA DRIVE
PART NO. QUANTITY UNIT	PART NO. QUANTITY UNIT	PART NO. QUANTITY UNIT	PART NO. QUANTITY UNIT
APPLICATION	APPLICATION	APPLICATION	APPLICATION

**BOLDOUT FRAME**

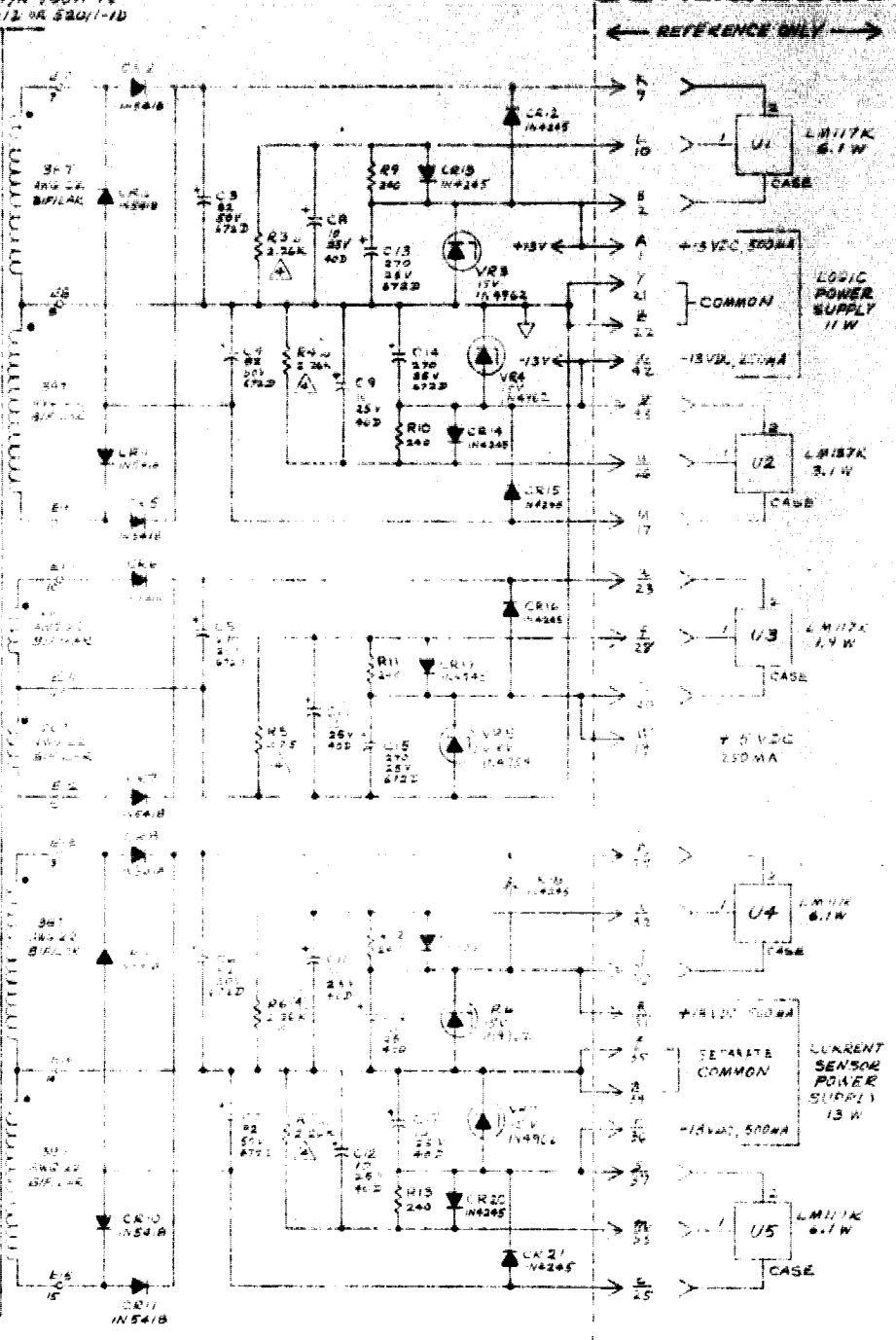
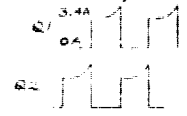
P1

MAGNETICS INC  
 CERT P/N 50011-12  
 57011-12 OR 52011-12

**ORIGINAL PAGE IS  
 OF POOR QUALITY**



POUT = 30W MIN  
 FREQ = 33KHZ FOR 100V  
 33KHZ FOR 140V  
 CORE LOSS = 1.1W @ 33KHZ  
 I PEAK PRI 2.5A



REFERENCE DESIGNATIONS	
LAST NO. USED	NO. NOT USED
C19	
CR24	
E15	
C5	
P1	RB
R34	
T1	
U1	
VR8	

- 5. HIGH RELIABLE PARTS ARE NOT TO BE SPECIFIED ON THIS PWR PARTS LIST
- 7. Q1 & Q2 ARE MOUNTED ON HEAT SINKS, THERMALLOY P/N: 6017 B
- 6. REFERENCE PARTS U1 - U5 ARE MOUNTED ON A PLATE HEAT SINK WITH INSULATING HDW. Pd TOTAL = 30W, WAKEFIELD P/N: 4771-5 INCH.

- ⚠ SELECT IN TEST KNC05
- ⚠ SELECT IN TEST KNC00
- 3. CAPACITANCE VALUES ARE IN MICROFARADS
- 2. RESISTANCE VALUES ARE IN OHMS, ± 2%
- 1. PARTIAL REFERENCE DESIGNATIONS ARE COMPLETE DESIGNATION PREFIX WITH UNIT & SUB ASSEMBLY DESIGNATORS.

NOTE: UNLESS OTHERWISE SPECIFIED

AA	AB	AC	AD	AE	AF	AG	AH	AI	AJ	AK	AL
1	2	3	4	5	6	7	8	9	10	11	12

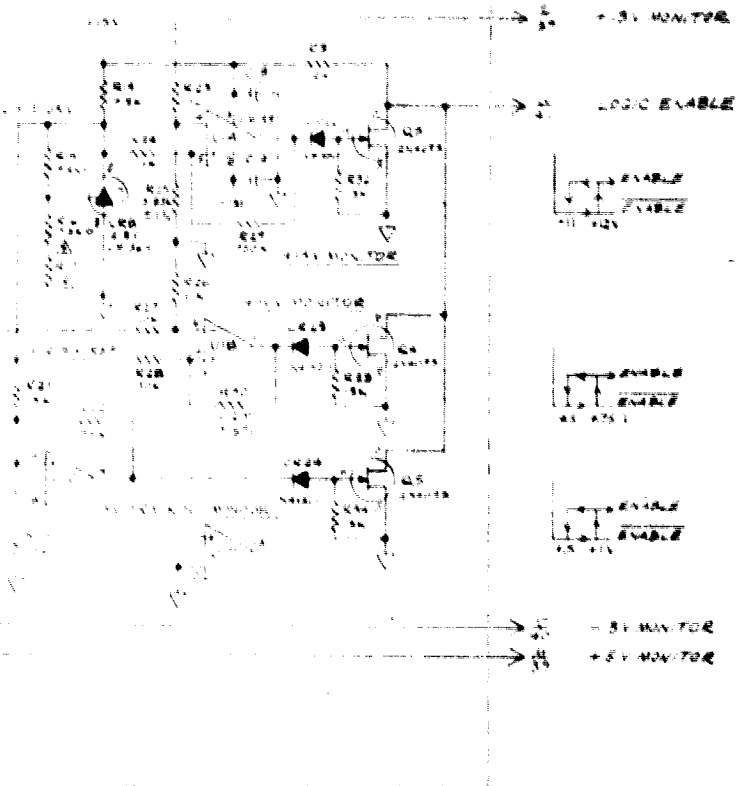
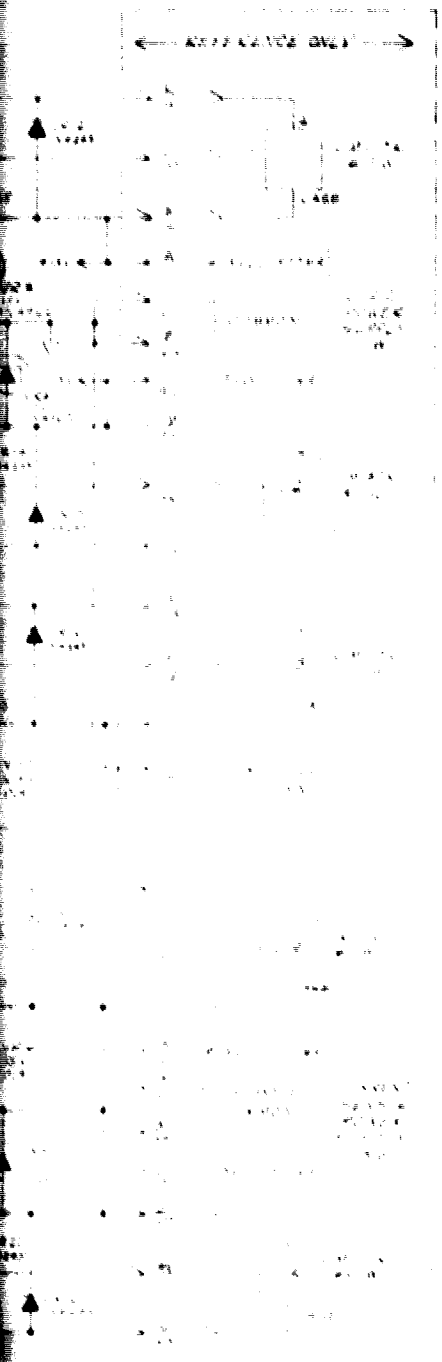


← DISTANCE ONLY →

2 FOLDOUT FRAME

ORIGINAL PAGE IS OF POOR QUALITY

PRECEDING PAGE BLANK NOT FILMED




REF DESIGN PREFIX: LOGIC RACK -A1A10

- 1. DESIGNATION OF PARTS
- 2. DESIGNATION OF PARTS
- 3. DESIGNATION OF PARTS
- 4. DESIGNATION OF PARTS
- 5. DESIGNATION OF PARTS
- 6. DESIGNATION OF PARTS
- 7. DESIGNATION OF PARTS
- 8. DESIGNATION OF PARTS
- 9. DESIGNATION OF PARTS
- 10. DESIGNATION OF PARTS

APPLICATION 1. 2. 3. 4. 5. 6. 7. 8. 9. 10.	DATE 1. 2. 3. 4. 5. 6. 7. 8. 9. 10.	DRAWN BY 1. 2. 3. 4. 5. 6. 7. 8. 9. 10.	CHECKED BY 1. 2. 3. 4. 5. 6. 7. 8. 9. 10.	APPROVED BY 1. 2. 3. 4. 5. 6. 7. 8. 9. 10.	ORGANIZATION ADVANCED RESEARCH AND DEVELOPMENT DIVISION
					PROJECT TITLE ELECTRICAL SCHEMATIC, LOGIC POWER SUPPLY, ADVANCED NASA DRIVE
PART NUMBER E 70210			DRAWING NUMBER 2001560		
SCALE 1:1					SHEET NO. 1 OF 1

2001560

A



8

7

6

5

4

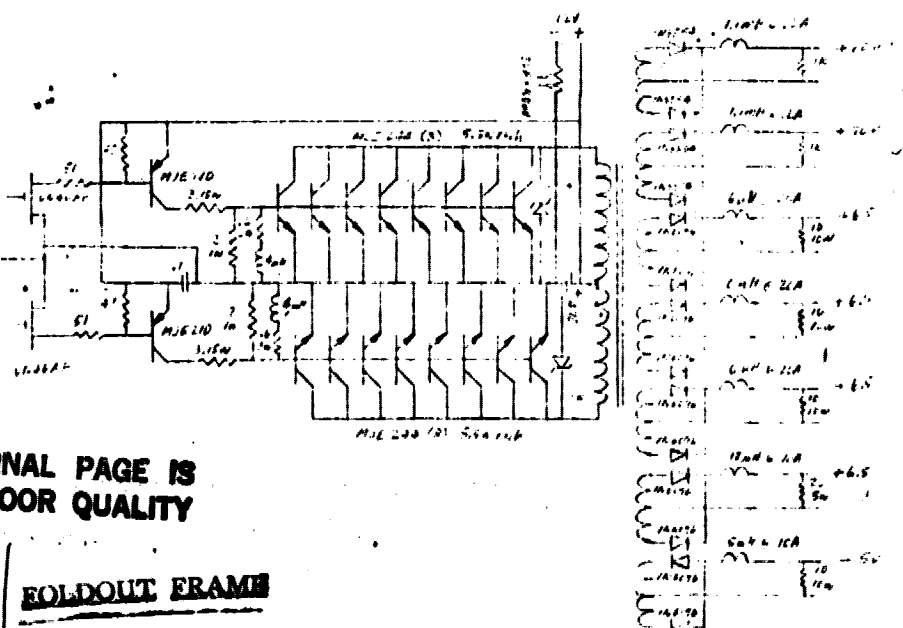
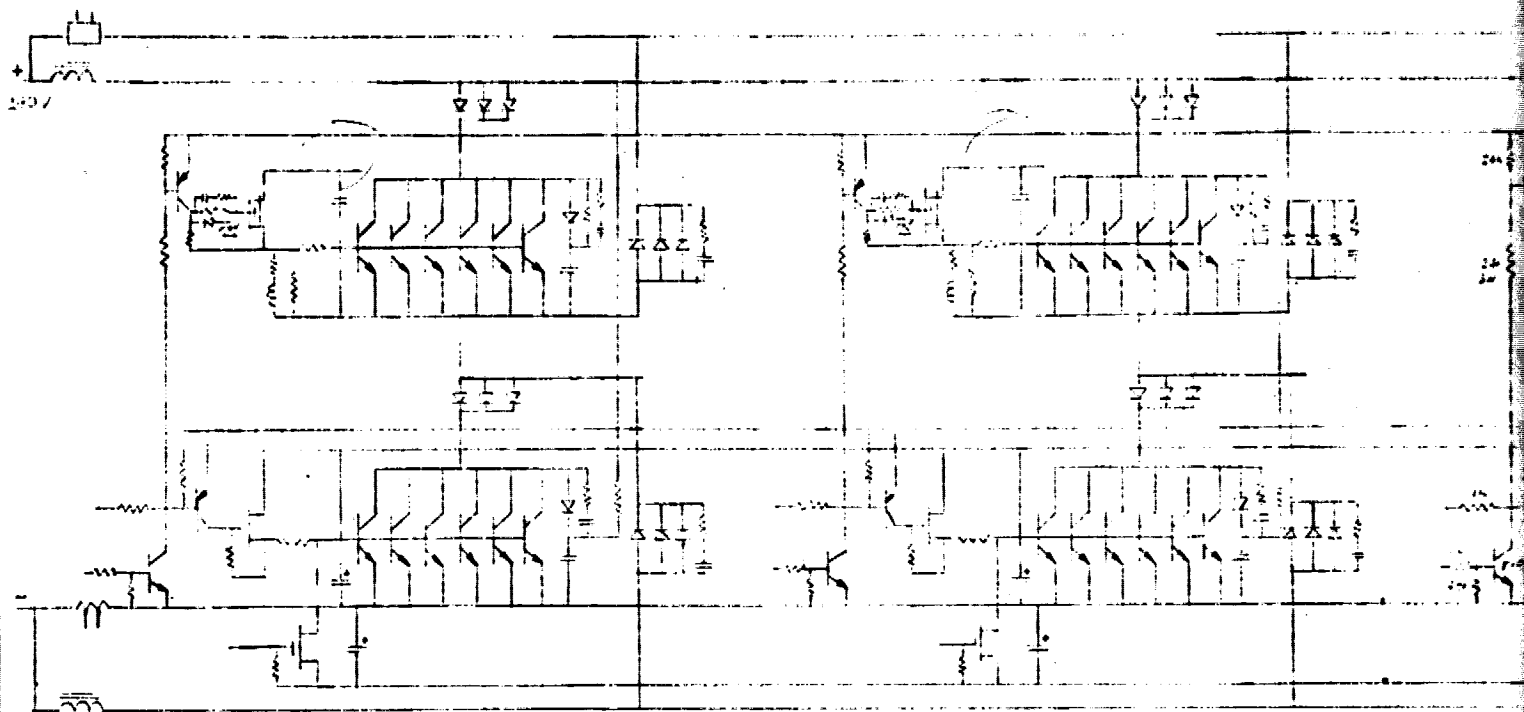
D

C

C

B

A



ORIGINAL PAGE IS  
OF POOR QUALITY

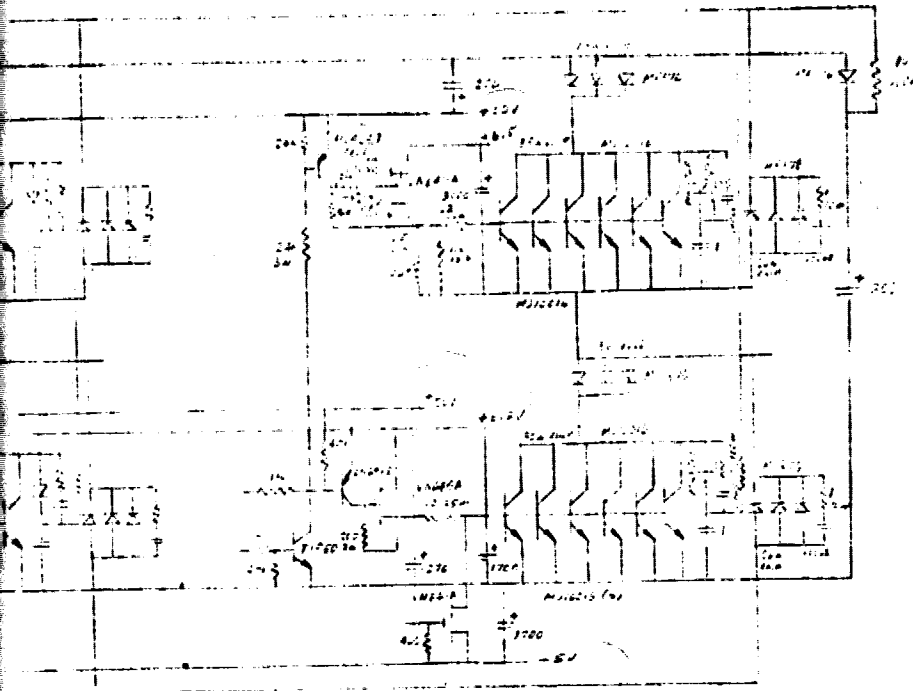
WOLDOUT FRAME

500W  
C 75AHz

Drive Power

3  
 This drawing shall be used only for the purpose of  
 illustrating the general nature of the invention  
 and shall not be construed as a limitation  
 thereof. It is to be understood that the  
 United States Government, this drawing may not  
 be used in any part to be reproduced or  
 used for manufacture of the part disclosed herein,  
 without the prior written permission of The Galt  
 Corporation.

REVISED		DATE	APPROVED
ZONE	LTR	DESCRIPTION	



ORIGINAL PAGE IS  
 OF POOR QUALITY

2 EOLDOUT FRAME

PRECEDING PAGE BLANK NOT FILMED

*Robert Underhill*

*1000 Galt Corporation Building*

*Yuba City, Texas*

AIRSEARCH MANUFACTURING COMPANY OF CALIFORNIA A DIVISION OF THE ROBERT EDUCATION YUBA CITY, CALIFORNIA		
D	70210	#1 SKPW 820910
SCALE	SHEET	

## APPENDIX F

### SHAFT POSITION SENSOR

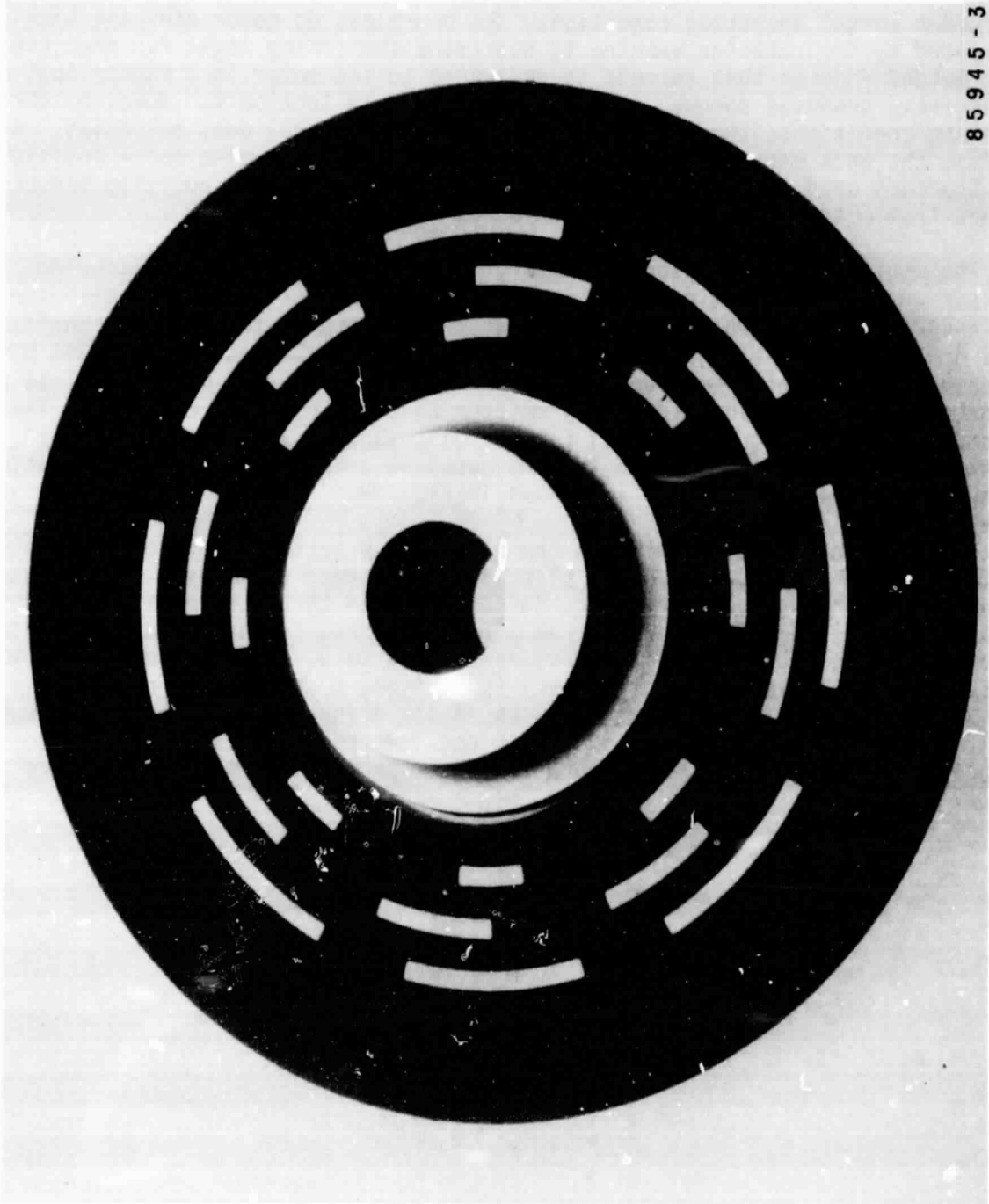
Under normal operating conditions, the brushless dc motor uses the back emf generated by the rotating machine to determine the firing logic for the inverter. This method ensures that current is delivered to the motor in a manner that most effectively produces torque. This was discussed in Section 4. However, during starting conditions, the back emf (proportional to speed) does not exist. At low speeds, the back emf is not sufficient to accurately determine rotor position. The approach used for this design was to incorporate a shaft position sensor for speeds from 0 to 10 percent of rated speed.

The shaft position sensor consists of an encoded disc, a light-coupled emitter and sensor pair, decoding logic, and the necessary mounting hardware. The encoded disc, shown in fig. 97, is attached directly to the motor shaft. The disc has three sets of slots, located at three different radii. The slot pattern repeats itself eight times over 360 mechanical deg since the machine has 16 poles (eight pole pairs). The stationary emitter assembly consists of 3 LED's located at radii equivalent to those used for the disc slots. The sensor assembly consists of 3 photodiodes, each located opposite an LED. Some of the mounting hardware and the encoded disc are shown in fig. 98.

The decoding logic, located in the electronics package, monitors the output of the three photodiodes. When a slot appears between the sensor and emitter, light passes through and photodiode turns on. When the disc blocks the light (between slots), the photodiode turns off. The three sensor outputs, therefore, each have a logic 0 or logic 1 output, resulting in 3, or eight possible logic states. The encoded disc slot pattern is arranged such that two of the possible combinations do not occur. This results in six unique logic states, corresponding to the six possible switch states in the inverter. The inverter logic decodes the emitter logic and ensures that the proper inverter switches are gated.

PRECEDING PAGE BLANK NOT FILMED

ORIGINAL PAGE IS  
OF POOR QUALITY



85945-3

Figure 97.--Position Sensor Encoded Disc.

ORIGINAL PAGE IS  
OF POOR QUALITY

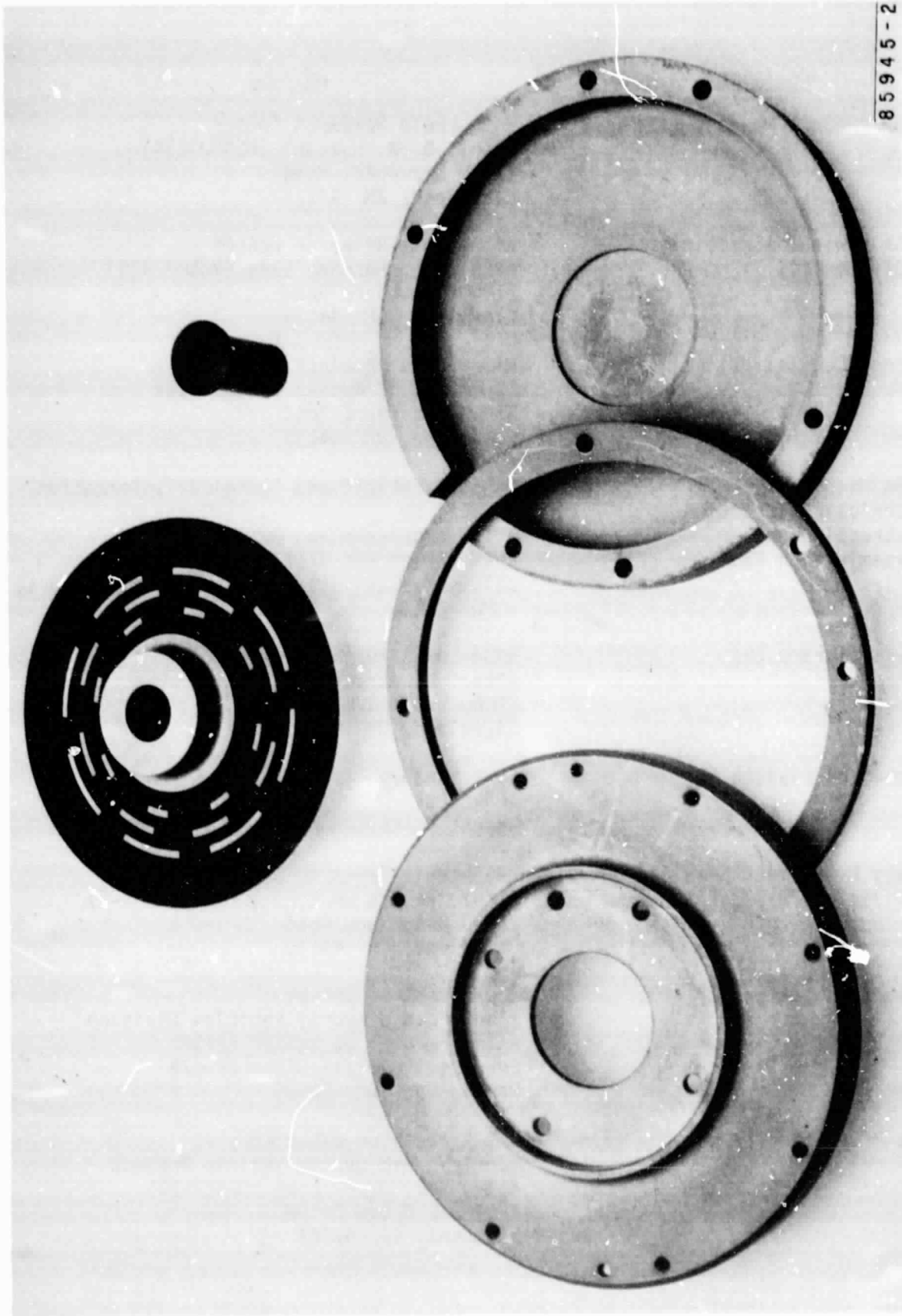


Figure 98.--Position Sensor Encoded Disc and Mounting Hardware.

<u>Recipient</u>	<u>Address</u>
NASA Project Manager (72)	NASA-Lewis Research Center Attn: B. R. Hatvani (MS500-214) 21000 Brookpark Road Cleveland, OH 44135
NASA Lewis Contracting Officer (1)	NASA-Lewis Research Center Attn: Mr. Anthony Long (MS500-305) 21000 Brookpark Road Cleveland, OH 44135
Patent Counsel (1)	NASA-Lewis Research Center Attn: N. T. Musial (MS500-113) 21000 Brookpark Road Cleveland, OH 44135
NASA Headquarters Technical Information Abstracting and Dissemination Facility (25)	NASA Scientific and Technical Information Facility Attn: Accessioning Department Post Office Box 8757 Baltimore/Washington International Airport, MD 21240
Lewis Library (2)	NASA-Lewis Research Center Attn: Library (MS 60-3) 21000 Brookpark Road Cleveland, OH 44135
Technical Liaison (1)	E. E. Bailey AFAPL/DO Wright Patterson AFB, OH 45433
Lewis Management Services Division (1)	NASA-Lewis Research Center Attn: Report Control Office (MS 5-5) 21000 Brookpark Road Cleveland, OH 44135
Department of Energy (20)	Department of Energy Electric and Hybrid Vehicles Division Attn: Mr. G. J. Walker CE132 Forrestal Building-Room GA-076 Washington, DC 20585
Jet Propulsion Laboratory (3)	Jet Propulsion Laboratory Electric and Hybrid Vehicle Project Attn: Mr. J. E. Long MS507-102 4800 Oak Grove Drive Pasadena, CA 91103

Recipient

Address

The Aerospace Company (3)

The Aerospace Company  
Attn: Mr. John H. Gower  
Suite 4000  
955 L'Enfant Plaza SW  
Washington, DC 20024

Argonne National Laboratory (3)

Argonne National Laboratory  
Attn: Dr. N. P. Yao Building 205  
9800 South Cass Avenue  
Argonne, IL 60439